

11-9-2021

Characterization of Biological Samples using Multi-modal Mass Spectrometry

Yarixa L. Cintron-Diaz
ycint002@fiu.edu

Follow this and additional works at: <https://digitalcommons.fiu.edu/etd>



Part of the [Analytical Chemistry Commons](#)

Recommended Citation

Cintron-Diaz, Yarixa L., "Characterization of Biological Samples using Multi-modal Mass Spectrometry" (2021). *FIU Electronic Theses and Dissertations*. 4854.
<https://digitalcommons.fiu.edu/etd/4854>

This work is brought to you for free and open access by the University Graduate School at FIU Digital Commons. It has been accepted for inclusion in FIU Electronic Theses and Dissertations by an authorized administrator of FIU Digital Commons. For more information, please contact dcc@fiu.edu.

FLORIDA INTERNATIONAL UNIVERSITY

Miami, Florida

CHARACTERIZATION OF BIOLOGICAL SAMPLES USING MULTI-MODAL
MASS SPECTROMETRY

A dissertation submitted in partial fulfillment of

the requirements for the degree of

DOCTOR OF PHILOSOPHY

in

CHEMISTRY

by

Yarixa L. Cintron-Diaz

2021

To: Dean Michael R. Heithaus
College of Arts, Sciences and Education

This dissertation, written by Yarixa L. Cintron-Diaz, and entitled Characterization of Biological Samples using Multi-modal Mass Spectrometry, having been approved in respect to style and intellectual content, is referred to you for judgment.

We have read this dissertation and recommend that it be approved.

Jeremy W. Chambers

Anthony P. DeCaprio

Bruce M. McCord

Piero R. Gardinali

Francisco A. Fernandez-Lima, Major Professor

Date of Defense: November 9, 2021

The dissertation of Yarixa L. Cintron-Diaz is approved.

Dean Michael R. Heithaus
College of Arts, Sciences and Education

Andrés G. Gil
Vice President for Research and Economic Development
and Dean of the University Graduate School

Florida International University, 2021

© Copyright 2021 by Yarixa L. Cintron-Diaz

All rights reserved.

DEDICATION

A mis abuelos, José Luis, Magdalena y Carmen, por siempre enseñarme que el cielo es el límite. A mi ángel de la guarda, mi Mamamery, por cuidarme y mimarme hasta tus últimos días. Ojalá pudiera escaparme un rato al cielo y abrazarlos una vez más.

Por ustedes, TODO.

ACKNOWLEDGMENTS

I would like to acknowledge Dr. Francisco Fernandez-Lima, for his consistent support throughout my years as a graduate student under his guidance. Thank you for always providing the necessary tools and motivation to achieve my goals. I am a better researcher thanks to you.

I am very grateful for my committee members, Dr. Jeremy Chambers, Dr. Anthony DeCaprio, Dr. Piero Gardinali, and Dr. Bruce McCord, for always being available and investing time in reading, listening, and providing feedback of my scientific progress. Your support and knowledge have guided and motivated me throughout my journey as a PhD student.

To my LimaLab family, Kevin, Dennys, Lilian, Clement, Khoa, Miguel, Sam and Cassandra, thanks for becoming my greatest support team and for all the fun times. Never a dull moment with you guys. To past members, Anthony and Alan, for guiding me throughout my first year as a PhD student and making the best cafecitos. To Jean and Jefferson, because your short stay was more than enough to make excellent friends and colleagues. I'm immensely grateful to Dr. Mario Gomez and Dr. Cesar Ramirez for the countless hours spent mentoring and helping during my efforts of becoming a better scientist. You both taught me so much, that I don't think I could ever pay you back.

During my PhD, I had the privilege to be funded by the National Science Foundation (NSF) through the Bridge to the Doctorate Fellowship. For that, I would like to thank Claudia Balzan for contacting me and preparing my application. Additionally, I would like to thank Dr. Lidia Kos, Dr. Sonja Montas-Hunter and Asfa Siddiqui for

organizing multiple workshops and activities that encouraged us to become better scientists.

I feel indebted to two amazing postdocs, Dr. Monica Rodriguez and Dr. Arlet Acanda, that even though I was not part of their lab, they had the patience and guidance to teach me many of the techniques I know today. I am also grateful for the many mentors, co-authors, and friends I have made along the way, especially Dr. Jeremy Chambers, Dr. Peter Verhaert, and Dr. Ivan Jozic.

I would like to acknowledge the Department of Chemistry and Biochemistry staff. Especially to Magali Autie, Dr. Kathleen Rein, and Dr. Watson Lees for providing the necessary tools to continue growing during our graduate studies and directing an excellent Chemistry Graduate Program.

Most importantly, I couldn't have reached this goal without the help of my amazing family, especially my parents, Aixa and Edgardo. Mami y papi, gracias por siempre ser mis mayores animadores y por esforzarse conmigo a través de los años. To my sister and brother, Aixa and Edgardito, thanks for being excellent role models and inspiring me to always reach for the stars. To my brother-in-law, Luis, for always making sure that I am happy and to my sister-in-law, Monique, for all the caring love and support you have given me. To my niece, Gabriela, for always putting a smile on my face. A mi segunda madre, Dinorah, por nunca faltar en los momentos mas difíciles y por quererme incondicionalmente. To all my family members, thank you. Con ustedes, todo en la vida es posible.

Finally, to all my friends. Thank you for bearing with me throughout the years and for always making me give my 200%. I'm eternally grateful.

ABSTRACT OF THE DISSERTATION
CHARACTERIZATION OF BIOLOGICAL SAMPLES USING MULTI-MODAL
MASS SPECTROMETRY

by

Yarixa L. Cintron-Diaz

Florida International University, 2021

Miami, Florida

Professor Francisco Fernandez-Lima, Major Professor

There is a need for fast, accurate and cost-effective protocols capable of assessing biomolecules at the molecular level (e.g., proteins, lipids and metabolites) from biological specimens. Mass spectrometry (MS) based techniques have become the analytical gold standard for identification and characterization of biomarkers in biological samples. The high throughput and short analysis time scales enables to follow biological processes while providing detailed chemical and spatial characterization. One of the current challenges in biological MS, is the high molecular complexity, chemical diversity and dynamic range. In this dissertation, the use of multi-modal mass spectrometry workflows -mass spectrometry imaging and ion mobility spectrometry - enables the untargeted and targeted analysis of biomolecules. The performance of mass spectrometry imaging techniques such as TOF-SIMS and MALDI-FTICR MS was evaluated for the spatial characterization of lipids, a chemotherapeutic drug agent, and neuropeptides. The orthogonality between ambient sampling liquid extraction surface analysis (LESA), ion mobility spectrometry and mass spectrometry (LESA-IMS-MS) was evaluated for the detection of small molecules from complex biological samples, such as common biological organs (e.g., liver, brain, and

skin) and three-dimensional multicellular spheroid (MCS) models of cancer cell lines. This dissertation showcases the development of new workflows that integrate ambient sampling with complementary gas-phase post-ionization separation techniques to study complex biological samples.

3.3.4. Trapped Ion Mobility Spectrometry CID TOF MS/MS	50
3.3.5. Liquid Chromatography-TIMS CID TOF MS/MS.....	51
3.3.6. Trapped Ion Mobility Spectrometry FT-ICR MS	52
3.3.7. Data Processing, Mobility Resolving Power and Mobility Resolution	52
3.4 Results and Discussion	53
3.5 Conclusions.....	63
3.6 Acknowledgements.....	64
3.7 References.....	65
CHAPTER 4: Mapping chemotherapeutic drug distribution in cancer cell spheroids using 2D-TOF-SIMS and LESA-TIMS-MS.....	72
4.1 Abstract.....	73
4.2 Introduction.....	74
4.3 Materials and Methods.....	77
4.3.1 Cell Culture.....	77
4.3.2. MCS Formation	78
4.3.3. Drug Treatment of MCS	78
4.3.4. MCS Embedding and Cryosectioning	79
4.3.5. Liquid Extraction Surface Analysis coupled to Trapped Ion Mobility Spectrometry Mass Spectrometry (LESA-TIMS-MS/MS)	80
4.3.6. Secondary Ion Mass Spectrometry (SIMS)	82
4.4 Results and Discussion	83
4.5 Conclusions.....	89
4.6 Acknowledgements.....	89
4.7 References.....	89
CHAPTER 5: Spatially resolved neuropeptide characterization from neuropathological FFPE tissue sections by a combination of MALDI MSHC and LESA-TIMS-MS	94
5.1 Abstract.....	95
5.2 Introduction.....	95
5.3 Materials and Methods.....	97
5.3.1 Chemicals.....	97
5.3.2. Sample collection, embedding, slicing and mounting	98
5.3.3. MALDI Matrix coating.....	99
5.3.4. MALDI Mass Spectrometry Imaging	99
5.3.5. Neuropeptide extraction from FFPE slides.....	100
5.3.6. LESA with Disulfide Bond reduction.....	100
5.3.7 nESI-TIMS-q-TOF MS/MS.....	101
5.3.8. Overall workflow scheme	101
5.4 Results and Discussion	102
5.4.1 MALDI FT-ICR MS	102
5.4.2. LESA-TIMS-TOF MS (/MS)	103
5.5 Conclusions.....	109
5.6 Acknowledgements.....	109

5.7 References.....	109
CHAPTER 6: Discovery and targeted analysis of saliva using LC-TIMS-TOF MS/MS	
.....	112
6.1 Abstract.....	113
6.2 Introduction.....	114
6.3 Materials and Methods.....	115
6.3.1 Chemicals.....	115
6.3.2. Samples.....	116
6.3.3. Sample preparation.....	116
6.3.4. LC-TIMS-TOF MS.....	117
6.3.5. Data Analysis.....	118
6.4 Results and Discussion.....	118
6.5 Conclusions.....	128
6.6 Acknowledgements.....	128
6.7 References.....	129
CHAPTER 7: Conclusions.....	133
APPENDICES.....	136
VITA.....	191

LIST OF TABLES

TABLE	PAGE
Table 2.1. Summary of the positive ionization mode LESA-FT-ICR-MS (MS1 and MS/MS) of a Mouse Brain sample. The molecular ion species, chemical composition, lipid class, theoretical mass, mass error, and identifiers are provided. HG denotes the head group and FA denotes fatty acids	29
Table 2.2. Summary of the positive ionization mode LESA-FT-ICR-MS (MS1 and MS/MS) of a Mouse Liver sample. The molecular ion species, chemical composition, lipid class, theoretical mass, mass error, and identifiers are provided. HG denotes the head group and FA denotes fatty acids	31
Table 2.3. Negative ion mode targeted MS/MS after preliminary MS1 accurate mass database search from the MB. The different lipid identification possibilities are shown, with the MS/MS fragment ion interpretations which refine the m/z identification	36
Table 6.1. Common unknown knowns detected in the saliva samples using LC-TIMS-TOF MS/MS	123

LIST OF FIGURES

FIGURE	PAGE
Figure 1.1. Liquid Extraction Surface Analysis (LESA) schematic.....	4
Figure 1.2. TOF-SIMS schematic.....	7
Figure 1.3. TIMS-TOF instrument schematic.....	10
Figure 1.4. cTWIMS-TOF instrument schematic.....	12
Figure 2.1 Graphical Abstract of Chapter 2.....	21
Figure 2.2. LESA-FT-ICR workflow developed for Chapter 2.....	26
Figure 2.3. Positive (a.) and negative (b.) ionization mode LESA-FT-ICR MS spectra of mouse brain (top, blue) and of mouse liver (bottom, red). The vertical lines on top of each spectrum represent the monoisotopic m/z peaks extracted for identification. The orange markers denote MS/MS identified peaks. The m/z peaks with unique and multiple lipid identifications are highlighted with pink and black markers. As proof-of-concept, the negative mode analysis of MB was subjected to targeted MS/MS experiments using MS1 accurate mass assignments (highlighted with green triangular markers).....	27
Figure 2.4. Extract from the mouse liver mass spectrum in negative mode from m/z 738.2 to 738.8. The black vertical lines represent the monoisotopic m/z peaks extracted for identification. The orange markers denote MS/MS identified peaks. The m/z peaks with unique and multiple lipid identifications are highlighted with pink and black markers.....	28
Figure 2.5. Representations of the identified lipid classes in MB and ML (from both MS/MS and MS1), weighted by the number of unique and distinct lipid identifications for each class. a. and c. represent positive ionization for MB and ML, respectively, and b. and d. represent negative ionization for both samples.....	34
Figure 2.6. Diagram of the lipid compositions (lipid classes) of healthy mouse brain and mouse liver samples identified from LESA-FT-ICR-MS (MS/MS and MS1) measurements, including both positive and negative ionization mode. The circle overlap represents the number of distinct lipids from the different lipid classes which were found in both tissues.....	35
Figure 3.1. Graphical Abstract of Chapter 3.....	45

Figure 3.2. Simplified schematics of the (a) LESA instrument used for ambient pressure lipid extraction from mouse brain and liver slices; (b) liquid chromatography-trapped ion mobility spectrometry using collision induced dissociation CID-TOF MS/MS (Bruker, USA); (c) cyclic traveling wave ion mobility instrument -TOF MS (Waters, UK) and (d) the trapped ion mobility spectrometry -TOF MS (Bruker, USA)49

Figure 3.3. 2D-IMS-MS contour plots from a LESA mouse brain lipid extract using cTWIMS-TOF MS (left) and TIMS-TOF MS (middle) and LC-TIMS-CID TOF MS (right). a., e., and i. represent fast, wide mobility ranges. The green dots in a. highlight ions previously identified using LESA-FT-ICR-MS(/MS)³⁵. The green rectangles highlight the mobility ranges isolated for higher-resolution targeted measurements. b. and c. represent the mobility-selected cTWIMS 3 pass and 5 pass measurements, with d. showing the mass spectrum of the cTWIMS 5 pass measurement. f. and g. showcase the TIMS mobility-selected measurements at higher resolving power with h. showing the mass spectrum of the TIMS Sr 0.3 V/ms measurement. j. and k. showcase the TIMS mobility-selected measurements at specific chromatographic time; 9.9-10.1 min and 29.9-30.1 min, respectively55

Figure 3.4. Typical IMS, IMS-LC and MS/MS profiles from m/z 810.60. a. cTWIMS -CID TOF MS/MS, b. TIMS-CID TOF MS/MS, c. OSA-TIMS-FT-ICR MS, d. TIMS-CID TOF MS/MS of lipid standards, and e. LC-TIMS-CID TOF MS/MS analysis.....58

Figure 3.5. a. Targeted nESI-TIMS-CID-TOF MS/MS and b. LC-TIMS-CID TOF MS/MS of m/z 782.56 from LESA mouse brain and liver lipid extracts. In the bottom, IMS and IMS-LC of lipid standards used for assignment validation60

Figure 3.6. a. Number of annotated lipid species per lipid class based on the extraction solvent and analytical workflow and b. number of annotated lipids per lipid class based on the observed adducts from the different solvents in the direct infusion experiments datasets62

Figure 4.1 Graphical Abstract of Chapter 4.....74

Figure 4.2. Workflow for MCS characterization using TOF-SIMS for chemical mapping and *in situ* LESA-TIMS-MS/MS for drug delivery secondary confirmation and quantitative analysis77

Figure 4.3. Typical HCT 116 MCS. (a) Optical images (4x) of the same MCS growth as a function of the culture time in a 15-day interval (b) Optical images (4x) of different MCS at day 15 prior to treatment and (c) Optical images (4x) of MCS shown in (b) after 24 hours exposure to ABT-737 at different concentrations.....83

Figure 4.4. (a) Optical (4x), total SI and m/z 811.25 (ABT-737 [M-H]⁻) images (left to right) of consecutive control MCS slices. (b) Optical (4x), total SI, endogenous

markers (m/z 159.93 HP_2O_6^- nuclei marker, m/z 255.23 $\text{C}_{18}\text{H}_{33}\text{O}_2^-$, Fatty Acid 16:0[M-H]⁻), and m/z 811.25 (ABT-737 [M-H]⁻) images (left to right) of consecutive slices from a 50 μM ABT-737 treated MCS. The line scan shows the intensity of ABT-737 across each slice of the spheroid.....85

Figure 4.5. (a) Schematic representation of the LESA extraction. (b) typical 2D-IMS-MS plots of from a 100 μM ABT-737 treated MCS, (c) 2D-IMS-MS blowouts of the Angiotensin II IS and ABT-737 signals. (e) ABT-737 typical fragmentation channels (f) mobility selected MS/MS spectra of the ABT-737 [M+H]⁺ signal from a standard and from a treated MCS (g) ABT-737 Calibration curve from LESA-TIMS-MS extracted from the MCS slices as a function of the ABT-737 concentration in the culture media. Error bars represent the standard deviation of the measurements (n=3).....88

Figure 5.1. Workflow for FFPE fixation, slicing and preparation for MSHC analysis...101

Figure 5.2. MALDI-FT ICR images of protonated (green), Schiff base (yellow) and sodiated (red) ions of Arg-Vasopressin species in sections through two different parts of human pituitary biopsy (a. part 1 and b. part 2). c. and d. showcase mass spectra and experimental isotopic patterns for each species in part 1 and part 2, respectively. e. theoretical isotopic patterns for each species103

Figure 5.3. Ion mobility, experimental isotopic pattern and fragmentation pattern of [M+H]⁺ species of Arg-Vasopressin. Red traces showcase comparison to standard..104

Figure 5.4. Ion mobility, experimental isotopic pattern and fragmentation pattern of [M+2H]²⁺ species of Arg-Vasopressin. Red traces showcase comparison to standard.....106

Figure 5.5. Ion mobility, experimental isotopic pattern and fragmentation pattern of [M+2H]²⁺ reduced Arg-Vasopressin species. Red traces showcase comparison to standard.....108

Figure 6.1. Representative features of the LC-TIMS-MS/MS workflow. (a) Merged positive and negative ion datasets into buckets representative of unique molecules observed using various ion forms (b). (c) Typical 2D-IMS-MS contour plots from healthy (HS) and allergy (AS) saliva samples; charge state trend lines are denoted.....119

Figure 6.2. Relative standard deviations of (a) RT and (b) CCS values. (c) mass error ($\Delta m/z$) for the annotated molecules based on the MS/MS confirmation. Data corresponds to n=6.....121

Figure 6.3. (A) Venn diagram showing molecular features in the healthy (HS) and allergy saliva samples (AS), and their relative observation depending on the ion mode.

(B) Distribution of annotated molecules across the mobility, m/z and detected ion mode. (C) Typical identification of unknowns for the case of structural isomers derived from caffeine; while two of them eluted at similar RT, they were all separated by mobility: theobromine (RT 15.81 min, CCS 131.6 Å²), theophylline (RT 15.82 min, CCS 139.8 Å²) and paraxanthine (RT 17.04 min, CCS 134.1 Å²). Theobromine (red, RT 15.81 min, CCS 131.6 Å²). Isotopic pattern of the parent ion and RT-CCS- separated MS/MS spectra are shown126

Figure 6.4. PCA statistical analysis based on the bucketing of the LC-TIMS-MS/MS dataset from the HS and AS sample using analytical triplicates. (a) Explained Variance, (b) Hotelling T² and (c) 3D scores127

ABBREVIATIONS AND ACRONYMS

ACN	Acetonitrile
ABT 737	Chemotherapeutic drug
CCS	Collision Cross-Section
CH ₃ Cl	Chloroform
CID	Collision Induced Dissociation
cTWIMS	Cyclic Travelling Wave Ion Mobility Spectrometry
DDA	Data Dependent Acquisition
DHB	Dihydroxybenzoic acid
ECD	Electron Capture Dissociation
EtOH	Ethanol
eV	Electron volt
FFPE	Formalin-Fixed Paraffin Embedded
FLD	Fluorescence Detector
FT-ICR MS	Fourier Transform Ton Cyclotron Mass Spectrometry
GC	Gas Chromatography
H ₂ O	Water
HCBU	High-Current Bunched mode
HCOOH	Formic Acid
HCT 116	Human Colon Cancer cell line
IC ₅₀	Half Maximal Inhibitory Concentration
ID	Identification

IMS	Ion Mobility Spectrometry
ITO	Indium-Tin Oxide
IPA	Isopropanol
K_0	Reduced mobility
kDA	kilo Dalton
LESA	Liquid Extraction Surface Analysis
LC	Liquid Chromatography
MALDI	Matrix-Assisted Laser Desorption Ionization
MB	Mouse Brain
MCS	Multi-cellular Spheroids
MeOH	Methanol
mL	Milli-liter
ML	Mouse Liver
mm	Milli-meter
MS	Mass Spectrometry
MSHC	Mass Spectrometry Histochemistry
MSI	Mass Spectrometry Imaging
MS/MS	Tandem mass spectrometry
m/z	mass-to-charge ratio
nESI	nano-Electro Spray Ionization
PASEF	Parallel Acquisition Serial Fragmentation
PCA	Principal Component Analysis
ppm	Parts-Per-Million

R	Resolving Power
r	Resolution
RF	Radio Frequency
RT	Retention Time
RPD	Relative Percentage Deviation
SIMS	Secondary Ion Mass Spectrometry
TIMS	Trapped Ion Mobility Spectrometry
TOF	Time-of-Flight
μL	Micro-liter
μm	Micro-meter
UV	Ultra-violet
UVPD	Ultra-Violet Photo Dissociation

CHAPTER 1: Introduction

1.1. Overview

As new challenges arise from the analysis of complex biological samples, there is a need for fast, accurate and cost-effective protocols capable of assessing molecular content, such as proteins, peptides, lipids, and metabolites. Throughout the years, we have seen an increase in biological knowledge, along with a range of methods and instrumentation that have become available to the scientific community. Nevertheless, many scientific problems are still in question, therefore the need to develop, optimize, and apply new methods and protocols for efficient analysis of biological samples. The discovery and validation of biomarkers, metabolic pathways and drug targets is mostly contingent of the sample size.¹ For example, samples from tumor biopsies are limited, making it challenging to obtain enough amounts of analyte to generate high quality data. Also, the detection of these specific analytes for biomarker discovery is a challenge due to the high molecular complexity, diversity and dynamic range¹ in biological samples. My dissertation focuses on the development, optimization, and application of multi-modal methodologies for the characterization of common biological samples: i) biological tissues (*e.g.*, liver, brain, and skin), ii) three-dimensional multicellular spheroid (MCS) models of cancer cell lines, and iii) common bodily fluid (*e. g.*, saliva).

To this day, a series of analytical tools have been used to perform targeted and untargeted analysis from biological samples, such as chromatography, mass spectrometry and nuclear magnetic resonance (NMR).² Analyses are typically performed using mass spectrometry (MS),³⁻⁶ with the use of separation techniques such as liquid chromatography (LC),^{4, 7} and ion mobility (IMS)⁸⁻¹⁰ to assist with characterization.

1. 2 Analytical Techniques for Sample Characterization

1.2.1 Liquid extraction Surface Analysis (LESA)

An emerging tool for the analysis of biological samples at ambient condition is Liquid Extraction Surface Analysis (LESA), which can be easily coupled to any MS instrument. With LESA, an alternative to surface mapping, a liquid micro-junction between the surface and an extraction tip is created, followed by direct nano-electrospray infusion.¹¹ LESA is performed by using a TriVersa Nanomate device (Advion, Ithaca, NY, USA). This device was developed in 2011 in collaboration with Dr. Gary van Berkel from Oak Ridge National Laboratories. In a LESA experiment, the solvent can be selected to extract the chemical class of choice. To perform the extraction, an automated arm relocates on top of the solvent well and aspirates a certain amount of solvent (5-20 μL). The robotic arm relocates on top of the desired spot in the sample and descends to a chosen dispensation height to place a droplet of solvent (0.5 – 2 μL) and form a liquid micro junction between the surface and the solvent. Solvent droplet stays in contact with the surface for a certain amount of time (5-60 s). If decided, the solvent droplet could be re-aspirated and re-dispensed for extra time. After this, the solvent is re-aspirated and directly nano-electrospray infused into the MS or dispensed into a specific well in a 96 well plate for collection.

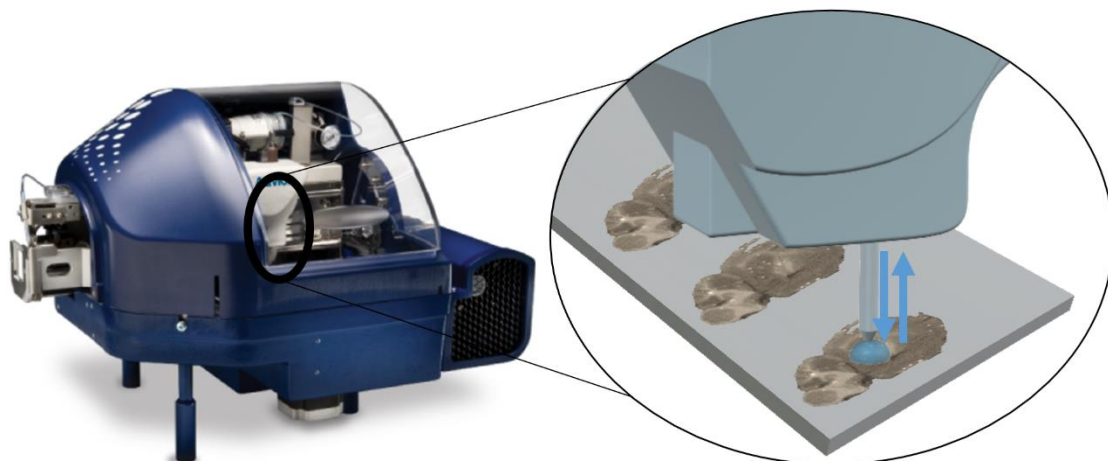


Figure 1.1. Liquid Extraction Surface Analysis (LESA) schematic

When compared to other extraction techniques or imaging experiments, LESA-MS significantly decreases sample preparation, experiment time and potential ionization suppression bias (e. g., MALDI matrix).¹² LESA-MS has shown to be more sensitive and avoids sample carryover due to the single use nature of its tips and nano sprayer.¹³ The pipetting accuracy of the Triversa NanoMate produces high throughput and high sensitivity experiments.

1.2.2 Liquid Chromatography

In chromatography, molecules in a mixture are physically separated by their interactions with a solid (stationary) phase, while moving with the aid of a mobile phase.¹⁴ These interactions can be dependent of molecule size, polarity, or hydrophobicity. In liquid chromatography, samples are injected into a solvent stream (mobile phase) and passed through a column (stationary phase) at a high pressure and flow rate. The separation of analytes depends greatly on the amount of time these molecules are allowed to interact

with the stationary phase. The time each analyte spends interacting with the column is known as the retention time (RT). Proper column selection is crucial for reversed-phase LC, as usually hydrophobic packing material (e.g. C18, C30, biphenyl) are best suited for lipids and peptides separations. At the time the analyte elutes from the column, it will pass through a detector, which can be an ultra-violet (UV) detector, a fluorescence detector (FLD), a mass spectrometer (MS), among others.¹⁵ Analyte separation is very dependent on the solvent gradient, flow rate, pressure, and temperature.

To this end, several technologies are under development in tandem with traditional liquid chromatography-mass spectrometry (LC-MS/MS). The most significant is ion mobility spectrometry (IMS);¹⁶ due to the short analysis time scales, analytical power and ease of coupling with MS platforms, which is thought to be the next generation gold standard for complex biological sample characterization (IMS-MS/MS).¹⁷

1.2.3 Mass Spectrometry

Mass spectrometry based techniques have become the analytical gold standard for identification and characterization of biomarkers in biological samples.¹⁸ The high throughput and short analysis time scales enables to follow biological processes while providing detailed chemical and spatial characterization. One of the current challenges in biological MS, is the high molecular complexity, diversity, and dynamic range.¹⁸ Many of the recent targeted and discovery workflows take advantage of complementary separations based on gas or liquid chromatography (GC, LC),¹⁹⁻²² ion mobility (IMS),²³⁻²⁵ and mass spectrometry (MS and MS/MS).^{22, 26-29} Several workflows for targeted and untargeted characterization of biomolecules from complex biological matrices (*e.g.*, urine,^{30, 31}

blood,^{32, 33} and tissue extracts^{12, 34, 35}) in tandem with high resolution (TOF-MS/MS)^{36, 37} and ultrahigh resolution (FT-ICR MS/MS)^{12, 38, 39} mass spectrometry have been developed. With the advent of commercial, high resolution IMS-MS platforms, several groups have shown the advantages of LC-IMS-MS/MS for the analysis of small molecules,^{23-25, 40} lipids,^{41, 42} and peptides.⁴³⁻⁴⁵ In particular, high resolution trapped IMS (TIMS, R up to 400) using custom-built instruments for the analysis of samples with high isomeric content (*e.g.*, small molecules,⁴⁶⁻⁴⁸ peptides,^{49, 50} lipids,⁵¹ and DNA fragments^{52, 53}) have been shown.

1.2.3.1 Mass Spectrometry Imaging (MSI)

Mass spectrometry imaging (MSI) allows for surface sampling and mapping without the need of knowing a preliminary targeted molecule, which is an important advantage when analyzing biological samples.⁵⁴ MSI is a label free technique that can provide information for the understanding of biological processes with high spatial resolution from sub-cellular to multicellular levels. MSI is a four-step process that involves the sample preparation, desorption and ionization, mass analysis and image registration.⁵⁵ Most widely used techniques are Matrix Assisted Laser Desorption Ionization (MALDI) and Secondary Ion Mass Spectrometer) coupled to a Time of Flight (ToF) spectrometer (TOF-SIMS).

1.2.3.1.1 Secondary Ion Mass Spectrometry (SIMS)

SIMS spectrometry is based on the emission of highly energetic primary ions from an ion gun in the direction of the sample. These primary ions will collide with surface molecules and provide energy by momentum transfer or charge transfer allowing atoms to get ejected from the surface. Some of these atoms are ionized (usually less than 1%) and

are referred to as secondary ions, which will be directed into the Time-of-Flight Mass Spectrometer for mass to charge ratio analysis. A full mass spectrum is acquired at each pixel point and by selecting a mass spectral signal of a particular ion, resolved images can be produced.⁵⁶ The high spatial resolution and sensitivity of the TOF-SIMS is able to achieve a lateral resolution in the micrometer to nanometers range depending on the desorption probe.

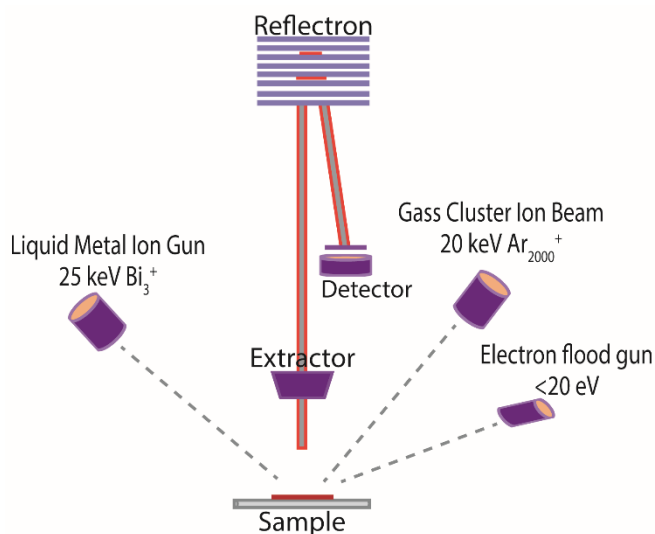


Figure 1.2. Simplified schematic of a dual beam IonTOF5 instrument.

1.2.3.1.2 Matrix Assisted Laser Desorption Ionization (MALDI)⁵⁷

MALDI spectrometry is based on the emission of a UV laser beam onto the surface of a sample. Prior to analysis, the sample will be mixed (in case of liquid sample) or coated (in case of solid sample) with a matrix, which absorbs the UV light and converts it to heat energy. The matrix heats rapidly and desorbs from the surface. In the process, the matrix and sample molecules vaporize to form ions which are accelerated into the mass spectrometer. Common MALDI sources provide spatial resolution of 20-25 μm and mass

range up to 100kDa. MALDI can also be used as a soft ionization source and is commonly coupled to a TOF or FT-ICR MS.

1.2.3.2 Fourier Transformed Ion Cyclotron Resonance (FT-ICR)⁵⁸

The highest mass resolution obtained to date has been with the use of a Fourier Transformed Ion Cyclotron Resonance mass spectrometer (FT-ICR MS). FTICR MS technique is based on the determination of the ion cyclotron frequencies of ions trapped in a Penning trap. The mass to charge ratio of the ions is determined from this frequency in first approximation by the equation:

$$\omega_c = \frac{qB}{m}$$

where ω_c is the reduced cyclotron frequency, q is the charge of the ion, B is the magnetic field, and m is the molecular weight of the ion.⁵⁸ In FTICR MS experiments, ions can be generated directly inside the ICR cell (ion trap) or by an ionization source (*e.g.*, nESI) and transported to the ICR cell. The ICR cell generally consists of two trap electrodes, two excitation electrodes and two detection electrodes. The cell electrodes define a parabolic trapping potential that confines the ions axially or radially by the magnetic field in which the ICR cell is positioned. After ions have been trapped and stored for a variable time, the ion cyclotron motion is excited by the application of a radio frequency (RF) excitation pulse on the excitation electrodes. As a result of this time-varying electric field the ions experience a net outward force which causes the ions to increase their cyclotron radius. The orbiting ions induce a corresponding image charge in the detection electrodes. The ICR signal is measured by digitizing the voltage difference between the two detection

electrodes as a function of time. This signal is often referred to as the ICR transient. Fourier transformation of the time- domain transient results in the cyclotron frequency spectra, which can subsequently be converted into mass spectra. FTICR MS delivers a unique combination of high mass spectral resolution and tandem mass spectrometric capabilities, allowing mass spectral separation of different species from complex systems.⁵⁸

1.2.3.3 Ion Mobility Spectrometry

Ion mobility spectrometry – mass spectrometry (IMS-MS) has multiple applications such as the detection of explosives,⁵⁹ illicit drugs,⁶⁰ petroleum,⁶¹ natural products,⁶² and many others. The separation between ions in these devices is based on differences in their ion mobilities under the influence of an electric field.⁶³ Since IMS-MS has proven to be very valuable, many designs have been developed.

1.2.3.3.1 Trapped Ion Mobility Spectrometry

In the recent years, Trapped Ion Mobility Spectrometry (TIMS) has been utilized for a variety of analytical applications like small molecules,⁴⁶⁻⁴⁸ proteomics,^{49, 50} lipidomic,⁵¹ DNA,^{52, 53} and many others. The ion mobility separation is determined by:

$$K_0 = \frac{V_g}{E} = \frac{A}{V_{elution} - V_{out}}$$

where K_0 is the reduced mobility, v_g is the gas flow velocity, $V_{elution}$ is the elution voltage and V_{out} is the base voltage.⁶⁴ The separation is carried out using Nitrogen (N_2) at room

temperature (T) with a gas flow velocity determined by the difference between the funnel entrance pressure (P1 = 2.6 mbar) and the funnel exit pressure (P2 = 1.1 mbar). Collision cross section (CCS, Ω) are determined by the Mason-Schamp equation:

$$\Omega = \frac{(18\pi)^{1/2}}{16} \frac{z}{(k_B T)^{1/2}} \left[\frac{1}{m_i} + \frac{1}{m_b} \right]^{1/2} \frac{1}{K_0} \frac{1}{N^*}$$

where z is the ion charge, k_B is the Boltzmann constant, N^* is the number density, and m_i and m_b are the masses of the ion and bath gas, respectively.^{64, 65} In a TIMS cell compared to other ion mobility instruments, ions are pushed forward by a bath gas while an electric field of increasing strength is being applied across the length of the cell. The electric field is reduced to allow ions to elute from largest to smallest. The rate at which the electric field is reduced can be controlled in a way that ions are “trapped” inside the cell for a specific amount of time. The pre-separation ability in the gas phase of TIMS is an emerging technique for the study of isomers, lipidomics, proteomics, and many others. This technology can be coupled to different mass spectrometers to allow high mass resolution.

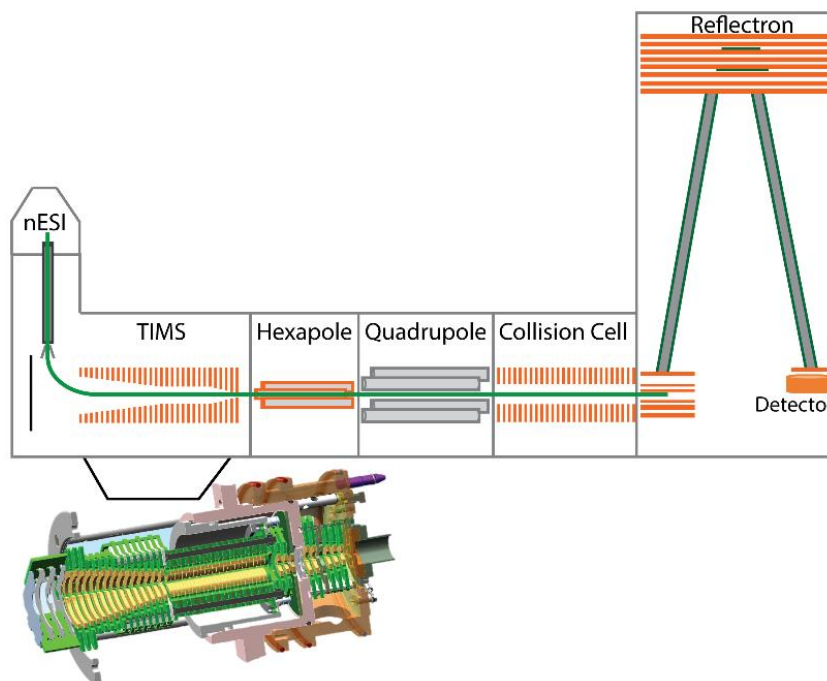


Figure 1.3. TIMS-TOF instrument schematic

1.2.2.3.2 Cyclic Travelling Wave Ion Mobility Spectrometry (cTWIMS)

The cTWIMS-TOF MS is based on a Synapt G2-Si instrument, where ions are guided from the source towards the quadrupole mass filter using a set of offset ion guides (StepWave). Following the quadrupole mass filter, the ions enter the trap cell where ion packets are formed for subsequent ion mobility separation. The ion packets are then transported into the helium cell and the pre-store ion guide operated in nitrogen. Following the pre-store ion guide, a multi-function array of electrodes constitutes the entry point of the 98-cm long, orthogonally-mounted cyclic ion mobility cell. In TWIMS, voltage pulses sweep the ion mobility cell electrodes, propelling the ions through a buffer gas, typically nitrogen. The ions are overtaken by the waves more or less often, depending on their mobility. Lower mobility ions take longer to travel through the IM cell than higher mobility ions, which

creates the time-dispersive (*i.e.*, arrival time) ion mobility separation.⁶⁶⁻⁶⁸ The mobility resolving power increases as \sqrt{n} , where n is the number of passes around the device. After the single- or multi-pass ion mobility separation, the array electrodes allow the ions to exit the cyclic IM cell towards the post-store ion guide and on to the ToF MS analyzer. The array operation allows isolation of the desired mobility range inside the cyclic IM (a mode employed in this work) as well as ejection of mobility-selected ions into the pre-/post-array stores. The selected ions can be then subjected to collision-induced dissociation (CID) (upon ejection or re-injection) followed by IM separation (IM^n).^{66, 69}

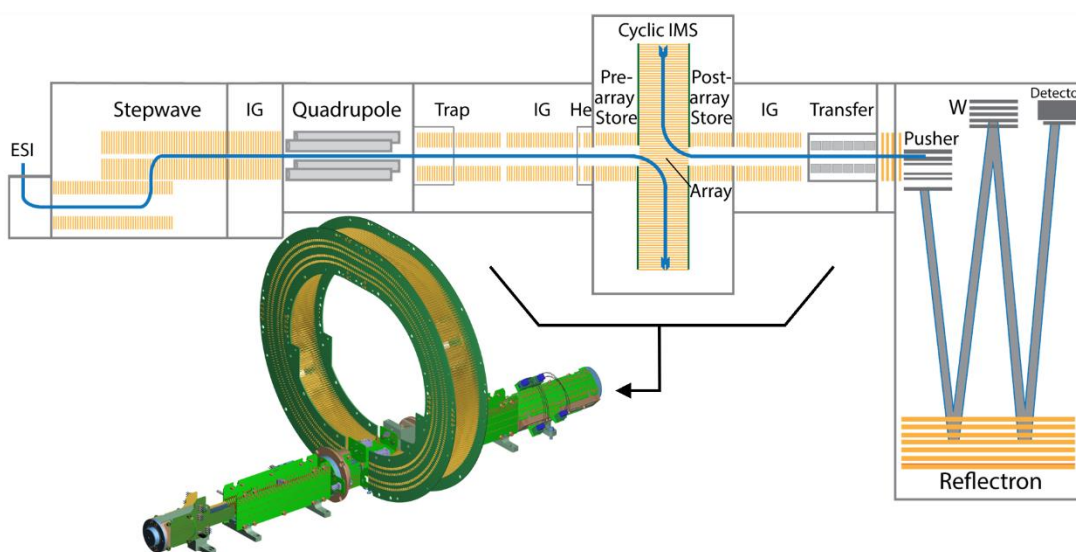


Figure 1.4. cTWMS-TOF instrument schematic

1.2.3.4 Collision Induced Dissociation (CID) Fragmentation

Tandem mass spectrometry (MS/MS) are a series of fragmentation techniques that provide detailed information for structural characterization of molecules. CID is a soft ionization technique where a buffer gas collides with a kinetically excited precursor

molecule. This collision imparts enough internal energy that causes bond breakage and produces fragment ions. The fragmentation spectra of an ion allows to determine the structure of both the precursor and fragments ions and also provides information of the relative energy of the precursor ion bonds. CID is the most common type of fragmentation technique reported in databases due to its availability in most mass spectrometry instruments.^{70, 71}

1.3 Objectives of the Dissertation

This dissertation is focused on the development, optimization and application of multi-modal analytical workflows for the characterization of small molecules (*e.g.*, lipids, peptides, drugs, and metabolites) in biological samples. Sample preparation was optimized to achieve the desired sensitivity, specificity, and accuracy for the identification of small molecules in complex biological matrices.

The following Chapters are arranged based on the analytical techniques utilized; LESA-FT-ICR, LESA-TIMS-TOF, LESA-cTWIMS-TOF, TOF-SIMS, MALDI-FT-ICR and LC-TIMS-TOF. As the Chapters progress, the introduction of multiple techniques is needed to study complex biological matrices and solve the question in hand. Chapter 2, published in *Analytical Methods*, is focused on the development of a workflow for fast lipid screening using LESA as an extraction solvent and a high-resolution mass spectrometer (*e.g.* FT-ICR) for accurate identification. Chapter 3, under review at *Talanta*, focuses on the advantages of LESA as an extraction technique and the need for high resolution pre-separation mobility measurements for the analysis of lipid isomers and isobars in complex mixtures. Chapter 4, published in *Analyst*, showcases high spatial

resolution imaging of three-dimensional cell spheroids treated with a chemotherapeutic drug agent. This Chapter combines the use of mass spectrometry imaging with LESA-TIMS-TOF for the unequivocal identification of a drug target in tissue. Chapter 5, under review in *JASMS*, combined high spatial resolution MALDI-FT ICR imaging with LESA-TIMS-TOF MS/MS to enable the characterization of neuropeptides in FFPE human pituitary tissue. Lastly, Chapter 6 involves the development of a workflow (from sample preparation to analysis) for discovery and targeted analysis of saliva using LC-TIMS-TOF MS/MS and will be submitted for a second round of reviews.

1.4 References

1. P. Feist and A. B. Hummon, *Int J Mol Sci*, 2015, **16**, 3537-3563.
2. B. S. B. Correia, R. S. Torrinhas, W. Y. Ohashi and L. Tasic, *Intech Open*, 2018, 1-20.
3. K. Yang and X. Han, *Trends Biochem Sci*, 2016, **41**, 954-969.
4. C. Giles, R. Takechi, V. Lam, S. S. Dhaliwal and J. C. L. Mamo, *Prog Lipid Res*, 2018, **71**, 86-100.
5. G. Dawson, *Biochim Biophys Acta*, 2015, **1851**, 1026-1039.
6. H. C. Lee and T. Yokomizo, *Biochem Biophys Res Commun*, 2018, **504**, 576-581.
7. A. Baglai, A. F. G. Gargano, J. Jordens, Y. Mengerink, M. Honing, S. van der Wal and P. J. Schoenmakers, *J Chromatogr A*, 2017, **1530**, 90-103.
8. C. Hinz, S. Liggi and J. L. Griffin, *Curr Opin Chem Biol*, 2018, **42**, 42-50.
9. J. C. May, C. R. Goodwin and J. A. McLean, *Curr Opin Biotechnol*, 2015, **31**, 117-121.
10. W. B. Ridenour, M. Kliman, J. A. McLean and R. M. Caprioli, *Anal Chem*, 2010, **82**, 1881-1889.
11. V. Kertesz and G. J. Van Berkel, *J Mass Spectrom*, 2010, **45**, 252-260.

12. J. R. N. Haler, E. K. Sisley, Y. L. Cintron-Diaz, S. N. Meitei, H. J. Cooper and F. Fernandez-Lima, *Anal Methods*, 2019, **11**, 2385-2395.
13. W. Rao, A. D. Celiz, D. J. Scurr, M. R. Alexander and D. A. Barrett, *J Am Soc Mass Spectrom*, 2013, **24**, 1927-1936.
14. M. E. LaCourse and W. R. LaCourse, in *Liquid Chromatography: Fundamentals and Instrumentation*, Elsevier, 2 edn., 2017, ch. 17, pp. 417-429.
15. W. M. N. Niessen, in *Chromatographic Sciences series*, Taylor and Francis, 3 edn., 2006, vol. 97, pp. 3-21.
16. K. Jeanne Dit Fouque and F. Fernandez-Lima, *Trends Analyt Chem*, 2019, **116**, 308-315.
17. X. Garcia, M. Sabaté, J. Aubets, J. Jansat and S. Sentellas, *Separations*, 2021, **8**, 33.
18. K. Chandramouli and P. Y. Qian, *Hum Genomics Proteomics*, 2009, **2009**, 1-22.
19. D. C. Mueller, M. Piller, R. Niessner, M. Scherer and G. Scherer, *J Proteome Res*, 2014, **13**, 1602-1613.
20. M. Ciborowski, A. Lipska, J. Godzien, A. Ferrarini, J. Korsak, P. Radziwon, M. Tomasiak and C. Barbas, *J Proteome Res*, 2012, **11**, 6231-6241.
21. O. C. Zeki, C. C. Eylem, T. Recber, S. Kir and E. Nemitlu, *J Pharm Biomed Anal*, 2020, **190**, 113509.
22. Y. Gao, Y. Chen, X. Yue, J. He, R. Zhang, J. Xu, Z. Zhou, Z. Wang, R. Zhang and Z. Abliz, *Anal Chim Acta*, 2018, **1037**, 369-379.
23. J. C. May, R. L. Gant-Branum and J. A. McLean, *Curr Opin Biotechnol*, 2016, **39**, 192-197.
24. M. Hernandez-Mesa, F. Monteau, B. Le Bizec and G. Dervilly-Pinel, *Anal Chim Acta*, 2019, **1**, 100006.
25. D. E. Davis, Jr., S. D. Sherrod, R. L. Gant-Branum, J. M. Colby and J. A. McLean, *Anal Chem*, 2020, **92**, 14648-14656.
26. K. Bingol, *High Throughput*, 2018, **7**, 1-11.

27. L. Lacalle-Bergeron, D. Izquierdo-Sandoval, J. V. Sancho, F. J. López, F. Hernández and T. Portolés, *Trends Analyt Chem*, 2021, **135**, 116161.
28. M. Vinaixa, E. L. Schymanski, S. Neumann, M. Navarro, R. M. Salek and O. Yanes, *Trends Analyt Chem*, 2016, **78**, 23-35.
29. J. F. Xiao, B. Zhou and H. W. Ransom, *Trends Analyt Chem*, 2012, **32**, 1-14.
30. H. Zhao, Y. Liu, Z. Li, Y. Song, X. Cai, Y. Liu, T. Zhang, L. Yang, L. Li, S. Gao, Y. Li and C. Yu, *Clin Chim Acta*, 2018, **486**, 192-198.
31. M. Huang, H. Zhao, S. Gao, Y. Liu, Y. Liu, T. Zhang, X. Cai, Z. Li, L. Li, Y. Li and C. Yu, *Clin Chim Acta*, 2019, **497**, 95-103.
32. J. R. Denery, A. A. Nunes and T. J. Dickerson, *Anal Chem*, 2011, **83**, 1040-1047.
33. M. H. Sarafian, M. Gaudin, M. R. Lewis, F. P. Martin, E. Holmes, J. K. Nicholson and M. E. Dumas, *Anal Chem*, 2014, **86**, 5766-5774.
34. V. A. Mikhailov, R. L. Griffiths and H. J. Cooper, *Int J Mass Spectrom*, 2017, **420**, 43-50.
35. E. K. Sisley, E. Illes-Toth and H. J. Cooper, *Trends Analyt Chem*, 2020, **124**, 115534.
36. M. Paul, J. Ippisch, C. Herrmann, S. Guber and W. Schultis, *Anal Bioanal Chem*, 2014, **406**, 4425-4441.
37. X. Qu, H. Gao, J. Sun, L. Tao, Y. Zhang, J. Zhai, Y. Song, T. Hu and Z. Li, *Toxicology*, 2020, **431**, 152366.
38. P. Benigni, C. J. Thompson, M. E. Ridgeway, M. A. Park and F. Fernandez-Lima, *Anal Chem*, 2015, **87**, 4321-4325.
39. E. R. Schenk, F. Nau, C. J. Thompson, Y. C. Tse-Dinh and F. Fernandez-Lima, *J Mass Spectrom*, 2015, **50**, 88-94.
40. C. Laphorn, F. Pullen and B. Z. Chowdhry, *Mass Spectrom Rev*, 2013, **32**, 43-71.
41. J. E. Kyle, X. Zhang, K. K. Weitz, M. E. Monroe, Y. M. Ibrahim, R. J. Moore, J. Cha, X. Sun, E. S. Lovelace, J. Wagoner, S. J. Polyak, T. O. Metz, S. K. Dey, R. D. Smith, K. E. Burnum-Johnson and E. S. Baker, *Analyst*, 2016, **141**, 1649-1659.

42. X. Zheng, R. D. Smith and E. S. Baker, *Curr Opin Chem Biol*, 2018, **42**, 111-118.
43. P. Venter, M. Muller, J. Vestner, M. A. Stander, A. G. J. Tredoux, H. Pasch and A. de Villiers, *Anal Chem*, 2018, **90**, 11643-11650.
44. E. S. Baker, K. E. Burnum-Johnson, Y. M. Ibrahim, D. J. Orton, M. E. Monroe, R. T. Kelly, R. J. Moore, X. Zhang, R. Theberge, C. E. Costello and R. D. Smith, *Proteomics*, 2015, **15**, 2766-2776.
45. A. Sidorina, G. Catesini, S. Levi Mortera, V. Marzano, L. Putignani, S. Boenzi, R. Taurisano, M. Garibaldi, F. Deodato and C. Dionisi-Vici, *J Inherit Metab Dis*, 2020, DOI: 10.1002/jimd.12344, 1-13.
46. A. McKenzie-Coe, J. D. DeBord, M. Ridgeway, M. Park, G. Eiceman and F. Fernandez-Lima, *Analyst*, 2015, **140**, 5692-5699.
47. P. Benigni, R. Marin and F. Fernandez-Lima, *Int J Ion Mobil Spectrom*, 2015, **18**, 151-157.
48. K. J. Adams, C. E. Ramirez, N. F. Smith, A. C. Munoz-Munoz, L. Andrade and F. Fernandez-Lima, *Talanta*, 2018, **183**, 177-183.
49. A. Garabedian, M. A. Baird, J. Porter, K. Jeanne Dit Fouque, P. V. Shliaha, O. N. Jensen, T. D. Williams, F. Fernandez-Lima and A. A. Shvartsburg, *Anal Chem*, 2018, **90**, 2918-2925.
50. F. Meier, A. D. Brunner, S. Koch, H. Koch, M. Lubeck, M. Krause, N. Goedecke, J. Decker, T. Kosinski, M. A. Park, N. Bache, O. Hoerning, J. Cox, O. Rather and M. Mann, *Mol Cell Proteomics*, 2018, **17**, 2534-2545.
51. K. Jeanne Dit Fouque, C. E. Ramirez, R. L. Lewis, J. P. Koelmel, T. J. Garrett, R. A. Yost and F. Fernandez-Lima, *Anal Chem*, 2019, **91**, 5021-5027.
52. A. Garabedian, D. Butcher, J. L. Lippens, J. Miksovska, P. P. Chapagain, D. Fabris, M. E. Ridgeway, M. A. Park and F. Fernandez-Lima, *Phys Chem Chem Phys*, 2016, **18**, 26691-26702.
53. D. Butcher, P. Chapagain, F. Leng and F. Fernandez-Lima, *J Phys Chem B*, 2018, **122**, 6855-6861.
54. A. Brunelle, D. Touboul and O. Laprevote, *J Mass Spectrom*, 2005, **40**, 985-999.
55. K. Chughtai and R. M. Heeren, *Chem Rev*, 2010, **110**, 3237-3277.

56. S. A. Schwarz, *Mater. Sci. Technol.*, 2001, **2**, 8624-8629.
57. M. Karas and R. Kruger, *Chem Rev*, 2003, **103**, 427-440.
58. E. N. Nikolaev, Y. I. Kostyukevich and G. Vladimirov, in *Fundamentals and Applications of Fourier Transform Mass Spectrometry*, Elsevier, 2019, ch. 4, pp. 89-111.
59. R. D. McCulloch and M. Amo-Gonzalez, *Rapid Commun Mass Spectrom*, 2019, **33**, 1455-1463.
60. H. Chen, C. Chen, W. Huang, M. Li, Y. Xiao, D. Jiang and H. Li, *Anal Chem*, 2019, **91**, 9138-9146.
61. J. Le Maitre, M. Hubert-Roux, B. Paupy, S. Marceau, C. P. Ruger, C. Afonso and P. Giusti, *Faraday Discuss*, 2019, **218**, 417-430.
62. E. A. Rue, J. A. Glinski, V. B. Glinski and R. B. van Breemen, *J Mass Spectrom*, 2019, DOI: 10.1002/jms.4377, 1-5.
63. H. Borsdorf and G. A. Eiceman, *Appl. Spectrosc. Rev.*, 2006, **41**, 323-375.
64. H. E. Revercomb and E. A. Mason, *Anal Chem*, 1975, **47**, 970-983.
65. E. A. Mason and E. W. McDaniel, *Transport Properties of Ions in Gases*, Wiley-Intersciences, 1988.
66. K. Giles, J. Ujma, J. Wildgoose, S. Pringle, K. Richardson, D. Langridge and M. Green, *Anal Chem*, 2019, **91**, 8564-8573.
67. J. R. N. Haler, P. Massonnet, J. Far, V. R. de la Rosa, P. Lecomte, R. Hoogenboom, C. Jerome and E. De Pauw, *J Am Soc Mass Spectrom*, 2019, **30**, 563-572.
68. A. A. Shvartsburg and R. D. Smith, *Anal Chem*, 2008, **80**, 9689-9699.
69. J. Ujma, D. Ropartz, K. Giles, K. Richardson, D. Langridge, J. Wildgoose, M. Green and S. Pringle, *J Am Soc Mass Spectrom*, 2019, **30**, 1028-1037.
70. A. R. Johnson and E. E. Carlson, *Anal Chem*, 2015, **87**, 10668-10678.
71. J. Y. Yang, L. M. Sanchez, C. M. Rath, X. Liu, P. D. Boudreau, N. Bruns, E. Glukhov, A. Wodtke, R. de Felicio, A. Fenner, W. R. Wong, R. G. Linington, L. Zhang, H. M. Debonsi, W. H. Gerwick and P. C. Dorrestein, *J Nat Prod*, 2013, **76**, 1686-1699.

CHAPTER 2. Fast Lipid Tissue Screening using LESA-FT-ICR-MS

Jean R. N. Haler, Emma K. Sisley, Yarixa Cintron-Diaz, Sanjib N. Meitei, Helen J. Cooper, and Francisco Fernandez-Lima

This chapter was published in *Analytical Methods* and reproduced with permission 2019, 11, 2385. DOI: 10.1039/c8ay02739k

2.1 Abstract

Lipid screening of biological substrates is an important component during biomarker detection and identification. In this work, a fast workflow is described capable of rapid screening for lipid components from biological tissues at ambient pressure based on liquid microjunction extraction in tandem with nano-electrospray ionization (nESI) with ultra-high resolution mass spectrometry, i.e., liquid extraction surface analysis (LESA) coupled to Fourier-transform ion cyclotron resonance (tandem) mass spectrometry (LESA-FT-ICR-MS/MS). Lipid profiles are presented for thin tissue sections of mouse brain (MB) and liver (ML) sample, analyzed in both positive and negative mode by data-dependent acquisition (DDA) tandem FT-ICR-MS/MS. Candidate assignments were based on fragmentation patterns using mostly SimLipid software and accurate mass using mostly the LipidMaps database (average sub-ppm mass error). A typical, single point surface analysis (< 1 mm spatial sampling resolution) lasted less than 15 minutes and resulted in the assignment of (unique and multiple) lipid identifications of ~190 (MB) and ~630 (ML) m/z values. Despite the biological complexity, this led to unique identifications of distinct lipid molecules (sub-ppm mass error) from 36 different lipid classes, corresponding to 25-30% of the lipid m/z identifications.

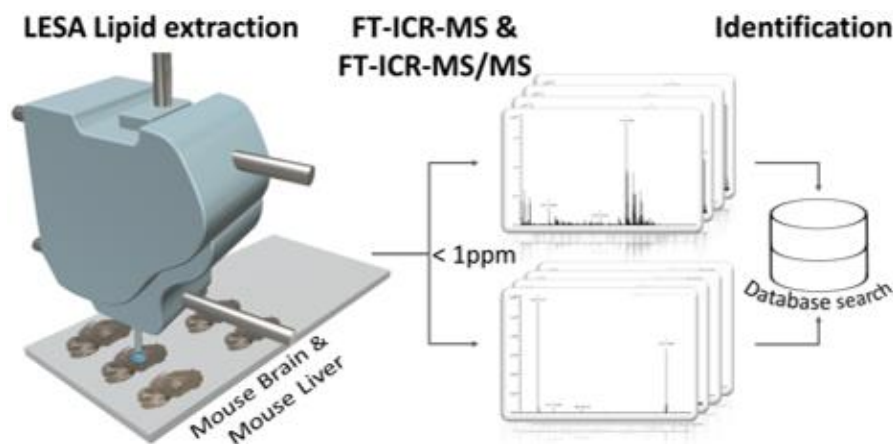


Figure 2.1. Graphical Abstract of Chapter 2

2.2 Introduction

Lipids are important components of living cells and frequently mediate biological processes.¹ Changes to a cell's environment are rapidly translated into changes in its lipid composition, making it an attractive target for biomarker discovery and disease screening and treatment.¹⁻³ Lipid analyses are typically performed using mass spectrometry (MS).^{1,3-8} The challenges for global mass spectrometry analyses of lipids (lipidomics) are twofold. First, the sample preparation can bias the lipid composition by selecting only a partial lipid content of the sample.^{4,5} Second, the mass spectrometry analysis must be capable of detecting both low and high abundance species, with a high resolving power and mass accuracy in order to resolve and confidently identify isobaric lipids. The latter challenge can be addressed by using instruments such as Fourier-transform ion cyclotron resonance mass spectrometers (FT-ICR MS). The choice of the sample preparation however depends on the ionization method used for the mass spectrometry analysis. For tissue analyses, imaging techniques such as secondary ion mass spectrometry (SIMS) or matrix assisted laser desorption ionization (MALDI) mass spectrometry are often used.⁹⁻¹⁷ Ionization

suppression and the matrix choice potentially bias the observed lipid composition.^{5,10,17,18} When using electrospray ionization (ESI), the MS analyses are usually preceded by liquid chromatography (LC) separations with long separation gradients (up to 2 hours) depending on the LC column, the LC solvent conditions, and the numbers of lipid classes.¹⁹ LC-LC couplings have shown some advantages in lipid separations, with the tradeoff of increased analysis times.^{5,20}

An alternative to lipid extraction (e.g., LC-MS/MS) or surface mapping (i.e., desorption electrospray ionization (DESI)^{21–24} or MALDI), is liquid extraction surface analysis (LESA) in which a liquid microjunction between the surface and an extraction tip is created, followed by direct nano-electrospray infusion.^{25–27} In a LESA experiment, the solvent (or solvent mixtures) of choice can direct the type of chemical class that is extracted (e.g., lipids or proteins).^{28,29,38,30–37} When compared to an LC-MS/MS or a MALDI-MS/MS experiment, LESA-MS/MS significantly decreases the sample preparation time and potential ionization suppression bias (e.g., MALDI matrix).

Here, we developed a fast, lipid tissue screening workflow based on LESA-FT-ICR-MS and MS/MS for ambient analysis of thin tissue sections. Examples shown include mouse brain and mouse liver analyzed using data dependent acquisition (DDA) with ultra-high mass resolution and high mass accuracy in positive and negative ion mode. Candidate lipid assignments were performed using different databases, based on MS/MS precursor m/z and fragmentation patterns, as well as on MS accurate mass measurements (< 3 ppm mass accuracy database searches).

2.3 Materials and Methods

2.3.1 Thin Tissue Sections

Liver and brain from wildtype mice (extraneous tissue from culled animals) were the gift of Prof. Steve Watson (University of Birmingham). Organs were frozen on dry ice prior to storage at -80 °C. Sections of murine liver tissue and brain tissue of area $\sim 1.5 \text{ cm}^2$ were obtained at a thickness of 10 μm using a CM1850 Cryostat (Leica Microsystems, Wetzlar, Germany) and thaw mounted onto glass slides.

2.3.2 LESA-MS/MS Analysis

Thin tissue section samples were loaded onto a universal LESA adapter plate and placed in the TriVersa Nanomate chip-based electrospray device (Advion, Ithaca, NY) coupled to a 7T Solarix XR FT-ICR MS (Bruker Daltonics, Germany). The solvent was EtOH/H₂O/HCOOH 80/19.9/0.1 (v/v/v). A total of 6 μL were aspirated from the solvent well. The robotic arm relocated to a position above the tissue and descended to a height 0.2 mm above the surface of the sample. A total of 3 μL of the solution was dispensed onto the sample surface to form a liquid microjunction. The liquid microjunction was maintained for 5 seconds; then 3.5 μL were reaspirated into the pipet tip. This liquid dispensing and reaspiration was repeated twice before MS injection.

The FT-ICR MS instrument was operated in both negative and positive ionization mode and data were collected for 15 minutes. Data dependent acquisition of MS/MS spectra was performed using the AutoMS/MS function and spectra were recorded with 500kW. Collision induced dissociation (CID) was utilized as a fragmentation tool

(typically 15-35 eV), with nominal mass quadrupole isolation prior to injection into the CID cell. Spectra were externally calibrated using a Tuning Mix solution (Agilent, SC)³⁹ and internally calibrated using single point correction with identified lipids. For example, the internal recalibration was performed using PC(34:1) ($m/z = 760.5856$) for MB and using PC(34:2) ($m/z = 758.5694$) for ML in positive mode and PC(34:1) ($m/z = 804.5760$) for MB and using PC(34:2) ($m/z = 802.5604$) for ML in negative mode. Data was analyzed using DataAnalysis 5.2 (Bruker Daltonics, Germany) and SimLipid software (Premier Biosoft, US). Assignments were manually curated using Alex123⁴⁰ and the LIPID MAPS Lipidomics Gateway^{41,42}. MS1 exact mass identifications were performed using the LIPID MAPS Lipidomics Gateway^{41,42} with a ± 3 ppm mass error search criterion. During lipid candidate assignments, protonated species (with and without the loss of H₂O according to the lipid class), sodium and potassium cation adduct species were considered for positive mode; deprotonated species, chloride and formate anion adduct species were considered for negative mode analysis. MS1 exact mass measurements were recorded with 4MW and 2MW for positive and negative modes, respectively. The mass resolution was around 170,000 at m/z 760.5856 and 758.5694 for positive mode MB and ML, respectively and around 60,000 at m/z 804.5760 and 802.5604 for negative mode MB and ML, respectively. For data completeness, targeted MS/MS after preliminary MS1 lipid assignment was performed on species where only little interfering m/z peaks were found in the spectra, using an Impact Q-ToF instrument (Bruker Daltonics Inc., Billerica, MA).

2.4 Results and Discussion

The fast lipid screening workflow is based on LESA of thin tissue sections (without any other surface treatment) followed by ultra-high-resolution MS/MS analysis (see Figure 2.2). The full-scan MS1 analyses and DDA MS/MS take advantage of the ultra-high mass resolution and high mass accuracy of the FT-ICR mass spectrometers. For example, during DDA using CID as a fragmentation method, typical neutral losses and lipid headgroups were utilized during candidate assignment with high mass accuracy. While not the focus of this paper, it should be noted that other MS/MS fragmentation techniques (e.g., EID, OzID, CTD)⁴³⁻⁴⁷ may be easily implemented and provide better and/or complementary structural information during lipid candidate assignment. In the proposed workflow, an initial search provides candidate lipids from the DDA dataset. Following DDA interpretation, the MS1 spectrum is processed (i.e., internal single point correction) and a list of monoisotopic m/z signals is created. This list is used to search among lipid databases using mass accuracy as a criterion. In many cases, the accurate mass database search will return multiple lipid hits, which will require secondary analysis (e.g., targeted MS/MS experiments). While not currently implemented, online processing of the MS1 scan using accurate mass lipid database searches can be performed to retrofit the DDA acquisition target list; this procedure can be easily implemented during static nESI since no major changes in the spray occur during 15 minutes, and each MS/MS acquisition requires typically 10-20 seconds.

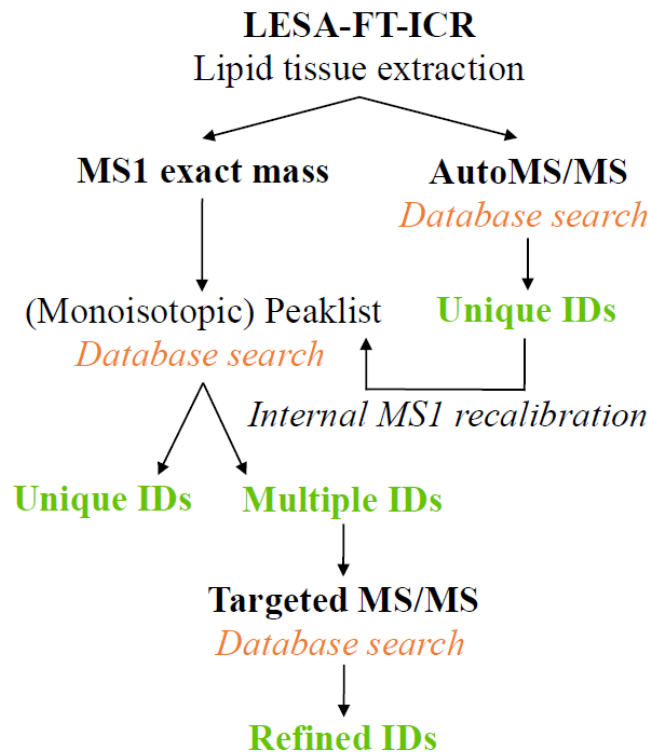


Figure 2.2. LESA-FT-ICR workflow developed for Chapter 2

The LESA-FT-ICR-MS (MS1 and MS/MS) analysis of two biological substrates (i.e., mouse brain, MB, and mouse liver, ML) resulted in the unique identification (within a ± 3 ppm database search for MS1) of distinct lipids from 36 different lipid classes in the 400-1000 m/z range. The unsupervised analysis resulted in the identification of ~190 (MB) and ~630 (ML) monoisotopic m/z peaks as lipids. Despite the biological complexity, 25-30% of these lipid identifications yielded unique lipid assignments (in contrast to multiple lipid assignments to one m/z peak; see Figure 2.3). The comparison of the MB and ML MS1 profiles (either positive or negative ionization mode) shows abundant lipid signal in the 700-900 m/z range. Overall, a larger number of monoisotopic m/z peaks were observed and picked in the ML sample when compared to the MB sample (e.g., 226

(MS⁺)/2215(MS⁻) for ML and 157(MS⁺)/174(MS⁻) for MB (see Appendix 1 for an extract of the negative mode spectra)). Figure 2.4 highlights the importance of performing these analyses using ultra-high-resolution mass spectrometers such as FT-ICR. Between m/z 738.2 and 738.8, 5 out of the 6 m/z values were correlated to lipid identifications.

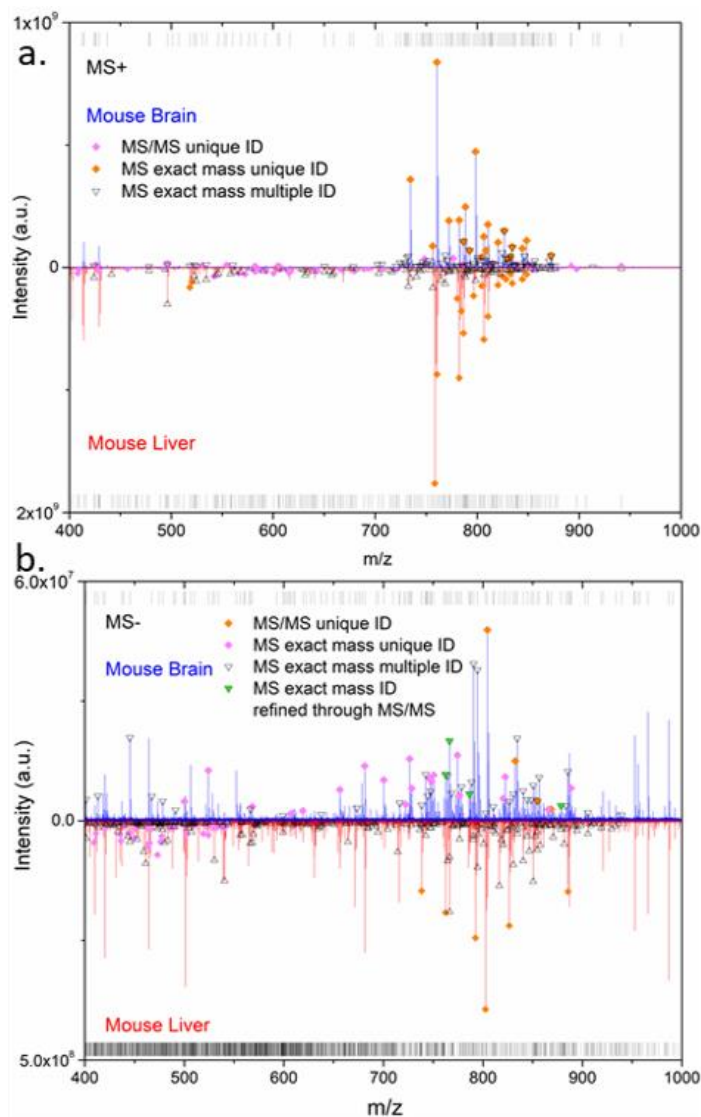


Figure 2.3. Positive (a.) and negative (b.) ionization mode LESA-FT-ICR MS spectra of mouse brain (top, blue) and of mouse liver (bottom, red). The vertical lines on top of each spectrum represent the monoisotopic m/z peaks extracted for identification. The orange markers denote MS/MS identified peaks. The m/z peaks with unique and multiple lipid identifications are highlighted with pink and black markers. As proof-of-concept, the negative mode analysis of MB was subjected to targeted MS/MS experiments using MS1 accurate mass assignments (highlighted with green triangular markers).

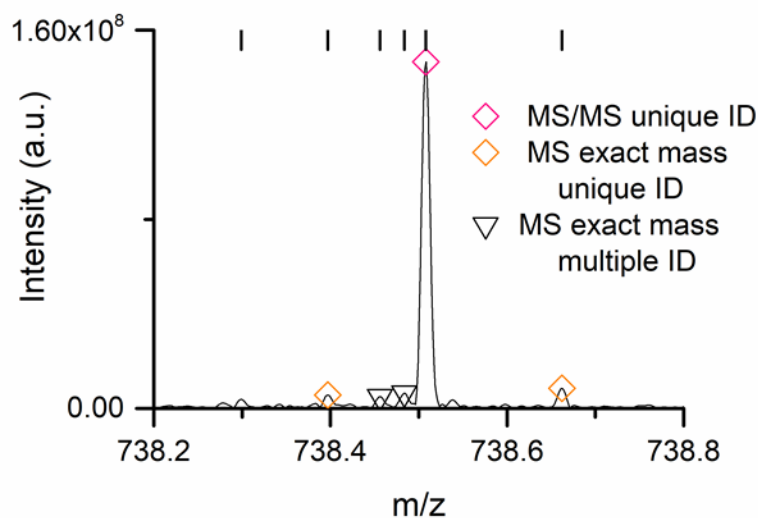


Figure 2.4. Extract from the mouse liver mass spectrum in negative mode from m/z 738.2 to 738.8. The black vertical lines represent the monoisotopic m/z peaks extracted for identification. The orange markers denote MS/MS identified peaks. The m/z peaks with unique and multiple lipid identifications are highlighted with pink and black markers.

In positive mode, the most intense m/z peaks with unique lipid identifications correspond to phosphatidylcholines (PC) in the MB and ML samples, with minor lipid signals corresponding to CAR, Cer, DG, DGDG, HexCer, LPA, LPC, LPG, LPIP, LPS, MG, MGDG, MIPC, PE, PS, and SQDG (see Table 2.1, Table 2.2, and Figure 2.5.a. and c.; all abbreviations are described in the Appendix 2). For the case of PC, the AutoMS/MS identification (without fatty acid chain or double bond identification) relied mostly on the detection of the headgroup and the neutral loss of a fatty acid chain; other lipid assignments were mostly based on MS1 accurate mass. Appendices 3 and 4 summarize all MS1 m/z signals with multiple lipid identifications within the ± 3 ppm database search. It should be noted that multiple adducts were observed for the most abundant lipids, increasing the confidence during their identifications. All uniquely-identified lipids yielded sub-ppm average m/z deviation (e.g., -0.90 ppm for MB and of -0.58 ppm for ML).

Table 2.1. Summary of the positive ionization mode LESA-FT-ICR-MS (MS1 and MS/MS) of a Mouse Brain sample. The molecular ion species, chemical composition, lipid class, theoretical mass, mass error, and identifiers are provided. HG denotes the head group and FA denotes fatty acids.

ID	Precursor m/z	Species	Chemical Composition	Main Class	Short Name	Theo. m/z	ppm	Identified fragments from AutoMS/MS or MS1 identification
1	426.3570	[M+H] ⁺	C25H48NO4	CAR	CAR(18:1)	426.3578	-2	MS1
2	496.3390	[M+Na] ⁺	C29H47NO4Na	CAR	CAR(22:5)	496.3397	1.39	MS1
3	604.5062	[M+K] ⁺	C36H71NO3K	Cer	Cer(d36:1)	604.5065	0.53	MS1
4	582.2952	[M+K] ⁺	C28H50NO7PK	LPC	LPC(20:4)	582.2956	0.77	MS1
5	606.2954	[M+K] ⁺	C30H50NO7PK	LPC	LPC(22:6)	606.2956	0.3	MS1
6	530.2871	[M+H-H2O] ⁺	C26H45NO8P	LPS	LPS(20:3)	530.2877	1.17	MS1
7	554.2871	[M+H-H2O] ⁺	C28H45NO8P	LPS	LPS(22:5)	554.2877	1.03	MS1
8	734.5698	[M+H] ⁺	C40H81NO8P	PC	PC(32:0)	734.5700	0.29	HG (184.0725)
8	756.5519	[M+Na] ⁺	C40H80NO8PNa	PC	PC(32:0)	756.5514	-0.6	HG (184.0724)
8	772.5260	[M+K] ⁺	C40H80NO8PK	PC	PC(32:0)	772.5253	-0.8	HG (184.0725)
9	760.5856	[M+H] ⁺	C42H83NO8P	PC	PC(34:1)	760.5856	0	HG (184.0725)
9	782.5671	[M+Na] ⁺	C42H82NO8PNa	PC	PC(34:1)	782.5670	-0.1	HG (184.0725)
9	798.5418	[M+K] ⁺	C42H82NO8PK	PC	PC(34:1)	798.5410	-0.9	HG (184.0725)
10	788.6171	[M+H] ⁺	C44H87NO8P	PC	PC(36:1)	788.6169	-0.3	HG (184.0725)
10	810.6020	[M+Na] ⁺	C44H86NO8PNa	PC	PC(36:1)	810.5983	-4.6	HG (184.0725)
10	826.5734	[M+K] ⁺	C44H86NO8PK	PC	PC(36:1)	826.5723	-1.3	HG (184.0728)
11	786.6015	[M+H] ⁺	C44H85NO8P	PC	PC(36:2)	786.6013	-0.2	HG (184.0725)
11	808.5863	[M+Na] ⁺	C44H84NO8PNa	PC	PC(36:2)	808.5827	-4.5	HG (184.0725)
12	806.5704	[M+Na] ⁺	C44H82NO8PNa	PC	PC(36:3)	806.5670	-4.2	HG (184.0725)
13	804.5522	[M+Na] ⁺	C44H80NO8PNa	PC	PC(36:4)	804.5514	-1	HG (184.0725)
13	820.5264	[M+K] ⁺	C44H80NO8PK	PC	PC(36:4)	820.5253	-1.3	HG (184.0725)
14	830.5108	[M+K] ⁺	C45H78NO8PK	PC	PC(37:6)	830.5097	-1.3	HG (184.0725)

Continue Table 2.1. Summary of the positive ionization mode LESA-FT-ICR-MS (MS1 and MS/MS) of a Mouse Brain sample. The molecular ion species, chemical composition, lipid class, theoretical mass, mass error, and identifiers are provided. HG denotes the head group and FA denotes fatty acids

ID	Precursor m/z	Species	Chemical Composition	Main Class	Short Name	Theo. m/z	ppm	Identified fragments from AutoMS/MS or MS1 identification
15	834.6019	[M+Na] ⁺	C46H86NO8PNa	PC	PC(38:3)	834.5983	-4.3	HG (184.0725)
16	810.6020	[M+H] ⁺	C46H85NO8P	PC	PC(38:4)	810.6013	-0.9	HG (184.0725)
16	832.5838	[M+Na] ⁺	C46H84NO8PNa	PC	PC(38:4)	832.5827	-1.4	HG (184.0725)
16	848.5579	[M+K] ⁺	C46H84NO8PK	PC	PC(38:4)	848.5566	-1.5	HG (184.0726)
17	844.5265	[M+K] ⁺	C46H80NO8PK	PC	PC(38:6)	844.5253	-1.5	HG (184.0725)
18	872.5581	[M+K] ⁺	C48H84NO8PK	PC	PC(40:6)	872.5566	-1.7	HG (184.0724)
19	838.6334	[M+H] ⁺	C48H89NO8P	PC	PC(40:4)	838.6320	-1.7	MS1
20	892.5268	[M+K] ⁺	C50H80NO8PK	PC	PC(42:10)	892.5253	-1.6	MS1
21	792.5546	[M+H] ⁺	C45H79NO8P	PE	PE(40:6)	792.5538	-1	M-C2H7NO3P-H2O (651.5296)
22	786.4842	[M+K] ⁺	C43H74NO7PK	PE	PE(P-38:6)	786.4834	-1	MS1
22	748.5280	[M+H] ⁺	C43H75NO7P	PE	PE(P-38:6)	748.5276	-0.6	MS1
23	814.5157	[M+K] ⁺	C45H78NO7PK	PE	PE(P-40:6)	814.5147	-1.2	MS1
23	776.5596	[M+H] ⁺	C45H79NO7P	PE	PE(P-40:6)	776.5589	-0.9	MS1
24	850.5559	[M+Na] ⁺	C45H82NO10PNa	PS	PS(39:3)	850.5569	1.23	MS1
25	941.6723	[M+H-H2O] ⁺	C53H97O11S	SQDG	SQDG(44:2)	941.6746	2.41	MS1

Table 2.2. Summary of the positive ionization mode LESA-FT-ICR-MS (MS1 and MS/MS) of a Mouse Liver sample. The molecular ion species, chemical composition, lipid class, theoretical mass, mass error, and identifiers are provided. HG denotes the head group and FA denotes fatty acids.

Mouse Liver MS+								
ID	Precursor <i>m/z</i>	Species	Chemical Composition	Main Class	Short Name	Theo. <i>m/z</i>	ppm	Identified fragments from AutoMS/MS or MS1 identification
1	408.3074	[M+Na] ⁺	C22H43NO4Na	CAR	CAR(15:0)	408.3084	-2.50	MS1
2	428.3724	[M+H] ⁺	C25H50NO4	CAR	CAR(18:0)	428.3734	-2.38	MS1
3	666.6390	[M+H] ⁺	C42H84NO4	Cer	Cer(t42:1)	666.6395	-0.80	MS1
4	589.4795	[M+Na] ⁺	C35H66O5Na	DG	DG(32:1)	589.4802	-1.19	MS1
5	617.5108	[M+Na] ⁺	C37H70O5Na	DG	DG(34:1)	617.5115	-1.07	MS1
6	615.4952	[M+Na] ⁺	C37H68O5Na	DG	DG(34:2)	615.4959	-1.19	MS1
7	613.4795	[M+Na] ⁺	C37H66O5Na	DG	DG(34:3)	613.4802	-1.08	MS1
8	643.5266	[M+Na] ⁺	C39H72O5Na	DG	DG(36:2)	643.5272	-0.95	MS1
9	641.5109	[M+Na] ⁺	C39H70O5Na	DG	DG(36:3)	641.5115	-0.87	MS1
10	639.4952	[M+Na] ⁺	C39H68O5Na	DG	DG(36:4)	639.4959	-1.05	MS1
11	897.5922	[M+H-H2O] ⁺	C49H85O14	DGDG	DGDG(34:3)	897.5934	-1.35	MS1
12	572.4513	[M+H-H2O] ⁺	C32H62NO7	HexCer	HexCer(d26:0)	572.4521	-1.48	MS1
13	586.4670	[M+H-H2O] ⁺	C33H64NO7	HexCer	HexCer(d27:0)	586.4677	-1.28	MS1
14	600.4826	[M+H-H2O] ⁺	C34H66NO7	HexCer	HexCer(d28:0)	600.4834	-1.27	MS1
15	409.2340	[M+H] ⁺	C19H38O7P	LPA	LPA(16:1)	409.2350	-2.42	MS1
16	542.3208	[M+Na] ⁺	C26H50NO7PNa	LPC	LPC(18:2)	542.3217	-1.64	MS1
17	566.3209	[M+Na] ⁺	C28H50NO7PNa	LPC	LPC(20:4)	566.3217	-1.39	MS1
17	582.2948	[M+K] ⁺	C28H50NO7PK	LPC	LPC(20:4)	582.2956	-1.31	MS1
18	606.2949	[M+K] ⁺	C30H50NO7PK	LPC	LPC(22:6)	606.2956	-1.09	MS1
19	495.3073	[M+H-H2O] ⁺	C24H48O8P	LPG	LPG(18:0)	495.3081	-1.72	MS1
20	689.2106	[M+K] ⁺	C25H48O15P2K	LPIP	LPIP(16:1)	689.2100	0.93	MS1

Continue Table 2.2. Summary of the positive ionization mode LESA-FT-ICR-MS (MS1 and MS/MS) of a Mouse Liver sample. The molecular ion species, chemical composition, lipid class, theoretical mass, mass error, and identifiers are provided. HG denotes the head group and FA denotes fatty acids.

ID	Precursor <i>m/z</i>	Species	Chemical Composition	Main Class	Short Name	Theo. <i>m/z</i>	ppm	Identified fragments from AutoMS/MS or MS1 identification
19	495.3073	[M+H-H ₂ O] ⁺	C24H48O8P	LPG	LPG(18:0)	495.3081	-1.72	MS1
20	689.2106	[M+K] ⁺	C25H48O15P2K	LPIP	LPIP(16:1)	689.2100	0.93	MS1
21	839.3513	[M+K] ⁺	C36H66O15P2K	LPIP	LPIP(27:3)	839.3509	0.44	MS1
22	580.3601	[M+H] ⁺	C28H55NO9P	LPS	LPS(22:1)	580.3609	-1.33	MS1
23	429.2966	[M+Na] ⁺	C25H42O4Na	MG	MG(22:4)	429.2975	-2.05	MS1
24	457.3279	[M+Na] ⁺	C27H46O4Na	MG	MG(24:4)	457.3288	-1.88	MS1
25	593.3288	[M+Na] ⁺	C30H50O10Na	MGDG	MGDG(21:3)	593.3296	-1.35	MS1
26	665.4232	[M+Na] ⁺	C35H62O10Na	MGDG	MGDG(26:2)	665.4235	-0.48	MS1
27	679.4389	[M+Na] ⁺	C36H64O10Na	MGDG	MGDG(27:2)	679.4392	-0.40	MS1
28	693.4546	[M+Na] ⁺	C37H66O10Na	MGDG	MGDG(28:2)	693.4548	-0.26	MS1
29	707.4703	[M+Na] ⁺	C38H68O10Na	MGDG	MGDG(29:2)	707.4705	-0.30	MS1
30	721.4859	[M+Na] ⁺	C39H70O10Na	MGDG	MGDG(30:2)	721.4861	-0.22	MS1
31	878.5396	[M+H-H ₂ O] ⁺	C44H81NO14P	MIPC	MIPC(m32:2)	878.5389	0.75	MS1
32	520.3388	[M+H] ⁺	C26H51NO7P	PC	PC(18:2)	520.3403	-2.8	M-C21H37O6P (104.1068), HG (184.0725), M-H ₂ O (502.3254)
33	518.3208	[M+H] ⁺	C26H49NO7P	PC	PC(18:3)	518.3247	-7.6	M-C21H35O6P (104.1068), HG (184.0725)
34	784.5853	[M+Na] ⁺	C42H84NO8PNa	PC	PC(34:0)	784.5827	3.25	HG (184.0725)
35	760.5851	[M+H] ⁺	C42H83NO8P	PC	PC(34:1)	760.5856	-0.7	HG (184.0725), M-FA 18:1 (496.3364)
35	782.5697	[M+Na] ⁺	C42H82NO8PNa	PC	PC(34:1)	782.5670	3.44	HG (184.0725)
36	758.5694	[M+H] ⁺	C42H81NO8P	PC	PC(34:2)	758.5694	-0	HG (184.0725)
36	780.5513	[M+Na] ⁺	C42H80NO8PNa	PC	PC(34:2)	780.5514	-0.1	HG (184.0725)

Continue Table 2.2. Summary of the positive ionization mode LESA-FT-ICR-MS (MS1 and MS/MS) of a Mouse Liver sample. The molecular ion species, chemical composition, lipid class, theoretical mass, mass error, and identifiers are provided. HG denotes the head group and FA denotes fatty acids.

ID	Precursor m/z	Species	Chemical Composition	Main Class	Short Name	Theo. m/z	ppm	Identified fragments from AutoMS/MS or MS1 identification
36	780.5513	[M+Na] ⁺	C42H80NO8PNa	PC	PC(34:2)	780.5514	-0.1	HG (184.0725)
36	796.5255	[M+K] ⁺	C42H80NO8PK	PC	PC(34:2)	796.5253	0.25	HG (184.0725)
37	786.6009	[M+H] ⁺	C44H85NO8P	PC	PC(36:2)	786.6013	-0.6	HG (184.0725)
37	824.5571	[M+K] ⁺	C44H84NO8PK	PC	PC(36:2)	824.5566	0.55	HG (184.0725)
38	804.5515	[M+Na] ⁺	C44H80NO8PNa	PC	PC(36:4)	804.5514	0.12	HG (184.0725)
38	820.5258	[M+K] ⁺	C44H80NO8PK	PC	PC(36:4)	820.5253	0.55	HG (184.0725), M-FA 20:4 (534.2914)
39	810.6011	[M+H] ⁺	C46H85NO8P	PC	PC(38:4)	810.6013	-0.2	HG (184.0725), M-C5H13NO3P-H2O (627.5343)
39	832.5857	[M+Na] ⁺	C46H84NO8PNa	PC	PC(38:4)	832.5827	3.58	HG (184.0725)
39	848.5572	[M+K] ⁺	C46H84NO8PK	PC	PC(38:4)	848.5566	0.75	HG (184.0725)
40	806.5698	[M+H] ⁺	C46H81NO8P	PC	PC(38:6)	806.5694	0.49	HG (184.0725)
40	828.5518	[M+Na] ⁺	C46H80NO8PNa	PC	PC(38:6)	828.5514	0.51	HG (184.0724)
40	844.5259	[M+K] ⁺	C46H80NO8PK	PC	PC(38:6)	844.5253	0.66	HG (184.0725), M-FA 20:5 (560.3077)
41	834.6013	[M+H] ⁺	C48H85NO8P	PC	PC(40:6)	834.6013	-0	HG (184.0725), M-C5H13NO3P-H2O (651.5293)
42	858.5861	[M+H] ⁺	C46H85NO11P	PS	PS(40:3(OH))	858.5855	0.72	MS1
43	854.5549	[M+H] ⁺	C46H81NO11P	PS	PS(40:5(OH))	854.5542	0.77	MS1
44	718.4624	[M+Na] ⁺	C35H70NO10PN a	PS	PS(O- 29:0(OH))	718.4630	-0.82	MS1

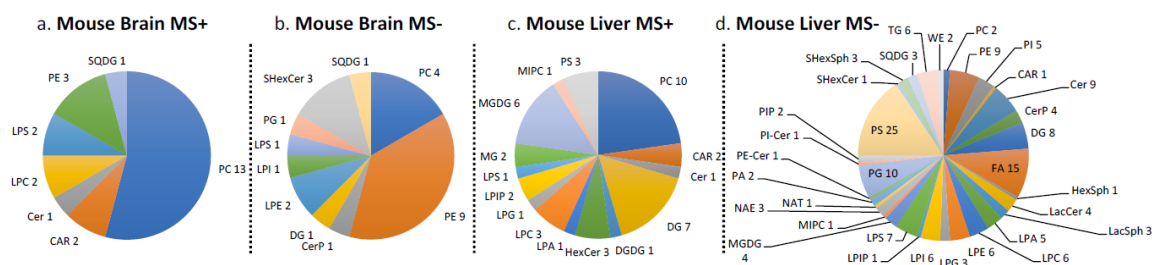


Figure 2.5. Representations of the identified lipid classes in MB and ML (from both MS/MS and MS1), weighted by the number of unique and distinct lipid identifications for each class. a. and c. represent positive ionization for MB and ML, respectively, and b. and d. represent negative ionization for both samples.

In negative mode, the lipid classes with the most unique identifications correspond to phosphatidylethanolamines (PE) and PC in MB, and to phosphatidylserines (PS), fatty acyls (FA) and glycerophosphoglycerols (PG) in ML (see Figure 2.5.b and d. and Appendices 5 and 6). Most of the AutoMS/MS assignments were based on the observation of the fatty acid losses and fragments; other lipids assignments were mostly based on MS1 accurate mass (see appendices 5 and 6). Further dataset descriptions can be found in Appendix 7 for both MB and ML in positive and negative ionization. All uniquely-identified lipids yielded sub-ppm average m/z deviation (e.g., 0.35 ppm for MB and -0.05 ppm for ML).

An estimate of the specificity of the LESA-FT-ICR-MS workflow as a function of the biological surface was obtained from the comparison of the unique lipid assignments in the MB and ML (see Figure 2.6, including both positive and negative mode MS1 and MS/MS identifications). 19 lipids were found common to the MB and ML, with the most abundant being 6 PC, 2 LPC, 2 LPE and 2 WE. One lipid from the PE, PS, LPS, LPI, SODG, SHexCer and NAT classes were found to be common. In the case of MB, 14 different lipid classes were identified (ranked according to the number of identified lipids: PC, PE, LPS, SHexCer, LPC, LPE, CAR, SODG, PS, PG, Cer, DG, LPI, CerP). The most

abundant lipid class for MB was PC (13 lipids), followed by PE (10 lipids) (see Appendix 8). In the case of ML, 36 different lipid classes were identified (ranked according to the number of identified lipids: PS, FA, PC, PG, PE, Cer, DG, LPS, MGDG, LPC, LPE, LPI, LPA, TG, PI, CerP, LacCer, LPG, SQDG, HexCer, LacSph, LPIP, NAE, SHexSph, CAR, MG, MIPC, PA, PIP, WE, SHexCer, DGDG, HexSph, PE-Cer, PI-Cer, NAT). The most abundant lipid class for ML was PS (27 lipids), followed by FA (15 lipids), and PC and PG (10 lipids).

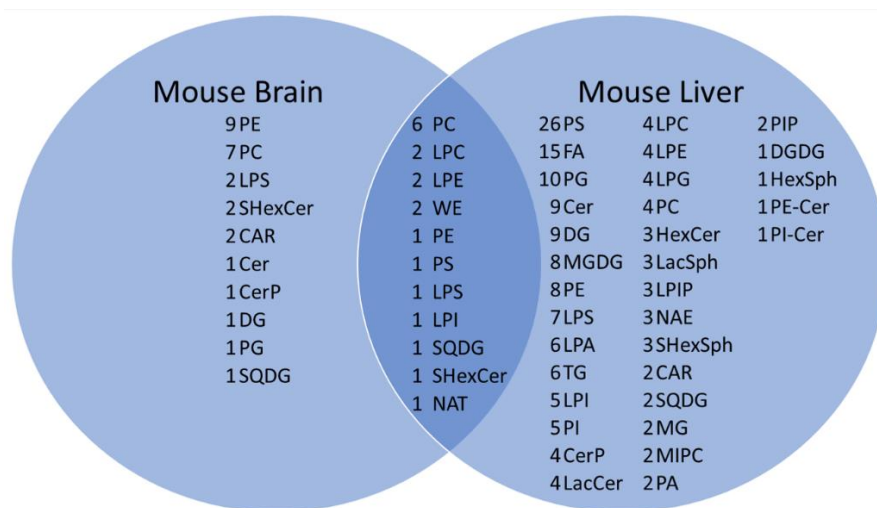


Figure 2.6. Diagram of the lipid compositions (lipid classes) of healthy mouse brain and mouse liver samples identified from LESA-FT-ICR-MS (MS/MS and MS1) measurements, including both positive and negative ionization mode. The circle overlap represents the number of distinct lipids from the different lipid classes which were found in both tissues.

An example of the use of targeted MS/MS following the MS1 accurate mass search is shown for the case of MB in negative ion mode (see Table 2.3). The added fragment ion information enables the exclusion of accurate mass identifications as well as to increase the structural information. For example, the identification of PE(22:6/16:0) ($m/z = 762.5079$) and PE(20:4/18:0) ($m/z = 766.5393$) is illustrated in Table 2.3.

Table 2.3. Negative ion mode targeted MS/MS after preliminary MS1 accurate mass database search from the MB. The different lipid identification possibilities are shown, with the MS/MS fragment ion interpretations which refine the m/z identification

Precursor <i>m/z</i>	species	Chemical Composition	Main Class	Short Name	Theo. <i>m/z</i>	ppm	Identified fragments from MS/MS	MS/MS refined identification																																														
762.5079	[M+H] ⁻	C43H73NO8P	PE	PE(38:6)	762.5079	0.05	FA 16:0(+COO) (255.2306), FA 22:6(-CO) (283.2423), FA 22:6(+COO) (327.2305), M-FA 22:6(-H) (452.2765)	PE(22:6/16:0)																																														
	[M+H] ⁻	C43H73NO8P	PE	PE(P- 38:6(OH))	762.5079	0.05			766.5393	[M+H] ⁻	C43H77NO8P	PE	PE(38:4)	766.5392	0.14	FA 18:0(+COO) (283.2615), FA 20:4(+COO) (303.2312), M-FA 20:4(+COO) (463.2978)	PE(20:4/18:0)	[M+H] ⁻	C43H77NO8P	PE	PE(O- 38:5(OH)) or PE(P- 38:4(OH))	766.5392	0.14	786.5276	[M+HCOO] ⁻	C42H77NO10P	PC	PC(33:3)	786.5291	-1.91	FA 18:1(+COO) (281.2468), M-FA 18:1(+HO)-C3H5NO2 (417.2372), M-C3H5NO2 (699.4904)	PS(18:1/18:1)	[M+HCOO] ⁻	C42H77NO10P	PE	PE(36:3)	786.5291	-1.91	[M+HCOO] ⁻	C42H77NO10P	PE	PE(O- 36:4(OH)) or PE(P- 36:3(OH))	786.5291	-1.91	[M+H] ⁻	C42H77NO10P	PS	PS(36:2)	786.5291	-1.91	[M+H] ⁻	C42H77NO10P	PS	PS(O- 36:3(OH)) or PS(P- 36:2(OH))
766.5393	[M+H] ⁻	C43H77NO8P	PE	PE(38:4)	766.5392	0.14	FA 18:0(+COO) (283.2615), FA 20:4(+COO) (303.2312), M-FA 20:4(+COO) (463.2978)	PE(20:4/18:0)																																														
	[M+H] ⁻	C43H77NO8P	PE	PE(O- 38:5(OH)) or PE(P- 38:4(OH))	766.5392	0.14			786.5276	[M+HCOO] ⁻	C42H77NO10P	PC	PC(33:3)	786.5291	-1.91	FA 18:1(+COO) (281.2468), M-FA 18:1(+HO)-C3H5NO2 (417.2372), M-C3H5NO2 (699.4904)	PS(18:1/18:1)	[M+HCOO] ⁻	C42H77NO10P	PE	PE(36:3)	786.5291	-1.91		[M+HCOO] ⁻	C42H77NO10P	PE	PE(O- 36:4(OH)) or PE(P- 36:3(OH))	786.5291	-1.91			[M+H] ⁻	C42H77NO10P	PS	PS(36:2)	786.5291	-1.91	[M+H] ⁻	C42H77NO10P	PS	PS(O- 36:3(OH)) or PS(P- 36:2(OH))	786.5291	-1.91	PS(O- 18:1/18:1(OH)) or PS(P- 18:0/18:1(OH))									
786.5276	[M+HCOO] ⁻	C42H77NO10P	PC	PC(33:3)	786.5291	-1.91	FA 18:1(+COO) (281.2468), M-FA 18:1(+HO)-C3H5NO2 (417.2372), M-C3H5NO2 (699.4904)	PS(18:1/18:1)																																														
	[M+HCOO] ⁻	C42H77NO10P	PE	PE(36:3)	786.5291	-1.91																																																
	[M+HCOO] ⁻	C42H77NO10P	PE	PE(O- 36:4(OH)) or PE(P- 36:3(OH))	786.5291	-1.91																																																
	[M+H] ⁻	C42H77NO10P	PS	PS(36:2)	786.5291	-1.91																																																
	[M+H] ⁻	C42H77NO10P	PS	PS(O- 36:3(OH)) or PS(P- 36:2(OH))	786.5291	-1.91			PS(O- 18:1/18:1(OH)) or PS(P- 18:0/18:1(OH))																																													

Continue Table 2.3. Negative ion mode targeted MS/MS after preliminary MS1 accurate mass database search from the MB. The different lipid identification possibilities are shown, with the MS/MS fragment ion interpretations which refine the m/z identification

Precursor <i>m/z</i>	species	Chemical Composition	Main Class	Short Name	Theo. <i>m/z</i>	ppm	Identified fragments from MS/MS	MS/MS refined identification
878.5913	[M+HCOO] ⁻	C49H85NO10P	PC	PC(40:6)	878.5917	-0.51	FA 12:5(-CO) (145.0618), FA 13:6(-CO) (157.0115), FA 13:5(+COO) (203.0207), FA 20:6(-CO) or FA 16:0(+COO) (255.2334), FA 22:6(-CO) or FA 18:0(+COO) (283.2650), FA 19:2(+COO) (293.1764), FA 24:6(-CO) or FA 20:0(+COO) (311.1719), FA 26:6(-CO) or FA 22:0(+COO) (339.2006), FA 23:1(+COO) (351.1385), M-CH3-HCOO (818.5718)	PC(40:6)
	[M+HCOO] ⁻	C49H85NO10P	PC	PC(P- 40:6(OH))	878.5917	-0.51		
	[M+HCOO] ⁻	C49H85NO10P	PE	PE(43:6)	878.5917	-0.51		
	[M+H] ⁻	C49H85NO10P	PS	PS(43:5)	878.5917	-0.51	FA 16:0(+COO) (255.2334), FA 18:0(+COO) (283.2650), FA 19:2(+COO) (293.1764), FA 20:0(+COO) (311.1719), FA 22:0(+COO) (339.2006), FA 23:1(+COO) (351.1385), M-C3H5NO2 (791.4671)	PS(43:5)

2.5 Conclusions

A fast and high-throughput analysis workflow for lipid screening in biological tissues at ambient conditions without the need for pre-separations or sample treatment is shown. The LESA-FT-ICR MS(/MS) analysis of mouse brain and liver sections resulted in the identification of 36 lipid classes in a single analysis (< 15 min), with lipid markers specific to each tissue. The combination of accurate mass and AutoMS/MS resulted in the identification of unique and common lipid molecules from the biological tissues, with average sub-ppm mass accuracy. The workflow was presented using CID as a proof of concept, but other fragmentation techniques providing further structural lipid information are equally suitable. The most abundant lipids species are typically observed and identified in several adduct forms (e.g., protonated, sodiated and potassiated), thus increasing the confidence in the molecular assignment. In the examples shown, ~190 (MB) and ~630 (ML) m/z values were identified by unique or multiple lipid assignments in positive and negative mode, with 25-30% of these identifications being unique and distinct lipids assignments. In addition to MS analysis, further integration on post-ionization mobility separation can provide additional structural information.^{20,48-51}

2.6 Acknowledgements

The work at FIU was supported by a NSF CAREER (CHE-1654274), with co-funding from the Division of Molecular and Cellular Biosciences to FFL. JRNH acknowledges the Fulbright for financial support. The work at UoB was supported by a IAS Vanguard Fellowship to FFL. HJC is an EPSRC Established Career Fellow (EP/L023490/1). EKS is funded by the EPSRC via the Centre for Doctoral Training

in Physical Sciences for Health (Sci-Phy-4-Health) (EP/L016346/1), in collaboration with UCB Pharma. The FT-ICR mass spectrometer used in this work was funded by BBSRC (BB/M012492/1).

2.7 References

- 1 A. Shamim, T. Mahmood, F. Ahsan, A. Kumar and P. Bagga, *Clin. Nutr. Exp.*, 2018, **20**, 1–19.
- 2 E. R. Schenk, F. Nau, C. J. Thompson, Y. C. Tse-Dinh and F. Fernandez-Lima, *J. Mass Spectrom.*, 2015, **50**, 88–94.
- 3 K. Yang and X. Han, *Trends Biochem. Sci.*, 2016, **41**, 954–969.
- 4 G. Dawson, *Biochim. Biophys. Acta - Mol. Cell Biol. Lipids*, 2015, **1851**, 1026–1039.
- 5 C. Giles, R. Takechi, V. Lam, S. S. Dhaliwal and J. C. L. Mamo, *Prog. Lipid Res.*, 2018, **71**, 86–100.
- 6 P. H. Axelsen and R. C. Murphy, *J. Lipid Res.*, 2010, **51**, 660–671.
- 7 H. C. Lee and T. Yokomizo, *Biochem. Biophys. Res. Commun.*, 2018, **504**, 576–581.
- 8 Y. H. Rustam and G. E. Reid, *Anal. Chem.*, 2018, **90**, 374–397.
- 9 B. M. Prentice, J. C. McMillen and R. M. Caprioli, *Int. J. Mass Spectrom.*, , DOI:10.1016/j.ijms.2018.06.006.
- 10 B. M. Ham, J. T. Jacob and R. B. Cole, *Anal. Chem.*, 2005, **77**, 4439–4447.
- 11 A. P. Bowman, R. M. A. Heeren and S. R. Ellis, *TrAC - Trends Anal. Chem.*, 2018, 1–10.
- 12 F. Barré, B. Rocha, M. Towers, P. Murray, E. Claude, B. C. Pastor, R. Heeren and T. P. Siegel, *Int. J. Mass Spectrom.*, , DOI:10.1016/j.ijms.2018.09.015.
- 13 M. L. Kraft and H. A. Klitzing, *Biochim. Biophys. Acta - Mol. Cell Biol. Lipids*, 2014, **1841**, 1108–1119.

- 14 K. J. Adams, J. D. DeBord and F. Fernandez-Lima, *J. Vac. Sci. Technol. B, Nanotechnol. Microelectron. Mater. Process. Meas. Phenom. JVST B*, 2016, **34**, 51804.
- 15 P. Sjövall, B. Johansson and J. Lausmaa, *Appl. Surf. Sci.*, 2006, **252**, 6966–6974.
- 16 H. Tian, J. S. Fletcher, R. Thuret, A. Henderson, N. Papalopulu, J. C. Vickerman and N. P. Lockyer, *J. Lipid Res.*, 2014, **55**, 1970–1980.
- 17 D. Gode and D. A. Volmer, *Analyst*, 2013, **138**, 1289–1315.
- 18 S. R. Ellis, S. H. Brown, M. In Het Panhuis, S. J. Blanksby and T. W. Mitchell, *Prog. Lipid Res.*, 2013, **52**, 329–353.
- 19 Y. Satomi, M. Hirayama and H. Kobayashi, *J. Chromatogr. B Anal. Technol. Biomed. Life Sci.*, 2017, **1063**, 93–100.
- 20 A. Baglai, A. F. G. Gargano, J. Jordens, Y. Mengerink, M. Honing, S. van der Wal and P. J. Schoenmakers, *J. Chromatogr. A*, 2017, **1530**, 90–103.
- 21 A. L. Rennó, M. Alves-Júnior, N. V. Schwab, M. N. Eberlin, A. A. Schenka and A. Sussulini, *Int. J. Mass Spectrom.*, 2017, **418**, 86–91.
- 22 J. I. Zhang, N. Talaty, A. B. Costa, Y. Xia, W. A. Tao, R. Bell, J. H. Callahan and R. G. Cooks, *Int. J. Mass Spectrom.*, 2011, **301**, 37–44.
- 23 M. Manikandan, Z. Kazibwe, N. Hasan, A. Deenadayalan, J. Gopal, T. Pradeep and S. Chun, *TrAC Trends Anal. Chem.*, 2016, **78**, 109–119.
- 24 L. S. Eberlin, C. R. Ferreira, A. L. Dill, D. R. Ifa and R. G. Cooks, *Biochim. Biophys. Acta - Mol. Cell Biol. Lipids*, 2011, **1811**, 946–960.
- 25 V. Kertesz, M. J. Ford and G. J. Van Berkel, *Anal. Chem.*, 2005, **77**, 7183–7189.
- 26 T. Wachs and J. Henion, *Anal. Chem.*, 2001, **73**, 632–638.
- 27 V. Kertesz and G. J. Van Berkel, *J. Mass Spectrom.*, 2010, **45**, 252–260.
- 28 R. L. Griffiths and H. J. Cooper, *Anal. Chem.*, 2016, **88**, 606–609.
- 29 N. J. Martin, R. L. Griffiths, R. L. Edwards and H. J. Cooper, *J. Am. Soc. Mass Spectrom.*, 2015, **26**, 1320–1327.

- 30 E. C. Randall, A. M. Race, H. J. Cooper and J. Bunch, *Anal. Chem.*, 2016, **88**, 8433–8440.
- 31 M. Wisztorski, A. Desmons, J. Quanico, B. Fatou, J. P. Gimeno, J. Franck, M. Salzet and I. Fournier, *Proteomics*, 2016, **16**, 1622–1632.
- 32 R. L. Griffiths, A. J. Creese, A. M. Race, J. Bunch and H. J. Cooper, *Anal. Chem.*, 2016, **88**, 6758–6766.
- 33 R. L. Griffiths, K. I. Kocurek and H. J. Cooper, *Curr. Opin. Chem. Biol.*, 2018, **42**, 67–75.
- 34 V. A. Mikhailov, R. L. Griffiths and H. J. Cooper, *Int. J. Mass Spectrom.*, 2017, **420**, 43–50.
- 35 Z. Hall, Y. Chu and J. L. Griffin, *Anal. Chem.*, 2017, **89**, 5161–5170.
- 36 N. N. Zhao, Y. F. Sun, L. Zong, S. Liu, F. R. Song, Z. Q. Liu and S. Y. Liu, *Int. J. Mass Spectrom.*, 2018, **434**, 29–36.
- 37 L. Zong, Z. Pi, S. Liu, J. Xing, Z. Liu and F. Song, *Rapid Commun. Mass Spectrom.*, 2018, **32**, 1683–1692.
- 38 S. A. Murfitt, P. Zacccone, X. Wang, A. Acharjee, Y. Sawyer, A. Koulman, L. D. Roberts, A. Cooke and J. L. Griffin, *J. Proteome Res.*, 2018, **17**, 946–960.
- 39 *United States of America Pat.*, 5872357, 1999.
- 40 J. K. Pauling, M. Hermansson, J. Hartler, K. Christiansen, S. F. Gallego, B. Peng, R. Ahrends and C. S. Ejsing, *PLoS One*, 2017, **12**, 1–21.
- 41 E. Fahy, S. Subramaniam, H. A. Brown, C. K. Glass, A. H. Merrill, R. C. Murphy, C. R. H. Raetz, D. W. Russell, Y. Seyama, W. Shaw, T. Shimizu, F. Spener, G. van Meer, M. S. VanNieuwenhze, S. H. White, J. L. Witztum and E. A. Dennis, *J. Lipid Res.*, 2005, **46**, 839–862.
- 42 E. Fahy, M. Sud, D. Cotter and S. Subramaniam, *Nucleic Acids Res.*, 2007, **35**, W606–W612.
- 43 X. Zheng, R. D. Smith and E. S. Baker, *Curr. Opin. Chem. Biol.*, 2018, **42**, 111–118.
- 44 H. J. Yoo and K. Håkansson, *Anal. Chem.*, 2010, **82**, 6940–6946.

- 45 J. W. Jones, C. J. Thompson, C. L. Carter and M. A. Kane, *J. Mass Spectrom.*, 2015, **50**, 1327–1339.
- 46 S. R. Ellis, H. T. Pham, M. In het Panhuis, A. J. Trevitt, T. W. Mitchell and S. J. Blanksby, *J. Am. Soc. Mass Spectrom.*, 2017, **28**, 1345–1358.
- 47 P. Li and G. P. Jackson, *J. Mass Spectrom.*, 2017, **52**, 271–282.
- 48 W. B. Ridenour, M. Kliman, J. A. McLean and R. M. Caprioli, *Anal. Chem.*, 2010, **82**, 1881–1889.
- 49 J. C. May, C. R. Goodwin and J. A. McLean, *Curr. Opin. Biotechnol.*, 2015, **31**, 117–121.
- 50 J. C. May, C. R. Goodwin, N. M. Lareau, K. L. Leaptrot, C. B. Morris, R. T. Kurulugama, A. Mordehai, C. Klein, W. Barry, E. Darland, G. Overney, K. Imatani, G. C. Stafford, J. C. Fjeldsted and J. A. McLean, *Anal. Chem.*, 2014, **86**, 2107–2116.
- 51 C. Hinz, S. Liggi and J. L. Griffin, *Curr. Opin. Chem. Biol.*, 2018, **42**, 42–50.

CHAPTER 3. Evaluation of Liquid Extraction Surface Analysis (LESA) with Time-Dispersive Cyclic Traveling Wave and Field-Dispersive Trapped Ion Mobility Spectrometries coupled to Mass Spectrometry for Fast Lipid Isomer/Isobar Screening

Yarixa L. Cintron-Diaz, Jean R. N. Haler, Jacob Porter and Francisco Fernandez-Lima

This chapter has been submitted to *Talanta* and is under review.

3.1 Abstract

The development of highly-sensitive, fast, analytical techniques in tandem with mass spectrometry (MS) has sparked increasing applications in the field of lipidomics and lipid biomarker discovery. In particular, gas-phase ion mobility spectrometry (IMS) has shown great potential in separating isomeric and isobaric lipid species, as well as providing lipid descriptors based on the collision cross-section (RPD<1%). In this work, we evaluate the direct analysis of biological surfaces using liquid extraction at ambient pressure complemented with two high-resolution ion mobility-mass spectrometry platforms: i) time-dispersive cyclic traveling wave IMS-MS (cTWIMS-MS) and ii) field-dispersive trapped IMS-MS (TIMS-MS). The workflows described have the common capacity to perform wide range mobility measurements (discovery mode) followed by higher resolution mobility targeted analysis of isomeric species (targeted mode). Unsupervised lipid identification is based on mobility selected fragmentation (CID-MS/MS), as well as the comparison with lipid standards. The application of these protocols to the analysis of lipids from wildtype mouse brain and liver sections is described based on the extraction solvent and the number and classes of lipids identified between direct infusion and the inclusion of a liquid chromatography step prior ionization (LC-TIMS-MS/MS using CID). Despite the complex nature of the biological samples, the high mobility resolution provided by cTWIMS and TIMS (resolving powers up to 310) allowed effective separation of isomeric lipids from the biological surfaces in a short time-scale (few min); a tradeoff of the direct analysis was the observation of the most abundant lipids when compared to the addition of a LC step prior to ionization.

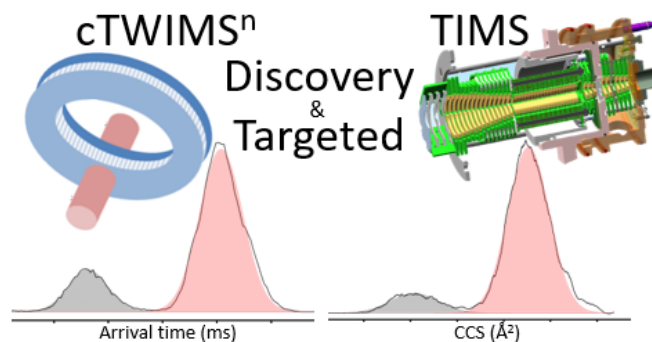


Figure 3.1. Graphical Abstract of Chapter 3

3.2 Introduction

In recent years, biomarker discovery has focused on the lipid content due to their role in many biological processes and the search for new therapeutic targets¹⁻⁶. From the analytical standpoint, lipid analysis is challenging due to their structural complexity and diversity⁷⁻¹². Lipid characterization at the level of lipid class/subclass, sum composition and/or, acyl chain composition has been made accessible mostly through mass spectrometric techniques^{3, 13-20}.

Biological tissue imaging using secondary ion mass spectrometry²¹⁻²⁵ (SIMS), matrix assisted laser desorption ionization^{2, 26-30} (MALDI), and liquid extraction surface analysis^{6, 31-37} (LESA), as well as bulk analysis using liquid chromatography (LC) coupling to mass spectrometry (MS)³⁸⁻⁴³, have brought high-throughput analysis strategies to the field of lipidomics. These high-throughput approaches coupled to different ion activation techniques mostly allow for lipid characterizations as the lipid (sub)class, the sum composition, and the individual acyl chain composition. Collision induced dissociation (CID) is the most widespread activation technique available in direct infusion or LC-MS

high-throughput analyses³⁸⁻⁴⁵. CID allows for the determination of the individual acyl chain lengths (and the number of double bonds), whereas more specific activation techniques, such as ozone induced dissociation (OzID), are able to elucidate the double bond positions^{13, 14, 16, 35, 46-49}.

The combination of ion mobility spectrometry (IMS) with mass spectrometry for lipid analysis^{45, 50-65}, with or without LC pre-separation, allows for the fast separation of the isomeric content based on differences in mobility^{45, 51, 54, 57, 66-76}. Whereas LC may be capable of separating lipid classes and isomers, typical LC-MS workflows require tens of minutes while similar results were obtained by direct infusion IMS-MS analyses with IMS separations performed in the millisecond-timescale^{55, 77}. We have recently shown the advantages of direct analysis at ambient pressure using LESA when combined with ultrahigh resolution mass spectrometry (LESA-FT-ICR MS/MS)³⁵. LESA can be easily coupled to any MS instrument and allow for surface mapping, where a liquid microjunction between the surface and an extraction tip is created, followed by direct nanoelectrospray infusion³². When compared to other extraction techniques or imaging experiments, LESA-MS significantly decreases sample preparation, experiment time, and potential ionization suppression bias (e. g., MALDI matrix)³⁵. Compared to DESI-MS, LESA-MS has shown to be more sensitive and avoids sample carryover due to the single use nature of its tips and nano sprayer⁷⁸.

Several IMS technologies have been coupled to mass spectrometry, such as traveling wave IMS (TWIMS and structures for lossless ion manipulations (SLIM))^{50, 58, 59, 64, 65, 79, 80}, drift tube IMS (DTIMS)^{51, 62, 81-84}, field asymmetric or differential IMS (FAIMS, DMS)^{54, 55, 85-87}, and trapped IMS (TIMS)^{60, 61, 73, 76, 88-90}. Several publications have shown

that high-resolution IMS-MS instruments have resolved cis/trans geometric isomers and double-bond positional lipid isomers^{51, 65, 73, 76, 79, 80, 83, 85}. For the (ultra)high-resolution DTIMS, TIMS and SLIM setups, separating acyl chain *sn*-1/2/3 positional isomers remains challenging^{51, 73, 76, 80, 91}, while FAIMS and DMS readily separate them^{76, 85, 87}. Other isomeric lipids differing (e.g. by their double bond positions), coelute in FAIMS and DMS but are resolved using DTIMS, TIMS and SLIM. While some of these platforms have been effective in analyzing lipid standards, they have yet to prove their performance during direct analysis of biological samples.

In the present work, we evaluate the performance of the direct analysis of biological surfaces using liquid extraction at ambient pressure complemented with two high-resolution, ion mobility-mass separation techniques: i) time-dispersive cyclic traveling wave IMS-MS (cTWIMS-MS)^{59, 91-94} and ii) field-dispersive trapped IMS-MS (TIMS-MS)^{60, 61, 73, 76, 88-90}. This is the first direct comparison of the two highest resolution IMS technologies successfully implemented in commercial TOF-MS instruments. Focus is made on the capacity of high resolution IMS to unravel the lipid isomeric content during direct sampling of biological surfaces in short time scale (few min). The showcased IMS experimental workflows incorporate wide scan mobility measurements (discovery mode) followed by targeted higher resolution ion mobility analyses (targeted mode) in tandem with CID MS/MS, resulting in mobility-selected CID MS/MS fragmentation pattern-based lipid assignments which are confirmed with measured ion mobility profiles of lipid standards. Examples are shown for the direct analysis of lipids from wildtype mouse brain and liver sections using ambient pressure liquid extraction surface analysis (LESA) followed by online cTWIMS-CID-TOF MS/MS and TIMS- CID TOF MS/MS. Two

traditional LESA extraction protocols were compared. Results from conventional LC-TIMS-TOF MS/MS analysis of the LESA extracts are discussed to evaluate the tradeoffs of the shorter time (few min compared to hours) direct infusion based analysis.

3.3 Materials and Methods

3.3.1 Biological samples

Wildtype mouse brain and liver samples were obtained from extraneous tissue from culled animals from Prof. Jeremy W. Chambers' laboratory at Florida International University (IACUC-15-017). After extractions, the organs were frozen and stored at -80 °C. Tissue sections were obtained with a thickness of 10 µm using a CM1850 Cryostat (Leica Microsystems, Wetzlar, Germany) and were thaw mounted onto glass slides.

3.3.2 LESA lipid extraction

Details on the LESA extraction of lipids from biological surfaces can be found elsewhere³⁵. Briefly, lipid extractions were performed using the TriVersa Nanomate (Advion, Ithaca, NY) by placing the thin tissue slices onto a universal LESA adapter plate (Figure 3.1.a). Two extraction solvent mixtures were considered: ethanol/water/formic acid (EtOH/H₂O/HCOOH) 80/19.9/0.1 (v/v/v) [LESA1] and isopropanol/methanol/chloroform (IPA/MeOH/CH₃Cl) 40/20/10 (v/v/v) with 10mM ammonium acetate [LESA2]. A total of 6 µL of solvent was aspirated from the well. The robotic arm descended to a height 0.2 mm above the surface of the sample for dispensing 3 µL onto the sample surface to form a liquid microjunction. The liquid microjunction was maintained for 5 seconds, before re-

aspirating 3.5 μL into the pipet tip. The liquid dispensing and re-aspiration was repeated three times. The lipid extracts were collected from four different spots ($\sim 1\text{mm}$ OD) and stored at $-20\text{ }^\circ\text{C}$ for direct analysis using cTWIMS-CID TOF MS/MS and nESI-TIMS-CID TOF MS/MS, as well as comparative LC-ESI-TIMS CID TOF MS/MS.

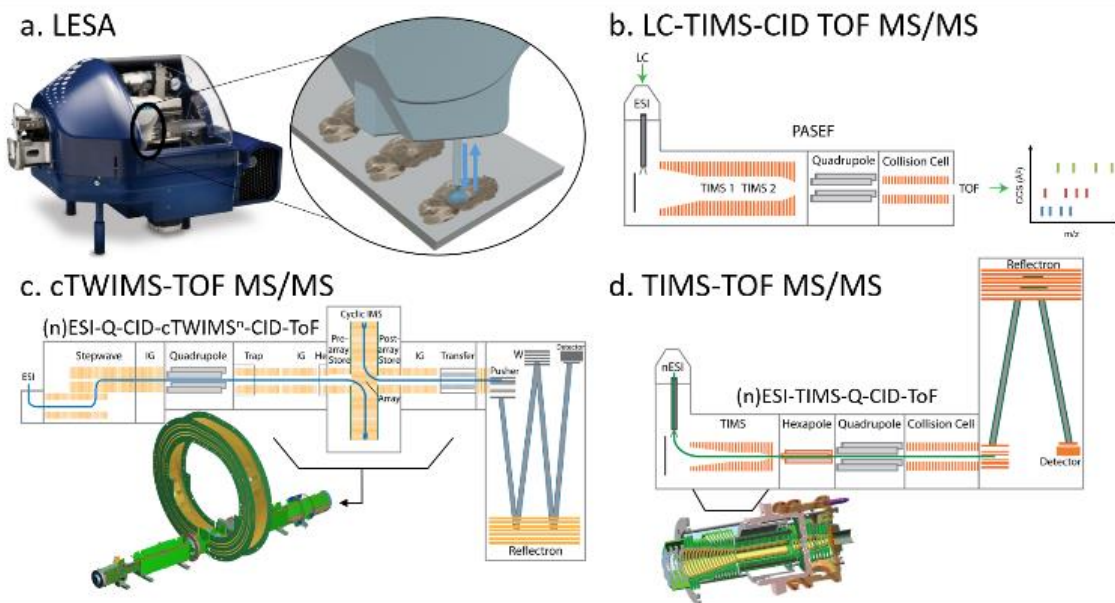


Figure 3.2. Simplified schematics of the (a) LESA instrument used for ambient pressure lipid extraction from mouse brain and liver slices; (b) liquid chromatography-trapped ion mobility spectrometry using collision induced dissociation CID-TOF MS/MS (Bruker, USA); (c) cyclic traveling wave ion mobility instrument - TOF MS (Waters, UK)⁵⁹ and (d) the trapped ion mobility spectrometry -TOF MS (Bruker, USA).

3.3.3 Cyclic Traveling Wave Ion Mobility Spectrometry-CID TOF MS/MS

The cTWIMS-TOF instrument used in these studies was a prototype of the commercially available system (Figure 3.1c). A detailed description of the operation of the cTWIMS instrument can be found elsewhere⁵⁹ and in the Supporting Information section. Samples were introduced using nano-electrospray ionization (nESI). The applied nESI

voltage ranged from 1.0-1.5 kV. The traveling wave height and velocity were 35 V and 375 m/s, respectively.

Non-targeted cTWIMS-TOF MS discovery runs were performed at 1 to 5 passes in the cTWIMS cell (i.e., no quadrupole precursor selection). The discovery runs use mobility selection to increase the resolution of a large range of lipids at the chosen range of arrival times. Targeted, quadrupole-selected cTWIMS-MS runs were performed at 1 to 30 passes in the cTWIMS cell. cTWIMS-CID TOF MS/MS was performed following the quadrupole and mobility selections of the precursor m/z , and a 40-45 V collision voltage in the CID transfer region. The mobility-selected MS/MS spectra allowed for lipid class assignments. The instrument was controlled using a web-based GUI and data was processed using MassLynx v.4.1, Driftscope v.2.4 and OriginPro 2016.

3.3.4 Trapped Ion Mobility Spectrometry-CID TOF MS/MS

Samples were introduced using a nano-electrospray (nESI) into a custom built nESI-TIMS analyzer coupled to an Impact Q-TOF MS^{60,61} (Figure 3.1.d; Bruker, Billerica, MA). The TIMS unit is equipped with the new quadrupolar, convex electrode geometry⁷⁶ and is controlled using a custom software in LabView (National Instruments) synchronized with the MS platform controls⁶⁰. A detailed description of the operation of the TIMS instrument can be found in the Supporting Information section.

The pulled nESI tips were biased at 600-750 V. Non-targeted, TIMS-TOF MS discovery runs (no quadrupole m/z isolation) were performed at different scan rates ($Sr = \Delta V_{\text{ramp}} / \text{ramp time}$). For example, $Sr = 2.8$ V/ms (100 ms ramp time and $\Delta V_{\text{ramp}} = 280$ V), 2.0 V/ms (100 ms ramp time and $\Delta V_{\text{ramp}} = 200$ V), 0.3 V/ms (100 ms ramp with

$\Delta V_{\text{ramp}} = 30 \text{ V}$), and 0.18 V/ms (500 ms ramp with $\Delta V_{\text{ramp}} = 90 \text{ V}$). The deflector voltage and base voltage were set to 60 V. The discovery runs used a wide mobility range selection (or wide electric field range). Targeted mobility and quadrupole-selected TIMS-CID TOF MS/MS runs were performed at lower scan rates. TIMS-TOF MS/MS was performed following the mobility and quadrupole selections of a predetermined precursor m/z , using a 40 V collision voltage in the CID cell. The mobility-selected MS/MS spectra allowed for lipid class assignments.

3.3.5 Liquid Chromatography – TIMS-CID TOF MS/MS

LESA extracts were also analyzed using a commercial timsTOF mass spectrometer (Bruker Daltonics, Germany) system coupled to a Prominence LC-20AD HPLC system (Shimadzu, Japan). Briefly, liquid chromatography separations were performed on a Accucore C₃₀ analytical column (Thermo Fisher Scientific, Sunnyvale, CA), using a gradient of 30:40:30 (ACN:H₂O:IPA) as mobile phase A and 10:5:85 (ACN: H₂O:IPA) as mobile phase B. Both phases contained 10 mM ammonium acetate and 0.1% formic acid. HPLC conditions were: injection volume of 5 μL , solvent flow rate of 0.25 mL/min and a total run time of 60min per sample. The chromatography was coupled to the MS instrument through an ESI source which operated under positive polarity. The timsTOF instrument was operated under parallel accumulation serial fragmentation (PASEF) mode⁹², an approach that enables four-dimensional (ion mobility, accurate mass, intensity and fragmentation) data acquisition with high sensitivity. The TIMS scan range was from 0.7-1.85 $\text{V}\cdot\text{s}/\text{cm}^2$ with a ramp time of 150 ms and the TOF analyzer was operated at m/z 50–1850. The scan rate used was 0.98 V/ms ($t_{\text{ramp}} = 150\text{ms}$ time and $\Delta V_{\text{ramp}} = 143.6 \text{ V}$). The

instrument was controlled using Compass Hystar and oTOF Control (Bruker Daltonics, Germany).

3.3.6 Trapped Ion Mobility Spectrometry-FT-ICR MS

LESA extracts were introduced using a nano-electrospray (nESI) into a custom built nESI-TIMS analyzer coupled to an 7T Solarix FT-ICR MS (Bruker Daltonics, Germany)⁹³. For oversampling experiments (OSA-TIMS-FT-ICR MS), a ΔV_{ramp} of 1V was used in the -70 to -62 V range, leading to a scan rate of 0.001 V/pulse, with a V_{step} of 0.05 V, and single mobility experiments were accumulated in the collision cell prior to injection in the FT-ICR MS cell and acquired at 4 MW (20 s transient using an average of 800 scans)⁹³. The total analysis time for the OSA-TIMS-FT-ICR MS experiments was 60 minutes. The mobility spectra were calibrated as described previously using Agilent Tune Mix^{89, 94}.

3.3.7 Data Processing, Mobility Resolving Power and Mobility Resolution

Data was processed using DataAnalysis 5.2, UIMFviewer v.1.4 and OriginPro 2016. The cTWIMS-MS/MS and TIMS-MS/MS spectra were interpreted based on fragmentation patterns reported in literature⁴⁷. Collected data from LC-TIMS-CID TOF MS/MS was annotated using the MetaboScape® 2021a software (Bruker Daltonics, Germany). Molecules were annotated based on the matching of accurate parent and fragment ion mass, isotopic pattern, and CCS from available online databases (e.g., LipidMaps). Mobility resolving power (R) and resolution (r) were calculated based on

equations 1 and 2. CCS values derived from calibrated TIMS measurements were used to estimate R values from cTWIMS data (Appendix 8).

$$R = \frac{CCS}{\Delta CCS} \quad (1)$$

$$r_{1-2} = \frac{|Apex_{peak1} - Apex_{peak2}|}{FWHM_{peak1} + FWHM_{peak2}} \times 1.18 \quad (2)$$

3.4 Results and Discussion

The analytical complexity of online direct lipid analyses using mass spectrometry (e.g., via direct infusion) originates from the small mass-to-charge (m/z) range within which most intact lipid species are detected: from m/z 500 to 1000, with some lipid subclasses above this m/z range. Within this 500 m/z range, many lipid species exhibit identical nominal masses, being isomers and isobars. The coupling of IMS to MS as a fast gas-phase pre-separation allows deconvoluting the lipid signals according to their mobilities (K_0) and m/z. When generating a 2D IMS-MS map, lipids cover a specific ion mobility region or trendline^{54, 95, 96}.

In the case of the TIMS setup, the scan rate ($Sr = \Delta V_{ramp} / \text{ramp time}$) correlates with the mobility resolving power; that is, wide voltage ranges or short ramp times yield lower resolution mobility measurements whereas narrow voltage ramps and long ramp times lead to higher resolution mobility measurements. By decreasing the TIMS voltage ramp range, the lipid regions of interest can be selectively isolated. The mobility resolving power can be increased nearly ~4x ($R = 60 - 295$), depending on the mobility range and scan time (data shown corresponds to a maximum of 500 ms per scan). For example, a mobility scan using

a $Sr = 0.18$ V/ms (90V over 500 ms) provides R up to 225 and separates ΔCCS of 1.9 \AA^2 for lipids in the 300-1500 m/z range. For visualization purposes, Appendix 9 shows the CCS profiles of three lipid standards as a function of the scan rate. These examples provide an estimate of the TIMS apparent resolving power as a function of the scan rate for the case of lipid species. Performance metrics showcasing peak resolutions and resolving powers using cTWIMS and TIMS for the lipid examples showcased in this work can be seen in Appendix 10.

One of the advantages of cTWIMS and TIMS is the possibility to adjust the mobility range of interest to increase the mobility resolution (Figure 3.2). In the case of cTWIMS, a portion of the mobility range (ATD window) is selected for subsequent supplementary IMS passes (or cycles), thus increasing the effective path length for these species leading to a net increase in the mobility resolution. As shown previously, in the case of TIMS, if the mobility range is decreased (ΔV_{ramp}) the slower scan rate will provide higher mobility resolution. These trends are illustrated for the case of the LESA mouse brain lipid extracts in Figure 3.2 and on standards in Appendix 9.

The 1-pass cTWIMS ($R \sim 70$)⁵⁹ and TIMS ($R \sim 60-70$ based on the lipid ions in Appendix 9) “discovery” measurements permit a quick overview of the lipids of interest from a complex biological sample. Given that the lipid m/z -mobility regions are well-defined, both the cTWIMS and TIMS instruments allow for increasing the mobility resolution by selectively isolating the mobility regions of interest. Green markers in Figure 3.2.a highlight previously- identified³⁵ lipid ions, using LESA-FT-ICR-MS(/MS) from wildtype mouse brain. In the cTWIMS setup, the identified specific arrival time region

from the low-resolution 1- pass measurement is then selected to undergo a higher-resolution 2-pass and 3-pass measurement (Figure 3.2.b).

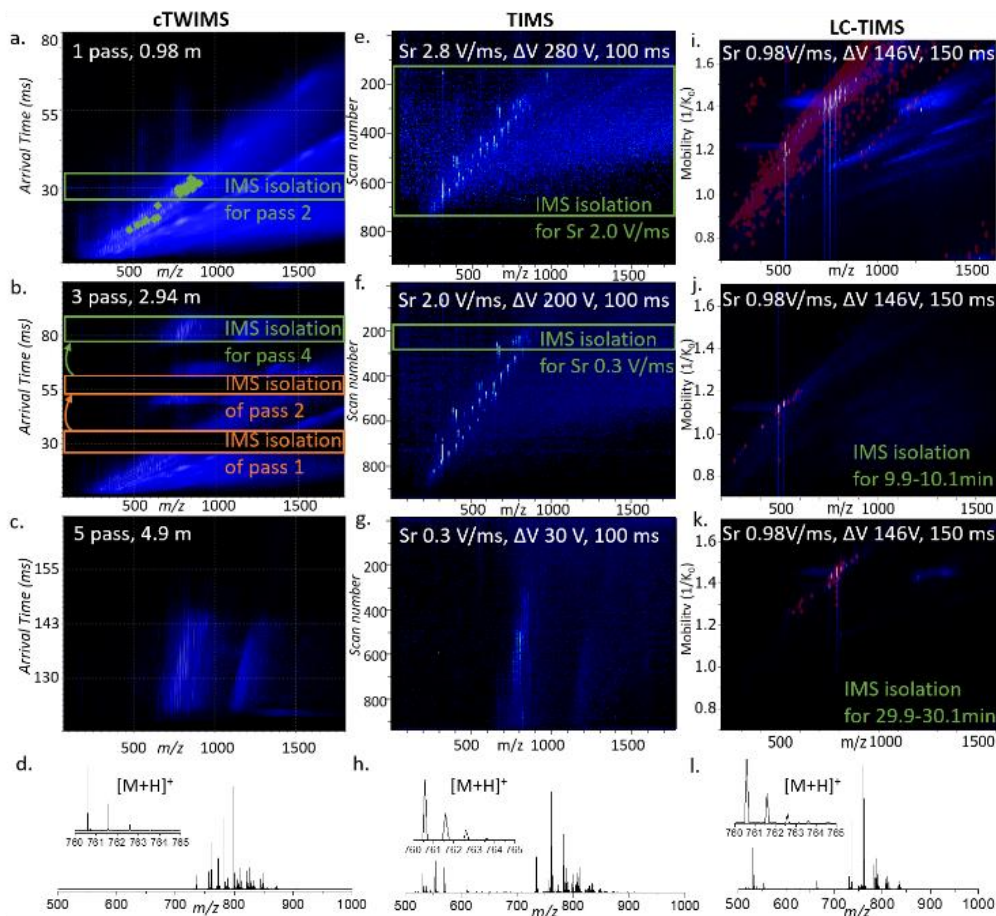


Figure 3.3. 2D-IMS-MS contour plots from a LESA mouse brain lipid extract using cTWIMS-TOF MS (left) and TIMS-TOF MS (middle) and LC-TIMS-CID TOF MS (right). a., e., and i. represent fast, wide mobility ranges. The green dots in a. highlight ions previously identified using LESA-FT-ICR-MS/(MS)³⁵. The green rectangles highlight the mobility ranges isolated for higher-resolution targeted measurements. b. and c. represent the mobility-selected cTWIMS 3 pass and 5 pass measurements, with d. showing the mass spectrum of the cTWIMS 5 pass measurement. f. and g. showcase the TIMS mobility-selected measurements at higher resolving power with h. showing the mass spectrum of the TIMS Sr 0.3 V/ms measurement. j. and k. showcase the TIMS mobility-selected measurements at specific chromatographic time; 9.9-10.1 min and 29.9-30.1 min, respectively.

The highest resolution mobility measurement while conserving the integrity of the lipid region of interest from m/z 700 to 950, is performed at 5 passes (Figure 3.2.c), where ions have then traveled a distance of about 4.90 m. According to experiments performed

on peptide standards, the cTWIMS resolving power scales as $70\sqrt{n}$ where n is the number of passes (e. g. $R\sim 155$ for $n=5$)⁵⁹. The higher resolution TIMS measurement also retains the m/z -mobility lipid region of interest (m/z 700-950; Figure 3.2.h).

The timescales required to achieve high mobility resolving power for both instruments are comparable and in the order of several hundred milliseconds for this mobility range. As a general guideline, the TIMS device can require ~ 400 - 500 ms to reach $R\sim 300$ (R /time ratio of ~ 0.55 ms^{-1}) while the cTWIMS device can require ~ 750 ms to reach $R\sim 305$ (R /time ratio of ~ 0.5 ms^{-1}). For example, the timescale of cTWIMS separation depends on the chosen T-wave height and velocity (here 35 V and 375 ms, respectively) and can be varied to achieve shorter (or longer) separation timescales. Analogously, the mobility range in the TIMS can be narrower, effectively lowering the scan rate over a shorter analysis time. For direct infusion experiments, the longer timescales provide a better analytical solution and can be effectively coupled to LESA extractions. For liquid chromatography separation experiments, shorter mobility separation timescales are a better fit to have enough sampling of the LC peaks, with the ultimate drawback of a lower mobility resolution.

The aim of the “discovery” mobility measurements is to obtain the highest possible mobility resolution over a wide mobility range. These discovery runs (non-targeted) allow for the screening of precursor molecular ions with potential (unresolved) multiple features in their mobility distributions. These chosen ions of interest can then be submitted to targeted ultrahigh-resolution mobility (resolving power > 200)⁹⁷ and quadrupole m/z selections combined with CID MS/MS to increase the confidence in the lipid assignment and limit potential interferences.

An example of a quadrupole-selected and mobility-selected “targeted” measurement is shown in Figure 3.3 for m/z 810.60 observed from the LESA mouse brain lipid extractions. Given that the required mass resolution to resolve the two potential isobaric candidates at m/z 800 is around 350k ($R=350k$), the use of ion mobility aided in the identification of potential candidates. The high-resolution cTWIMS and TIMS resolved two mobility bands and mobility-selected CID MS/MS provided the lipid identification. The identification of unique/characteristic fragments in the mobility selected CID MS/MS permitted the isobaric lipid species identification (see Appendix 11 for mobility selected CID MS/MS spectra from cTWIMS-qCID-TOF and TIMS-qCID-TOF, and Appendix 12 for fragment ion identification). The $[M+H]^+$ PC (18:0_20:4) corresponds to the mobility band at 295.3 \AA^2 (gray) and the $[M+Na]^+$ PC (18:0_18:1) to the mobility band at 298.6 \AA^2 (red). Also, two mobility bands and further confirmation using accurate mass of the assigned lipid species is brought by mobility-selected CID performed on a TIMS-FT-ICR MS (Figure 3.3c and Appendix 10). In the case that very high mass resolutions are needed but are not accessible, the quadrupole-selected and mobility-selected “targeted” CID MS/MS measurement allows to resolve and determine the identity of the isobaric species. Moreover, these assignments were confirmed with measured ion mobility profiles of lipid standards (Figure 3.3d).

The analysis of the same LESA extracts using LC-TIMS-CID TOF MS/MS provided confirmation of the two lipid assignments by their separation species in the LC domain and characteristic MS/MS patterns (Figure 3.3e.); however, the higher scan speed of the TIMS analyzer utilized during the LC operation did not resolve the two mobility bands (when considering only the m/z -IMS dimensions). This example illustrates the

advantages of high resolution IMS during direct infusion analysis for fast and accurate isobaric species identifications, with a significant reduction in the analysis time when compared to the LC-workflows.

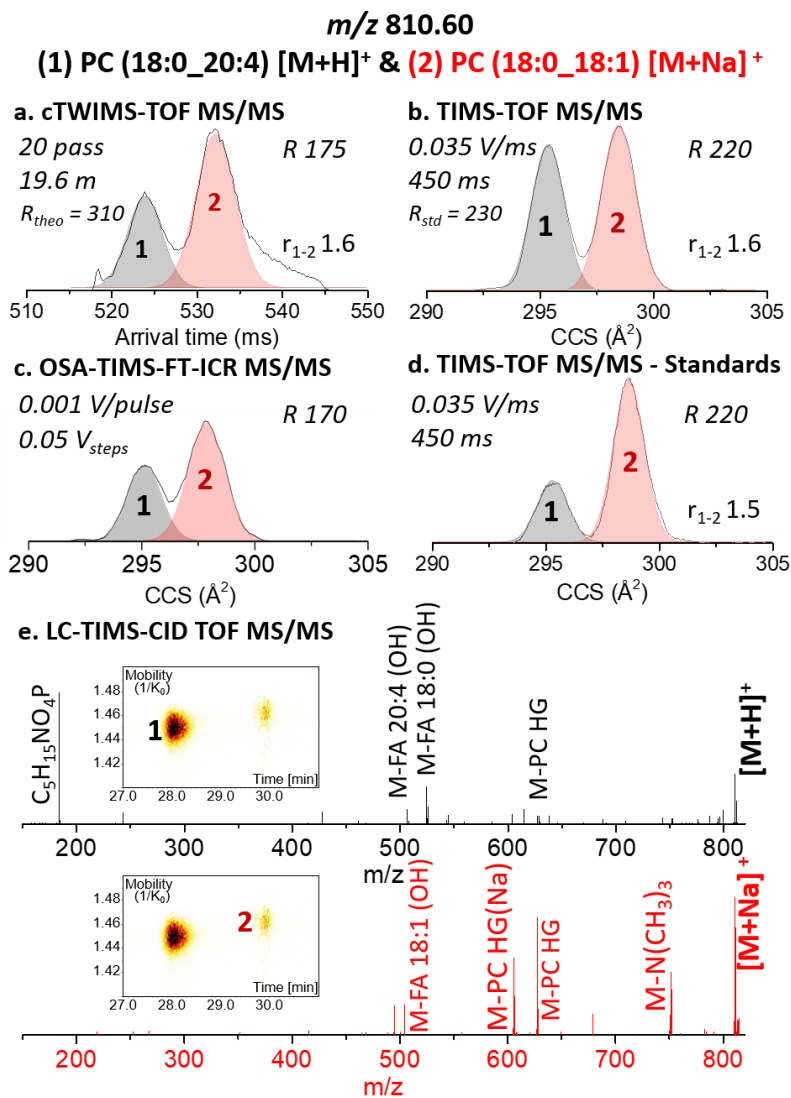


Figure 3.4. Typical IMS, IMS-LC and MS/MS profiles from m/z 810.60. a. cTWIMS-CID TOF MS/MS, b. TIMS-CID TOF MS/MS, c. OSA-TIMS-FT-ICR MS, d. TIMS-CID TOF MS/MS of lipid standards, and e. LC-TIMS-CID TOF MS/MS analysis. FA refers to Fatty Acid chain and HG refers to Headgroup.

During the direct analysis of the LESA extracts from the mouse brain and liver, cTWIMS-TOF and TIMS-TOF also allow for the investigation of isomeric lipids. An example is shown for the case of m/z 782.56. In both LESA extracts, m/z 782.56 exhibits two mobility bands with different relative intensities (Figure 3.4a). The mobility selected CID MS/MS spectra identified the both IMS bands as $[M+H]^+$ PC (36:4) (see Appendix 12 and Appendix 13 however, no information on the acyl chains was obtained from the positive mode fragments. A negative mode TIMS-MS/MS analysis of the corresponding the $[M+HCOO]^-$ ion suggested the presence of the 20:4 and 16:0 acyl chains (see Appendix 12 and 14). The LC-TIMS-CID MS/MS analysis of the LESA extracts provided complementary information on the sample isomeric complexity (Figure 3.4b). Three positional isomers were separated in the chromatography domain with respective CCS measurements (Appendix 12). Further lipid annotation was based on the comparison with lipid standards. By comparing the RT, CCS and mobility-selected CID MS/MS fragmentation pattern with the lipid standards, the isomeric mixture was identified as two acyl chain positional *sn*-1,2 isomers of $[M+H]^+$: 1) PC (20:4_16:0) and 2) PC (16:0_20:4), and the isomer 3) PC (18:2_18:2). This example illustrates the complexity of the isomeric content in biological samples as well as the analytical power of high resolution IMS. Besides the lipid isomeric assignment, the relative abundances can be derived from the IMS profiles per LESA extract. While the LC-TIMS-CID MS/MS and comparison with standards enabled the lipid isomeric assignment, the high-resolution “targeted” direct analysis provided the PC lipid class (head group in the MS/MS) and suggested the existence of positional isomers.

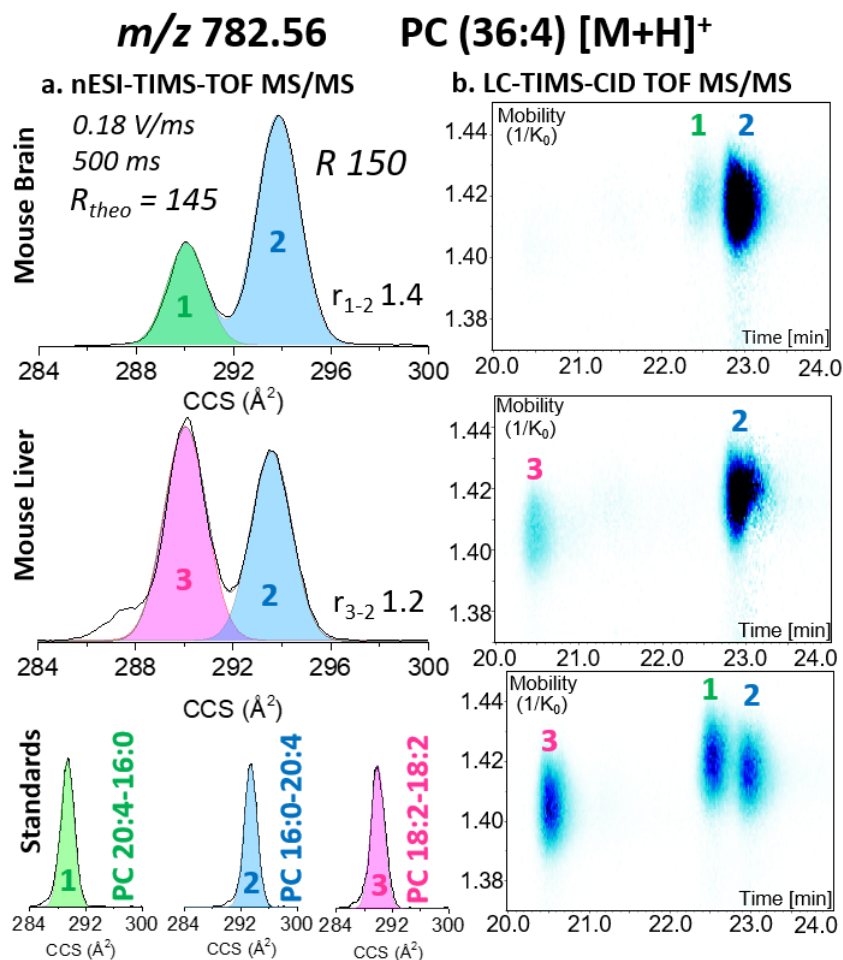


Figure 3.5. a. Targeted nESI-TIMS-CID-TOF MS/MS and b. LC-TIMS-CID TOF MS/MS of m/z 782.56 from LESA mouse brain and liver lipid extracts. In the bottom, IMS and IMS-LC of lipid standards used for assignment validation.

The direct infusion experiments of the LESA extracted samples from mouse brain and liver were compared with LC-based experiments. The LC-TIMS-CID MS/MS analysis were processed, and lipid assignments were made based on the comparison of MS/MS score and chemical formula with lipid libraries. Figure 3.5a shows the annotated lipid species per lipid class from the direct infusion experiments (nESI-LESA) and LC runs (LC LESA), where two LESA extraction solvents were used (LESA1 and LESA2, *cf.* Materials

and Methods section). The LC analysis provided a better lipid coverage when compared to the direct infusion analysis. A list of annotated lipid species from direct infusion and LC can be found in Appendix 15; molecular ion form, experimental mass, mass error, CCS values from direct infusion dataset and RT, CCS, MS/MS score and mass error from LC datasets are reported. Inspection of the relative abundances in the LC datasets suggest that lower abundance species were suppressed during direct infusion analysis; we attribute these to matrix effects during the ionization of the LESA extracts.

The influence of the LESA solvent on the lipid assignments is summarized in Figure 3.5b. Most of the lipids are observed in different molecular ion forms (e.g., several adducts or a water loss) regardless of the LESA solvent composition. In the case of the direct analysis of complex biological samples, the observation of different adducts is preferred for added confirmation of a specific lipid; a tradeoff to this approach compared to a unique adduct species (e.g., ammonium or sodium adduct) is that the observation of lower abundant species can be compromised. For example, most LPC lipid species were annotated by the protonated, sodiated and potassiated ion forms.

During the selection of the LESA solvent, an important criterion is the LESA solvent surface tension, which significantly influences the extraction capabilities and sample handling. To this end, water containing solvent are usually more effective for LESA operations. For both solvents, the predominant ion are the $[M+H]^+$, followed by the $[M+Na]^+$ and $[M+K]^+$. It can be observed that LESA1 solvent was able to extract some DG species that were not observed from LESA2 solvent dataset. Overall, both solvent extractions provided similar amounts of annotated lipid species. The use of both extraction

solvents allowed for the comparison of the extraction capacity of different lipid classes to select the best for lipid extraction from biological tissues⁹⁸.

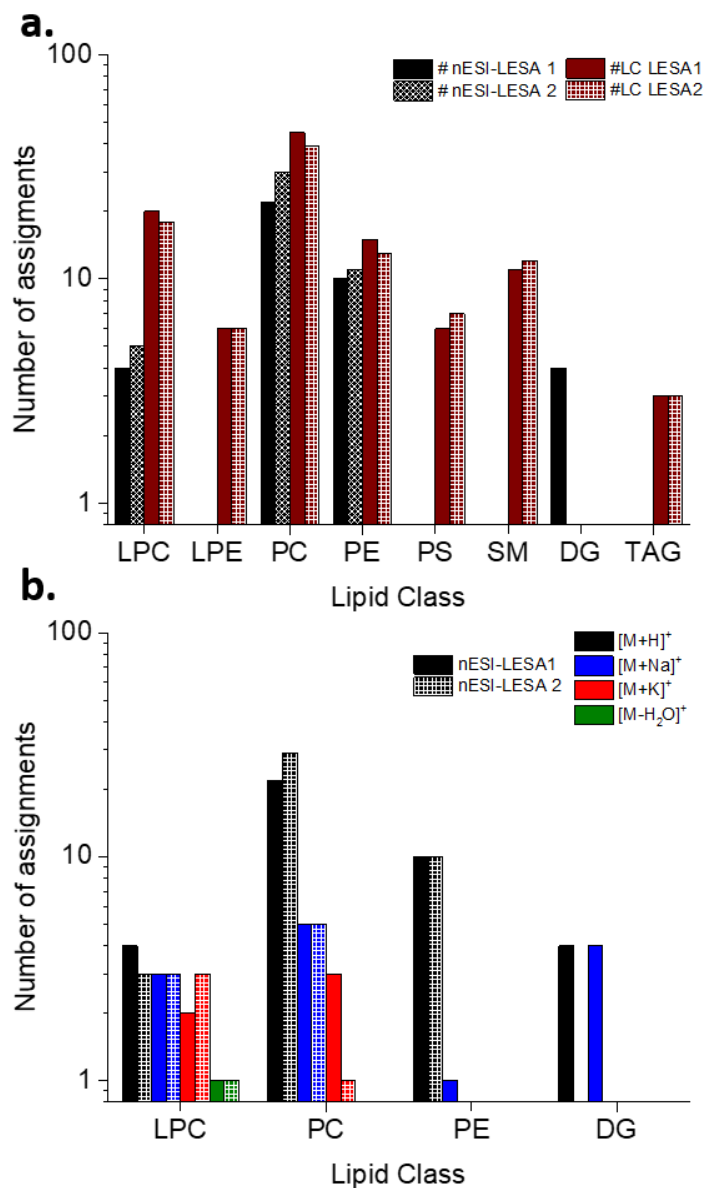


Figure 3.5. a. Number of annotated lipid species per lipid class based on the extraction solvent and analytical workflow and b. number of annotated lipids per lipid class based on the observed adducts from the different solvents in the direct infusion experiments datasets.

3.5 Conclusions

The performance of LESA direct infusion analysis by two high-resolution IMS-MS platforms – nESI-cTWIMSⁿ-CID-TOF MS/MS and nESI-TIMS-qCID-TOF MS/MS – from complex biological samples (wildtype mouse brain and liver) was evaluated. The potential of the direct infusion “discovery” and “targeted” ion mobility-mass spectrometry workflows were effectively illustrated on both instrument platforms. During the discovery runs, a wide mobility range covering lipids of m/z 300-1500 was selected, which allowed the lipid class differentiation and evaluation of the isomeric content. Lipid species exhibiting multiple ion mobility features underwent targeted ultrahigh-resolution mobility- and quadrupole-selected CID MS/MS. The comparison between the mouse brain and liver analyses showed the need for isomeric and/or isobaric separation during direct analysis; examples are shown where the same m/z signal was present in both samples while corresponding to different isomeric lipids at different levels.

The TIMS and cTWIMS separations yielded similar mobility apparent resolving powers ($R \sim 300$) under the conditions employed. In cases where similar mobility bands and features were observed, the TIMS measurements were performed at slightly shorter timescales (400-500 ms) when compared to the multi-pass cTWIMS experiments (500-750 ms). These numbers are provided as indicators of the experiment timescale, and further optimizations are possible depending on the analytical challenge. The presented data highlights the feasibility of LESA with high-resolution IMS-MS technologies for direct lipid profiling of biological surfaces. All in all, both setups were able to efficiently detect the presence of multiple lipid isomers/isobars during direct infusion analysis of complex biological samples.

Despite the complex nature of the biological samples, the high mobility resolution provided by cTWIMS and TIMS (resolving powers up to 310 in the applied experimental conditions in the present study) allowed the direct sampling of isomeric lipids from the biological surfaces in a short timescale (few min). A tradeoff of the direct infusion analysis was the observation of a lower number of lipid species when compared to the more time-consuming LC-based analysis of the LESA extracts (~1h). Indeed, the LC separation prior to ESI ionization allows for a better lipid coverage even though only lower ion mobility resolutions are accessible within the LC separation timeframe. This higher coverage resulted from the observation of lower abundance species and the reduction of ionization matrix effects.

LESA solvents containing water showed advantages during the sample handling with similar lipid IDs and ionic forms compared to organic LESA solvents. The observation of multiple molecular ion forms (e.g., adducts and water loss) provided more confidence during the lipid assignment based on mobility-selected CID MS/MS. Further implementation of alternative MS/MS techniques (e.g., OzID) can provide complementary information for the isomeric lipid assignment.

3.6 Acknowledgements

Prof. Helen J. Cooper and Emma K. Sisley (University of Birmingham) are thanked for their help with the LESA extraction protocols. Prof. Jeremy W. Chambers and Dr. Monica Rodríguez-Silva (Florida International University) are acknowledged for providing the wildtype mouse tissues used in this study. The work at FIU was supported by a National Institute of Allergy and Infectious Diseases (R21AI135469) and a NSF

CAREER (CHE-1654274), with co-funding from the Division of Molecular and Cellular Biosciences to FFL. JRNH acknowledges the Fulbright and Wallonie-Bruxelles International (WBI.WORLD) for financial support. YCD acknowledges the financial support from NSF FGLSAMP FIU Bridge to the Doctorate award HRD # 1810974. Waters (Wilmslow, UK) are gratefully acknowledged for access to a prototype cTWIMS instrument.

3.7 References

1. A. Shamim, T. Mahmood, F. Ahsan, A. Kumar and P. Bagga, *Clin Nutr Exp*, 2018, **20**, 1-19.
2. E. R. Schenk, F. Nau, C. J. Thompson, Y. C. Tse-Dinh and F. Fernandez-Lima, *J Mass Spectrom*, 2015, **50**, 88-94.
3. K. Yang and X. Han, *Trends Biochem Sci*, 2016, **41**, 954-969.
4. S. Furse, L. Richardson and A. Koulman, *Nutr Bull*, 2018, **43**, 296-300.
5. S. A. Murfitt, P. Zacccone, X. Wang, A. Acharjee, Y. Sawyer, A. Koulman, L. D. Roberts, A. Cooke and J. L. Griffin, *J Proteom Res*, 2018, **17**, 946-960.
6. N.-N. Zhao, Y.-F. Sun, L. Zong, S. Liu, F.-R. Song, Z.-Q. Liu and S.-Y. Liu, *Int J Mass Spectrom*, 2018, **434**, 29-36.
7. E. Fahy, M. Sud, D. Cotter and S. Subramaniam, *Nucleic Acids Res*, 2007, **35**, W606-612.
8. E. Fahy, S. Subramaniam, H. A. Brown, C. K. Glass, A. H. Merrill, Jr., R. C. Murphy, C. R. Raetz, D. W. Russell, Y. Seyama, W. Shaw, T. Shimizu, F. Spener, G. van Meer, M. S. VanNieuwenhze, S. H. White, J. L. Witztum and E. A. Dennis, *J Lipid Res*, 2005, **46**, 839-861.
9. E. Fahy, S. Subramaniam, R. C. Murphy, M. Nishijima, C. R. Raetz, T. Shimizu, F. Spener, G. van Meer, M. J. Wakelam and E. A. Dennis, *J Lipid Res*, 2009, **50 Suppl**, S9-14.
10. J. K. Pauling, M. Hermansson, J. Hartler, K. Christiansen, S. F. Gallego, B. Peng, R. Ahrends and C. S. Ejsing, *PLoS One*, 2017, **12**, e0188394.

11. G. van Meer, D. R. Voelker and G. W. Feigenson, *Nat Rev Mol Cell Biol*, 2008, **9**, 112-124.
12. C. Bielow, G. Mastrobuoni, M. Orioli and S. Kempa, *Anal Chem*, 2017, **89**, 2986-2994.
13. B. L. J. Poad, D. L. Marshall, E. Harazim, R. Gupta, V. R. Narreddula, R. S. E. Young, E. Duchoslav, J. L. Campbell, J. A. Broadbent, J. Cvacka, T. W. Mitchell and S. J. Blanksby, *J Am Soc Mass Spectrom*, 2019, **30**, 2135-2143.
14. J. W. Jones, C. J. Thompson, C. L. Carter and M. A. Kane, *J Mass Spectrom*, 2015, **50**, 1327-1339.
15. C. Giles, R. Takechi, V. Lam, S. S. Dhaliwal and J. C. L. Mamo, *Prog Lipid Res*, 2018, **71**, 86-100.
16. P. Li and G. P. Jackson, *J Mass Spectrom*, 2017, **52**, 271-282.
17. S. Sethi and E. Brietzke, *Prostag Oth Lipid M*, 2017, **128-129**, 8-16.
18. R. C. Murphy, *Trends Analyt Chem*, 2018, **107**, 91-98.
19. C. Hu, C. Wang, L. He and X. Han, *Trends Analyt Chem*, 2019, **120**.
20. A. P. Bowman, R. M. A. Heeren and S. R. Ellis, *Trends Analyt Chem*, 2019, **120**, 1-10.
21. P. Sjövall, B. Johansson and J. Lausmaa, *Appl Surf Sci*, 2006, **252**, 6966-6974.
22. K. J. Adams, J. D. DeBord and F. Fernandez-Lima, *J Vac Sci Technol B Nanotechnol Microelectron*, 2016, **34**, E051804.
23. M. L. Kraft and H. A. Klitzing, *Biochim Biophys Acta*, 2014, **1841**, 1108-1119.
24. D. Gode and D. A. Volmer, *Analyst*, 2013, **138**, 1289-1315.
25. A. Castellanos, C. E. Ramirez, V. Michalkova, M. Nouzova, F. G. Noriega and F. L. Francisco, *J Anal At Spectrom*, 2019, **34**, 874-883.
26. B. M. Prentice, J. C. McMillen and R. M. Caprioli, *Int J Mass Spectrom*, 2019, **437**, 30-37.
27. C. Schone, H. Hofler and A. Walch, *Clin Biochem*, 2013, **46**, 539-545.
28. F. Barré, B. Rocha, F. Dewez, M. Towers, P. Murray, E. Claude, B. Cillero-Pastor, R. Heeren and T. Porta Siegel, *Int J Mass Spectrom*, 2019, **437**, 38-48.

29. A. S. Mohammadi, N. T. Phan, J. S. Fletcher and A. G. Ewing, *Anal Bioanal Chem*, 2016, **408**, 6857-6868.
30. B. Fuchs, *J Chromatogr A*, 2012, **1259**, 62-73.
31. V. Kertesz, M. J. Ford and G. J. Van Berkel, *Anal Chem*, 2005, **77**, 7183-7189.
32. V. Kertesz and G. J. Van Berkel, *J Mass Spectrom*, 2010, **45**, 252-260.
33. T. Wachs and J. Henion, *Anal Chem*, 2001, **73**, 632-638.
34. E. C. Randall, A. M. Race, H. J. Cooper and J. Bunch, *Anal Chem*, 2016, **88**, 8433-8440.
35. J. R. N. Haler, E. K. Sisley, Y. L. Cintron-Diaz, S. N. Meitei, H. J. Cooper and F. Fernandez-Lima, *Anal Methods*, 2019, **11**, 2385-2395.
36. L. Zong, Z. Pi, S. Liu, J. Xing, Z. Liu and F. Song, *Rapid Commun Mass Spectrom*, 2018, **32**, 1683-1692.
37. R. Almeida, Z. Berzina, E. C. Arnspang, J. Baumgart, J. Vogt, R. Nitsch and C. S. Ejsing, *Anal Chem*, 2015, **87**, 1749-1756.
38. Y. Satomi, M. Hirayama and H. Kobayashi, *J Chromatogr B* 2017, **1063**, 93-100.
39. M. Lisa, E. Cifkova, M. Khalikova, M. Ovcacikova and M. Holcapek, *J Chromatogr A*, 2017, **1525**, 96-108.
40. W. Lv, X. Shi, S. Wang and G. Xu, *Trends Analyt Chem*, 2018, **120**, 115302.
41. S. Bhattacharya, *Lipidomics: Methods and Protocols*, Humana Press, 1 edn., 2017.
42. T. Cajka and O. Fiehn, *Anal Chem*, 2016, **88**, 524-545.
43. H. C. Lee and T. Yokomizo, *Biochem Biophys Res Commun*, 2018, **504**, 576-581.
44. E. Altuntaş and U. S. Schubert, *Anal Chim Acta*, 2014, **808**, 56-69.
45. T. P. Lintonen, P. R. Baker, M. Suoniemi, B. K. Ubhi, K. M. Koistinen, E. Duchoslav, J. L. Campbell and K. Ekroos, *Anal Chem*, 2014, **86**, 9662-9669.
46. M. C. Thomas, T. W. Mitchell, D. G. Harman, J. M. Deeley, J. R. Nealon and S. J. Blanksby, *Anal Chem*, 2008, **80**, 303-311.
47. J. Godzien, M. Ciborowski, M. P. Martinez-Alcazar, P. Samczuk, A. Kretowski and C. Barbas, *J Proteome Res*, 2015, **14**, 3204-3216.

48. S. Rojas-Betancourt, J. R. Stutzman, F. A. Londry, S. J. Blanksby and S. A. McLuckey, *Anal Chem*, 2015, **87**, 11255-11262.
49. S. R. Ellis, H. T. Pham, M. In Het Panhuis, A. J. Trevitt, T. W. Mitchell and S. J. Blanksby, *J Am Soc Mass Spectrom*, 2017, **28**, 1345-1358.
50. K. Giles, S. D. Pringle, K. R. Worthington, D. Little, J. L. Wildgoose and R. H. Bateman, *Rapid Commun Mass Spectrom*, 2004, **18**, 2401-2414.
51. M. Groessl, S. Graf and R. Knochenmuss, *Analyst*, 2015, **140**, 6904-6911.
52. J. C. May, J. N. Dodds, R. T. Kurulugama, G. C. Stafford, J. C. Fjeldsted and J. A. McLean, *Analyst*, 2015, **140**, 6824-6833.
53. A. A. Shvartsburg, *Differential Ion Mobility Spectrometry: Nonlinear Ion Transport and Fundamentals of FAIMS*, CRC Press, 1st edn., 2008.
54. A. A. Shvartsburg, G. Isaac, N. Leveque, R. D. Smith and T. O. Metz, *J Am Soc Mass Spectrom*, 2011, **22**, 1146-1155.
55. V. Gabelica, A. A. Shvartsburg, C. Afonso, P. Barran, J. L. P. Benesch, C. Bleiholder, M. T. Bowers, A. Bilbao, M. F. Bush, J. L. Campbell, I. D. G. Campuzano, T. Causon, B. H. Clowers, C. S. Creaser, E. De Pauw, J. Far, F. Fernandez-Lima, J. C. Fjeldsted, K. Giles, M. Groessl, C. J. Hogan, Jr., S. Hann, H. I. Kim, R. T. Kurulugama, J. C. May, J. A. McLean, K. Pagel, K. Richardson, M. E. Ridgeway, F. Rosu, F. Sobott, K. Thalassinou, S. J. Valentine and T. Wytenbach, *Mass Spectrom Rev*, 2019, **38**, 291-320.
56. C. G. Vasilopoulou, K. Sulek, A. Brunner, N. S. Meitei, U. Schweiger-Hufnagel, S. Meyer, A. Barsch, M. Mann and F. Meier, *Nat Commun*, 2020, **11**, 1-11.
57. C. Hinz, S. Liggi and J. L. Griffin, *Curr Opin Chem Biol*, 2018, **42**, 42-50.
58. K. Giles, J. P. Williams and I. Campuzano, *Rapid Commun Mass Spectrom*, 2011, **25**, 1559-1566.
59. K. Giles, J. Ujma, J. Wildgoose, S. Pringle, K. Richardson, D. Langridge and M. Green, *Anal Chem*, 2019, **91**, 8564-8573.
60. F. A. Fernandez-Lima, D. A. Kaplan and M. A. Park, *Rev Sci Instrum*, 2011, **82**, 126106.
61. F. A. Fernandez-Lima, D. A. Kaplan, J. Suetering and M. A. Park, *Int J Ion Mobil Spectrom*, 2011, **14**.
62. P. Dugourd, H. R. R., D. E. Clemmer and M. F. Jarrold, *Rev Sci Instrum*, 1996, **68**, 1122-1129.

63. P. R. Kemper, N. F. Dupuis and M. T. Bowers, *Int J Mass Spectrom*, 2009, **287**, 46-57.
64. L. Deng, Y. M. Ibrahim, A. M. Hamid, S. V. Garimella, I. K. Webb, X. Zheng, S. A. Prost, J. A. Sandoval, R. V. Norheim, G. A. Anderson, A. V. Tolmachev, E. S. Baker and R. D. Smith, *Anal Chem*, 2016, **88**, 8957-8964.
65. L. Deng, I. K. Webb, S. V. B. Garimella, A. M. Hamid, X. Zheng, R. V. Norheim, S. A. Prost, G. A. Anderson, J. A. Sandoval, E. S. Baker, Y. M. Ibrahim and R. D. Smith, *Anal Chem*, 2017, **89**, 4628-4634.
66. J. Tu, Z. Zhou, T. Li and Z. Zhu, *Trends Analyt Chem*, 2019, **116**, 332-339.
67. R. A. Harris, K. L. Leaptrot, J. C. May and J. A. McLean, *Trends Analyt Chem*, 2019, **116**, 316-323.
68. K. E. Burnum-Johnson, X. Zheng, J. N. Dodds, J. Ash, D. Fourches, C. D. Nicora, J. P. Wendler, T. O. Metz, K. M. Waters, J. K. Jansson, R. D. Smith and E. S. Baker, *Trends Analyt Chem*, 2019, **116**, 292-299.
69. S. Trimpin, C. A. Lutomski, T. J. El-Baba, D. W. Woodall, C. D. Foley, C. D. Manly, B. Wang, C. Liu, B. M. Harless, R. Kumar, L. F. Imperial and E. D. Inutan, *Int J Mass Spectrom*, 2015, **377**, 532-545.
70. J. C. May, C. R. Goodwin, N. M. Lareau, K. L. Leaptrot, C. B. Morris, R. T. Kurulugama, A. Mordehai, C. Klein, W. Barry, E. Darland, G. Overney, K. Imatani, G. C. Stafford, J. C. Fjeldsted and J. A. McLean, *Anal Chem*, 2014, **86**, 2107-2116.
71. X. Zheng, R. D. Smith and E. S. Baker, *Curr Opin Chem Biol*, 2018, **42**, 111-118.
72. K. M. Hines, J. C. May, J. A. McLean and L. Xu, *Anal Chem*, 2016, **88**, 7329-7336.
73. K. Jeanne Dit Fouque, C. E. Ramirez, R. L. Lewis, J. P. Koelmel, T. J. Garrett, R. A. Yost and F. Fernandez-Lima, *Anal Chem*, 2019, **91**, 5021-5027.
74. A. Baglai, A. F. G. Gargano, J. Jordens, Y. Mengerink, M. Honing, S. van der Wal and P. J. Schoenmakers, *J Chromatogr A*, 2017, **1530**, 90-103.
75. W. B. Ridenour, M. Kliman, J. A. McLean and R. M. Caprioli, *Anal Chem*, 2010, **82**, 1881-1889.
76. K. Jeanne Dit Fouque and F. Fernandez-Lima, *Trends Analyt Chem*, 2019, **116**, 308-315.

77. E. A. Mason and E. W. McDaniel, *Transport Properties of Ions in Gases*, Wiley, New York, 1988.
78. W. Rao, A. D. Celiz, D. J. Scurr, M. R. Alexander and D. A. Barrett, *J Am Soc Mass Spectrom*, 2013, **24**, 1927-1936.
79. L. Deng, Y. M. Ibrahim, E. S. Baker, N. A. Aly, A. M. Hamid, X. Zhang, X. Zheng, S. V. B. Garimella, I. K. Webb, S. A. Prost, J. A. Sandoval, R. V. Norheim, G. A. Anderson, A. V. Tolmachev and R. D. Smith, *ChemistrySelect*, 2016, **1**, 2396-2399.
80. R. Wojcik, I. K. Webb, L. Deng, S. V. Garimella, S. A. Prost, Y. M. Ibrahim, E. S. Baker and R. D. Smith, *Int J Mol Sci*, 2017, **18**.
81. D. E. Clemmer and M. F. Jarrold, *J Mass Spectrom*, 1997, **32**, 577-592.
82. G. von Helden, M. Hsu, P. R. Kemper and M. T. Bowers, *J Chem Phys*, 1991, **95**, 3835-3837.
83. S. I. Merenbloom, R. S. Glaskin, Z. B. Henson and D. E. Clemmer, *Anal Chem*, 2009, **81**, 1482-1487.
84. R. S. Glaskin, M. A. Ewing and D. E. Clemmer, *Anal Chem*, 2013, **85**, 7003-7008.
85. A. P. Bowman, R. R. Abzalimov and A. A. Shvartsburg, *J Am Soc Mass Spectrom*, 2017, **28**, 1552-1561.
86. A. A. Shvartsburg, F. Li, K. Tang and R. D. Smith, *Anal Chem*, 2007, **79**, 1523-1528.
87. A. T. Maccarone, J. Duldig, T. W. Mitchell, S. J. Blanksby, E. Duchoslav and J. L. Campbell, *J Lipid Res*, 2014, **55**, 1668-1677.
88. M. E. Ridgeway, J. J. Wolff, J. A. Silveira, C. Lin, C. E. Costello and M. A. Park, *Int J Ion Mobil Spectrom*, 2016, **19**, 77-85.
89. D. R. Hernandez, J. D. DeBord, M. E. Ridgeway, D. A. Kaplan, M. A. Park and F. Fernandez-Lima, *Analyst*, 2014, **139**, 1913-1921.
90. J. R. N. Haler, P. Massonnet, F. Chiro, C. Kune, C. Comby-Zerbino, J. Jordens, M. Honing, Y. Mengerink, J. Far, P. Dugourd and E. De Pauw, *J Am Soc Mass Spectrom*, 2018, **29**, 114-120.
91. J. E. Kyle, X. Zhang, K. K. Weitz, M. E. Monroe, Y. M. Ibrahim, R. J. Moore, J. Cha, X. Sun, E. S. Lovelace, J. Wagoner, S. J. Polyak, T. O. Metz, S. K. Dey, R. D. Smith, K. E. Burnum-Johnson and E. S. Baker, *Analyst*, 2016, **141**, 1649-1659.

92. F. Meier, S. Beck, N. Grassl, M. Lubeck, M. A. Park, O. Raether and M. Mann, *J Proteome Res*, 2015, **14**, 5378-5387.
93. P. Benigni and F. A. Fernandez-Lima, *Anal Chem*, 2016, **88**, 7404-7412.
94. *United States of America Pat.*, 5872357, 1999.
95. J. C. May, C. B. Morris and J. A. McLean, *Anal Chem*, 2017, **89**, 1032-1044.
96. J. C. May, C. R. Goodwin and J. A. McLean, *Curr Opin Biotechnol*, 2015, **31**, 117-121.
97. A. T. Kirk, A. Bohnhorst, C. R. Raddatz, M. Allers and S. Zimmermann, *Anal Bioanal Chem*, 2019, **411**, 6229-6246.
98. S. R. Ellis, C. J. Ferris, K. J. Gilmore, T. W. Mitchell, S. J. Blanksby and M. in het Panhuis, *Anal Chem*, 2012, **84**, 9679-9683.

**CHAPTER 4. Mapping chemotherapeutic drug distribution in cancer cell spheroids
using 2D-TOF-SIMS and LESA-TIMS-MS**

Yarixa L. Cintron-Diaz, Arlet M. Acanda de la Rocha, Anthony Castellanos, Jeremy
Chambers and Francisco Fernandez-Lima,

This chapter was published in Analyst and reproduced with permission.
2020, DOI: 10.1039/C9AN02245G

4.1 Abstract

Three-dimensional (3D) cancer cell cultures grown in the form of spheroids are effective models for the study of *in-vivo-like* processes simulating cancer tumor pharmacological dynamics and morphology. In this study, we show the advantages of Time-of-Flight Secondary Ion Mass Spectrometry (TOF-SIMS) combined with *in-situ* Liquid Extraction Surface Analysis coupled to trapped Ion Mobility Spectrometry Mass Spectrometry (LESA-TIMS-TOF MS) for high spatial resolution mapping and quantitation of ABT-737, a chemotherapeutic drug, at the level of single human colon carcinoma cell spheroids (HCT 116 MCS). 2D-TOF-SIMS studies of consecutive sections (~16 μm thick slices) showed that ABT-737 is homogeneously distributed in the outer layers of the HCT 116 MCS. Complementary *in situ* LESA-TIMS-TOF MS/MS measurements confirmed the presence of the ABT-737 drug in the MCS slides by the observation of the molecular ion $[M+H]^+$ m/z and mobility, and characteristic fragmentation pattern. The LESA-TIMS-TOF MS allowed a quantitative assessment of the ABT-737 drug of the control MCS slice spiked with ABT-737 standard over the 0.4 – 4.1 ng range and MCS treated starting at 10 μM for 24h ($\text{IC}_{50} \sim 17.5 \mu\text{M}$). These experiments showcase an effective protocol for unambiguous characterization and 3D mapping of chemotherapeutic drug distribution at single MCS level.

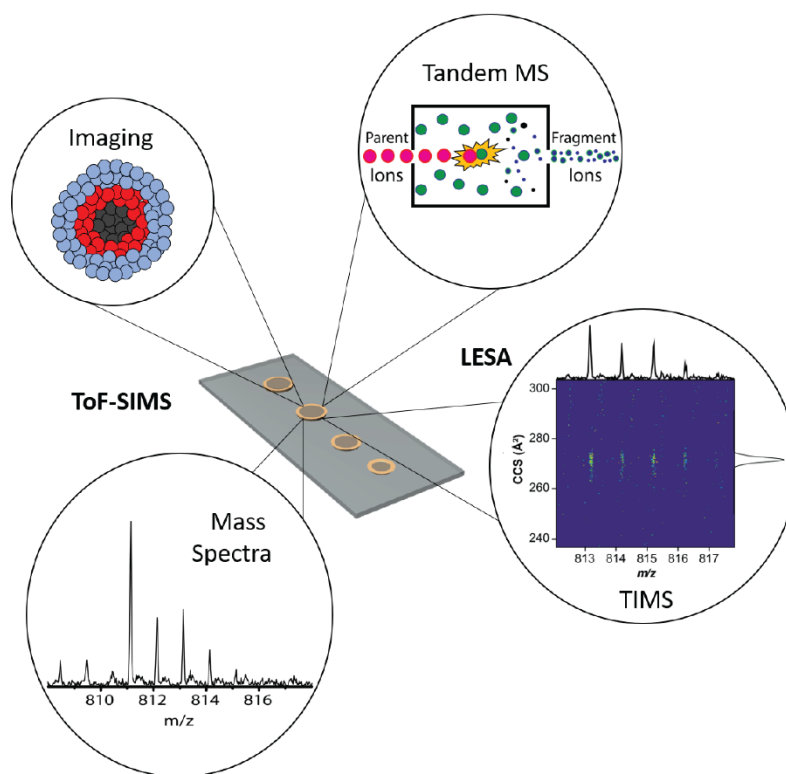


Figure 4.1 Graphical Abstract of Chapter 4

4.2 Introduction

Three-dimensional multicellular spheroids (MCSs) are emerging as an alternative model to study the physiology of cancer tumors and evaluate drug distribution within a tumor¹. These 3D tumor models permits the analysis of *in-vivo-like* processes and cell conditions, including differences in cell types within each MCS². When compared to the use of animal models to follow tumor development, MCS present several advantages in reproducibility, rate of growth and cost effectiveness³.

Mass spectrometry (MS) techniques have been used for the study of various cancers^{4,5}, ranging from cancer cell proteomics to clinical applications⁶. MS has proven to be a powerful tool to investigate the molecular content from biological samples and to map

at the molecular level their complex spatial distributions⁷. For example, in the case of MCS, MS has been successfully employed to identify extracellular compounds⁸. Mass spectrometry imaging (MSI) has provided information on the protein content within MCS⁹. Chemotherapeutic agents and their metabolites (e.g. Irinotecan and their metabolites) have been characterized in MCS with high spatial resolution MS¹⁰.

Recent advancements in ion sources for Secondary Ion Mass Spectrometry (SIMS) has extended their use in biological applications with high spatial resolution (submicrometric)¹¹. In a recent work, we showcase the potential of SIMS to follow the drug delivery of ABT-737 at the single cell level using 3D-TOF SIMS¹². In addition, SIMS has been successfully applied to differentiate cancerous and non-cancerous tissues based on lipid profiles, and it has been suggested as diagnostic tools for screening purposes¹³.

While most of the MSI probes require special sample preparation, Liquid Extraction Surface Analysis (LESA) is rapidly emerging as an ambient pressure solution for fast screening and characterization of biological samples that can be easily coupled to traditional MS workflows (e.g., lipid^{14, 15} and protein¹⁶⁻¹⁸ profiling). When complemented with other separation techniques (e.g., Liquid chromatography, LC¹⁹, and/or ion mobility spectrometry, IMS²⁰⁻²²), LESA can provide extensive characterization with minimum sample preparation¹⁴. Previous reports have demonstrated how LESA can serve as a profiling tool for drug and metabolite distribution (e.g. terfenadine and chloroquine) in whole-body tissue sections^{23, 24}. It has also been proved how LESA can be used for lipidomic profiling of various cancer cell lines¹⁵.

In this study, we showcase the potential of MSI-TOF-SIMS for the identification, localization, and distribution of ABT-737 drug in a HCT 116 cell spheroid model. ABT-

737 is a Bcl-2 small-molecule inhibitor which has been proved to be beneficial in preclinical and clinical cancer treatment²⁵. ABT-737 is a BH3 mimetic drug that, by binding and inhibiting Bcl-2 proteins, promotes pro-apoptotic proteins that trigger cell death²⁶. The use of TOF-SIMS allows for high spatial resolution analysis. Complementary *in situ* LESA-IMS-MS measurements will increase the confidence and quantify the levels of ABT-737 per MCS as a function of the drug concentration in the cell media.

IMS has shown many advantages for trace detection of small molecules (e.g., explosives²⁷, illicit drugs²⁸, petroleum²⁹, and natural products³⁰ among others). In particular, one of the IMS variants, trapped IMS (TIMS³¹⁻³³) has shown several advantages due to higher mobility resolution³⁴, ease of coupling to MS and high sensitivity in a wide range of analytical applications (e.g., small molecules³⁵⁻³⁸, proteomics^{39, 40}, lipidomic⁴¹, and DNA^{42, 43} among others). The ABT-737 drug per MCS secondary conformation and quantitation will be performed based on the ABT-737 [M+H]⁺ mobility and fragmentation pattern in a LESA-TIMS-TOF MS/MS platform.

4.3 Materials and Methods

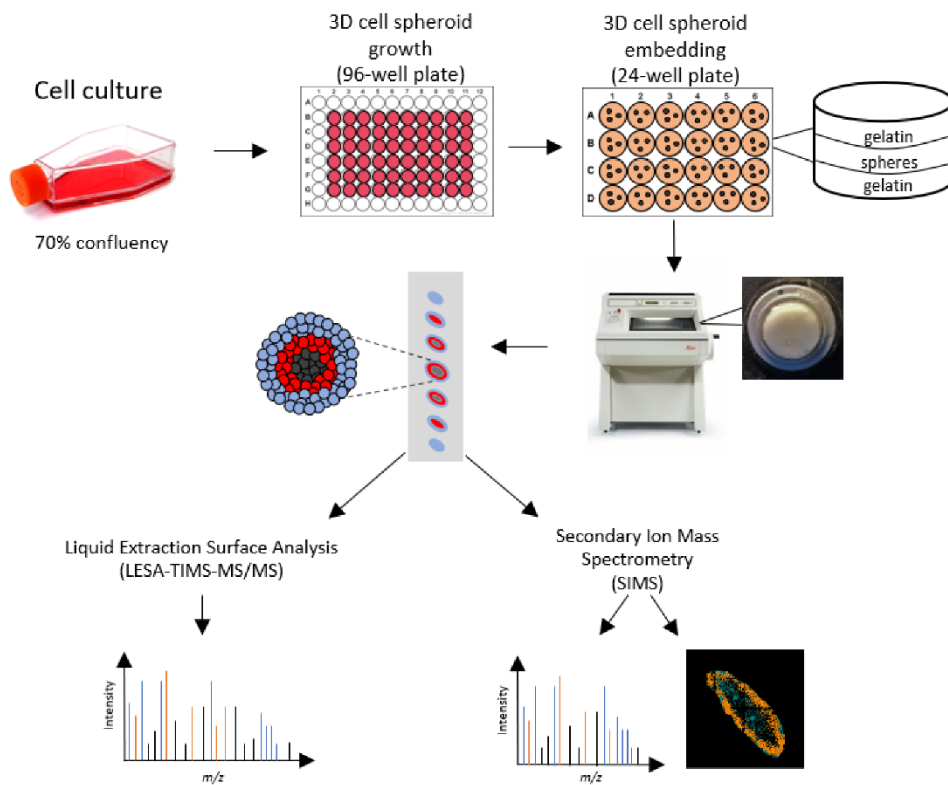


Figure 4.2. Workflow for MCS characterization using TOF-SIMS for chemical mapping and *in situ* LESA-TIMS-MS/MS for drug delivery secondary confirmation and quantitative analysis.

4.3.1 Cell Culture

Human colon cancer cell line HCT-116 was purchased from American Type Culture Collection (ATCC, Manassas, VA). Cell line was cultured according to the supplier's instructions in McCoy's 5A media (Corning), supplemented with 10% Fetal Bovine Serum (Gibco), 1000 U/mL Penicillin, 100 mg/mL Streptomycin (Gibco), 1% l-glutamax and 5 $\mu\text{g}/\text{mL}$ Plasmocin (Invivogen, San Diego, CA). Cells were grown under normal cell culture conditions at 37 $^{\circ}\text{C}$ and under 5% CO_2 . Cell passage was performed every four days. HCT-116 cell line was used within three months after resuscitation of

frozen aliquots thawed from liquid nitrogen. The provider assured the authentication of these cell lines.

4.3.2 MCS Formation

Friedrich et al. protocol was used to generate the spheres in a flat-bottomed 96-well microtiter plates (ThermoFisher)⁴⁴. Briefly, an agarose solution was prepared by dissolving 0.15 g of agarose (Bio-Rad, Hercules, CA) in 10 mL of McCoy's 5a cell culture media and autoclaved for 30 min at 120 °C and 200 kPa. A volume of 50 µL of the agarose solution was added to the inner 60 wells of a 96-well plate. The agarose solidified in around 30 s after being transferred into the well. The plate was covered to allow it to cool down at room temperature and then stored in a 4°C refrigerator.

Cell suspension was prepared by enzymatic dissociation using a 0.25% Trypsin solution (Gibco) and the cells were counted using a hemocytometer. The cell suspension was diluted in McCoy's 5A cell culture media to ~30 cells/µL. Cells were seeded into each of the wells in the agarose-coated cell culture plate at a density of 6000 cells/well in a final volume of 200 µL/well. The cells were incubated under normal cell culture conditions at 37 °C and under 5% CO₂, and the culture media was carefully replenished every 3-5 days until spheres reached an average size of ~1 mm. The uniform and compact MCSs were used for follow-up studies. MCSs were analyzed in biological triplicates.

4.3.3 Drug Treatment of MCS

BH3-only mimetic ABT-737 was purchased from Santa Cruz Biotechnology (Dallas, TX, USA). The stock solution of ABT-737 was prepared in dimethyl sulfoxide

(DMSO; Sigma-Aldrich, St. Louis, MO, USA) and further diluted into McCoy's 5A cell culture media as needed. We evaluated the efficacy after 72 hours of MCS exposure to ABT-737 over a 0-100 μM range. The relative amount of cell death in the population of cells outside of the necrotic core of the MCS was determined using Calcein AM staining combined with propidium iodide, as previously reported^{45,46}. An IC_{50} of $28 \pm 12 \mu\text{M}$ was detected for ABT-737 in HCT-116 MCS at 72 hours. The reported IC_{50} cell viability value of ABT-737 in HCT-116 cells is $17.5 \mu\text{M}$ ⁴⁷. Moreover, during clinical treatment, the ABT-737 plasma concentration levels are $5.4 - 7.7 \mu\text{M}$ ⁴⁸. Since the IC_{50} value measured for MCS is likely supraphysiological, we treated the MCS starting with a lower range to address clinically relevant levels. That is, MCS were treated for 24 h with varying drug concentrations: control, 1 μM , 5 μM , 10 μM , 15 μM , 25 μM , 50 μM , and 100 μM . The treatment time was chosen to assure drug uptake without significant cell death. Untreated MCSs were used for control purposes.

4.3.4 MCSs Embedding and Cryosectioning

A 24 well plate was prepared by adding 100 μL of warm gelatin into each well, as proposed by Li and collaborators⁹. Cell spheroids were gently transferred via a serological pipette and placed on top of the already solidified gelatin. A second layer of 100 μL of gelatin was added to cover the spheroids. The 24 well plate was stored in a -80°C freezer before sectioning. The embedded cells were removed from the 24 well plate and sliced to 16 μm thickness using a Leica CM 3050 cryostat (Leica Biosystems, Nussloch, Germany) and thaw mounted into glass slides. Approximately 20 slices at varying depths per MCS were obtained, but only the top half (~10 slices) of the MCS was sampled.

4.3.5. Liquid Extraction Surface Analysis coupled to Trapped Ion Mobility Spectrometry-Mass Spectrometry (LESA-TIMS-MS/MS)

Glass slides with MCS slices were placed on the LESA universal adaptor plate and the location of extraction was manually identified. Liquid Extraction Surface Analysis (LESA) was performed using a TriVersa Nanomate device (Advion, Ithaca, NY, USA) in micro-junction mode. To perform the extraction, an automated arm was relocated on top of the solvent well and aspirated 5 μL of solvent. The robotic arm relocated on top of the desired spot in the MCS sample and descended to a 1.9 mm dispensation height to place 1.0 μL of solvent and form a liquid micro junction between the surface and the solvent. Solvent droplet stayed in contact with the surface for 10 s, re-aspirated and re-dispensed for another 10 s. After this time, 1.5 μL of solvent was re-aspirated and dispensed into a specific well in a 96 well plate. Each extraction covered the entire MCS section on the slide. A peptide internal standard (Human Angiotensin II, 1046 m/z) was prepared to 1 μM concentration and added to the extraction solvent ethanol, water and formic acid (60:39.9:0.1); the peptide internal standard allowed to correct for variations in the LESA tip extraction and nESI spraying conditions across experiments. A calibration curve was developed using control MCS slides spiked with a 0.5 μL drop of ABT-737 standards in the 0.406-4.066 ng range. The calibration curve points used were 0.406 ng, 0.813 ng, 1.219 ng, 1.626 ng, 2.033 ng, 3.253 ng, and 4.066 ng). Extraction was performed as previously described.

A volume of 5 μL of LESA extract was loaded in a quartz glass pull-tip capillary (O.D.: 1.0mm and I.D.: 0.70mm) and sprayed at 600 – 1000 V into a custom built nESI-TIMS coupled to a Bruker impact q-TOF Mass Spectrometer (Bruker Daltonics, Billerica,

MA, USA)¹⁶. The TOF component was operated at 10 kHz and m/z range from 50 - 2000, using the maXis Impact Q-TOF acquisition program. The TIMS component was operated by Lab View, an in-house software, in synchronization with the TOF controls¹⁷. Details regarding the TIMS operation and calibration procedure can be found elsewhere¹⁷⁻²⁰. The ion mobility is determined by,

$$K_0 = \frac{V_g}{E} = \frac{A}{V_{elution} - V_{out}}$$

where K_0 is the reduced mobility, v_g is the gas flow velocity, $V_{elution}$ is the elution voltage and V_{out} is the base voltage. The constant A was determined using a Tuning Mix (Agilent Technologies, Santa Clara, CA, USA) calibration standard of known reduced mobilities. The separation was carried out using Nitrogen (N_2) at room temperature (T) with a gas flow velocity determined by the difference between the funnel entrance pressure ($P1 = 2.6$ mbar) and the funnel exit pressure ($P2 = 1.1$ mbar)

Collision cross section (CCS, Ω) were determined by the Mason-Schamp equation:

$$\Omega = \frac{(18\pi)^{1/2}}{16} \frac{z}{(k_B T)^{1/2}} \left[\frac{1}{m_i} + \frac{1}{m_b} \right]^{1/2} \frac{1}{K_0} \frac{1}{N^*}$$

where z is the ion charge, k_B is the Boltzmann constant, N^* is the number density, and m_i and m_b are the masses of the ion and bath gas, respectively⁴⁹. Tandem mass spectrometry (MS/MS) experiments were obtained using collision induced dissociation (CID). The mobility profiles and fragmentation patterns of the ABT-737 doped MCS were compared to those of the ABT-737 standard for validation. Data from the LESA-TIMS-TOF MS/MS was analyzed using DataAnalysis version 5.2 and all IMS values were determined using OriginPro version 8.0.

4.3.6. Secondary Ion Mass Spectrometry (SIMS)

Glass slides containing MCS slices were freeze-dried using a custom-built vacuum drier for 2 h, similar to our previous report¹⁰. Samples were slowly warmed up to room temperature and transferred into the TOF-SIMS analysis vacuum chamber.

A TOF-SIMS instrument (ION-TOF, Münster, Germany) equipped with a high spatial resolution liquid metal ion gun analytical beam (25 keV, Bi³⁺) was used for chemical mapping. The instrument was operated in high current bunched (HCBU) spectral mode at a current of 0.215 pA and a total primary ion dose of $\sim 5 \times 10^{12}$ ion/cm². Charge accumulation was compensated using a low energy electron flooding gun (21 eV). Secondary ions were detected by a hybrid detector, composed of a micro-channel plate, a scintillator, and a photomultiplier⁵⁰, efficiently transmitting low mass ions ($m/z < 2000$). A mass resolving power of $m/\Delta m \sim 6,000$ at m/z 400 and spatial resolution of 1.2 μm was measured in negative polarity analyses. Secondary ion images were collected with the 2D large area stage raster mode with a field of view of 1.0 mm x 1.0mm, a patch side length of 0.3 mm (total 16 patches) and a pixel density of 256 pixels/mm.

Data from the TOF-SIMS was analysed using SurfaceLab 6 software (ION-TOF, Münster, Germany). An internal calibration was achieved with C⁻, CH⁻, CH₂⁻, C₂⁻, C₃⁻, C₄H⁻ and C₁₈H₃₃O₂⁻. After obtaining a full 2D large area image, regions of interest (ROI) were selected based on the distribution of ABT 737 in the MCSs.

4.4 Results and Discussion

The formation and growth of 3D HCT 116 cancer cell spheres is a fast and reliable way of studying cancer tumor models in a relatively cheap and quick manner⁵¹. The spheres

assimilate cancer tumors by having the same structure of a poorly vascularized tumor where the outer cells have access to nutrients and the inner cells become hypoxic, leading to cell death⁵². The growth of MCS was monitored every 2-3 days to have a closer inspection of the growth rate. After 15 days, the spheres had grown to around 1mm (Figure 4.3.a), which is an optimal size to exhibit 3D cell-cell and cell-matrix interactions and establish chemical gradients of oxygen, nutrients and catabolites⁵³.

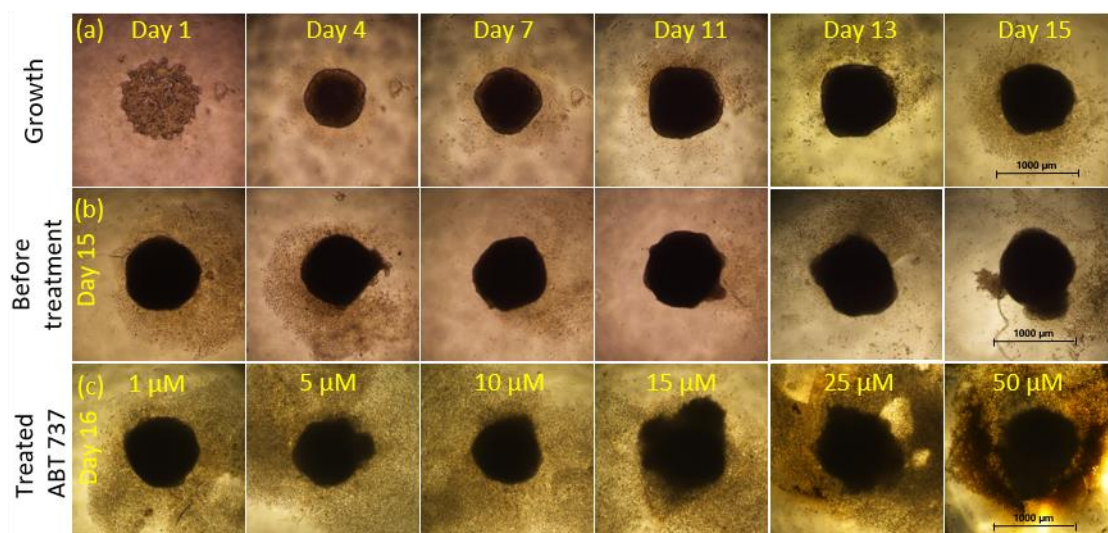


Figure 4.3. Typical HCT 116 MCS. (a) Optical images (4x) of the same MCS growth as a function of the culture time in a 15-day interval (b) Optical images (4x) of different MCS at day 15 prior to treatment and (c) Optical images (4x) of MCS shown in (b) after 24 hours exposure to ABT-737 at different concentrations.

Our goal was to assess whether clinically relevant concentrations of drug could be detected within the spheroids. MCS were treated with increasing concentrations of ABT-737 which resulted in some cellular detachment from the sphere shape after 24 hours; in particular, at higher concentrations of ABT 737 some spheres lost their shape making it hard to section and transfer for TOF-SIMS analysis. MCS treated with 1 μM, 5 μM, 10

μM , 15 μM , 25 μM and 50 μM of ABT 737 maintained the spherical shape, although cellular detachment was also observed to a lesser extent. In Figure 4.3 we can observe how each MCS was before (b) and after treatment (c).

The TOF-SIMS analysis under HCBU mode provided high mass resolution and permitted the detection of the ABT-737 molecular ion (i.e., $[\text{M-H}]^-$ at 811 m/z). The comparison between the TOF-SIMS analysis of control MCS, ABT-737 standard and MCS treated with ABT-737 drug can be found in Appendix 18. Closer inspection of Appendix 18 shows that there is no signal at 811 m/z for the control MCS samples, whereas there is a predominant signal in the ABT-737 standard and ABT-737 treated MCS samples. This high contrast allowed for the chemical mapping of ABT-737 without major endogenous interferences.

To visualize the distribution of ABT-737 in the MCS, Figure 4.4 a-b presents optical and TOF-SIMS images of consecutive MCS slices. Across the 16 μm thick slices, there is consistently a high contrast between the 811 m/z signal observed from the control MCS (low intensity background) and the ABT-737 treated MCS samples. Endogenous signals at 159 m/z (nuclei marker HP_2O_6^-) and 255.23 m/z (fatty acid 16:0, $\text{C}_{18}\text{H}_{33}\text{O}_2^-$) allowed for visualization of the MCS on the glass slide. Closer inspection of 811 m/z in Figure 4.4b shows that the 811 m/z signal corresponding to the ABT-737 drug distribution from the ABT-737 treated MCS is clearly defined and restricted to the outer layers of the MCS, while the homogenous distribution of 811 m/z from the control MCS is just a low signal background. A line scan shows the intensity of the 811 m/z ion across the sphere and how it is highly intense in the borders and less intense in the center for the case of the ABT-737 treated MCS. A three-dimensional visualization is provided to aid the correlation

between the MCS slices and the original 3D MCS (Figure 4.4b right panel); in the 3D MCS schematic, the ABT-737 signal (gold color) from the outer MCS layers is consistently observed across the slices. While TOF-SIMS analysis of MCS and comparison with between MCS control, ABT-737 standard, and ABT-737 treated MCS provided a clear localization and identification of the ABT-737 drug, secondary confirmation was obtained using *in-situ* LESA-TIMS-TOF MS/MS analysis.

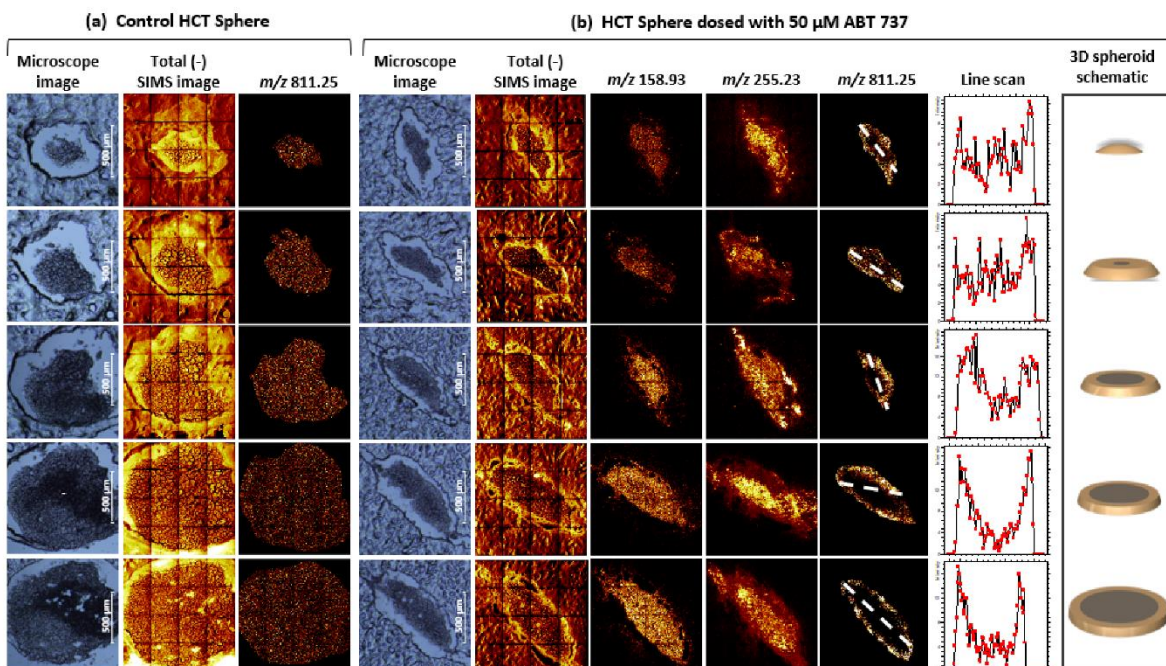


Figure 4.4. (a) Optical (4x), total SI and m/z 811.25 (ABT-737 [M-H]⁻) images (left to right) of consecutive control MCS slices. (b) Optical (4x), total SI, endogenous markers (m/z 159.93 HP_2O_6^- nuclei marker, m/z 255.23 $\text{C}_{18}\text{H}_{33}\text{O}_2^-$ Fatty Acid 16:0[M-H]⁻), and m/z 811.25 (ABT-737 [M-H]⁻) images (left to right) of consecutive slices from a 50 μM ABT-737 treated MCS. The line scan shows the intensity of ABT-737 across each slice of the spheroid.

Previous reports have shown the existence of multiple components at the level of nominal mass in biological samples⁵⁴. Mobility selected fragmentation patterns were utilized for confirmation of the presence of ABT-737 in the treated MCS samples. One of

the remarkable advantages of the LESA-TIMS-TOF MS/MS workflow is the fast screening from biological surfaces at ambient pressure (Figure 4.5). A typical LESA extraction is performed in less than 1 minute for a single point analysis (~1mm spatial resolution), followed by a short MS analysis, lasting less than 5 minutes per sample, which is a major advantage compared to long LC-MS run times. Different from the TOF-SIMS analysis, the LESA-TIMS-TOF MS was performed in positive ion mode using a nESI source, since better S/N was observed for the ABT-737 parent ion signal from the complex biological mixture across experiments. The extraction solvent ethanol, water and formic acid (60:39.9:0.1) - was chosen based on the affinity of ABT-737 drug to bind to the hydrophobic grooves of BCl-2 type proteins⁵⁵. The 2D-IMS-MS contour maps allow for a quick identification of the ABT-737 parent ion (813 m/z, [M+H]⁺) and the Angiotensin II internal standard signal (1046 m/z, [M+H]⁺) by their *m/z* (~1 ppm mass accuracy) and CCS values in the complex mixture biological extract. The CCS value for ABT-737 [M+H]⁺ and Angiotensin II [M+H]⁺ are 273 Å² and 303 Å², respectively. In addition to the accurate mass and mobility of the parent ions, mobility selected MS/MS were used for tertiary confirmation of the ABT 737 signal using the fragment ions [M-NO₂]⁺, [M-C₄H₁₁N]⁺, [M-C₁₈H₂₄N₄O₄S₂]⁺, and [M-C₃₀H₂₈ClN₅O₅S]⁺.

A calibration curve for ABT-737 using LESA-TIMS-TOF MS was generated from MCS control samples spiked at different concentrations of ABT-737. The extractions were performed in triplicates and the extraction volume covered the entire MCS sections. The amount of drug per slice was determined from the linear regression of the calibration curve (Figure 4.5g). The calibration curve was plotted using the ABT-737 parent ion (813 m/z, [M+H]⁺) signal and the Angiotensin II internal standard signal (1046 m/z, [M+H]⁺). A limit

of detection of 0.3 ng was determined from the standard deviation of the response and the slope of the curve. Using the calibration equation, a typical mass of drug per middle-MCS slice was estimated to be 0.81 ng, 1.22 ng, 1.41 ng, 1.75 ng, and 2.47 ng for the 10 μ M, 15 μ M, 25 μ M, 50 μ M and 100 μ M ABT-737 concentration in the cell culture media over 24h, respectively. Signals for MCCs treated below 5 μ M for 24h (slightly above our LOD) were not observed. Extrapolating these numbers based on the area of the drug relative to the slice and the MCS volume, 474 ng, 719 ng, 831 ng, 1031 ng, and 1457 ng for the 10 μ M, 15 μ M, 25 μ M, 50 μ M and 100 μ M during 24h incubation, respectively are estimated per MCS. This methodology allows for further assessment of the ABT-737 generated toxicity at the MCS level. This method is particularly advantageous for cases when the drug is localized and is not homogeneously distributed across the MCS or cancer tumor.

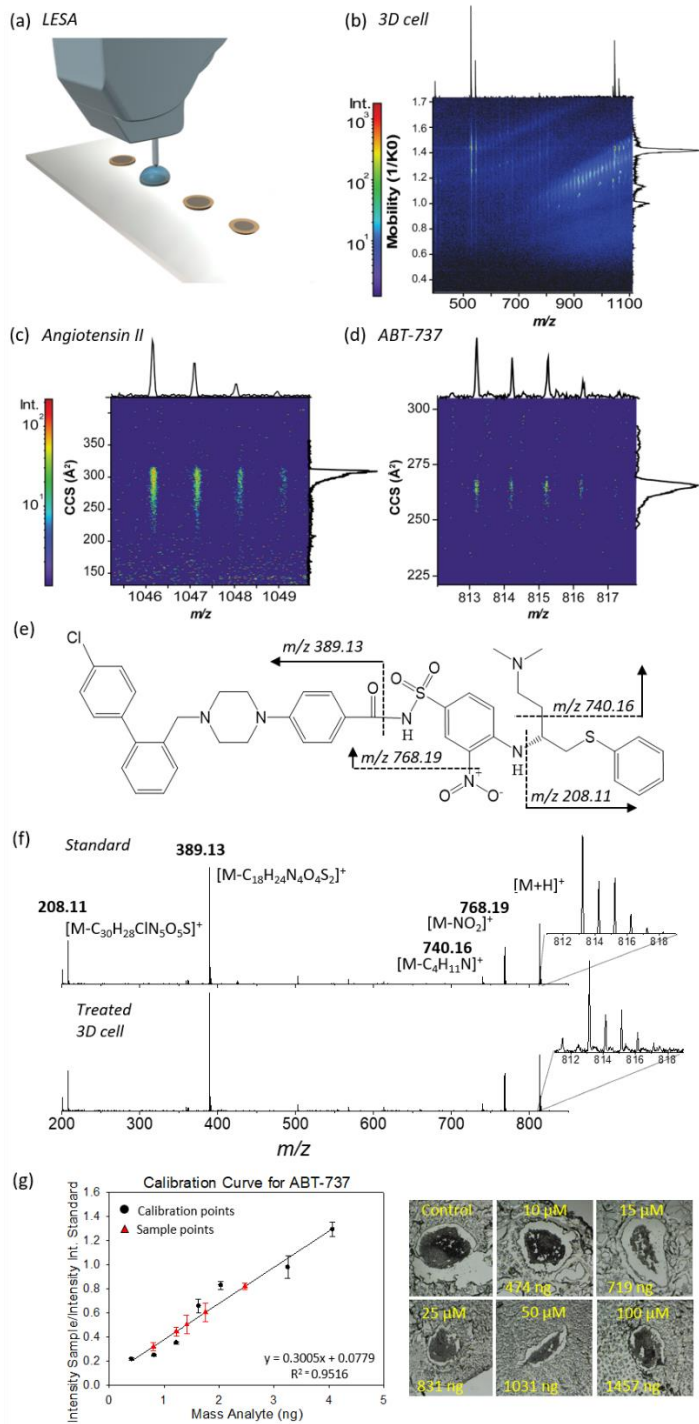


Figure 4.5. (a) Schematic representation of the LESA extraction. (b) typical 2D-IMS-MS plots of from a 100 μM ABT-737 treated MCS, (c) 2D-IMS-MS blowouts of the Angiotensin II IS and ABT-737 signals. (e) ABT-737 typical fragmentation channels (f) mobility selected MS/MS spectra of the ABT-737 $[\text{M}+\text{H}]^+$ signal from a standard and from a treated MCS (g) ABT-737 Calibration curve from LESA-TIMS-MS extracted from the MCS slices as a function of the ABT-737 concentration in the culture media. Error bars represent the standard deviation of the measurements ($n=3$).

4.5 Conclusions

An analytical workflow capable of estimating the amount of drug incorporated per MCS based and their localization based on complementary TOF-SIMS and LESA-TIMS-TOF MS/MS is described. The use of TOF-SIMS allowed for high spatial resolution chemical mapping (~1.2 μm) of ABT-737 drug in single MCS slices. Complementary, *in-situ* LESA-TIMS-TOF MS using internal standards allowed secondary confirmation based on mobility selected fragmentation pattern and 3D quantitation of the amount of ABT-737 drug per MCS slices. This methodology enables further assessment of the fate and uptake of drugs by cancer tumors, particularly when drugs are not homogeneously distributed inside the tumor volume.

4.6 Acknowledgements

YCD acknowledge the financial support from NSF FGLSAMP FIU Bridge to the Doctorate award HRD # 1810974. AC was fully supported by NSF grant HRD-1547798 awarded to Florida International University as part of the Centers for Research Excellence in Science and Technology (CREST) Program

4.7 References

1. X. Cui, Y. Hartanto and H. Zhang, *J R Soc Interface*, 2017, **14**.
2. L. B. Weiswald, D. Bellet and V. Dangles-Marie, *Neoplasia*, 2015, **17**, 1-15.
3. Y. Fang and R. M. Eglén, *SLAS Discov*, 2017, **22**, 456-472.

4. M. Sans, K. Gharpure, R. Tibshirani, J. Zhang, L. Liang, J. Liu, J. H. Young, R. L. Dood, A. K. Sood and L. S. Eberlin, *Cancer Res*, 2017, **77**, 2903-2913.
5. S. Guenther, L. J. Muirhead, A. V. Speller, O. Golf, N. Strittmatter, R. Ramakrishnan, R. D. Goldin, E. Jones, K. Veselkov, J. Nicholson, A. Darzi and Z. Takats, *Cancer Res*, 2015, **75**, 1828-1837.
6. J. F. Timms, O. J. Hale and R. Cramer, *Expert Rev Proteomics*, 2016, **13**, 593-607.
7. M. Sans, C. L. Feider and L. S. Eberlin, *Curr Opin Chem Biol*, 2018, **42**, 138-146.
8. M. Sun, X. Tian and Z. Yang, *Anal Chem*, 2017, **89**, 9069-9076.
9. H. Li and A. B. Hummon, *Anal Chem*, 2011, **83**, 8794-8801.
10. X. Liu, E. M. Weaver and A. B. Hummon, *Anal Chem*, 2013, **85**, 6295-6302.
11. L. J. Gamble and C. R. Anderton, *Micros Today*, 2016, **24**, 24-31.
12. Q. P. Vanbellinghen, A. Castellanos, M. Rodriguez-Silva, I. Paudel, J. W. Chambers and F. A. Fernandez-Lima, *J Am Soc Mass Spectrom*, 2016, **27**, 2033-2040.
13. S. Ninomiya, K. Yoshimura, L. C. Chen, S. Takeda and K. Hiraoka, *Mass Spectrom*, 2017, **6**, 1-6.
14. J. R. N. Haler, E. K. Sisley, Y. L. Cintron-Diaz, S. N. Meitei, H. J. Cooper and F. Fernandez-Lima, *Anal Methods*, 2019, **11**, 2385-2395.
15. S. S. Basu, E. C. Randall, M. S. Regan, B. G. C. Lopez, A. R. Clark, N. D. Schmitt, J. N. Agar, D. A. Dillon and N. Y. R. Agar, *Anal Chem*, 2018, **90**, 4987-4991.
16. V. A. Mikhailov, R. L. Griffiths and H. J. Cooper, *Int J Mass Spectrom*, 2017, **420**, 43-50.
17. D. J. Ryan, D. Nei, B. M. Prentice, K. L. Rose, R. M. Caprioli and J. M. Spraggins, *Rapid Commun Mass Spectrom*, 2018, **32**, 442-450.
18. J. Havlikova, E. C. Randall, R. L. Griffiths, J. G. Swales, R. J. A. Goodwin, J. Bunch, I. B. Styles and H. J. Cooper, *Anal Chem*, 2019, **91**, 14198-14202.

19. D. J. Ryan, N. H. Patterson, N. E. Putnam, A. D. Wilde, A. Weiss, W. J. Perry, J. E. Cassat, E. P. Skaar, R. M. Caprioli and J. M. Spraggins, *Anal Chem*, 2019, **91**, 7578-7585.
20. H. Borsdorf and G. A. Eiceman, *Appl. Spectrosc. Rev.*, 2006, **41**, 323-375.
21. E. K. Sisley, E. Illes-Toth and H. J. Cooper, *Trends Analyt Chem*, 2020, **124**, 115534.
22. R. L. Griffiths, A. J. Creese, A. M. Race, J. Bunch and H. J. Cooper, *Anal Chem*, 2016, **88**, 6758-6766.
23. D. Eikel, M. Vavrek, S. Smith, C. Bason, S. Yeh, W. A. Korfmacher and J. D. Henion, *Rapid Commun Mass Spectrom*, 2011, **25**, 3587-3596.
24. W. B. Parson, S. L. Koeniger, R. W. Johnson, J. Erickson, Y. Tian, C. Stedman, A. Schwartz, E. Tarcsa, R. Cole and G. J. Van Berkel, *J Mass Spectrom*, 2012, **47**, 1420-1428.
25. R. L. Zinn, E. E. Gardner, I. Dobromilskaya, S. Murphy, L. Marchionni, C. L. Hann and C. M. Rudin, *Mol Cancer*, 2013, **12**, 1-9.
26. M. Broecker-Preuss, N. Becher-Boveleth, S. Muller and K. Mann, *Cancer Cell Int*, 2016, **16**, 27.
27. R. D. McCulloch and M. Amo-Gonzalez, *Rapid Commun Mass Spectrom*, 2019, **33**, 1455-1463.
28. H. Chen, C. Chen, W. Huang, M. Li, Y. Xiao, D. Jiang and H. Li, *Anal Chem*, 2019, **91**, 9138-9146.
29. J. Le Maitre, M. Hubert-Roux, B. Paupy, S. Marceau, C. P. Ruger, C. Afonso and P. Giusti, *Faraday Discuss*, 2019, **218**, 417-430.
30. E. A. Rue, J. A. Glinski, V. B. Glinski and R. B. van Breemen, *J Mass Spectrom*, 2019, DOI: 10.1002/jms.4377, 1-5.
31. F. A. Fernandez-Lima, D. A. Kaplan and M. A. Park, *Rev. Sci. Instr.*, 2011, **82**, 126106.
32. F. Fernandez-Lima, D. Kaplan, J. Suetering and M. Park, *Int. J. Ion Mobility Spectrom.*, 2011, **14**, 93-98.
33. K. Jeanne Dit Fouque and F. Fernandez-Lima, *Trends Analyt Chem*, 2019, **116**, 308-315.

34. K. J. Adams, D. Montero, D. Aga and F. Fernandez-Lima, *Int J Ion Mobil Spectrom*, 2016, **19**, 69-76.
35. A. McKenzie-Coe, J. D. DeBord, M. Ridgeway, M. Park, G. Eiceman and F. Fernandez-Lima, *Analyst*, 2015, **140**, 5692-5699.
36. P. Benigni, R. Marin and F. Fernandez-Lima, *Int J Ion Mobil Spectrom*, 2015, **18**, 151-157.
37. K. J. Adams, C. E. Ramirez, N. F. Smith, A. C. Munoz-Munoz, L. Andrade and F. Fernandez-Lima, *Talanta*, 2018, **183**, 177-183.
38. K. J. Adams, N. F. Smith, C. E. Ramirez and F. Fernandez-Lima, *Int J Mass Spectrom*, 2018, **427**, 133-140.
39. A. Garabedian, M. A. Baird, J. Porter, K. Jeanne Dit Fouque, P. V. Shliaha, O. N. Jensen, T. D. Williams, F. Fernandez-Lima and A. A. Shvartsburg, *Anal Chem*, 2018, **90**, 2918-2925.
40. F. Meier, A. D. Brunner, S. Koch, H. Koch, M. Lubeck, M. Krause, N. Goedecke, J. Decker, T. Kosinski, M. A. Park, N. Bache, O. Hoerning, J. Cox, O. Rather and M. Mann, *Mol Cell Proteomics*, 2018, **17**, 2534-2545.
41. K. Jeanne Dit Fouque, C. E. Ramirez, R. L. Lewis, J. P. Koelmel, T. J. Garrett, R. A. Yost and F. Fernandez-Lima, *Anal Chem*, 2019, **91**, 5021-5027.
42. A. Garabedian, D. Butcher, J. L. Lippens, J. Miksovska, P. P. Chapagain, D. Fabris, M. E. Ridgeway, M. A. Park and F. Fernandez-Lima, *Phys Chem Chem Phys*, 2016, **18**, 26691-26702.
43. D. Butcher, P. Chapagain, F. Leng and F. Fernandez-Lima, *J Phys Chem B*, 2018, **122**, 6855-6861.
44. J. Friedrich, C. Seidel, R. Ebner and L. A. Kunz-Schughart, *Nat Protoc*, 2009, **4**, 309-324.
45. W. Senkowski, X. Zhang, M. H. Olofsson, R. Isacson, U. Hoglund, M. Gustafsson, P. Nygren, S. Linder, R. Larsson and M. Fryknas, *Mol Cancer Ther*, 2015, **14**, 1504-1516.
46. X. Gong, C. Lin, J. Cheng, J. Su, H. Zhao, T. Liu, X. Wen and P. Zhao, *PLoS One*, 2015, **10**, 1-18.
47. K. Okumura, S. Huang and F. A. Sinicrope, *Clin Cancer Res*, 2008, **14**, 8132-8142.

48. C. Tse, A. R. Shoemaker, J. Adickes, M. G. Anderson, J. Chen, S. Jin, E. F. Johnson, K. C. Marsh, M. J. Mitten, P. Nimmer, L. Roberts, S. K. Tahir, Y. Xiao, X. Yang, H. Zhang, S. Fesik, S. H. Rosenberg and S. W. Elmore, *Cancer Res*, 2008, **68**, 3421-3428.
49. E. W. McDaniel and E. A. Mason, *Mobility and diffusion of ions in gases*, John Wiley and Sons, Inc., New York, New York, 1973.
50. A. Brunelle, D. Touboul and O. Laprevote, *J Mass Spectrom*, 2005, **40**, 985-999.
51. J. Hoarau-Vechot, A. Rafii, C. Touboul and J. Pasquier, *Int J Mol Sci*, 2018, **19**.
52. D. Lv, Z. Hu, L. Lu, H. Lu and X. Xu, *Oncol Lett*, 2017, **14**, 6999-7010.
53. F. Hirschhaeuser, H. Menne, C. Dittfeld, J. West, W. Mueller-Klieser and L. A. Kunz-Schughart, *J Biotechnol*, 2010, **148**, 3-15.
54. J. D. DeBord, D. F. Smith, C. R. Anderton, R. M. Heeren, L. Pasa-Tolic, R. H. Gomer and F. A. Fernandez-Lima, *PLoS One*, 2014, **9**, e99319.
55. S. Cory and J. M. Adams, *Cancer Cell*, 2005, **8**, 5-6.

CHAPTER 5. Spatially resolved neuropeptide characterization from neuropathological FFPE tissue sections by a combination of Imaging MALDI FT-ICR MSHC and LESA-TIMS-MS

Yarixa L. Cintron-Diaz, Mario E. Gomez-Hernandez, Marthe M. H. A. Verhaert, Peter D. E. M. Verhaert, and Francisco Fernandez-Lima,

This chapter has been submitted to *JASMS* and is under review.

5.1 Abstract

Recent advances in mass spectrometry histochemistry (MSHC) have focused on the label-free top-down MS analysis of neuropeptides in sections of paraffin embedded formalin-fixed (FFPE) human clinical samples out of the vast tissue collections documented in biobanks. Besides the detection and localization of neuropeptide and other MS signals in biological tissues, there is great interest in their molecular identification and full characterization. Whereas MALDI MSI using ultra, high-resolution FT ICR MS on DHB coated five-micron sections of human FFPE pituitary provides clear isotope patterns and chemical formulae assignment for the general case of neuropeptides (vasopressin for the case here presented), there is a need for complementary sequence characterization. In the present work, we performed LESA extractions on consecutive (uncoated) tissue slices deposited on non-ITO coated microscope glasses and characterized the presence of vasopressin by their mobility pattern, accurate mass (~1ppm) and MS/MS fragmentation pattern. Differences in sequence coverage are discussed based on the mobility selected CID, ECD and UVPD MS/MS. In the case of peptide with disulfide bonds (Arg-Vasopressin), the use of LESA with a disulfide reduction agent is illustrated for effective sequencing using mobility selected CID, ECD and UVPD MS/MS.

5.2 Introduction

Biological tissues comprise the various organs and organ systems in our body and consist of large groups of heterogeneous cells which together complete a shared function. Cells within tissues are known to respond to their surrounding extracellular environment and communicate with each other by a combination of physical signals (through

specialized intercellular junctions), and biochemical molecular signals. This enables multicellular tissues to operate as functional units¹. Endogenous peptides are an essential part of a living cell as they are known to be biological messengers that carry information from one tissue to another through the bloodstream². Their function is dependent on the amino acid chain and shape, therefore the need to elucidate their sequence and structure and resolve their spatial distribution within a biological tissue.

A series of analytical tools have been used to study changes related to endogenous peptides in a cell or an organism, such as chromatography, mass spectrometry and nuclear magnetic resonance (NMR)³. Most analyses are typically performed using mass spectrometry (MS),⁴⁻⁶ with the use of separation techniques such as liquid chromatography (LC),⁷⁻¹⁰ and ion mobility (IMS)¹¹⁻¹⁵ which assist with characterization. The caveat of these techniques is the lack of spatial distribution of peptides within the tissue. Mass spectrometry imaging (MSI) allows for surface sampling and mapping without the need of knowing a preliminary targeted molecule, which is an important advantage when analyzing biological samples¹⁶. MSI is a label free technique that can provide information for the understanding of biological processes with high spatial resolution from sub-cellular to multicellular levels. MSI is a four-step process that involves the sample preparation, desorption and ionization, mass analysis and image registration¹⁷. Most widely used techniques are Matrix Assisted Laser Desorption Ionization (MALDI) and Secondary Ion Mass Spectrometry coupled to a Time of Flight spectrometers (TOF-SIMS).

Formalin-fixed, paraffin-embedded (FFPE) tissues are widely found in hospital sample archives and are extensively used for histological and histochemical studies¹⁸. However, there are not many reported studies of the analysis of FFPE by MSI, given that

these techniques are typically considered to require fresh (or fresh frozen) tissue preparations. The detection, characterization, and localization of endogenous peptides by MSI has only been showcased by two independent groups, Lemaire *et al.*¹⁹ and Paine *et al.*²⁰, both using slightly different sample preparation workflows (and yielding different conclusions as to the usefulness of FFPE tissues for MSI for 'top down' peptide analyses.

In the present work, MALDI MSI using an ultrahigh resolution 7T FT-ICR MS was performed on DHB coated sections of human pituitary (FFPE) tissue. As an orthogonal, complementary technique, liquid extraction surface analysis – trapped ion mobility spectrometry- tandem mass spectrometry (LESA-TIMS-MS/MS) was performed on consecutive FFPE tissue slices to confirm the peptide sequence based on the mobility pattern, accurate mass and mobility selected MS/MS fragmentation pattern. LESA has become an alternative technique to surface mapping, where a liquid micro-junction between the surface and an extraction tip is created, followed by direct nano-electrospray infusion²¹. Differences in sequence coverage are discussed based on the mobility selected CID, ECD and UVPD MS/MS. In the case of peptide with disulfide bonds (Arg-Vasopressin), the use of LESA with a disulfide reduction agent is illustrated for effective sequencing using mobility selected CID, ECD and UVPD MS/MS.

5.3 Materials and Methods

5.3.1. Chemicals

HPLC-grade ethanol (dehydrated) was purchased from Biosolve B.V. (Valkenswaard, The Netherlands). Xylene (>99%), HPLC-grade acetonitrile (ACN; >99.93%), 2,5-dihydroxybenzoic acid (DHB; >99.0%), and trifluoroacetic acid (TFA; 99%)

were from Sigma-Aldrich (Zwijndrecht, The Netherlands). Vasopressin standard (synthetic [Arg8]-Vasopressin (AVP) peptide) was purchased from AnaSpec Inc. (Fremont, CA, USA).

5.3.2. Sample collection, embedding, slicing and mounting

Formaldehyde-fixed paraffin-embedded (FFPE) human pituitary tissues were obtained from the FFPE biobank at the Neuropathology Department of Leuven University (UZ-Leuven, Belgium). Tissues from patient biopsies of pituitary adenomas, were especially selected for inclusion parts of the neurohypophysis (i.e. posterior pituitary). These pituitary parts are known to store and release endogenous neuropeptides, including the nonapeptides vasopressin and oxytocin. The tissues had been fixed and embedded following a routine standard protocol employed for histopathology, all in accordance with national laws and regulations, and in full respect of human rights²⁰. Briefly, fixation of tissues with 10% formalin (i.e. 40% formaldehyde, fixative volume 5-10 times tissue volume) was performed at room temperature for 24-48 hours. Fixed tissues (trimmed to appropriate size and shape) were placed in embedding cassettes. Paraffin embedding was performed according to the following schedule (total 16 hours); 70% ethanol (3 x 1h); 80% ethanol (2 x 1h); 95% ethanol (2 x 1h); 100% ethanol (3 x 1.5h); xylene (3 x 1.5h); paraffin wax (58-60 °C) (1 x 2h; 1 x >2h). Afterwards, embedded tissues were brought back to room temperature, allowing the paraffin to solidify. Paraffin blocks were trimmed as necessary and sectioned at 5 µm thickness on a semi-automated microtome (Microm) equipped with a Zeiss Stemi 2000 binocular loupe. Sections were collected in a water bath at room temperature and mounted onto regular microscope slides (Thermo Superfrost) using

distilled water. Sections were stretched on a hotplate (50 °C) and air-dried for at least 30 minutes with optional overnight baking in an oven (45-50 °C).

Prior to mass spectrometry histochemistry (MSHC) analysis, sections were deparaffinized in 2 changes of xylene (3 and 2 min respectively), xylene was removed by ethanol through 2 changes of 100% ethanol (2 min each), according to the MSHC protocol we published before (Paine et al., 2018).

5.3.3. MALDI Matrix coating

After deparaffinization, tissues on the microscope slides were coated with a matrix solution of 2,5-dihydroxybenzoic acid (DHB; 50 mg/mL) in ACN/H₂O/TFA (49.95:49.95:0.1 v/v). The matrix solution was applied as a nebulized spray using a TM sprayer (HTX Technologies, NC, U.S.A.) with the following settings: flow rate, 0.1 mL/min; spray nozzle velocity, 1200 mm/min; spray nozzle temperature, 75 °C; number of passes, 3; nitrogen gas pressure, 10 psi; track spacing, 1 mm; drying time between passes, 10 s.

5.2.4. MALDI-Mass Spectrometry Imaging

MALDI Imaging experiments were done on a Bruker Solarix 7T FT-ICR MS system (Bruker Daltonics, Billerica, MA, USA) equipped with a 355nm Nd:YAG Laser Smartbeam technology. A total of 1000 laser shots were acquired per spectrum, with 100 shots per raster site. Raster width was set to 25 µm. Data was processed using Data Analysis 4.0 and the Bruker Imaging Suite. Mass spectra internally calibrated using known peaks.

5.2.5. Neuropeptide extraction from FFPE slides

Glass slides containing deparaffinized human pituitary tissue slices were placed on the LESA universal adaptor plate was performed using a TriVersa Nanomate device (Advion, Ithaca, NY, USA) in micro-junction mode. Extraction spots were determined manually. To start, an automated arm aspirated 5 μL of solvent from the solvent well and relocated on top of the desired spot in the tissue. The tip descended to a 1.9 mm dispensation height to place 1.0 μL of solvent forming a liquid micro-junction between the surface of the tissue sample and the solvent. Solvent droplet stayed in contact with the surface for 60 s, re-aspirated and re-dispensed for another 60 s for a total of 5 times. Ultimately, 1.5 μL of solvent was re-aspirated and dispensed into a specific well in a 96 well plate. As many spots as possible were extracted depending on tissue size. A peptide internal standard (human angiotensin II, 1046 m/z) was prepared to 1 μM concentration and added to the extraction solvent acetonitrile:water:formic acid (40:59:1; v/v/v). The use of an internal standard allowed to correct for variations in the LESA tip extraction and nESI spraying conditions.

5.2.6. LESA with Disulfide Bond reduction

A 10 μL of LESA extract was reduced by adding 1 μL of 10mM of Tris(2-carboxyethyl)phosphine (TCEP) at 50 °C for 15 min. Reduced solutions were analyzed immediately after dilution to avoid re-formation of the disulfide bond.

5.2.7. nESI-TIMS-q-TOF MS/MS

A volume of 10 μL of LESA extract was loaded in a quartz glass pull-tip capillary (O.D.: 1.0mm and I.D.: 0.70mm) and sprayed at 800 – 1200 V into a custom built nESI-TIMS coupled to a q-TOF MS instrument (Impact q-TOF, Bruker Daltonics, Billerica, MA, USA)²². The TOF component was operated at 10 kHz and m/z range from 50 – 2000, using the maXis Impact Q-TOF acquisition program. The TIMS component was operated by Lab View, an in-house software, in synchronization with the TOF controls. This TIMS-q-TOF MS/MS prototype is also equipped with a CID cell, a custom-built EMS cell (for electron capture dissociation) and a trap for mobility selected UV photodissociation (213 nm) prior to TOF MS. Data were analyzed using Data Analysis version 5.2.

5.2.8. Overall workflow scheme

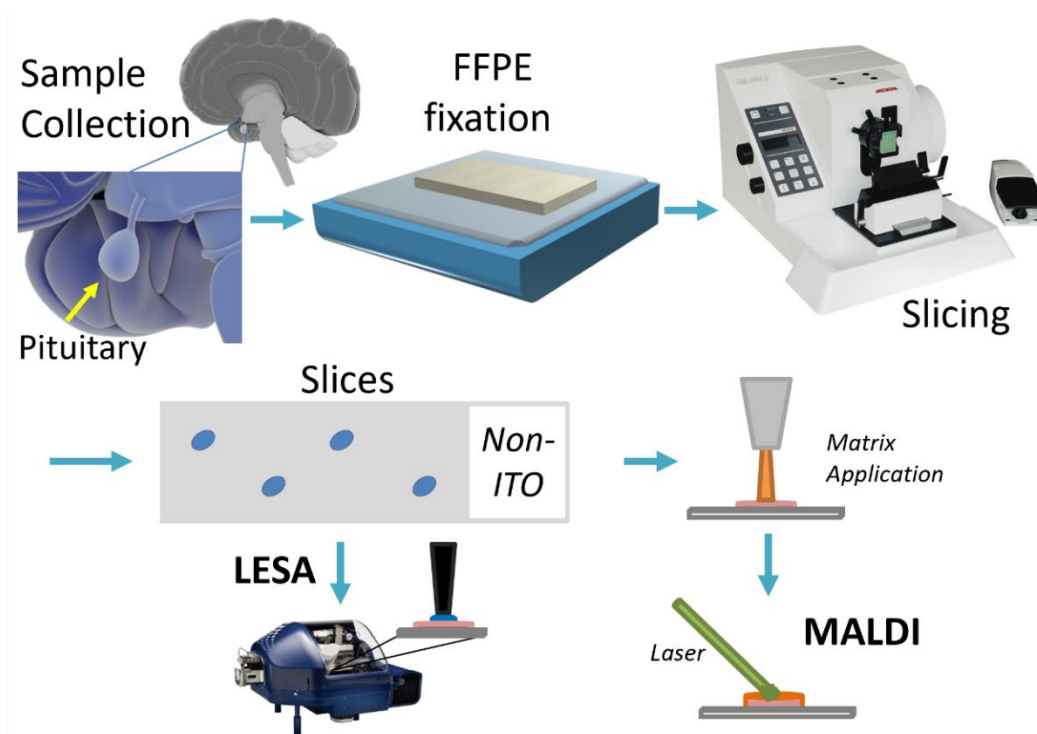


Figure 5.1. Workflow for FFPE fixation, slicing and preparation for MSHC analysis.

5.3 Results and Discussion

5.3.1. MALDI-FT ICR MS

MSHC analysis by MALDI MSI FT ICR MS provided ultra-high mass resolution measurements in the range of m/z 500-2000 (see two sections in Figure 2 a and b). Endogenous neuropeptide signals for Arg-vasopressin (1084.44 m/z $[M+H]^+$; Figure 2, green) and Oxytocin (1029.45 m/z $[M+Na]^+$, Figure S11.) were detected. The protonated signals were accompanied by the Schiff base ($[M+12]^+$, yellow) and sodiated adducts ($[M+Na]^+$, red) of Arg-Vasopressin, providing similar MSHC images to that of the $[M+H]^+$ signal (Figure 2a. and 2b.). Figure 2c. and 2d. showcase the MS and isotopic patterns for all the species with the corresponding mass error. One of the advantages of this MALDI setup is that the use of conductive slides did not appear to be critical.

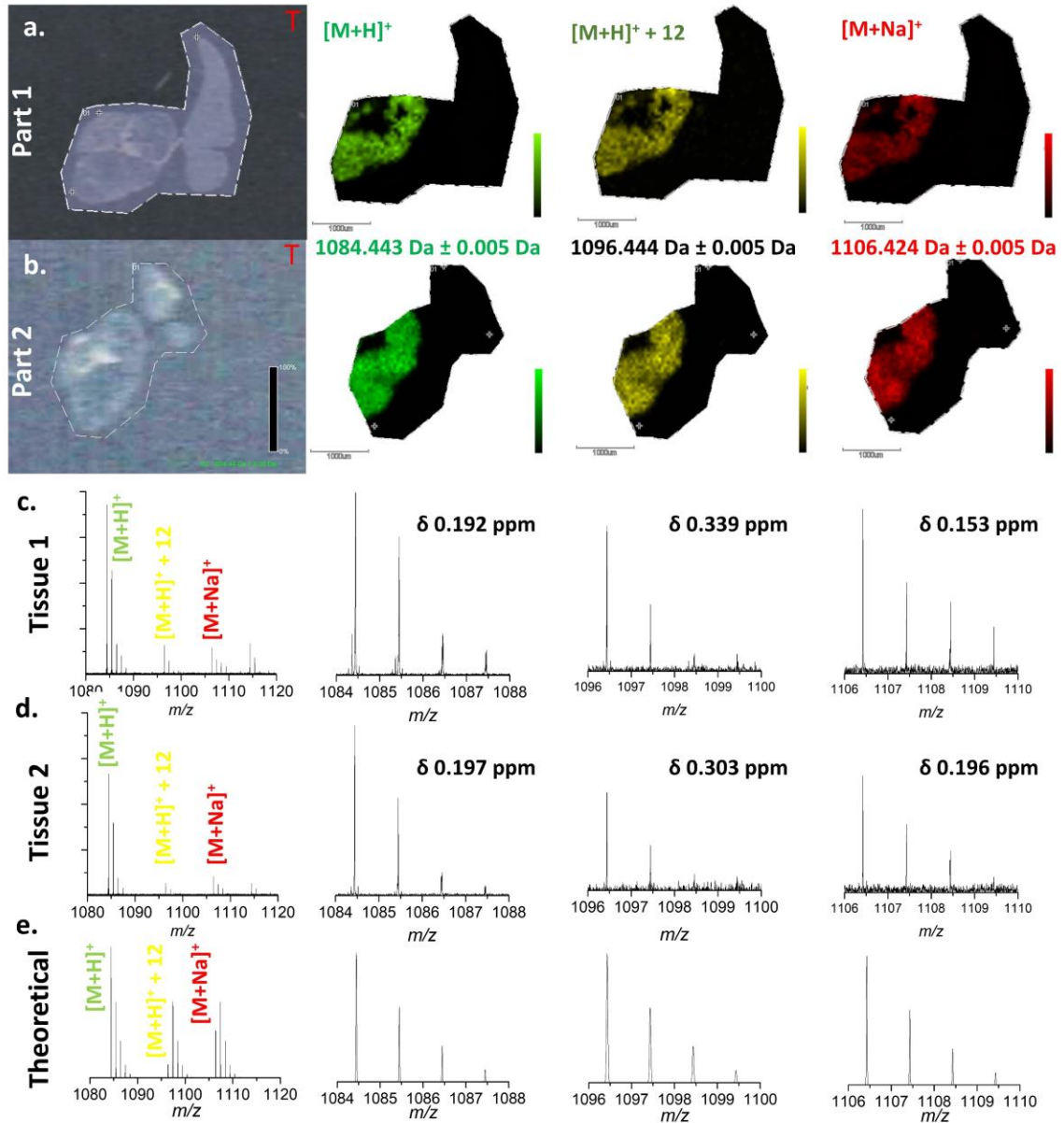


Figure 5.2. MALDI-FT ICR images of protonated (green), Schiff base (yellow) and sodiated (red) ions of Arg-Vasopressin species in sections through two different parts of human pituitary biopsy (a. part 1 and b. part 2). c. and d. showcase mass spectra and experimental isotopic patterns for each species in part 1 and part 2, respectively. e. theoretical isotopic patterns for each species.

5.3.2. LESA-TIMS-TOF MS (/MS)

LESA-nESI-TIMS-TOF MS/MS provided a complementary, quick identification of vasopressin ($1084\ m/z\ [M+H]^+$ and $542\ m/z\ [M+2H]^{2+}$) from the tissue sample (Figures 3

and 4, respectively). Interestingly, the Arg-vasopressin $[M+H]^+$ yielded two mobility bands (302 \AA^2 and 310 \AA^2 ; Figure 3a), while the $[M+2H]^{2+}$ showed a single band (340 \AA^2) (Figure 4a). These results were compared to the analysis of a Arg-vasopressin standard in the same solvent conditions (red trace in both Figure 3 and 4). The mobility selected CID MS/MS of the singly charged Arg-vasopressin ions from the LESA extract yielded characteristic fragment ions (b_6 , b_8 and y_3), in good agreement to that observed from the Arg-vasopressin standard (Figure 3).

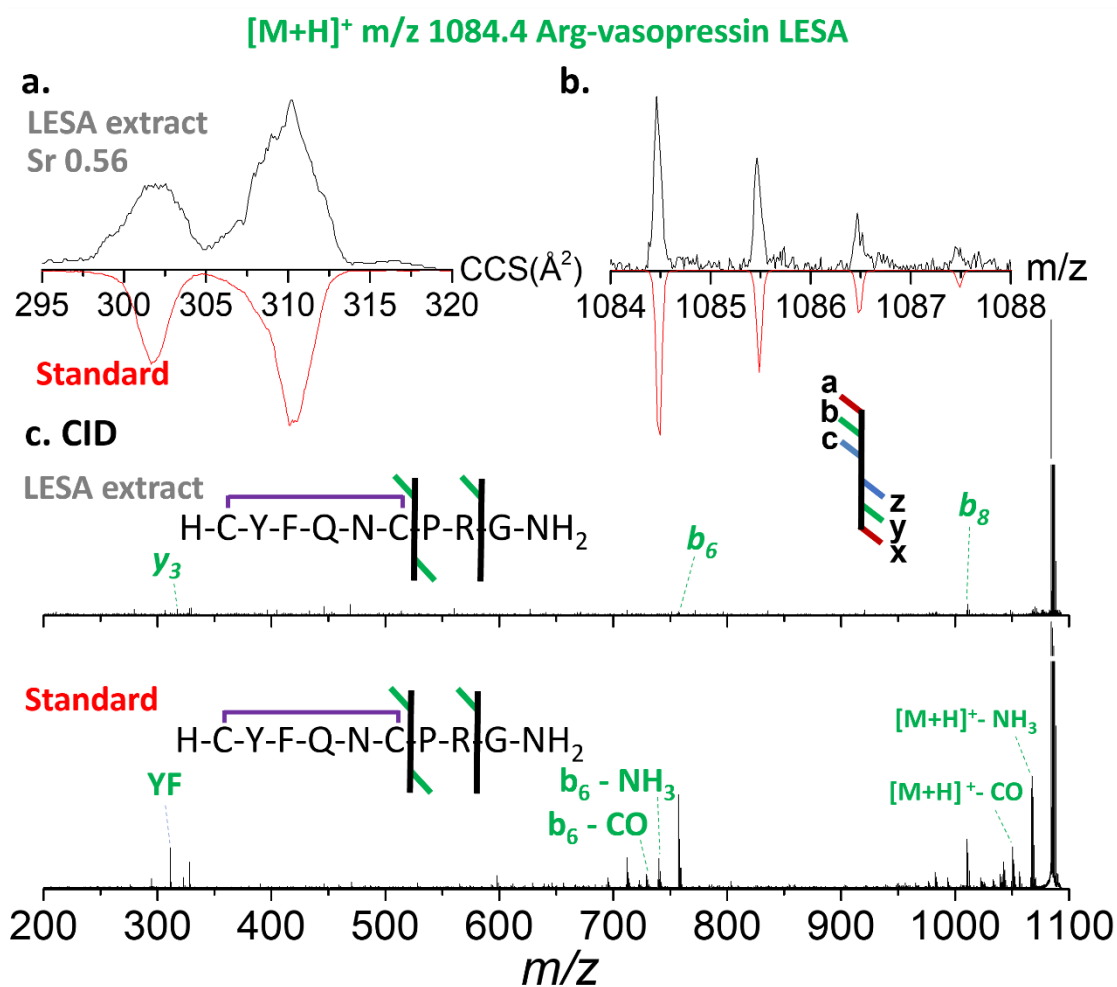


Figure 5.3. Ion mobility, experimental isotopic pattern and fragmentation pattern of $[M+H]^+$ species of Arg-Vasopressin. Red traces showcase comparison to standard.

The mobility selected CID MS/MS of the doubly charged Arg-vasopressin ions from the LESA extract yielded characteristic fragment ions (b_6 , b_7 , b_8 and y_3), in good agreement to that observed from the Arg-vasopressin standard (Figure 4). In contrast to CID, mobility selected ECD MS/MS from the LESA extract showed better sequence coverage (b_5 , b_6 , b_7 , b_8 , y_3 , y_5 , and y_6), in good agreement to that observed from the Arg-vasopressin standard and previous CID/ECD comparisons.²³⁻²⁵ The mobility selected UV photodissociation (213 nm) of the double charged Arg-vasopressin standard showed complete sequence coverage (b_5 , a_6 , b_6 , b_7 , b_8 , y_3 , y_5 , y_6 , x_7 , y_7 , x_8 and y_8); note that exposure of peptides to 213 nm photons selectively cleaves disulfide bonds by UVPD fragmentations.²⁶ The caveat of ECD and UVPD over CID is the lower fragmentation efficiencies (0.9 %, 9.7% and 114% respectively based on the most abundant product ion relative to the precursor ion), which combined with the low peptide concentration typically observed in the LESA extracts from FFPE makes this approach more challenging.

An alternative suitable for LESA samples, is the addition of a disulfide reduction agent prior the nESI-TIMS-TOF MS/MS analysis (Figure 5). Interestingly, when the disulfide bond is reduced, the mobility profiles of the doubly charged Arg-vasopressin ions now presents two mobility bands and the reduction can be clearly seen by the A+2 profile. Moreover, the mobility selected CID MS/MS of the doubly charged reduced Arg-vasopressin ions from the LESA extract provided full sequence information (b_3 , b_4 , b_5 , b_6 , b_7 , b_8^{2+} , y_3 , y_4 , y_5 , y_6 , y_7 , y_7^{2+} and y_8^{2+}) (Figure 5c), in good agreement to that observed from the Arg-vasopressin standard (Figure 5d).

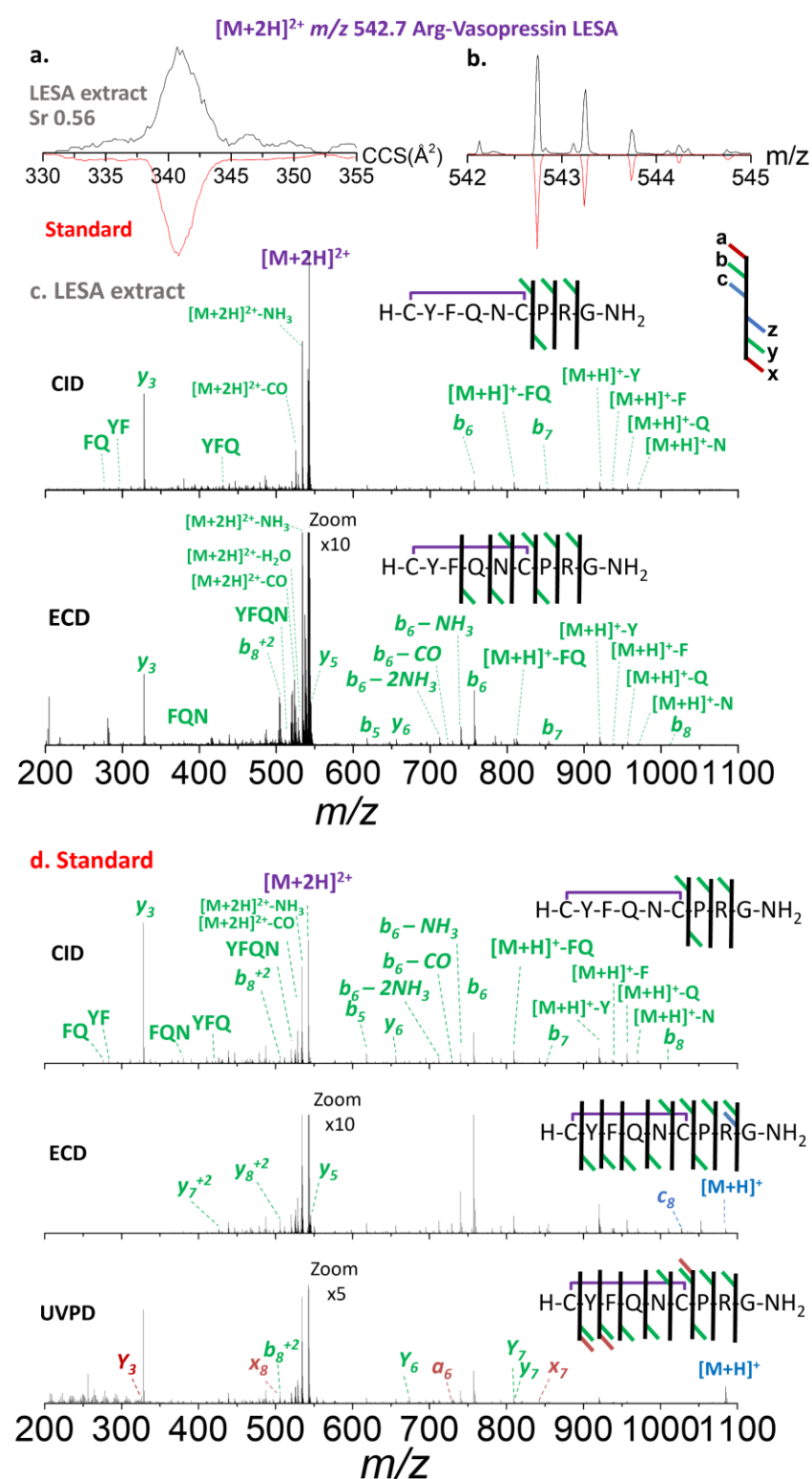


Figure 5.4. Ion mobility, experimental isotopic pattern and fragmentation pattern of [M+2H]²⁺ species of Arg-Vasopressin. Red traces showcase comparison to standard.

The mobility selected ECD and UVPD MS/MS of the doubly charged reduced Arg-vasopressin ions from the showed better sequence than CID. a_2 , b_2 , b_3 , c_3 , b_4 , b_5 , c_5 , b_6 , b_7 , b_8 , c_8 , y_2 , y_3 , y_4 , y_5 , y_6 , z_6 , y_7 , z_7^{2+} , y_8 and z_8 were observed for ECD and a_2 , b_2 , b_3 , c_3 , a_4 , b_4 , a_5 , b_5 , b_6 , b_7 , b_8^{2+} , y_2 , y_3 , y_4 , y_5 , y_6 , z_6 , y_7 , z_7^{2+} , and y_8^{2+} for UVPD. The same caveat was observed for the case of the S-S reduced LESA extract: the lower fragmentation efficiency of ECD and UVPD (2.7% and 10.0 % respectively based on the most abundant product ion relative to the precursor ion), over CID (156%) did not provided meaningful fragmentation information. Overall, with the cysteine bond present, sequencing of the inner amino acids was not achieved by mobility selected CID. However, by reducing the S-S bond, sequencing of the full peptide was obtained.

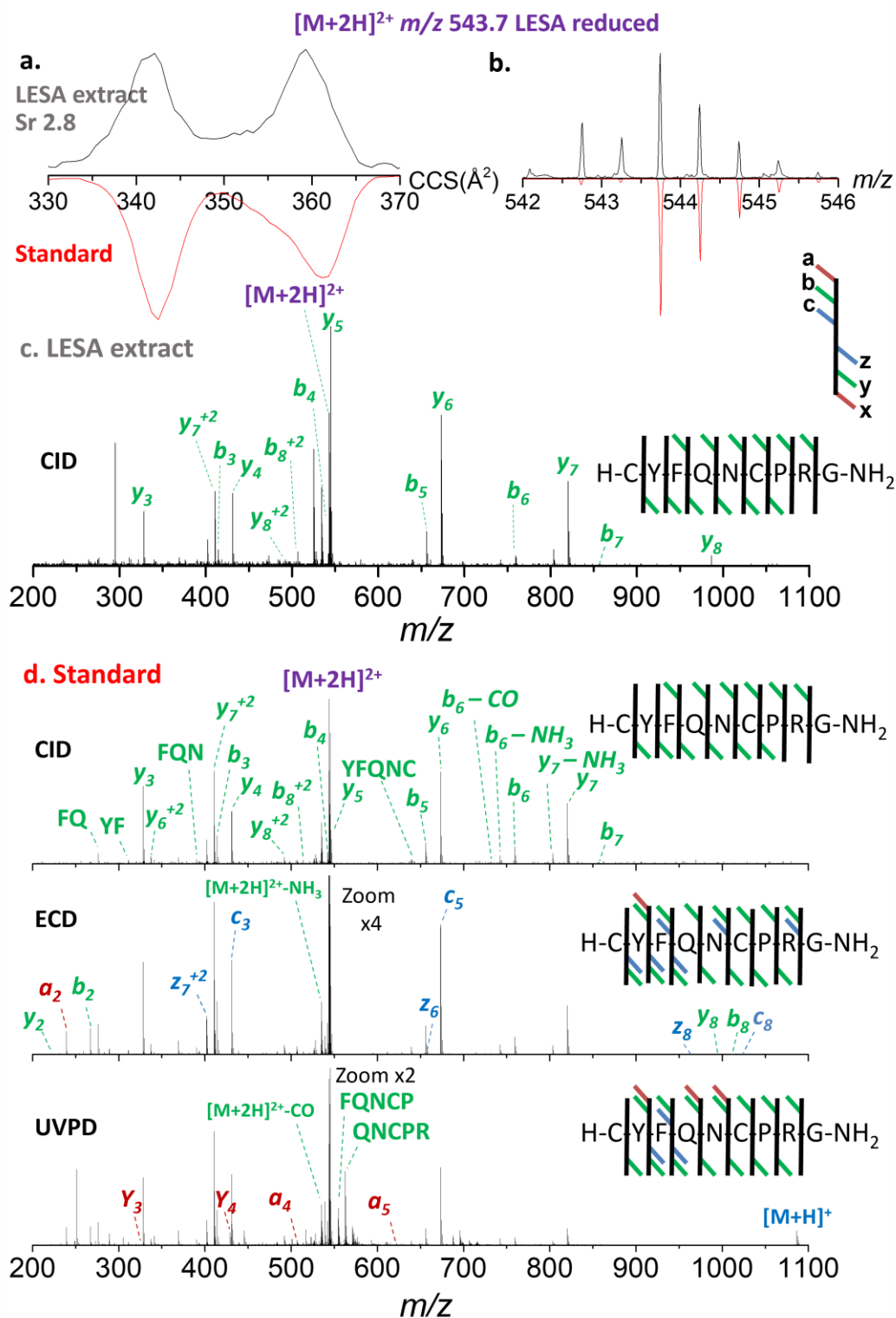


Figure 5.5. Ion mobility, experimental isotopic pattern and fragmentation pattern of [M+2H]²⁺ reduced Arg-Vasopressin species. Red traces showcase comparison to standard.

5.4. Conclusion

This paper described the utilization of complementary MALDI MSI FT-ICR MS and LESA-TIMS-TOF MS/MS for the analysis of neuropeptides from FFPE slides. The workflow allows for the localization based on MALDI MSI with sub-ppm mass accuracy and effective peptide identification using mobility profiles, accurate m/z , and fragmentation patterns. In the case of peptides with disulfide bonds, the LESA workflows allows for the addition of reduction agents effectively leading to full sequence coverage using CID techniques. The use of alternative mobility selected ECD and UVPD techniques showed better sequence coverage but lower fragmentation efficiencies when compared to mobility selected CID.

5.5. Acknowledgements

YCD acknowledges the financial support from NSF FGLSAMP FIU Bridge to the Doctorate award HRD # 1810974. We also acknowledge the financial support from the National Science Foundation Division of Chemistry, under CAREER award CHE-1654274, with co-funding from the Division of Molecular and Cellular Biosciences and funding from National Institutes of General Medicine (R01GM134247) to FFL.

5.6 References

1. M. H. Ross and W. Pawlina, *Histology: a text and atlas: with correlated cell and molecular biology*, Wolters Kluwer, 7th edn., 2016.
2. G. Baggerman, P. Verleyen, E. Clynen, J. Huybrechts, A. De Loof and L. Schoofs, *J Chromatogr B Analyt Technol Biomed Life Sci*, 2004, **803**, 3-16.

3. B. S. B. Correia, R. S. Torrinhas, W. Y. Ohashi and L. Tasic, *Intech Open*, 2018, 1-20.
4. S. A. Trauger, W. Webb and G. Siuzdak, *Spectroscopy*, 2002, 15-28.
5. F. Meng, M. C. Wiener, J. R. Sachs, C. Burns, P. Verma, C. P. Paweletz, M. T. Mazur, E. G. Deyanova, N. A. Yates and R. C. Hendrickson, *J Am Soc Mass Spectrom*, 2007, **18**, 226-233.
6. S. Chiang, W. Zhang, C. Farnsworth, Y. Zhu, K. Lee and Z. Ouyang, *J Proteome Res*, 2020, **19**, 2043-2052.
7. H. John, M. Walden, S. Schafer, S. Genz and W. G. Forssmann, *Anal Bioanal Chem*, 2004, **378**, 883-897.
8. P. M. v. Midwoud, L. Rieux, R. Bischoff, E. Verpoorte and H. A. G. Niederla, *J. Proteome Res.*, 2006, **6**, 781-791.
9. Y. V. Karpievitch, A. D. Polpitiya, G. A. Anderson, R. D. Smith and A. R. Dabney, *Ann Appl Stat*, 2010, **4**, 1797-1823.
10. Y. Bian, R. Zheng, F. P. Bayer, C. Wong, Y. C. Chang, C. Meng, D. P. Zolg, M. Reinecke, J. Zecha, S. Wiechmann, S. Heinzlmeir, J. Scherr, B. Hemmer, M. Baynham, A. C. Gingras, O. Boychenko and B. Kuster, *Nat Commun*, 2020, **11**, 157.
11. S. J. Valentine, M. Kulchania, C. A. S. Barnes and D. E. Clemmer, *Int J Mass Spectrom*, 2001, **212**, 97-109.
12. W. B. Ridenour, M. Kliman, J. A. McLean and R. M. Caprioli, *Anal Chem*, 2010, **82**, 1881-1889.
13. E. S. Baker, E. A. Livesay, D. J. Orton, R. J. Moore, W. F. D. III, D. C. Prior, Y. M. Ibrahim, B. L. LaMarche, A. M. Mayampurath, A. A. Schepmoes, D. F. Hopkins, K. Tang, R. D. Smith and M. E. Belov, *J Proteome Res*, 2010, **9**, 997-1006.
14. E. S. Baker, K. E. Burnum-Johnson, Y. M. Ibrahim, D. J. Orton, M. E. Monroe, R. T. Kelly, R. J. Moore, X. Zhang, R. Theberge, C. E. Costello and R. D. Smith, *Proteomics*, 2015, **15**, 2766-2776.
15. J. C. May, C. R. Goodwin and J. A. McLean, *Curr Opin Biotechnol*, 2015, **31**, 117-121.
16. A. Brunelle, D. Touboul and O. Laprevote, *J Mass Spectrom*, 2005, **40**, 985-999.
17. K. Chughtai and R. M. Heeren, *Chem Rev*, 2010, **110**, 3237-3277.

18. T. J. Kokkat, M. S. Patel, D. McGarvey, V. A. LiVolsi and Z. W. Baloch, *Biopreserv Biobank*, 2013, **11**, 101-106.
19. R. Lemaire, A. Desmons, J. C. Tabet, R. Day, M. Salzet and I. Fournier, *J Proteome Res*, 2007, **6**, 1295-1305.
20. M. R. L. Paine, S. R. Ellis, D. Maloney, R. M. A. Heeren and P. Verhaert, *Anal Chem*, 2018, **90**, 9272-9280.
21. V. Kertesz and G. J. Van Berkel, *J Mass Spectrom*, 2010, **45**, 252-260.
22. F. A. Fernandez-Lima, D. A. Kaplan and M. A. Park, *Rev Sci Instrum*, 2011, **82**, 126106.
23. K. Jeanne Dit Fouque, J. D. Hegemann, M. Santos-Fernandez, T. T. Le, M. Gomez-Hernandez, W. A. van der Donk and F. Fernandez-Lima, *Anal Bioanal Chem*, 2021, **413**, 4815-4824.
24. K. Jeanne Dit Fouque, V. Bisram, J. D. Hegemann, S. Zirah, S. Rebuffat and F. Fernandez-Lima, *Anal Bioanal Chem*, 2019, **411**, 6287-6296.
25. K. Jeanne Dit Fouque, H. Lavanant, S. Zirah, J. D. Hegemann, C. D. Fage, M. A. Marahiel, S. Rebuffat and C. Afonso, *Analyst*, 2018, **143**, 1157-1170.
26. J. S. Brodbelt, L. J. Morrison and I. Santos, *Chem Rev*, 2020, **120**, 3328-3380.

**CHAPTER 6. Discovery and targeted analysis of saliva using LC-TIMS-TOF
MS/MS**

Yarixa L. Cintron-Diaz, Cesar E. Ramirez, Heino Hayeman, and Francisco Fernandez-
Lima.

6.1 Abstract

The chemical and structural complexity of biological samples have challenged the development of complementary analytical techniques capable of biomarker screening. Saliva contains a variety of molecular and microbial analytes that can be effective indicators of both local and systemic disorders while carrying many advantages over blood sampling. There is a need for analytical workflows capable of identifying molecular panels indicative for early disease prognosis and disease state. A complimentary liquid chromatography trapped ion mobility spectrometry and tandem MS/MS workflow is presented for small molecule analysis from saliva samples. The proof-of-concept and potential are illustrated for the comparison of healthy (HS) and seasonal allergy (AS) human saliva samples. Complementary positive and negative ion mode generated [RT; CCS; MS; MS/MS] datasets were automatically processed and annotated. The analysis of HS and AS samples resulted in the observation of over 5,200 molecules. The proposed LC-TIMS-TOF MS/MS workflow resulted in small deviations in RT ($\leq 1\%$ RSD), CCS ($\leq 1\%$ RSD), and high mass accuracy (≤ 2 ppm). The PCA analysis provided over 90% discrimination between the saliva samples using 3 components. The potential of complementary LC-TIMS-TOF MS for the analysis of saliva samples is demonstrated for the case of healthy and seasonal allergy individuals. The combination of a 4-dimensional system allowed for the identification and discovery of potential biomarkers. Noteworthy is the observation of characteristic endogenous (e.g., metabolites and peptides) and exogenous (e.g., drugs, food markers, contaminants, etc.) and their complementary detection using various ion forms (e.g., ion modes, charge states, adduct ion forms and neutral losses).

6.2 Introduction

The use of biological samples such as blood, urine, saliva, and sweat as a source for biomarkers screening has been documented¹⁻⁴. Serum and plasma are the most popular sources used for clinical analysis; however, there have been several attempts to use non-invasive matrices (e.g., saliva and exhaled breath condensate (EBC)) for drug monitoring and biomarker discovery⁵. For example, blood sampling requires highly trained personnel, while saliva collection can be done by anyone, including self-collection. Blood sampling is invasive, while saliva collection is painless, reducing the discomfort most individuals endure from biopsies and repeated blood draws. Also, samples are safer to handle, given that EBC and salivary secretions contain factors that inhibit the infectivity of certain viruses (e.g. HIV), resulting in extremely low or negligible rates of oral transmission⁶. Finally, samples are easier to ship and store given that saliva does not clot and requires less manipulation than blood, making it a more economical procedure resulting in fewer costs for patients and healthcare providers. Saliva contains a variety of molecular and microbial analytes that can be effective indicators of both local and systemic disorders, ranging from cancer to infectious diseases⁷⁻⁹. The analysis of saliva can provide metabolomic information¹⁰, as well as proteomic and transcriptomic indicators¹¹. However, some disadvantages come with the collection and analysis of saliva such as variability in volume collection, analyte concentration and possible contamination between individuals, as well as content diurnal variability from the same individual¹². Therefore, the need for an analytical protocol on sample collection, preparation, and analysis is needed.

Many of the recent targeted and discovery workflows take advantage of complementary separations based on gas or liquid chromatography (GC, LC)¹³⁻¹⁶, ion

mobility (IMS)¹⁷⁻¹⁹ and mass spectrometry (MS and MS/MS)^{16, 20-23}. Several workflows for targeted and untargeted characterization of biomolecules from complex biological matrices (e.g., urine^{24, 25}, blood^{26, 27}, and tissue extracts²⁸⁻³⁰) in tandem with high resolution (TOF-MS/MS)^{31, 32} and ultrahigh resolution (FT-ICR MS/MS)^{28, 33, 34} mass spectrometry have been developed. With the advent of commercial, high resolution IMS-MS platforms, several groups have shown the advantages of LC-IMS-MS/MS for the analysis of small molecules^{17-19, 35}, lipids^{36, 37} and peptides³⁸⁻⁴⁰. In particular, we have shown the advantages of high resolution trapped IMS (TIMS, R up to 400) using custom-built instruments for the analysis of samples with high isomeric content (e.g., small molecules⁴¹⁻⁴³, peptides^{44, 45}, lipids⁴⁶, and DNA fragments^{47, 48}).

In this study, we discuss an LC-TIMS-TOF MS/MS workflow based on a commercial timsTOF instrument for small molecule biomarker detection from saliva samples. The goal of this report is to provide the scientific community with the expected metrics (accuracy and reproducibility on the RT, CCS, and MS measurements) for further development of multidimensional data processing and library-based validation tools for high throughput biomarker analysis based on LC-IMS-MS/MS.

6.3 Materials and Methods

6.3.1 Chemicals

LC-MS grade solvents, Acetonitrile, and Water containing 0.1% Formic Acid, were purchased from Thermo Fisher Scientific (Waltham, MA, USA). Caffeine-D3 was purchased from Toronto Research Chemicals (Ontario, Canada).

6.3.2 Samples

Single Donor Human Saliva sample (HS) was purchased from Innovative Research (LOT: 32120; Peary Court, Novi, MI, USA), and Single Donor Seasonal Allergy (AS) saliva sample was purchased from Bio IVT (LOT HMN467869; Westbury, NY). Upon arrival, saliva samples were centrifuged at 3000 rpm for 10 min at 4 °C, the supernatant was transferred to a clean tube and stored at -80 °C.

6.3.3 Sample preparation

Saliva samples were thawed on ice. An aliquot of 500 µL of saliva was transferred to a falcon tube, spiked with Caffeine-D3 to a concentration of 10 ppb as internal standard and vortexed for 1 min. 2 mL of cold acetonitrile were added and vortexed for 1 minute. Four (4) separate aliquots were transferred into 1.5 mL centrifuge tubes and centrifuged at 14,000 rpm for 10min at 4 C. The supernatant of each tube was transferred to a new 1.5 mL centrifuge tube and frozen for at least 3h at -80 C. Frozen samples were lyophilized using a custom-built vacuum drier for 3 h at 100 mTorr. Sample residues of the combined aliquots were reconstituted in 100 µL of acetonitrile/water containing 0.1% formic acid (50:50 v/v; preconcentration factor = 20). Blank samples consisted of 500 µL of ultrapure water spiked with 10 µL of Caffeine-D3 [100 ppb] as internal standard and following the same sample preparation procedure for saliva samples. Samples were prepared in triplicates.

6.3.4 LC – TIMS- MS

Reconstituted samples were analyzed using a commercial timsTOF mass spectrometer (Bruker Daltonics, Germany) system coupled to a Prominence LC-20AD HPLC system (Shimadzu, Japan). Briefly, liquid chromatography separations were performed on a Acclaim Polar Advantage II C18 analytical column (4.6 x 150 mm, 5 μ m particle size) from Thermo Fisher Scientific (Waltham, MA), using water with 0.1% of formic acid (mobile phase A) and acetonitrile with 0.1% formic acid (mobile phase B). Liquid chromatography gradient was: 5% B for 0.5 min; increase to 98% in 36.50 min; hold 98% for 4 min; return to 5% in 1.5 min; hold 5% for 2.5 min (total run time: 45 min). Flow rate was varied as follows: hold 0.250 mL/min for 30 min; increase to 0.500 mL/min in 7 min and hold until the end of the run. External valves were used to introduce calibrants as follows: a 20 μ L sample loop filled with 10 mM sodium formate clusters (50% water, 50% isopropanol; accurate mass) at 1 min; a 20 μ L sample loop filled with diluted ESI Tuning Mix (50% tunemix, 2.5 % mobile phase B and 47.5% mobile phase A; ion mobility, Agilent, Santa Clara, CA) at 1.5 min. The chromatograph was coupled to the MS instrument through an ESI source which operated under positive or negative polarities at capillary and end voltages fixed at 4500 and 500 V, respectively, with a nitrogen flow of 1.8 L/min and 250 °C. Each sample and blank were analyzed a minimum of three times in each polarity. The timsTOF instrument was operated under parallel accumulation serial fragmentation (PASEF) mode⁴⁹, an approach that enables four-dimensional (ion mobility, accurate mass, intensity and fragmentation) data acquisition with high sensitivity. The TIMS scan range was from 0.40-1.30 V·s/cm² with a ramp time of 150 ms and the TOF analyzer was operated at m/z 50–950. The scan rate used was 0.93 V/ms ($t_{\text{ramp}} = 150\text{ms}$

time and $\Delta V_{\text{ramp}} = 137.8 \text{ V}$) in the positive polarity and 0.98 V/ms ($t_{\text{ramp}} = 150 \text{ ms}$ ramp time and $\Delta V_{\text{ramp}} = 147.1 \text{ V}$) in the negative polarity. The instrument was controlled using Compass Hystar and oTOF Control (Bruker Daltonics, Germany).

6.3.5 Data Analysis

Collected data from LC-TIMS-TOF under PASEF was visualized with Compass Data Analysis 5.3 and annotated using the MetaboScape[®] 2021a software (Bruker Daltonics, Germany). Molecules were annotated based on the matching of accurate parent and fragment ion mass, isotopic pattern and CCS from available online databases (e.g., Human Metabolomics Data Base project) and *in silico* generated MS/MS profiles. MS/MS spectra were scored based on the matching to the spectral libraries. Peaks Studio X Pro (Bioinformatics Solutions Inc., Canada) was utilized to search for potential peptide molecules.

6.4 Results and discussion

The LC-TIMS-TOF MS/MS datasets are organized in buckets using automatic detection (i.e., T-ReX[®] 4D algorithm) of retention time, m/z pattern (precursor and fragments) and mobility (Figure 6.1a). The processing of positive and negative datasets resulted in over 5,200 buckets. Each bucket contains all the measured features associated with a molecule: retention time, neutral mass (derived from all the detected parent and fragment ion forms considered and corresponding CCS values)⁵⁰⁻⁵³. While most of the detected signals corresponded to single charge molecular ions (e.g., $[M+H]^{1+}$ or $[M-H]^{1-}$), doubly charged, molecular adduct ions and water loss were also observed (Figure 6.1b).

The increase in peak capacity over traditional LC-MS/MS workflows can be observed from the inspection of the 2D-IMS-MS contour plots for the HS and AS saliva samples (Figure 6.1c).

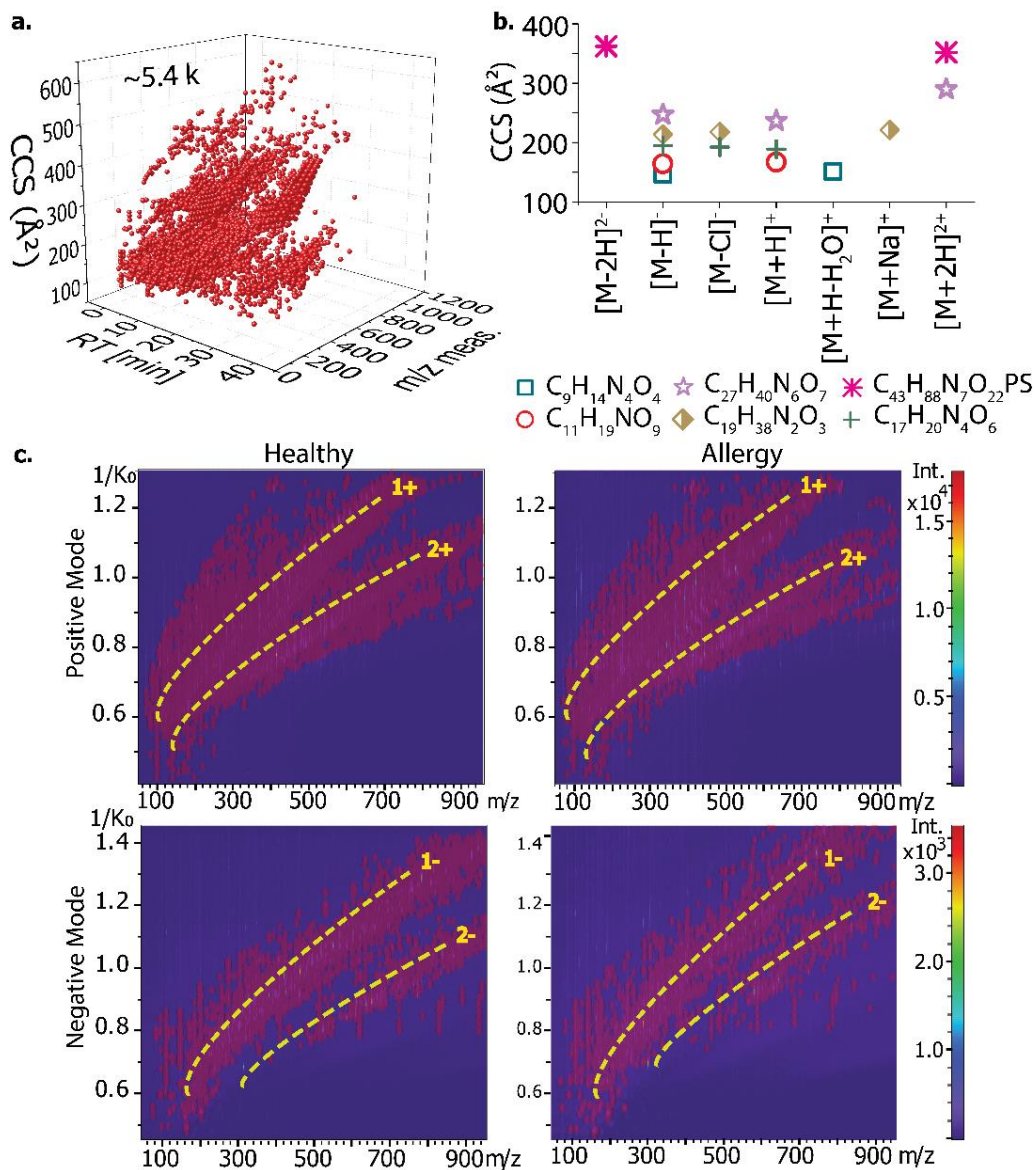


Figure 6.1. Representative features of the LC-TIMS-MS/MS workflow. (a) Merged positive and negative ion datasets into buckets representative of unique molecules observed using various ion forms (b). (c) Typical 2D-IMS-MS contour plots from healthy (HS) and allergy (AS) saliva samples; charge state trend lines are denoted.

The LC-TIMS-TOF MS/MS workflow was optimized to increase the reproducibility across runs (Figure 6.2). Low deviations in RT ($\leq 1\%$ RSD), CCS ($\leq 1\%$ RSD), and m/z (≤ 2 ppm) were observed across the analytical replicates ($n=6$); noteworthy is that most of the CCS measurements have $\leq 0.3\%$ RSD. The inclusion of calibration segments and the beginning of the LC runs allowed for automatic mobility and mass internal calibration per dataset, lowering the RSD of the CCS and m/z by 2-3x. In addition, the high mobility ($R = 80 - 120$ for $Sr = 0.93$ V/ms) and mass ($R > 50k$) resolution combined with the fast quadrupole switching (PASEF) of the current hardware permitted high analytical separation and increased numbers of MS/MS per run, respectively^{45, 49}. These are significant improvements compared to other MS platforms where typical m/z deviations are of the order of 5-10 ppm^{54, 55}. Caffeine-D3 was added to all samples as internal standard and used for normalization (Appendix 21). To further increase the confidence across chemical classes due to potential dependence on the molecular ion formation with the ion source and operating conditions, further workflows should also include the use of internal standards for the most common molecular classes annotated.

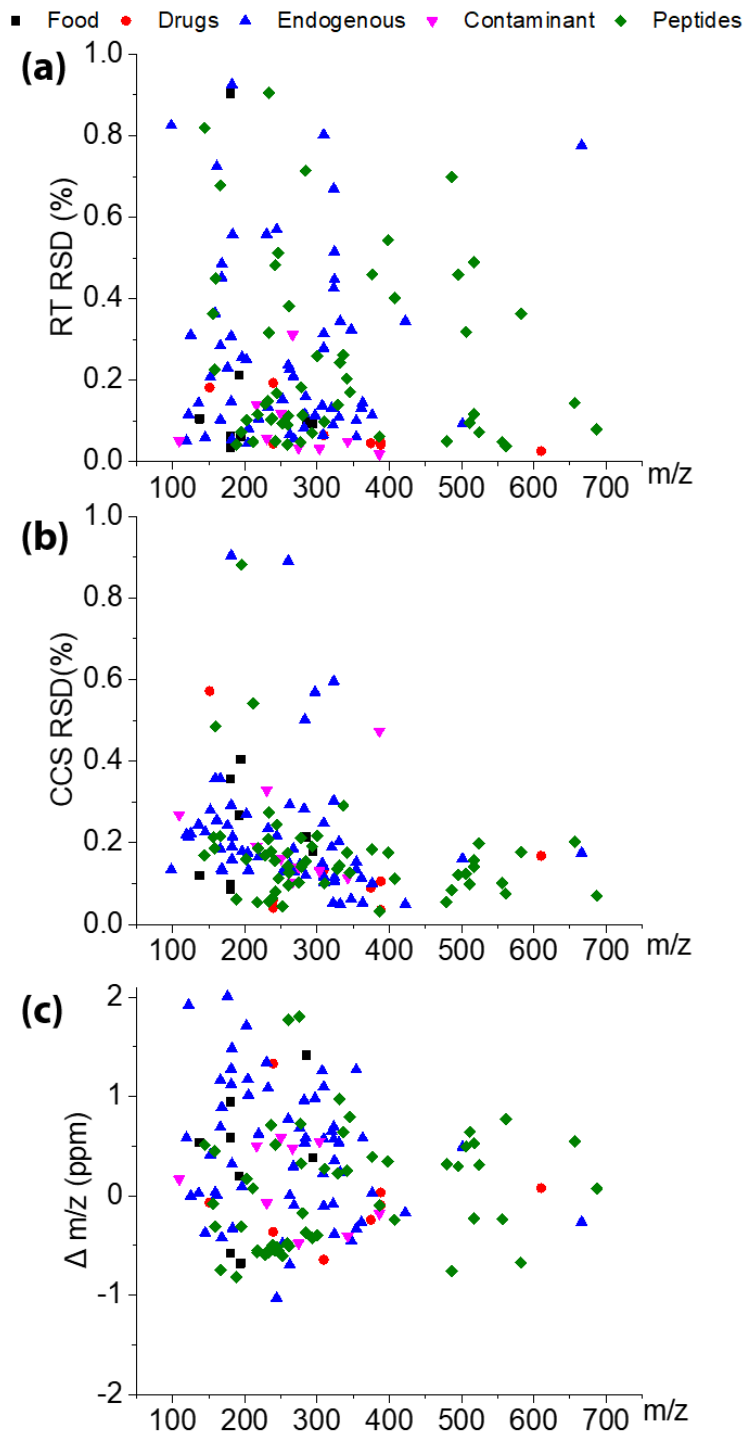


Figure 6.2. Relative standard deviations of (a) RT and (b) CCS values. (c) mass error ($\Delta m/z$) for the annotated molecules based on the MS/MS confirmation. Data corresponds to $n=6$.

The annotated analytes were organized by categories such as endogenous molecules (e.g., metabolites, vitamins, etc), drugs (medications), food, contaminants, and naturally occurring peptides. Although the latter may fall into the “endogenous molecule” category, we decided to separate these and only include molecules that are known to be present in saliva, such as vitamins, metabolites, enzymes, and nitrogenous products. Table 6.1 includes a short list of common compounds for each category (complete list; Appendix 22). The processing of the LC-TIMS-MS/MS datasets from the saliva HS and AS samples resulted in 3351 and 1730 features respectively, out of which 250 features were present in both sample types (Figure 6.3a.). Closer inspection shows that the use of negative and positive ion modes provides complementary information (Figure 6.3a), with only ~10% of observed features occurring in both ionization modes. For example, pantothenic acid and riboflavin were detected in the HS and AS samples and identified in both positive and negative mode runs. Moreover, the AS sample uniquely contained compounds associated to allergy treatment (e.g., cetirizine (RT 24.22 min, CCS 199.9 Å², ion form [M+H]⁺, and 730.7 MSMS score), albuterol (RT 13.01 min, CCS 159.5 Å², ion form [M+H]⁺, and 988.0 MSMS score), hydroxyzine (RT 22.09 min, CCS 197.2 Å², ion form [M+H]⁺, and 995.8 MSMS score)), and other medications (e. g., nadolol (RT 15.43 min, CCS 172.6 Å², ion form [M+H]⁺, and 970.9 MSMS score)), while acetaminophen (RT 19.02 min, CCS 132.6 Å², ion form [M+H]⁺, and 951.1 MSMS score), was uniquely detected in the HS sample.

Table 6.1. Common unknown knowns detected in the saliva samples using LC-TIMS-TOF MS/MS.

Identification	RT (min)	Molecular Ion Form	CCS (Å ²)	Neutral Mass	Chemical Formula	MS/MS score
Endogenous compounds						
Indole-3-acetaldehyde	25.17	[M-H] ⁺	129.9	159.0684	C ₁₀ H ₉ NO	755.7
Panhotenic Acid	15.45	[M+H] ⁺ [M-H] ⁻	149.0 146.7	219.1104	C ₉ H ₁₇ NO ₅	871.9
Uric Acid	9.86	[M+H] ⁺ [M-H] ⁻	130.9 124.6	168.0285	C ₅ H ₄ N ₄ O ₃	875.7
Drugs						
Acetaminophen ^a	19.02	[M+H] ⁺	132.6	151.0633	C ₈ H ₉ NO ₂	951.1
Albuterol ^b	13.01	[M+H] ⁺ [M-H] ⁻	159.5 163.4	239.1521	C ₁₃ H ₂₁ NO ₃	988.0
Cetirizine ^b	24.22	[M+H] ⁺ [M-H] ⁻	199.9 195.3	388.1552	C ₂₁ H ₂₅ ClN ₂ O ₃	730.7
Food						
Caffeine ^a	18.67	[M+H] ⁺	142.5	195.0875	C ₈ H ₁₀ N ₄ O ₂	996.9
D-(-)-Quinic acid	8.16	[M-H] ⁻	134.1	191.0562	C ₇ H ₁₂ O ₆	757.4
Theobromine	15.81	[M+H] ⁺	131.6	180.0721	C ₇ H ₈ N ₄ O ₂	829.1
Theophylline	17.04	[M+H] ⁺ [M-H] ⁻	139.8 131.1	180.0721	C ₇ H ₈ N ₄ O ₂	909.5

Continue Table 6.1. Common unknown knowns detected in the saliva samples using LC-TIMS-TOF MS/MS.

Identification	RT (min)	Molecular Ion Form	CCS (Å²)	Neutral Mass	Chemical Formula	MS/MS score
Contaminants						
2-Aminonaphthalene	7.27	[M+H] ⁺	132.4	110.0713	C ₅ H ₇ N ₃	992.0
Bis(p-methylbenzylidene)sorbitol	32.8	[M+H] ⁺	195.3	387.1802	C ₂₂ H ₂₆ O ₆	991.6
Bisphenol S	29.97	[M-H] ⁻	155.0	249.0229	C ₁₂ H ₁₀ O ₄ S	918.1
Peptides						
Ala Pro Pro Gln Pro Phe	16.88	[M+H] ⁺	234.4	656.3406	C ₂₃ H ₄₅ N ₇ O ₈	-
Diprotin B	15.7	[M+H] ⁺	178.8	328.2232	C ₁₆ H ₂₉ N ₃ O ₄	-
gamma-Glutamylglutamine	7.18	[M-H] ⁻	159.6	274.1051	C ₁₀ H ₁₇ N ₃ O ₆	-

^a Only present in HS sample ; ^b Only present in AS sample

One of the advantages of the proposed workflow is the complementary separation based on mobility when compared to traditional LC-MS/MS workflows (Figure 6.3b). For example, caffeine was only detected in the HS sample and can be quantified relative to the internal standard Caffeine-D3 (Appendix 21). Moreover, three structural isomers derived from caffeine were also detected; while two of them eluted at similar RT, they were all separated by mobility (Figure 6.3c): theobromine (RT 15.81 min, CCS 131.6 Å²), theophylline (RT 15.82 min, CCS 139.8 Å²) and paraxanthine (RT 17.04 min, CCS 134.1 Å²). The acetaminophen and caffeine metabolite CCS values are consistent with those in the Unified CCS Compendium⁵⁶. The cases above represent the ultimate potential for discovery analysis of unknown knowns using the LC-TIMS-MS/MS workflow and library matching.

Unbiased principal component analysis (PCA) showed that the first 3 principal components can account for over 90% of the information, meaning that the AS and HS samples can be easily differentiated based on the LC-TIMS-MS/MS datasets (Figure 6.4). Moreover, representative Hotelling T² and 3D PC1-PC3 box plots shows that the samples are clearly different in the first two components. While further evaluation will require the use of clinical replicates, these proof-of-concept experiments showcase the analytical potential of the LC-TIMS-MS/MS for clinical analysis. It should be noted that the use of clinical replicates will enable the use of other statistical tools to better identify the panel of biomarker significant to the clinical question not just based on their detection, but also based on their relative abundances^{57, 58}.

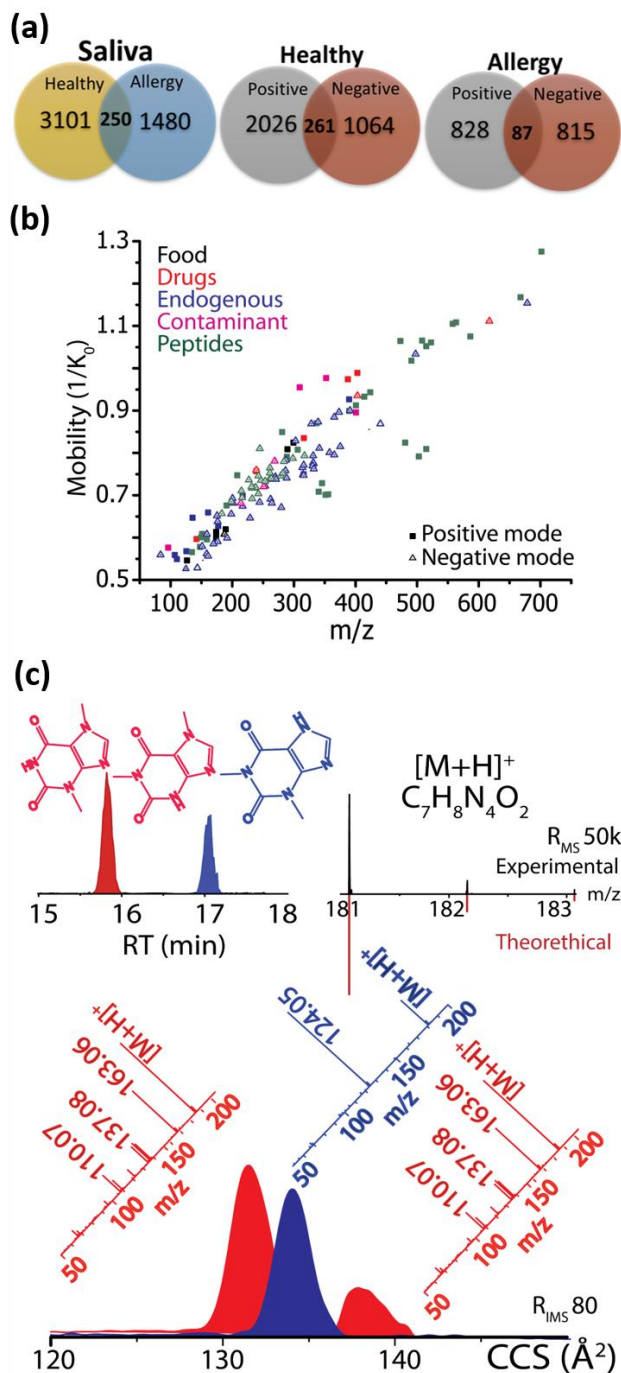


Figure 6.3. (A) Venn diagram showing molecular features in the healthy (HS) and allergy saliva samples (AS), and their relative observation depending on the ion mode. (B) Distribution of annotated molecules across the mobility, m/z and detected ion mode. (C) Typical identification of unknown knows for the case of structural isomers derived from caffeine; while two of them eluted at similar RT, they were all separated by mobility: theobromine (RT 15.81 min, $CCS 131.6 \text{ \AA}^2$), theophylline (RT 15.82 min, $CCS 139.8 \text{ \AA}^2$) and paraxanthine (RT 17.04 min, $CCS 134.1 \text{ \AA}^2$). Theobromine (red, RT 15.81 min, $CCS 131.6 \text{ \AA}^2$). Isotopic pattern of the parent ion and RT-/CCS- separated MS/MS spectra are shown.

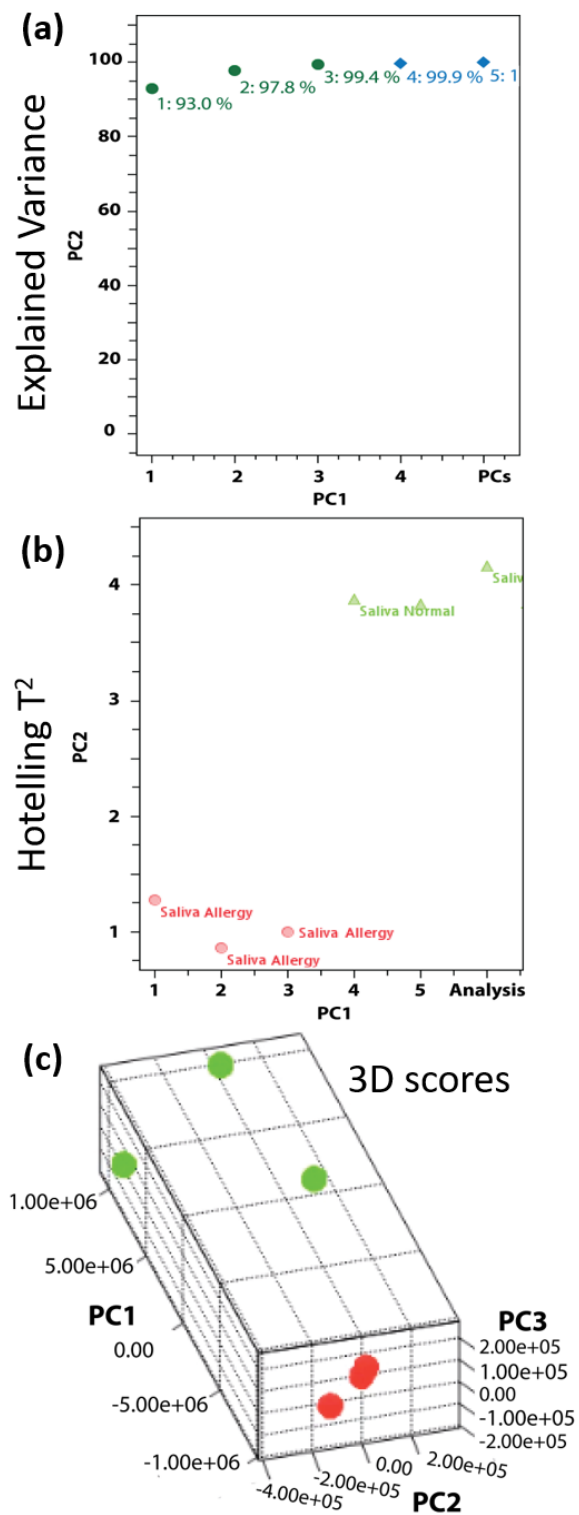


Figure 6.4. PCA statistical analysis based on the bucketing of the LC-TIMS-MS/MS dataset from the HS and AS sample using analytical triplicates. (a) Explained Variance, (b) Hotelling T² and (c) 3D scores.

6.5 Conclusions

In this study, we successfully evaluated the potential of an LC-TIMS-TOF MS/MS workflow based on a commercial timsTOF MS platform. The unbiased analysis of two human saliva samples showed the potential for the detection of different chemical classes of endogenous and exogenous compounds based on RT, CCS, accurate mass (<2 ppm), and MS/MS profile combined with library-based compound identification. Noteworthy is the increase in the analytical power with the use of complementary separation tools as well as the high reproducibility (RPD <1%) and accuracy across measurements. Additionally, this workflow offers the capability to separate molecular isomers (RT and CCS) and to identify unknown knowns using complementary ion forms with high mass accuracy and MS/MS patterns. While significant separations were observed between the two saliva samples, further evaluation with a larger number of clinical samples (at least n=30 per test group) will enable the use of more powerful statistical tools for the determination of biomarker panels associated with disease states. This basic research serves as a proof-of-concept of the capability of the sample preparation and analysis by LC-TIMS-TOF MS/MS for the potential detection of salivary markers in a clinical study. The idea is to develop an analytical workflow capable of analyzing the complexity of biological samples for salivary biomarker detection.

6.6 Acknowledgments

YCD acknowledges the financial support from NSF FGLSAMP FIU Bridge to the Doctorate award HRD # 1810974. We also acknowledge the technical support from Heiko Neuweger, Aiko Barsch, and Lucy Woods from Bruker Daltonik GmbH (Germany).

6.7 References

1. M. Harpole, J. Davis and V. Espina, *Expert Rev Proteomic*, 2016, **13**, 609-626.
2. J. M. Jacobs, J. N. Adkins, W.-J. Qian, T. Liu, Y. Shen, D. G. C. II and R. D. Smith, *J. Proteome Res.*, 2005, **4**, 1073-1085.
3. M. M. Raiszadeh, M. M. Ross, P. S. Russo, M. A. Schaepper, W. Zhou, J. Deng, D. Ng, A. Dickson, C. Dickson, M. Strom, C. Osorio, T. Soepron, J. D. Wulfschuhle, E. F. Petricoin, L. A. Liotta and W. M. Kirsch, *J. Proteome Res.*, 2012, **11**, 2127-2139.
4. N. J. Bonne and D. T. W. Wong, *Genome Med*, 2012, **4**, 1-12.
5. A. Krilaviciute, J. A. Heiss, M. Leja, J. Kupcinskas, H. Haick and H. Brenner, *Oncotarget*, 2015, **6**, 38643-38657.
6. E. A. Dietrich, K. H. Gebhard, C. E. Fasching, R. A. Giacaman, J. C. Kappes, K. F. Ross and M. C. Herzberg, *AIDS Res Hum Retroviruses*, 2012, **28**, 1574-1578.
7. N. Rathnayake, S. Akerman, B. Klinge, N. Lundegren, H. Jansson, Y. Tryselius, T. Sorsa and A. Gustafsson, *PLoS One*, 2013, **8**, e61356.
8. Y.-H. Lee and D. T. Wong, *Am J Dent.*, 2009, **22**, 241-248.
9. J. M. Yoshizawa, C. A. Schafer, J. J. Schafer, J. J. Farrell, B. J. Paster and D. T. Wong, *Clin Microbiol Rev*, 2013, **26**, 781-791.
10. Z. T. Dame, F. Aziat, R. Mandal, R. Krishnamurthy, S. Bouatra, S. Borzouie, A. C. Guo, T. Sajed, L. Deng, H. Lin, P. Liu, E. Dong and D. S. Wishart, *Metabolomics*, 2015, **11**, 1864-1883.
11. S. K. Al-Tarawneh, M. B. Border, C. F. Dibble and S. Bencharit, *OMICS*, 2011, **15**, 353-361.
12. R. Farah, H. Haraty, Z. Salame, Y. Fares, D. M. Ojcius and N. Said Sadier, *Biomed J*, 2018, **41**, 63-87.
13. D. C. Mueller, M. Piller, R. Niessner, M. Scherer and G. Scherer, *J Proteome Res*, 2014, **13**, 1602-1613.

14. M. Ciborowski, A. Lipska, J. Godzien, A. Ferrarini, J. Korsak, P. Radziwon, M. Tomasiak and C. Barbas, *J Proteome Res*, 2012, **11**, 6231-6241.
15. O. C. Zeki, C. C. Eylem, T. Recber, S. Kir and E. Nemutlu, *J Pharm Biomed Anal*, 2020, **190**, 113509.
16. Y. Gao, Y. Chen, X. Yue, J. He, R. Zhang, J. Xu, Z. Zhou, Z. Wang, R. Zhang and Z. Abliz, *Anal Chim Acta*, 2018, **1037**, 369-379.
17. J. C. May, R. L. Gant-Branum and J. A. McLean, *Curr Opin Biotechnol*, 2016, **39**, 192-197.
18. M. Hernandez-Mesa, F. Monteau, B. Le Bizec and G. Dervilly-Pinel, *Anal Chim Acta*, 2019, **1**, 100006.
19. D. E. Davis, Jr., S. D. Sherrod, R. L. Gant-Branum, J. M. Colby and J. A. McLean, *Anal Chem*, 2020, **92**, 14648-14656.
20. K. Bingol, *High Throughput*, 2018, **7**, 1-11.
21. L. Lacalle-Bergeron, D. Izquierdo-Sandoval, J. V. Sancho, F. J. López, F. Hernández and T. Portolés, *Trends Analyt Chem*, 2021, **135**, 116161.
22. M. Vinaixa, E. L. Schymanski, S. Neumann, M. Navarro, R. M. Salek and O. Yanes, *Trends Analyt Chem*, 2016, **78**, 23-35.
23. J. F. Xiao, B. Zhou and H. W. Ransom, *Trends Analyt Chem*, 2012, **32**, 1-14.
24. H. Zhao, Y. Liu, Z. Li, Y. Song, X. Cai, Y. Liu, T. Zhang, L. Yang, L. Li, S. Gao, Y. Li and C. Yu, *Clin Chim Acta*, 2018, **486**, 192-198.
25. M. Huang, H. Zhao, S. Gao, Y. Liu, Y. Liu, T. Zhang, X. Cai, Z. Li, L. Li, Y. Li and C. Yu, *Clin Chim Acta*, 2019, **497**, 95-103.
26. J. R. Denery, A. A. Nunes and T. J. Dickerson, *Anal Chem*, 2011, **83**, 1040-1047.
27. M. H. Sarafian, M. Gaudin, M. R. Lewis, F. P. Martin, E. Holmes, J. K. Nicholson and M. E. Dumas, *Anal Chem*, 2014, **86**, 5766-5774.
28. J. R. N. Haler, E. K. Sisley, Y. L. Cintron-Diaz, S. N. Meitei, H. J. Cooper and F. Fernandez-Lima, *Anal Methods*, 2019, **11**, 2385-2395.
29. V. A. Mikhailov, R. L. Griffiths and H. J. Cooper, *Int J Mass Spectrom*, 2017, **420**, 43-50.

30. E. K. Sisley, E. Illes-Toth and H. J. Cooper, *Trends Analyt Chem*, 2020, **124**, 115534.
31. M. Paul, J. Ippisch, C. Herrmann, S. Guber and W. Schultis, *Anal Bioanal Chem*, 2014, **406**, 4425-4441.
32. X. Qu, H. Gao, J. Sun, L. Tao, Y. Zhang, J. Zhai, Y. Song, T. Hu and Z. Li, *Toxicology*, 2020, **431**, 152366.
33. P. Benigni, C. J. Thompson, M. E. Ridgeway, M. A. Park and F. Fernandez-Lima, *Anal Chem*, 2015, **87**, 4321-4325.
34. E. R. Schenk, F. Nau, C. J. Thompson, Y. C. Tse-Dinh and F. Fernandez-Lima, *J Mass Spectrom*, 2015, **50**, 88-94.
35. C. Laphorn, F. Pullen and B. Z. Chowdhry, *Mass Spectrom Rev*, 2013, **32**, 43-71.
36. J. E. Kyle, X. Zhang, K. K. Weitz, M. E. Monroe, Y. M. Ibrahim, R. J. Moore, J. Cha, X. Sun, E. S. Lovelace, J. Wagoner, S. J. Polyak, T. O. Metz, S. K. Dey, R. D. Smith, K. E. Burnum-Johnson and E. S. Baker, *Analyst*, 2016, **141**, 1649-1659.
37. X. Zheng, R. D. Smith and E. S. Baker, *Curr Opin Chem Biol*, 2018, **42**, 111-118.
38. P. Venter, M. Muller, J. Vestner, M. A. Stander, A. G. J. Tredoux, H. Pasch and A. de Villiers, *Anal Chem*, 2018, **90**, 11643-11650.
39. E. S. Baker, K. E. Burnum-Johnson, Y. M. Ibrahim, D. J. Orton, M. E. Monroe, R. T. Kelly, R. J. Moore, X. Zhang, R. Theberge, C. E. Costello and R. D. Smith, *Proteomics*, 2015, **15**, 2766-2776.
40. A. Sidorina, G. Catesini, S. Levi Mortera, V. Marzano, L. Putignani, S. Boenzi, R. Taurisano, M. Garibaldi, F. Deodato and C. Dionisi-Vici, *J Inherit Metab Dis*, 2020, DOI: 10.1002/jimd.12344, 1-13.
41. A. McKenzie-Coe, J. D. DeBord, M. Ridgeway, M. Park, G. Eiceman and F. Fernandez-Lima, *Analyst*, 2015, **140**, 5692-5699.
42. P. Benigni, R. Marin and F. Fernandez-Lima, *Int J Ion Mobil Spectrom*, 2015, **18**, 151-157.
43. K. J. Adams, C. E. Ramirez, N. F. Smith, A. C. Munoz-Munoz, L. Andrade and F. Fernandez-Lima, *Talanta*, 2018, **183**, 177-183.

44. A. Garabedian, M. A. Baird, J. Porter, K. Jeanne Dit Fouque, P. V. Shliaha, O. N. Jensen, T. D. Williams, F. Fernandez-Lima and A. A. Shvartsburg, *Anal Chem*, 2018, **90**, 2918-2925.
45. F. Meier, A. D. Brunner, S. Koch, H. Koch, M. Lubeck, M. Krause, N. Goedecke, J. Decker, T. Kosinski, M. A. Park, N. Bache, O. Hoerning, J. Cox, O. Rather and M. Mann, *Mol Cell Proteomics*, 2018, **17**, 2534-2545.
46. K. Jeanne Dit Fouque, C. E. Ramirez, R. L. Lewis, J. P. Koelmel, T. J. Garrett, R. A. Yost and F. Fernandez-Lima, *Anal Chem*, 2019, **91**, 5021-5027.
47. A. Garabedian, D. Butcher, J. L. Lippens, J. Miksovska, P. P. Chapagain, D. Fabris, M. E. Ridgeway, M. A. Park and F. Fernandez-Lima, *Phys Chem Chem Phys*, 2016, **18**, 26691-26702.
48. D. Butcher, P. Chapagain, F. Leng and F. Fernandez-Lima, *J Phys Chem B*, 2018, **122**, 6855-6861.
49. F. Meier, S. Beck, N. Grassl, M. Lubeck, M. A. Park, O. Raether and M. Mann, *J Proteome Res*, 2015, **14**, 5378-5387.
50. A. Goes, P. Lapuhs, T. Kuhn, E. Schulz, R. Richter, F. Panter, C. Dahlem, M. Koch, R. Garcia, A. K. Kiemer, R. Muller and G. Fuhrmann, *Cells*, 2020, **9**, 1-17.
51. L. Olmo-García, K. Wendt, N. Kessler, A. Bajoub, A. Fernández-Gutiérrez, C. Baessmann and A. Carrasco-Pancorbo, *Eur J Lipid Sci Technol*, 2019, 1-13.
52. M. Schroeder, S. W. Meyer, H. M. Heyman, A. Barsch and L. W. Sumner, *Metabolites*, 2019, **10**, 1-17.
53. C. G. Vasilopoulou, K. Sulek, A. D. Brunner, N. S. Meitei, U. Schweiger-Hufnagel, S. W. Meyer, A. Barsch, M. Mann and F. Meier, *Nat Commun*, 2020, **11**, 1-11.
54. T. De Vijlder, D. Valkenburg, F. Lemiere, E. P. Romijn, K. Laukens and F. Cuyckens, *Mass Spectrom Rev*, 2018, **37**, 607-629.
55. T. Kind, H. Tsugawa, T. Cajka, Y. Ma, Z. Lai, S. S. Mehta, G. Wohlgemuth, D. K. Barupal, M. R. Showalter, M. Arita and O. Fiehn, *Mass Spectrom Rev*, 2018, **37**, 513-532.
56. J. A. Picache, B. S. Rose, A. Balinski, K. L. Leaptrot, S. D. Sherrod, J. C. May and J. A. McLean, *Chem Sci*, 2019, **10**, 983-993.

57. M. Gosho, K. Nagashima and Y. Sato, *Sensors*, 2012, **12**, 8966-8986.
58. J. E. McDermott, J. Wang, H. Mitchell, B. J. Webb-Robertson, R. Hafen, J. Ramey and K. D. Rodland, *Expert Opin Med Diagn*, 2013, **7**, 37-51.

CHAPTER 7: Conclusions

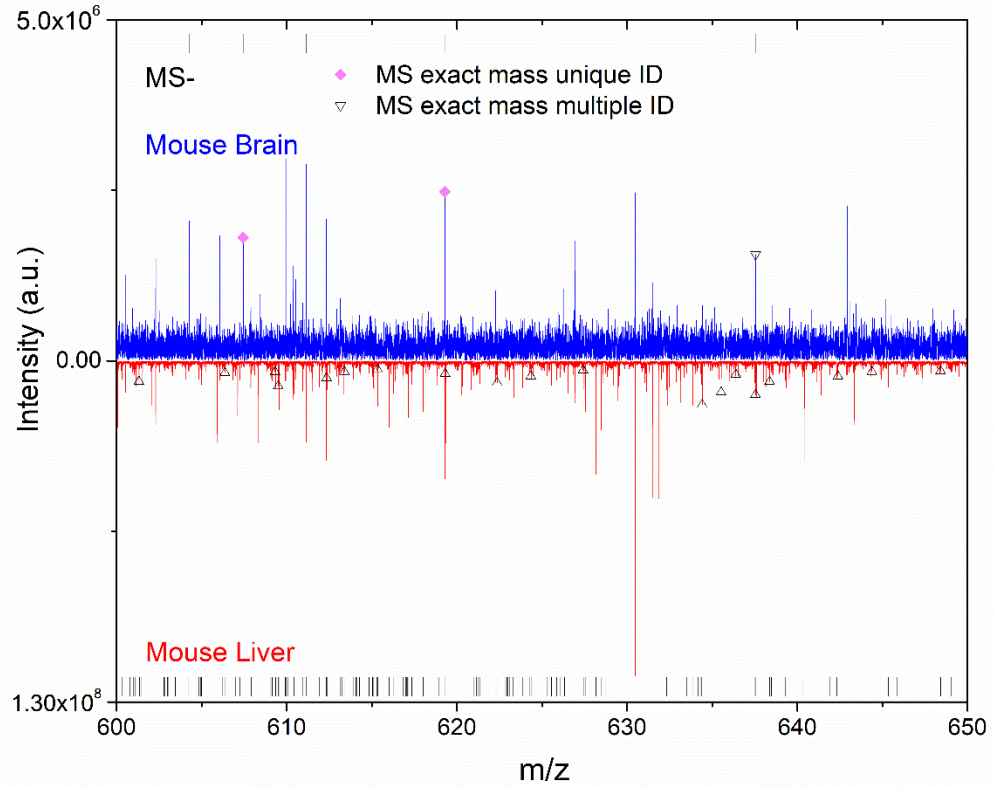
The development and application of multiple workflows in these chapters exemplify the advantages of utilizing multimodal approaches for the untargeted and targeted characterization of biological samples. In Chapter 2, a fast and high-throughput analysis workflow for lipid screening in biological tissues at ambient conditions without the need for pre-separations or sample treatment is shown. The LESA-FT-ICR MS(/MS) analysis of mouse brain and liver sections resulted in the identification of 36 lipid classes in a single analysis (< 15 min), with lipid markers specific to each tissue. In Chapter 3, the performance of LESA direct infusion analysis by two high-resolution IMS-MS platforms – nESI-cTWIMSⁿ-CID-TOF MS/MS and nESI-TIMS-qCID-TOF MS/MS – from complex biological samples (wildtype mouse brain and liver) was evaluated. The potential of the direct infusion “discovery” and “targeted” ion mobility-mass spectrometry workflows were effectively illustrated on both instrument platforms. In Chapter 4, an analytical workflow was described, where the use of TOF-SIMS allowed for high spatial resolution chemical mapping (~1.2 μm) of ABT-737 drug in single MCS slices and complementary, *in-situ* LESA-TIMS-TOF MS using internal standards allowed secondary confirmation based on mobility selected fragmentation pattern. As well, in Chapter 5, the combination of MALDI FT-ICR MS and LESA-TIMS-MS/MS allowed for the identification and localization of neuropeptides in FFPE tissues from non-ITO glass slides by their mobility pattern, accurate mass (~1ppm) and MS/MS fragmentation pattern. In the final chapter, an LC-TIMS-TOF MS/MS workflow, based on a commercial timsTOF MS platform, was developed for unbiased analysis of human saliva samples for the detection of different chemical classes of endogenous and exogenous compounds based on RT, CCS, accurate mass (<2 ppm),

In general, these chapters demonstrate the applicability of multiple mass spectrometry techniques for the unbiased and accurate identification of biomolecules in biological samples. The combination of multiple techniques allows to increase the degree of confidence of the suggested identifications in complex matrices.

Most importantly, these workflows can be implemented for the analysis of biological samples in clinical settings. The use of LESA as an extraction technique can become a gold standard for the extraction of specific biomolecules from fresh tissue biopsies and/or tissues that have been stored for years in clinical biobanks without the need of any sample preparation. The capability of changing the extraction solvent and tailoring it to extract the biomolecule (or exogenous molecule) of interest allows for the analysis of a wide range of biological tissues. In the case of the wide variety of FFPE tissues available in hospital archives, LESA has been shown to tackle the formalin fixation problem by adding a cleaning step prior to extraction. By implementing FT-ICR MS into the workflow, we can provide high mass accuracy identifications of specific molecules of interest. On the other hand, by implementing ion mobility separations, we can use high mobility resolution platforms to separate isomers and isobars from complex mixtures. Additionally, by utilizing mass spectrometry imaging platforms such as MALDI and SIMS, we can provide information of the spatial distribution of the molecule (s) of interest. All in all, the extraction, analysis, characterization, and localization of small molecules has proven to be a necessity for biomarker discovery, disease screening and development of new therapeutic agents.

APPENDICES

Appendix 1. Extract from the negative ionization mode LESA-FT-ICR-MS spectra of mouse brain (top blue) and mouse liver (bottom red). The vertical lines on top of each spectrum represent the monoisotopic m/z peaks extracted for identification. The m/z peaks with unique and multiple lipid identifications are highlighted with pink and black markers.



Appendix 2. List of used lipid abbreviations

CAR: Acyl carnitines
Cer: Ceramides
CerP: Cer-1-phosphates
DG: Di(acyl/alkyl)glycerols
DGDG: Monogalactosyldiacylglycerols
FA: Fatty acyls
HexCer: Hexosylceramides
HexSph: Hexosylsphingosines
LacCer: Lactosylceramides
LacSph: Lactosylsphingosine
LPA: Lysophosphatidic acid
LPC: Lysophosphatidylcholines
LPE: Lysophosphatidylethanolamines
LPG: Lysophosphatidylglycerol
LPI: Lysophosphatidylinositol
LPIP: Lysophosphatidylinositol monophosphate
LPS: Lysophosphatidylserine
MG: Mono(acyl/alkyl)glycerols
MGDG: Monogalactosyldiacylglycerols
MIPC: Mannosyl-PI-ceramides
NAE: N-acyl ethanolamines
NAT: N-acyl taurines
PA: Phosphatidic acids
PC: Phosphatidylcholines
PE: Phosphatidylethanolamines
PE-Cer: PE-ceramides
PG: Phosphatidylglycerols
PI: Phosphatidylinositols
PI-Cer: PI-ceramides
PIP: Phosphatidylinositol phosphates
PS: Phosphatidylserines
SHexCer: Sulfatides
SQDG: Sulfoquinovosyldiacylglycerols
TG: Tri(acyl/alkyl)glycerols
WE: Wax esters

Appendix 3. Summary of the mouse brain positive ionization LESA-FT-ICR MS1 exact mass assignments with multiple lipid identifications. The molecular ion species, chemical composition, lipid identifiers, theoretical mass, and mass error are provided.

Precursor m/z	species	Chemical Composition	Short Name	Theo. m/z	ppm
424.28148	[M+K] ⁺	C22H43NO4K	CAR(15:0)	424.2824	-2.17
424.28148	[M+H] ⁺	C20H43NO6P	S1P(t20:1)	424.2822	-1.70
478.32835	[M+H-H2O] ⁺	C24H49NO6P	LPC(16:0)	478.3292	-1.78
478.32835	[M+H-H2O] ⁺	C24H49NO6P	LPE(19:0)	478.3292	-1.78
496.33901	[M+H] ⁺	C24H51NO7P	LPC(16:0)	496.3398	1.59
496.33901	[M+H] ⁺	C24H51NO7P	LPE(19:0)	496.3398	1.59
518.32101	[M+Na] ⁺	C24H50NO7PNa	LPC(16:0)	518.3217	1.33
518.32101	[M+Na] ⁺	C24H50NO7PNa	LPE(19:0)	518.3217	1.33
522.35472	[M+H] ⁺	C26H53NO7P	CerP(t26:1)	522.3554	1.30
522.35472	[M+H] ⁺	C26H53NO7P	LPC(18:1)	522.3554	1.30
522.35472	[M+H-H2O] ⁺	C26H53NO7P	LPS(O-20:0)	522.3554	1.30
524.37031	[M+Na] ⁺	C31H51NO4Na	CAR(24:5)	524.371	1.32
524.37031	[M+H] ⁺	C26H55NO7P	CerP(t26:0)	524.3711	1.51
524.37031	[M+H] ⁺	C26H55NO7P	LPC(18:0)	524.3711	1.51
524.37031	[M+H] ⁺	C26H55NO7P	LPE(21:0)	524.3711	1.51
534.29497	[M+K] ⁺	C24H50NO7PK	LPC(16:0)	534.2956	1.18
534.29497	[M+K] ⁺	C24H50NO7PK	LPE(19:0)	534.2956	1.18
560.31074	[M+K] ⁺	C26H52NO7PK	CerP(t26:1)	560.3113	1.00
560.31074	[M+K] ⁺	C26H52NO7PK	LPC(18:1)	560.3113	1.00
560.31074	[M+H] ⁺	C24H50NO11S	SHexSph(t18:0)	560.3099	-1.50
650.43913	[M+H] ⁺	C33H65NO9P	LPS(27:1)	650.4391	-0.05
650.43913	[M+H] ⁺	C33H65NO9P	PC(25:1(OH))	650.4391	-0.05
650.43913	[M+H] ⁺	C33H65NO9P	PE(28:1(OH))	650.4391	-0.05
678.47071	[M+H] ⁺	C35H69NO9P	PC(27:1(OH))	678.4704	-0.46
678.47071	[M+H] ⁺	C35H69NO9P	PE(30:1(OH))	678.4704	-0.46
678.47071	[M+H] ⁺	C35H69NO9P	PS(P-29:0)	678.4704	-0.46
702.54339	[M+H] ⁺	C39H77NO7P	PC(P-31:1)	702.5432	-0.27
702.54339	[M+H] ⁺	C39H77NO7P	PE(O-34:2)	702.5432	-0.27
702.54339	[M+H] ⁺	C39H77NO7P	PE(P-34:1)	702.5432	-0.27
706.53831	[M+H] ⁺	C38H77NO8P	PC(30:0)	706.5381	-0.30
706.53831	[M+H] ⁺	C38H77NO8P	PC(O-30:1(OH))	706.5381	-0.30
706.53831	[M+H] ⁺	C38H77NO8P	PC(P-30:0(OH))	706.5381	-0.30
706.53831	[M+H] ⁺	C38H77NO8P	PE(33:0)	706.5381	-0.30
706.53831	[M+H] ⁺	C38H77NO8P	PE(O-33:1(OH))	706.5381	-0.30
706.53831	[M+H] ⁺	C38H77NO8P	PE(P-33:0(OH))	706.5381	-0.30
720.59057	[M+H] ⁺	C40H83NO7P	CerP(t40:0)	720.5902	-0.51
720.59057	[M+H] ⁺	C40H83NO7P	LPC(32:0)	720.5902	-0.51
720.59057	[M+H] ⁺	C40H83NO7P	PC(O-32:0)	720.5902	-0.51
720.59057	[M+H] ⁺	C40H83NO7P	PE(O-35:0)	720.5902	-0.51
724.52804	[M+H] ⁺	C41H75NO7P	PE(O-36:5)	724.5276	-0.61
724.52804	[M+H] ⁺	C41H75NO7P	PE(P-36:4)	724.5276	-0.61
728.55917	[M+H] ⁺	C41H79NO7P	PC(P-33:2)	728.5589	-0.37
728.55917	[M+H] ⁺	C41H79NO7P	PE(O-36:3)	728.5589	-0.37
728.55917	[M+H] ⁺	C41H79NO7P	PE(P-36:2)	728.5589	-0.37

Continue Appendix 3. Summary of the mouse brain positive ionization LESA-FT-ICR MS1 exact mass assignments with multiple lipid identifications.

Precursor m/z	species	Chemical Composition	Short Name	Theo. m/z	ppm
729.59077	[M+H] ⁺	C41H82N2O6P	PE-Cer(d39:2)	729.5905	-0.37
729.59077	[M+H] ⁺	C41H82N2O6P	SM(d36:2)	729.5905	-0.37
730.57489	[M+H] ⁺	C41H81NO7P	PC(O-33:2)	730.5745	-0.53
730.57489	[M+H] ⁺	C41H81NO7P	PC(P-33:1)	730.5745	-0.53
730.57489	[M+H] ⁺	C41H81NO7P	PE(O-36:2)	730.5745	-0.53
730.57489	[M+H] ⁺	C41H81NO7P	PE(P-36:1)	730.5745	-0.53
731.60646	[M+H] ⁺	C41H84N2O6P	PE-Cer(d39:1)	731.6061	-0.49
731.60646	[M+H] ⁺	C41H84N2O6P	SM(d36:1)	731.6061	-0.49
732.55413	[M+H] ⁺	C40H79NO8P	PC(32:1)	732.5538	-0.45
732.55413	[M+H] ⁺	C40H79NO8P	PC(P-32:1(OH))	732.5538	-0.45
732.55413	[M+H] ⁺	C40H79NO8P	PE(35:1)	732.5538	-0.45
732.55413	[M+H] ⁺	C40H79NO8P	PE(O-35:2(OH))	732.5538	-0.45
732.55413	[M+H] ⁺	C40H79NO8P	PE(P-35:1(OH))	732.5538	-0.45
732.55413	[M+H-H2O] ⁺	C40H79NO8P	LPS(34:0)	732.5538	-0.45
740.49924	[M+K] ⁺	C39H76NO7PK	PC(P-31:1)	740.4991	-0.19
740.49924	[M+K] ⁺	C39H76NO7PK	PE(O-34:2)	740.4991	-0.19
740.49924	[M+K] ⁺	C39H76NO7PK	PE(P-34:1)	740.4991	-0.19
740.49924	[M+H] ⁺	C37H74NO11S	SHexCer(d31:0)	740.4977	-2.08
740.52297	[M+H] ⁺	C41H75NO8P	PC(33:4)	740.5225	-0.63
740.52297	[M+H] ⁺	C41H75NO8P	PE(36:4)	740.5225	-0.63
740.52297	[M+H] ⁺	C41H75NO8P	PE(O-36:5(OH))	740.5225	-0.63
740.52297	[M+H] ⁺	C41H75NO8P	PE(P-36:4(OH))	740.5225	-0.63
744.49434	[M+K] ⁺	C38H76NO8PK	PC(30:0)	744.494	-0.46
744.49434	[M+K] ⁺	C38H76NO8PK	PC(O-30:1(OH))	744.494	-0.46
744.49434	[M+K] ⁺	C38H76NO8PK	PC(P-30:0(OH))	744.494	-0.46
744.49434	[M+K] ⁺	C38H76NO8PK	PE(33:0)	744.494	-0.46
744.49434	[M+K] ⁺	C38H76NO8PK	PE(O-33:1(OH))	744.494	-0.46
744.49434	[M+K] ⁺	C38H76NO8PK	PE(P-33:0(OH))	744.494	-0.46
744.49434	[M+Na] ⁺	C41H72NO7PNa	PE(P-36:5)	744.4939	-0.59
744.55423	[M+H] ⁺	C41H79NO8P	PC(33:2)	744.5538	-0.58
744.55423	[M+H] ⁺	C41H79NO8P	PC(P-33:2(OH))	744.5538	-0.58
744.55423	[M+H] ⁺	C41H79NO8P	PE(36:2)	744.5538	-0.58
744.55423	[M+H] ⁺	C41H79NO8P	PE(O-36:3(OH))	744.5538	-0.58
744.55423	[M+H] ⁺	C41H79NO8P	PE(P-36:2(OH))	744.5538	-0.58
744.59077	[M+H] ⁺	C42H83NO7P	CerP(t42:2)	744.5902	-0.77
744.59077	[M+H] ⁺	C42H83NO7P	PC(O-34:2)	744.5902	-0.77
744.59077	[M+H] ⁺	C42H83NO7P	PC(P-34:1)	744.5902	-0.77
744.59077	[M+H] ⁺	C42H83NO7P	PE(O-37:2)	744.5902	-0.77
744.59077	[M+H] ⁺	C42H83NO7P	PE(P-37:1)	744.5902	-0.77
746.56979	[M+H] ⁺	C41H81NO8P	PC(33:1)	746.5694	-0.52
746.56979	[M+H] ⁺	C41H81NO8P	PC(O-33:2(OH))	746.5694	-0.52
746.56979	[M+H] ⁺	C41H81NO8P	PC(P-33:1(OH))	746.5694	-0.52
746.56979	[M+H] ⁺	C41H81NO8P	PE(36:1)	746.5694	-0.52
746.56979	[M+H] ⁺	C41H81NO8P	PE(O-36:2(OH))	746.5694	-0.52
746.56979	[M+H] ⁺	C41H81NO8P	PE(P-36:1(OH))	746.5694	-0.52

Continue Appendix 3. Summary of the mouse brain positive ionization LESA-FT-ICR MS1 exact mass assignments with multiple lipid identifications.

Precursor m/z	species	Chemical Composition	Short Name	Theo. m/z	ppm
746.6063	[M+H] ⁺	C42H85NO7P	CerP(t42:1)	746.6058	-0.67
746.6063	[M+H] ⁺	C42H85NO7P	PC(O-34:1)	746.6058	-0.67
746.6063	[M+H] ⁺	C42H85NO7P	PC(P-34:0)	746.6058	-0.67
746.6063	[M+H] ⁺	C42H85NO7P	PE(O-37:1)	746.6058	-0.67
746.6063	[M+H] ⁺	C42H85NO7P	PE(P-37:0)	746.6058	-0.67
750.5439	[M+H] ⁺	C43H77NO7P	PE(O-38:6)	750.5432	-0.93
750.5439	[M+H] ⁺	C43H77NO7P	PE(P-38:5)	750.5432	-0.93
752.55942	[M+H] ⁺	C43H79NO7P	PE(O-38:5)	752.5589	-0.69
752.55942	[M+H] ⁺	C43H79NO7P	PE(P-38:4)	752.5589	-0.69
753.58872	[M+Na] ⁺	C41H83N2O6PNa	PE-Cer(d39:1)	753.5881	-0.82
753.58872	[M+Na] ⁺	C41H83N2O6PNa	SM(d36:1)	753.5881	-0.82
754.53611	[M+Na] ⁺	C40H78NO8PNa	PC(32:1)	754.5357	-0.54
754.53611	[M+Na] ⁺	C40H78NO8PNa	PE(35:1)	754.5357	-0.54
754.53611	[M+Na] ⁺	C40H78NO8PNa	PC(P-32:1(OH))	754.5357	-0.54
754.53611	[M+Na] ⁺	C40H78NO8PNa	PE(O-35:2(OH))	754.5357	-0.54
754.53611	[M+H] ⁺	C42H77NO8P	PC(34:4)	754.5381	2.64
754.53611	[M+Na] ⁺	C40H78NO8PNa	PE(P-35:1(OH))	754.5357	-0.54
754.53611	[M+H] ⁺	C42H77NO8P	PE(37:4)	754.5381	2.64
754.53611	[M+H] ⁺	C42H77NO8P	PC(P-34:4(OH))	754.5381	2.64
764.523	[M+H] ⁺	C43H75NO8P	PC(35:6)	764.5225	-0.65
764.523	[M+H] ⁺	C43H75NO8P	PE(38:6)	764.5225	-0.65
764.523	[M+H] ⁺	C43H75NO8P	PE(P-38:6(OH))	764.5225	-0.65
768.55439	[M+H] ⁺	C43H79NO8P	PC(35:4)	768.5538	-0.77
768.55439	[M+H] ⁺	C43H79NO8P	PE(38:4)	768.5538	-0.77
768.55439	[M+H] ⁺	C43H79NO8P	PE(O-38:5(OH))	768.5538	-0.77
768.55439	[M+H] ⁺	C43H79NO8P	PE(P-38:4(OH))	768.5538	-0.77
770.5103	[M+K] ⁺	C40H78NO8PK	PC(32:1)	770.5097	-0.78
770.5103	[M+K] ⁺	C40H78NO8PK	PE(35:1)	770.5097	-0.78
770.5103	[M+K] ⁺	C40H78NO8PK	PC(P-32:1(OH))	770.5097	-0.78
770.5103	[M+K] ⁺	C40H78NO8PK	PE(O-35:2(OH))	770.5097	-0.78
770.5103	[M+K] ⁺	C40H78NO8PK	PE(P-35:1(OH))	770.5097	-0.78
770.5103	[M+H] ⁺	C38H76NO12S	SHexCer(t32:0)	770.5083	-2.60
770.5103	[M+Na] ⁺	C43H74NO7PNa	PE(P-38:6)	770.5095	-1.04
774.60142	[M+H] ⁺	C43H85NO8P	PC(35:1)	774.6007	-0.93
774.60142	[M+H] ⁺	C43H85NO8P	PC(O-35:2(OH))	774.6007	-0.93
774.60142	[M+H] ⁺	C43H85NO8P	PE(38:1)	774.6007	-0.93
774.60142	[M+H] ⁺	C43H85NO8P	PC(P-35:1(OH))	774.6007	-0.93
774.60142	[M+H] ⁺	C43H85NO8P	PE(O-38:2(OH))	774.6007	-0.93
774.60142	[M+H] ⁺	C43H85NO8P	PE(P-38:1(OH))	774.6007	-0.93
774.63802	[M+H] ⁺	C44H89NO7P	CerP(t44:1)	774.6371	-1.19
774.63802	[M+H] ⁺	C44H89NO7P	PC(O-36:1)	774.6371	-1.19
774.63802	[M+H] ⁺	C44H89NO7P	PC(P-36:0)	774.6371	-1.19
774.63802	[M+H] ⁺	C44H89NO7P	PE(P-39:0)	774.6371	-1.19
780.55186	[M+Na] ⁺	C42H80NO8PNa	PC(34:2)	780.5514	-0.59
780.55186	[M+Na] ⁺	C42H80NO8PNa	PE(37:2)	780.5514	-0.59

Continue Appendix 3. Summary of the mouse brain positive ionization LESA-FT-ICR MS1 exact mass assignments with multiple lipid identifications.

Precursor m/z	species	Chemical Composition	Short Name	Theo. m/z	ppm
780.55186	[M+H] ⁺	C44H79NO8P	PC(36:5)	780.5538	2.49
780.55186	[M+Na] ⁺	C42H80NO8PNa	PC(O-34:3(OH))	780.5514	-0.59
780.55186	[M+H] ⁺	C44H79NO8P	PE(39:5)	780.5538	2.49
780.55186	[M+Na] ⁺	C42H80NO8PNa	PC(P-34:2(OH))	780.5514	-0.59
780.55186	[M+H] ⁺	C44H79NO8P	PC(P-36:5(OH))	780.5538	2.49
780.55186	[M+Na] ⁺	C42H80NO8PNa	PE(P-37:2(OH))	780.5514	-0.59
780.59097	[M+H] ⁺	C45H83NO7P	PE(O-40:5)	780.5902	-0.99
780.59097	[M+H] ⁺	C45H83NO7P	PE(P-40:4)	780.5902	-0.99
782.51	[M+K] ⁺	C41H78NO8PK	PC(33:2)	782.5097	-0.38
782.51	[M+K] ⁺	C41H78NO8PK	PE(36:2)	782.5097	-0.38
782.51	[M+K] ⁺	C41H78NO8PK	PC(P-33:2(OH))	782.5097	-0.38
782.51	[M+H] ⁺	C39H76NO12S	SHexCer(t33:1)	782.5083	-2.17
782.51	[M+K] ⁺	C41H78NO8PK	PE(O-36:3(OH))	782.5097	-0.38
782.51	[M+K] ⁺	C41H78NO8PK	PE(P-36:2(OH))	782.5097	-0.38
784.56232	[M+K] ⁺	C42H84NO7PK	CerP(t42:1)	784.5617	-0.79
784.56232	[M+K] ⁺	C42H84NO7PK	PC(O-34:1)	784.5617	-0.79
784.56232	[M+K] ⁺	C42H84NO7PK	PC(P-34:0)	784.5617	-0.79
784.56232	[M+K] ⁺	C42H84NO7PK	PE(O-37:1)	784.5617	-0.79
784.56232	[M+K] ⁺	C42H84NO7PK	PE(P-37:0)	784.5617	-0.79
786.5051	[M+Na] ⁺	C43H74NO8PNa	PC(35:6)	786.5044	-0.89
786.5051	[M+Na] ⁺	C43H74NO8PNa	PE(38:6)	786.5044	-0.89
786.5051	[M+K] ⁺	C40H78NO9PK	PC(32:1(OH))	786.5046	-0.64
786.5051	[M+K] ⁺	C40H78NO9PK	PE(35:1(OH))	786.5046	-0.64
786.5051	[M+H] ⁺	C45H73NO8P	PE(40:9)	786.5068	2.16
786.5051	[M+Na] ⁺	C43H74NO8PNa	PE(P-38:6(OH))	786.5044	-0.89
786.5051	[M+K] ⁺	C40H78NO9PK	PS(O-34:1)	786.5046	-0.64
786.5051	[M+K] ⁺	C40H78NO9PK	PS(P-34:0)	786.5046	-0.64
786.54126	[M+K] ⁺	C41H82NO8PK	PC(33:0)	786.541	-0.33
786.54126	[M+K] ⁺	C41H82NO8PK	PE(36:0)	786.541	-0.33
786.54126	[M+K] ⁺	C41H82NO8PK	PC(O-33:1(OH))	786.541	-0.33
786.54126	[M+K] ⁺	C41H82NO8PK	PC(P-33:0(OH))	786.541	-0.33
786.54126	[M+Na] ⁺	C44H78NO7PNa	PC(P-36:5)	786.5408	-0.58
786.54126	[M+K] ⁺	C41H82NO8PK	PE(O-36:1(OH))	786.541	-0.33
786.54126	[M+K] ⁺	C41H82NO8PK	PE(P-36:0(OH))	786.541	-0.33
786.60147	[M+H] ⁺	C44H85NO8P	PC(36:2)	786.6007	-0.98
786.60147	[M+H] ⁺	C44H85NO8P	PE(39:2)	786.6007	-0.98
786.60147	[M+H] ⁺	C44H85NO8P	PC(O-36:3(OH))	786.6007	-0.98
786.60147	[M+H] ⁺	C44H85NO8P	PC(P-36:2(OH))	786.6007	-0.98
790.51554	[M+K] ⁺	C43H78NO7PK	PE(O-38:5)	790.5147	-1.06
790.51554	[M+K] ⁺	C43H78NO7PK	PE(P-38:4)	790.5147	-1.06
790.53578	[M+Na] ⁺	C43H78NO8PNa	PC(35:4)	790.5357	-0.10
790.53578	[M+H] ⁺	C45H77NO8P	PC(37:7)	790.5381	2.93
790.53578	[M+Na] ⁺	C43H78NO8PNa	PE(38:4)	790.5357	-0.10
790.53578	[M+H] ⁺	C45H77NO8P	PE(40:7)	790.5381	2.93
790.53578	[M+Na] ⁺	C43H78NO8PNa	PE(O-38:5(OH))	790.5357	-0.10

Continue Appendix 3. Summary of the mouse brain positive ionization LESA-FT-ICR MS1 exact mass assignments with multiple lipid identifications.

Precursor m/z	species	Chemical Composition	Short Name	Theo. m/z	ppm
790.53578	[M+Na] ⁺	C43H78NO8PNa	PE(P-38:4(OH))	790.5357	-0.10
792.55455	[M+H] ⁺	C45H79NO8P	PC(37:6)	792.5538	-0.95
792.55455	[M+H] ⁺	C45H79NO8P	PE(40:6)	792.5538	-0.95
792.55455	[M+H] ⁺	C45H79NO8P	PE(P-40:6(OH))	792.5538	-0.95
796.52609	[M+K] ⁺	C42H80NO8PK	PC(34:2)	796.5253	-0.99
796.52609	[M+K] ⁺	C42H80NO8PK	PE(37:2)	796.5253	-0.99
796.52609	[M+H] ⁺	C40H78NO12S	SHexCer(t34:1)	796.5239	-2.75
796.52609	[M+K] ⁺	C42H80NO8PK	PC(O-34:3(OH))	796.5253	-0.99
796.52609	[M+K] ⁺	C42H80NO8PK	PC(P-34:2(OH))	796.5253	-0.99
796.52609	[M+K] ⁺	C42H80NO8PK	PE(P-37:2(OH))	796.5253	-0.99
796.58594	[M+H] ⁺	C45H83NO8P	PC(37:4)	796.5851	-1.05
796.58594	[M+H] ⁺	C45H83NO8P	PE(40:4)	796.5851	-1.05
796.58594	[M+H] ⁺	C45H83NO8P	PE(O-40:5(OH))	796.5851	-1.05
796.58594	[M+H] ⁺	C45H83NO8P	PE(P-40:4(OH))	796.5851	-1.05
800.53995	[M+Na] ⁺	C41H80NO10PNa	PS(35:0)	800.5412	1.56
800.53995	[M+Na] ⁺	C41H80NO10PNa	PS(O-35:1(OH))	800.5412	1.56
800.53995	[M+Na] ⁺	C41H80NO10PNa	PS(P-35:0(OH))	800.5412	1.56
800.55745	[M+K] ⁺	C42H84NO8PK	PC(34:0)	800.5566	-1.06
800.55745	[M+K] ⁺	C42H84NO8PK	PE(37:0)	800.5566	-1.06
800.55745	[M+K] ⁺	C42H84NO8PK	PC(O-34:1(OH))	800.5566	-1.06
800.55745	[M+K] ⁺	C42H84NO8PK	PC(P-34:0(OH))	800.5566	-1.06
800.55745	[M+K] ⁺	C42H84NO8PK	PE(O-37:1(OH))	800.5566	-1.06
800.55745	[M+Na] ⁺	C45H80NO7PNa	PE(O-40:6)	800.5565	-1.19
800.55745	[M+K] ⁺	C42H84NO8PK	PE(P-37:0(OH))	800.5566	-1.06
800.55745	[M+Na] ⁺	C45H80NO7PNa	PE(P-40:5)	800.5565	-1.19
802.47923	[M+K] ⁺	C43H74NO8PK	PC(35:6)	802.4784	-1.03
802.47923	[M+K] ⁺	C43H74NO8PK	PE(38:6)	802.4784	-1.03
802.47923	[M+K] ⁺	C43H74NO8PK	PE(P-38:6(OH))	802.4784	-1.03
806.51057	[M+K] ⁺	C43H78NO8PK	PC(35:4)	806.5097	-1.08
806.51057	[M+K] ⁺	C43H78NO8PK	PE(38:4)	806.5097	-1.08
806.51057	[M+K] ⁺	C43H78NO8PK	PE(O-38:5(OH))	806.5097	-1.08
806.51057	[M+K] ⁺	C43H78NO8PK	PE(P-38:4(OH))	806.5097	-1.08
808.5705	[M+H] ⁺	C42H83NO11P	PS(36:0(OH))	808.5698	-0.87
808.5705	[M+K] ⁺	C44H83NO9K	HexCer(t38:2)	808.5699	-0.74
808.5705	[M+H] ⁺	C42H83NO11P	PI-Cer(d36:1)	808.5698	-0.87
808.5705	[M+H-H ₂ O] ⁺	C42H83NO11P	PI-Cer(t36:0)	808.5698	-0.87
812.55756	[M+K] ⁺	C43H84NO8PK	PC(35:1)	812.5566	-1.18
812.55756	[M+K] ⁺	C43H84NO8PK	PE(38:1)	812.5566	-1.18
812.55756	[M+K] ⁺	C43H84NO8PK	PC(O-35:2(OH))	812.5566	-1.18
812.55756	[M+K] ⁺	C43H84NO8PK	PC(P-35:1(OH))	812.5566	-1.18
812.55756	[M+H] ⁺	C41H82NO12S	SHexCer(t35:0)	812.5552	-2.90
812.55756	[M+K] ⁺	C43H84NO8PK	PE(O-38:2(OH))	812.5566	-1.18
812.55756	[M+K] ⁺	C43H84NO8PK	PE(P-38:1(OH))	812.5566	-1.18
812.55756	[M+Na] ⁺	C46H80NO7PNa	PC(P-38:6)	812.5565	-1.30
812.61737	[M+H] ⁺	C46H87NO8P	PC(38:3)	812.6164	-1.19

Continue Appendix 3. Summary of the mouse brain positive ionization LESA-FT-ICR MS1 exact mass assignments with multiple lipid identifications.

Precursor m/z	species	Chemical Composition	Short Name	Theo. m/z	ppm
812.61737	[M+H] ⁺	C46H87NO8P	PE(41:3)	812.6164	-1.19
812.61737	[M+H] ⁺	C46H87NO8P	PC(O-38:4(OH))	812.6164	-1.19
812.61737	[M+H] ⁺	C46H87NO8P	PC(P-38:3(OH))	812.6164	-1.19
813.68517	[M+H] ⁺	C47H94N2O6P	PE-Cer(d45:2)	813.6844	-0.95
813.68517	[M+H] ⁺	C47H94N2O6P	SM(d42:2)	813.6844	-0.95
814.5367	[M+Na] ⁺	C45H78NO8PNa	PC(37:6)	814.5357	-1.23
814.5367	[M+Na] ⁺	C45H78NO8PNa	PE(40:6)	814.5357	-1.23
814.5367	[M+K] ⁺	C42H82NO9PK	PC(34:1(OH))	814.5359	-0.98
814.5367	[M+K] ⁺	C42H82NO9PK	PE(37:1(OH))	814.5359	-0.98
814.5367	[M+H] ⁺	C47H77NO8P	PE(42:9)	814.5381	1.72
814.5367	[M+Na] ⁺	C45H78NO8PNa	PE(P-40:6(OH))	814.5357	-1.23
814.5367	[M+K] ⁺	C42H82NO9PK	PS(O-36:1)	814.5359	-0.98
814.5367	[M+K] ⁺	C42H82NO9PK	PS(P-36:0)	814.5359	-0.98
814.63308	[M+H] ⁺	C46H89NO8P	PC(38:2)	814.632	-1.33
814.63308	[M+H] ⁺	C46H89NO8P	PE(41:2)	814.632	-1.33
814.63308	[M+H] ⁺	C46H89NO8P	PC(O-38:3(OH))	814.632	-1.33
814.63308	[M+H] ⁺	C46H89NO8P	PC(P-38:2(OH))	814.632	-1.33
816.64866	[M+H] ⁺	C46H91NO8P	PC(38:1)	816.6477	-1.18
816.64866	[M+H] ⁺	C46H91NO8P	PE(41:1)	816.6477	-1.18
816.64866	[M+H] ⁺	C46H91NO8P	PC(O-38:2(OH))	816.6477	-1.18
816.64866	[M+H] ⁺	C46H91NO8P	PC(P-38:1(OH))	816.6477	-1.18
816.64866	[M+H] ⁺	C46H91NO8P	PE(P-41:1(OH))	816.6477	-1.18
822.542	[M+K] ⁺	C44H82NO8PK	PC(36:3)	822.541	-1.22
822.542	[M+K] ⁺	C44H82NO8PK	PE(39:3)	822.541	-1.22
822.542	[M+H] ⁺	C42H80NO12S	SHexCer(t36:2)	822.5396	-2.92
822.542	[M+K] ⁺	C44H82NO8PK	PC(O-36:4(OH))	822.541	-1.22
822.542	[M+K] ⁺	C44H82NO8PK	PC(P-36:3(OH))	822.541	-1.22
824.55766	[M+K] ⁺	C44H84NO8PK	PC(36:2)	824.5566	-1.29
824.55766	[M+K] ⁺	C44H84NO8PK	PE(39:2)	824.5566	-1.29
824.55766	[M+H] ⁺	C42H82NO12S	SHexCer(t36:1)	824.5552	-2.98
824.55766	[M+K] ⁺	C44H84NO8PK	PC(O-36:3(OH))	824.5566	-1.29
824.55766	[M+K] ⁺	C44H84NO8PK	PC(P-36:2(OH))	824.5566	-1.29
826.57337	[M+K] ⁺	C44H86NO8PK	PC(36:1)	826.5723	-1.29
826.57337	[M+K] ⁺	C44H86NO8PK	PE(39:1)	826.5723	-1.29
826.57337	[M+H] ⁺	C42H84NO12S	SHexCer(t36:0)	826.5709	-2.99
826.57337	[M+K] ⁺	C44H86NO8PK	PC(O-36:2(OH))	826.5723	-1.29
826.57337	[M+K] ⁺	C44H86NO8PK	PC(P-36:1(OH))	826.5723	-1.29
826.57337	[M+Na] ⁺	C47H82NO7PNa	PE(P-42:6)	826.5721	-1.54
828.49509	[M+K] ⁺	C45H76NO8PK	PC(37:7)	828.494	-1.32
828.49509	[M+K] ⁺	C45H76NO8PK	PE(40:7)	828.494	-1.32
828.55244	[M+K] ⁺	C43H84NO9PK	PC(35:1(OH))	828.5515	-1.13
828.55244	[M+Na] ⁺	C46H80NO8PNa	PC(38:6)	828.5514	-1.26
828.55244	[M+H] ⁺	C48H79NO8P	PC(40:9)	828.5538	1.64
828.55244	[M+K] ⁺	C43H84NO9PK	PE(38:1(OH))	828.5515	-1.13
828.55244	[M+Na] ⁺	C46H80NO8PNa	PE(41:6)	828.5514	-1.26

Continue Appendix 3. Summary of the mouse brain positive ionization LESA-FT-ICR MS1 exact mass assignments with multiple lipid identifications.

Precursor m/z	species	Chemical Composition	Short Name	Theo. m/z	ppm
828.55244	[M+Na] ⁺	C46H80NO8PNa	PC(P-38:6(OH))	828.5514	-1.26
828.55244	[M+K] ⁺	C43H84NO9PK	PS(O-37:1)	828.5515	-1.13
828.55244	[M+K] ⁺	C43H84NO9PK	PS(P-37:0)	828.5515	-1.13
830.56796	[M+Na] ⁺	C46H82NO8PNa	PC(38:5)	830.567	-1.16
830.56796	[M+Na] ⁺	C46H82NO8PNa	PE(41:5)	830.567	-1.16
830.56796	[M+K] ⁺	C43H86NO9PK	PC(35:0(OH))	830.5672	-0.92
830.56796	[M+H] ⁺	C48H81NO8P	PC(40:8)	830.5694	1.73
830.56796	[M+K] ⁺	C43H86NO9PK	PE(38:0(OH))	830.5672	-0.92
830.56796	[M+H] ⁺	C48H81NO8P	PE(43:8)	830.5694	1.73
830.56796	[M+Na] ⁺	C46H82NO8PNa	PC(O-38:6(OH))	830.567	-1.16
830.56796	[M+Na] ⁺	C46H82NO8PNa	PC(P-38:5(OH))	830.567	-1.16
830.56796	[M+K] ⁺	C43H86NO9PK	PS(O-37:0)	830.5672	-0.92
832.58384	[M+H] ⁺	C48H83NO8P	PC(40:7)	832.5851	1.51
832.58384	[M+H] ⁺	C48H83NO8P	PE(43:7)	832.5851	1.51
832.58384	[M+Na] ⁺	C46H84NO8PNa	PC(38:4)	832.5827	-1.37
832.58384	[M+Na] ⁺	C46H84NO8PNa	PE(41:4)	832.5827	-1.37
832.58384	[M+Na] ⁺	C46H84NO8PNa	PC(O-38:5(OH))	832.5827	-1.37
832.58384	[M+Na] ⁺	C46H84NO8PNa	PC(P-38:4(OH))	832.5827	-1.37
834.54203	[M+K] ⁺	C45H82NO8PK	PC(37:4)	834.541	-1.23
834.54203	[M+K] ⁺	C45H82NO8PK	PE(40:4)	834.541	-1.23
834.54203	[M+K] ⁺	C45H82NO8PK	PE(O-40:5(OH))	834.541	-1.23
834.54203	[M+K] ⁺	C45H82NO8PK	PE(P-40:4(OH))	834.541	-1.23
834.60189	[M+H] ⁺	C48H85NO8P	PC(40:6)	834.6007	-1.43
834.60189	[M+H] ⁺	C48H85NO8P	PE(43:6)	834.6007	-1.43
834.60189	[M+H] ⁺	C48H85NO8P	PC(P-40:6(OH))	834.6007	-1.43
836.54449	[M+H] ⁺	C46H79NO10P	PS(40:6)	836.5436	-1.06
836.54449	[M+H] ⁺	C46H79NO10P	PS(P-40:6(OH))	836.5436	-1.06
836.60147	[M+K] ⁺	C46H87NO9K	HexCer(t40:2)	836.6012	-0.32
836.60147	[M+H] ⁺	C44H87NO11P	PI-Cer(d38:1)	836.6011	-0.44
836.60147	[M+H-H ₂ O] ⁺	C44H87NO11P	PI-Cer(t38:0)	836.6011	-0.44
836.60147	[M+H] ⁺	C44H87NO11P	PS(38:0(OH))	836.6011	-0.44
836.61779	[M+H] ⁺	C48H87NO8P	PC(40:5)	836.6164	-1.66
836.61779	[M+H] ⁺	C48H87NO8P	PE(43:5)	836.6164	-1.66
836.61779	[M+H] ⁺	C48H87NO8P	PC(O-40:6(OH))	836.6164	-1.66
836.61779	[M+H] ⁺	C48H87NO8P	PC(P-40:5(OH))	836.6164	-1.66
838.63343	[M+H] ⁺	C48H89NO8P	PC(40:4)	838.632	-1.71
838.63343	[M+H] ⁺	C48H89NO8P	PE(43:4)	838.632	-1.71
838.63343	[M+H] ⁺	C48H89NO8P	PC(O-40:5(OH))	838.632	-1.71
838.63343	[M+H] ⁺	C48H89NO8P	PC(P-40:4(OH))	838.632	-1.71
842.66472	[M+H] ⁺	C48H93NO8P	PC(40:2)	842.6633	-1.69
842.66472	[M+H] ⁺	C48H93NO8P	PE(43:2)	842.6633	-1.69
842.66472	[M+H] ⁺	C48H93NO8P	PC(O-40:3(OH))	842.6633	-1.69
842.66472	[M+H] ⁺	C48H93NO8P	PC(P-40:2(OH))	842.6633	-1.69
842.66472	[M+H] ⁺	C48H93NO8P	PE(O-43:3(OH))	842.6633	-1.69

Continue Appendix 3. Summary of the mouse brain positive ionization LESA-FT-ICR MS1 exact mass assignments with multiple lipid identifications.

Precursor m/z	species	Chemical Composition	Short Name	Theo. m/z	ppm
844.68004	[M+H] ⁺	C48H95NO8P	PC(40:1)	844.679	-1.23
844.68004	[M+H] ⁺	C48H95NO8P	PE(43:1)	844.679	-1.23
844.68004	[M+H] ⁺	C48H95NO8P	PC(O-40:2(OH))	844.679	-1.23
844.68004	[M+H] ⁺	C48H95NO8P	PC(P-40:1(OH))	844.679	-1.23
844.68004	[M+H] ⁺	C48H95NO8P	PE(P-43:1(OH))	844.679	-1.23
846.52697	[M+K] ⁺	C42H82NO11PK	PS(36:0(OH))	846.5257	-1.50
846.52697	[M+K] ⁺	C42H82NO11PK	PI-Cer(d36:1)	846.5257	-1.50
846.52697	[M+Na] ⁺	C45H78NO10PNa	PS(39:5)	846.5256	-1.62
846.54218	[M+K] ⁺	C46H82NO8PK	PC(38:5)	846.541	-1.39
846.54218	[M+K] ⁺	C46H82NO8PK	PE(41:5)	846.541	-1.39
846.54218	[M+K] ⁺	C46H82NO8PK	PC(O-38:6(OH))	846.541	-1.39
846.54218	[M+K] ⁺	C46H82NO8PK	PC(P-38:5(OH))	846.541	-1.39
848.63881	[M+K] ⁺	C48H91NO8K	HexCer(d42:2)	848.6376	-1.43
848.63881	[M+H-H ₂ O] ⁺	C46H91NO10P	PI-Cer(d40:0)	848.6375	-1.54
848.63881	[M+H] ⁺	C46H91NO10P	PS(40:0)	848.6375	-1.54
848.63881	[M+H] ⁺	C46H91NO10P	PS(O-40:1(OH))	848.6375	-1.54
848.63881	[M+H] ⁺	C46H91NO10P	PS(P-40:0(OH))	848.6375	-1.54
850.57386	[M+K] ⁺	C46H86NO8PK	PC(38:3)	850.5723	-1.83
850.57386	[M+K] ⁺	C46H86NO8PK	PE(41:3)	850.5723	-1.83
850.57386	[M+K] ⁺	C46H86NO8PK	PC(O-38:4(OH))	850.5723	-1.83
850.57386	[M+K] ⁺	C46H86NO8PK	PC(P-38:3(OH))	850.5723	-1.83
852.58906	[M+K] ⁺	C46H88NO8PK	PC(38:2)	852.5879	-1.36
852.58906	[M+K] ⁺	C46H88NO8PK	PE(41:2)	852.5879	-1.36
852.58906	[M+K] ⁺	C46H88NO8PK	PC(O-38:3(OH))	852.5879	-1.36
852.58906	[M+K] ⁺	C46H88NO8PK	PC(P-38:2(OH))	852.5879	-1.36
854.56805	[M+Na] ⁺	C48H82NO8PNa	PC(40:7)	854.567	-1.23
854.56805	[M+H] ⁺	C50H81NO8P	PC(42:10)	854.5694	1.58
854.56805	[M+Na] ⁺	C48H82NO8PNa	PE(43:7)	854.567	-1.23
854.56805	[M+K] ⁺	C45H86NO9PK	PC(37:2(OH))	854.5672	-0.99
854.56805	[M+K] ⁺	C45H86NO9PK	PE(40:2(OH))	854.5672	-0.99
854.60484	[M+K] ⁺	C46H90NO8PK	PC(38:1)	854.6036	-1.45
854.60484	[M+K] ⁺	C46H90NO8PK	PE(41:1)	854.6036	-1.45
854.60484	[M+K] ⁺	C46H90NO8PK	PC(O-38:2(OH))	854.6036	-1.45
854.60484	[M+K] ⁺	C46H90NO8PK	PC(P-38:1(OH))	854.6036	-1.45
854.60484	[M+K] ⁺	C46H90NO8PK	PE(P-41:1(OH))	854.6036	-1.45
854.60484	[M+Na] ⁺	C49H86NO7PNa	PE(P-44:6)	854.6034	-1.68
856.58405	[M+Na] ⁺	C48H84NO8PNa	PC(40:6)	856.5827	-1.58
856.58405	[M+Na] ⁺	C48H84NO8PNa	PC(P-40:6(OH))	856.5827	-1.58
856.58405	[M+Na] ⁺	C48H84NO8PNa	PE(43:6)	856.5827	-1.58
856.58405	[M+K] ⁺	C45H88NO9PK	PC(37:1(OH))	856.5828	-1.46
856.58405	[M+H] ⁺	C50H83NO8P	PC(42:9)	856.5851	1.23
856.58405	[M+K] ⁺	C45H88NO9PK	PE(40:1(OH))	856.5828	-1.46
856.58405	[M+K] ⁺	C45H88NO9PK	PS(P-39:0)	856.5828	-1.46
858.59918	[M+Na] ⁺	C48H86NO8PNa	PC(40:5)	858.5983	-1.02
858.59918	[M+Na] ⁺	C48H86NO8PNa	PC(O-40:6(OH))	858.5983	-1.02

Continue Appendix 3. Summary of the mouse brain positive ionization LESA-FT-ICR MS1 exact mass assignments with multiple lipid identifications.

Precursor m/z	species	Chemical Composition	Short Name	Theo. m/z	ppm
858.59918	[M+Na] ⁺	C48H86NO8PNa	PC(P-40:5(OH))	858.5983	-1.02
858.59918	[M+Na] ⁺	C48H86NO8PNa	PE(43:5)	858.5983	-1.02
858.59918	[M+K] ⁺	C45H90NO9PK	PC(37:0(OH))	858.5985	-0.79
858.59918	[M+H] ⁺	C50H85NO8P	PC(42:8)	858.6007	1.77
858.59918	[M+K] ⁺	C45H90NO9PK	PE(40:0(OH))	858.5985	-0.79
858.59918	[M+H] ⁺	C50H85NO8P	PE(45:8)	858.6007	1.77
858.59918	[M+K] ⁺	C45H90NO9PK	PS(O-39:0)	858.5985	-0.79
860.61865	[M+H] ⁺	C50H87NO8P	PC(42:7)	860.6164	-2.61
860.61865	[M+H] ⁺	C50H87NO8P	PE(45:7)	860.6164	-2.61
863.6499	[M+Na] ⁺	C49H93O8PNa	PA(46:2)	863.65	0.12
863.6499	[M+H] ⁺	C51H92O8P	PA(48:5)	863.6524	2.89
863.6499	[M+Na] ⁺	C49H93O8PNa	PA(O-46:3(OH))	863.65	0.12
863.6499	[M+H] ⁺	C51H92O8P	PA(O-48:6(OH))	863.6524	2.89
863.6499	[M+Na] ⁺	C49H93O8PNa	PA(P-46:2(OH))	863.65	0.12
863.6499	[M+H] ⁺	C51H92O8P	PA(P-48:5(OH))	863.6524	2.89
870.54239	[M+K] ⁺	C48H82NO8PK	PC(40:7)	870.541	-1.60
870.54239	[M+K] ⁺	C48H82NO8PK	PE(43:7)	870.541	-1.60
870.69646	[M+H] ⁺	C50H97NO8P	PC(42:2)	870.6946	-2.14
870.69646	[M+H] ⁺	C50H97NO8P	PC(O-42:3(OH))	870.6946	-2.14
870.69646	[M+H] ⁺	C50H97NO8P	PC(P-42:2(OH))	870.6946	-2.14
870.69646	[M+H] ⁺	C50H97NO8P	PE(45:2)	870.6946	-2.14
870.69646	[M+H] ⁺	C50H97NO8P	PE(O-45:3(OH))	870.6946	-2.14
870.69646	[M+H] ⁺	C50H97NO8P	PE(P-45:2(OH))	870.6946	-2.14
872.55812	[M+K] ⁺	C48H84NO8PK	PC(40:6)	872.5566	-1.74
872.55812	[M+K] ⁺	C48H84NO8PK	PC(P-40:6(OH))	872.5566	-1.74
872.55812	[M+K] ⁺	C48H84NO8PK	PE(43:6)	872.5566	-1.74
872.71185	[M+H] ⁺	C50H99NO8P	PC(42:1)	872.7103	-1.78
872.71185	[M+H] ⁺	C50H99NO8P	PC(O-42:2(OH))	872.7103	-1.78
872.71185	[M+H] ⁺	C50H99NO8P	PC(P-42:1(OH))	872.7103	-1.78
872.71185	[M+H] ⁺	C50H99NO8P	PE(45:1)	872.7103	-1.78
872.71185	[M+H] ⁺	C50H99NO8P	PE(O-45:2(OH))	872.7103	-1.78
872.71185	[M+H] ⁺	C50H99NO8P	PE(P-45:1(OH))	872.7103	-1.78
876.58935	[M+K] ⁺	C48H88NO8PK	PC(40:4)	876.5879	-1.65
876.58935	[M+K] ⁺	C48H88NO8PK	PC(O-40:5(OH))	876.5879	-1.65
876.58935	[M+K] ⁺	C48H88NO8PK	PC(P-40:4(OH))	876.5879	-1.65
876.58935	[M+K] ⁺	C48H88NO8PK	PE(43:4)	876.5879	-1.65
913.6454	[M+K] ⁺	C53H95O7PK	PA(O-50:6)	913.6447	-0.77
913.6454	[M+K] ⁺	C53H95O7PK	PA(P-50:5)	913.6447	-0.77
913.6454	[M+H-H ₂ O] ⁺	C51H93O11S	SQDG(42:2)	913.6433	-2.30

Appendix 4. Summary of the mouse liver positive ionization LESA-FT-ICR MS1 exact mass assignments with multiple lipid identifications. The molecular ion species, chemical composition, lipid identifiers, theoretical mass, and mass error are provided.

Precursor m/z	species	Chemical Composition	Short Name	Theo. m/z	ppm
424.28133	[M+K] ⁺	C22H43NO4K	CAR(15:0)	424.2824	-2.52
424.28133	[M+H] ⁺	C20H43NO6P	S1P(t20:1)	424.2822	-2.05
441.23911	[M+H-H2O] ⁺	C23H38O6P	LPA(20:4)	441.24	-2.02
441.23911	[M+K] ⁺	C25H38O4K	MG(22:6)	441.2402	-2.47
478.32818	[M+H-H2O] ⁺	C24H49NO6P	LPC(16:0)	478.3292	-2.13
478.32818	[M+H-H2O] ⁺	C24H49NO6P	LPE(19:0)	478.3292	-2.13
494.3231	[M+Na] ⁺	C29H45NO4Na	CAR(22:6)	494.3241	-2.02
494.3231	[M+H-H2O] ⁺	C24H49NO7P	LPS(O-18:0)	494.3241	-2.02
494.3231	[M+H] ⁺	C24H49NO7P	LPC(16:1)	494.3241	-2.02
496.3388	[M+Na] ⁺	C29H47NO4Na	CAR(22:5)	496.3397	-1.81
496.3388	[M+H] ⁺	C24H51NO7P	LPC(16:0)	496.3398	-2.01
496.3388	[M+H] ⁺	C24H51NO7P	LPE(19:0)	496.3398	-2.01
522.35447	[M+H] ⁺	C26H53NO7P	CerP(t26:1)	522.3554	-1.78
522.35447	[M+H-H2O] ⁺	C26H53NO7P	LPS(O-20:0)	522.3554	-1.78
522.35447	[M+H] ⁺	C26H53NO7P	LPC(18:1)	522.3554	-1.78
524.37012	[M+Na] ⁺	C31H51NO4Na	CAR(24:5)	524.371	-1.68
524.37012	[M+H] ⁺	C26H55NO7P	CerP(t26:0)	524.3711	-1.87
524.37012	[M+H] ⁺	C26H55NO7P	LPC(18:0)	524.3711	-1.87
524.37012	[M+H] ⁺	C26H55NO7P	LPE(21:0)	524.3711	-1.87
534.29472	[M+K] ⁺	C24H50NO7PK	LPC(16:0)	534.2956	-1.65
534.29472	[M+K] ⁺	C24H50NO7PK	LPE(19:0)	534.2956	-1.65
544.33886	[M+Na] ⁺	C26H52NO7PNa	CerP(t26:1)	544.3374	2.68
544.33886	[M+Na] ⁺	C26H52NO7PNa	LPC(18:1)	544.3374	2.68
544.33886	[M+H] ⁺	C28H51NO7P	LPC(20:4)	544.3398	-1.73
546.35209	[M+Na] ⁺	C26H54NO7PNa	CerP(t26:0)	546.353	-1.67
546.35209	[M+Na] ⁺	C26H54NO7PNa	LPC(18:0)	546.353	-1.67
546.35209	[M+Na] ⁺	C26H54NO7PNa	LPE(21:0)	546.353	-1.67
558.29478	[M+K] ⁺	C26H50NO7PK	LPC(18:2)	558.2956	-1.47
558.29478	[M+H] ⁺	C24H48NO11S	SHexSph(t18:1)	558.2943	0.86
562.32608	[M+K] ⁺	C26H54NO7PK	CerP(t26:0)	562.3269	-1.46
562.32608	[M+K] ⁺	C26H54NO7PK	LPC(18:0)	562.3269	-1.46
562.32608	[M+K] ⁺	C26H54NO7PK	LPE(21:0)	562.3269	-1.46
568.33897	[M+Na] ⁺	C28H52NO7PNa	LPC(20:3)	568.3374	2.76
568.33897	[M+H] ⁺	C30H51NO7P	LPC(22:6)	568.3398	-1.46
577.51788	[M+Na] ⁺	C35H70O4Na	DG(O-32:0)	577.5166	2.22
577.51788	[M+H] ⁺	C37H69O4	DG(O-34:3)	577.519	-1.94
577.51788	[M+H] ⁺	C37H69O4	DG(P-34:2)	577.519	-1.94
577.51788	[M+H-H2O] ⁺	C37H69O4	DG(34:1)	577.519	-1.94
577.51788	[M+Na] ⁺	C35H70O4Na	MG(32:0)	577.5166	2.22
590.32095	[M+Na] ⁺	C30H50NO7PNa	LPC(22:6)	590.3217	-1.27
590.32095	[M+K] ⁺	C27H54NO8PK	PE(22:0)	590.3219	-1.61
605.45345	[M+K] ⁺	C35H66O5K	DG(32:1)	605.4542	-1.24
605.45345	[M+H] ⁺	C33H66O7P	LPA(30:1)	605.4541	-1.07
605.45345	[M+H] ⁺	C33H66O7P	PA(O-30:1)	605.4541	-1.07

Continue Appendix 4. Summary of the mouse liver positive ionization LESA-FT-ICR MS1 exact mass assignments with multiple lipid identifications.

Precursor m/z	species	Chemical Composition	Short Name	Theo. m/z	ppm
605.45345	[M+H] ⁺	C33H66O7P	PA(P-30:0)	605.4541	-1.07
609.30281	[M+Na] ⁺	C26H51O12PNa	LPI(17:0)	609.301	2.97
609.30281	[M+K] ⁺	C30H50O10K	MGDG(21:3)	609.3036	-1.30
627.53411	[M+Na] ⁺	C39H72O4Na	DG(O-36:3)	627.5323	2.88
627.53411	[M+H] ⁺	C41H71O4	DG(O-38:6)	627.5347	-0.94
627.53411	[M+Na] ⁺	C39H72O4Na	DG(P-36:2)	627.5323	2.88
627.53411	[M+H] ⁺	C41H71O4	DG(P-38:5)	627.5347	-0.94
627.53411	[M+H-H2O] ⁺	C41H71O4	DG(38:4)	627.5347	-0.94
629.45358	[M+K] ⁺	C37H66O5K	DG(34:3)	629.4542	-0.98
629.45358	[M+Na] ⁺	C33H67O7PNa	LPA(30:0)	629.4517	2.99
629.45358	[M+Na] ⁺	C33H67O7PNa	PA(O-30:0)	629.4517	2.99
631.46919	[M+K] ⁺	C37H68O5K	DG(34:2)	631.4698	-0.97
631.46919	[M+H] ⁺	C35H68O7P	PA(P-32:1)	631.4697	-0.81
633.48487	[M+K] ⁺	C37H70O5K	DG(34:1)	633.4855	-0.99
633.48487	[M+H] ⁺	C35H70O7P	LPA(32:1)	633.4854	-0.84
633.48487	[M+H] ⁺	C35H70O7P	PA(O-32:1)	633.4854	-0.84
633.48487	[M+H] ⁺	C35H70O7P	PA(P-32:0)	633.4854	-0.84
638.60753	[M+H] ⁺	C40H80NO4	CAR(33:0)	638.6082	-1.05
638.60753	[M+H] ⁺	C40H80NO4	Cer(t40:1)	638.6082	-1.05
650.43861	[M+H] ⁺	C33H65NO9P	LPS(27:1)	650.4391	-0.75
650.43861	[M+H] ⁺	C33H65NO9P	PC(25:1(OH))	650.4391	-0.75
650.43861	[M+H] ⁺	C33H65NO9P	PE(28:1(OH))	650.4391	-0.75
655.46929	[M+K] ⁺	C39H68O5K	DG(36:4)	655.4698	-0.78
655.46929	[M+H] ⁺	C37H68O7P	LPA(34:4)	655.4697	-0.63
655.46929	[M+H] ⁺	C37H68O7P	PA(O-34:4)	655.4697	-0.63
655.46929	[M+H] ⁺	C37H68O7P	PA(P-34:3)	655.4697	-0.63
657.48492	[M+K] ⁺	C39H70O5K	DG(36:3)	657.4855	-0.88
657.48492	[M+Na] ⁺	C35H71O7PNa	LPA(32:0)	657.483	2.92
657.48492	[M+Na] ⁺	C35H71O7PNa	PA(O-32:0)	657.483	2.92
657.48492	[M+H] ⁺	C37H70O7P	PA(O-34:3)	657.4854	-0.73
657.48492	[M+H] ⁺	C37H70O7P	PA(P-34:2)	657.4854	-0.73
659.5006	[M+K] ⁺	C39H72O5K	DG(36:2)	659.5011	-0.76
659.5006	[M+H] ⁺	C37H72O7P	PA(O-34:2)	659.501	-0.61
659.5006	[M+H] ⁺	C37H72O7P	PA(P-34:1)	659.501	-0.61
672.42067	[M+Na] ⁺	C33H64NO9PNa	LPS(27:1)	672.4211	-0.64
672.42067	[M+Na] ⁺	C33H64NO9PNa	PC(25:1(OH))	672.4211	-0.64
672.42067	[M+Na] ⁺	C33H64NO9PNa	PE(28:1(OH))	672.4211	-0.64
676.45443	[M+H] ⁺	C35H67NO9P	LPS(29:2)	676.4548	-0.55
676.45443	[M+H] ⁺	C35H67NO9P	PC(27:2(OH))	676.4548	-0.55
676.45443	[M+H] ⁺	C35H67NO9P	PE(30:2(OH))	676.4548	-0.55
681.48501	[M+K] ⁺	C41H70O5K	DG(38:5)	681.4855	-0.72
681.48501	[M+Na] ⁺	C37H71O7PNa	PA(O-34:2)	681.483	2.95
681.48501	[M+H] ⁺	C39H70O7P	PA(O-36:5)	681.4854	-0.57
681.48501	[M+Na] ⁺	C37H71O7PNa	PA(P-34:1)	681.483	2.95
681.48501	[M+H] ⁺	C39H70O7P	PA(P-36:4)	681.4854	-0.57

Continue Appendix 4. Summary of the mouse liver positive ionization LESA-FT-ICR MS1 exact mass assignments with multiple lipid identifications.

Precursor <i>m/z</i>	species	Chemical Composition	Short Name	Theo. <i>m/z</i>	ppm
703.57453	[M+H-H ₂ O] ⁺	C39H80N2O6P	PE-Cer(t37:0)	703.5748	-0.38
703.57453	[M+H] ⁺	C39H80N2O6P	PE-Cer(d37:1)	703.5748	-0.38
703.57453	[M+H] ⁺	C39H80N2O6P	SM(d34:1)	703.5748	-0.38
714.58749	[M+H] ⁺	C41H80NO8	HexCer(d35:1)	714.5878	-0.43
714.58749	[M+H-H ₂ O] ⁺	C41H80NO8	HexCer(t35:0)	714.5878	-0.43
716.52218	[M+H] ⁺	C39H75NO8P	PC(31:2)	716.5225	-0.45
716.52218	[M+Na] ⁺	C37H76NO8PNa	PC(O-29:0(OH))	716.5201	2.90
716.52218	[M+H] ⁺	C39H75NO8P	PE(34:2)	716.5225	-0.45
716.52218	[M+Na] ⁺	C37H76NO8PNa	PE(O-32:0(OH))	716.5201	2.90
716.52218	[M+H] ⁺	C39H75NO8P	PE(O-34:3(OH))	716.5225	-0.45
716.52218	[M+H] ⁺	C39H75NO8P	PE(P-34:2(OH))	716.5225	-0.45
720.58996	[M+H] ⁺	C40H83NO7P	CerP(t40:0)	720.5902	-0.33
720.58996	[M+H] ⁺	C40H83NO7P	LPC(32:0)	720.5902	-0.33
720.58996	[M+H] ⁺	C40H83NO7P	PC(O-32:0)	720.5902	-0.33
720.58996	[M+H] ⁺	C40H83NO7P	PE(O-35:0)	720.5902	-0.33
730.538	[M+H] ⁺	C40H77NO8P	PC(32:2)	730.5381	-0.14
730.538	[M+H] ⁺	C40H77NO8P	PE(35:2)	730.5381	-0.14
730.538	[M+H] ⁺	C40H77NO8P	PE(P-35:2(OH))	730.5381	-0.14
732.55363	[M+H-H ₂ O] ⁺	C40H79NO8P	LPS(34:0)	732.5538	-0.23
732.55363	[M+H] ⁺	C40H79NO8P	PC(32:1)	732.5538	-0.23
732.55363	[M+H-H ₂ O] ⁺	C40H79NO8P	PS(O-34:0)	732.5538	-0.23
732.55363	[M+H] ⁺	C40H79NO8P	PE(35:1)	732.5538	-0.23
732.55363	[M+H] ⁺	C40H79NO8P	PC(P-32:1(OH))	732.5538	-0.23
732.55363	[M+H] ⁺	C40H79NO8P	PE(O-35:2(OH))	732.5538	-0.23
732.55363	[M+H] ⁺	C40H79NO8P	PE(P-35:1(OH))	732.5538	-0.23
734.43664	[M+Na] ⁺	C38H66NO9PNa	LPS(32:5)	734.4367	-0.08
734.43664	[M+Na] ⁺	C38H66NO9PNa	PC(30:5(OH))	734.4367	-0.08
734.43664	[M+Na] ⁺	C38H66NO9PNa	PE(33:5(OH))	734.4367	-0.08
734.43664	[M+K] ⁺	C35H70NO10PK	PS(O-29:0(OH))	734.4369	-0.35
734.56932	[M+H] ⁺	C40H81NO8P	PC(32:0)	734.5694	-0.11
734.56932	[M+H] ⁺	C40H81NO8P	PC(O-32:1(OH))	734.5694	-0.11
734.56932	[M+H] ⁺	C40H81NO8P	PE(35:0)	734.5694	-0.11
734.56932	[M+H] ⁺	C40H81NO8P	PC(P-32:0(OH))	734.5694	-0.11
734.56932	[M+H] ⁺	C40H81NO8P	PE(O-35:1(OH))	734.5694	-0.11
734.56932	[M+H] ⁺	C40H81NO8P	PE(P-35:0(OH))	734.5694	-0.11
738.50754	[M+H] ⁺	C41H73NO8P	PC(33:5)	738.5068	1.00
738.50754	[M+H] ⁺	C41H73NO8P	PE(36:5)	738.5068	1.00
738.50754	[M+H] ⁺	C41H73NO8P	PE(P-36:5(OH))	738.5068	1.00
740.52237	[M+H] ⁺	C41H75NO8P	PC(33:4)	740.5225	-0.18
740.52237	[M+H] ⁺	C41H75NO8P	PE(36:4)	740.5225	-0.18
740.52237	[M+H-H ₂ O] ⁺	C41H75NO8P	PS(P-35:2)	740.5225	-0.18
740.52237	[M+H] ⁺	C41H75NO8P	PE(O-36:5(OH))	740.5225	-0.18
740.52237	[M+H] ⁺	C41H75NO8P	PE(P-36:4(OH))	740.5225	-0.18
742.61907	[M+H] ⁺	C43H84NO8	HexCer(d37:1)	742.6191	-0.04

Continue Appendix 4. Summary of the mouse liver positive ionization LESA-FT-ICR MS1 exact mass assignments with multiple lipid identifications.

Precursor <i>m/z</i>	species	Chemical Composition	Short Name	Theo. <i>m/z</i>	ppm
742.61907	[M+H-H ₂ O] ⁺	C43H84NO8	HexCer(t37:0)	742.6191	-0.04
744.55371	[M+H] ⁺	C41H79NO8P	PC(33:2)	744.5538	-0.12
744.55371	[M+H] ⁺	C41H79NO8P	PE(36:2)	744.5538	-0.12
744.55371	[M+H] ⁺	C41H79NO8P	PC(P-33:2(OH))	744.5538	-0.12
744.55371	[M+H] ⁺	C41H79NO8P	PE(O-36:3(OH))	744.5538	-0.12
744.55371	[M+H] ⁺	C41H79NO8P	PE(P-36:2(OH))	744.5538	-0.12
744.55371	[M+H-H ₂ O] ⁺	C41H79NO8P	PS(O-35:1)	744.5538	-0.12
744.55371	[M+H-H ₂ O] ⁺	C41H79NO8P	PS(P-35:0)	744.5538	-0.12
746.56949	[M+H] ⁺	C41H81NO8P	PC(33:1)	746.5694	0.12
746.56949	[M+H] ⁺	C41H81NO8P	PC(O-33:2(OH))	746.5694	0.12
746.56949	[M+H] ⁺	C41H81NO8P	PE(36:1)	746.5694	0.12
746.56949	[M+H] ⁺	C41H81NO8P	PC(P-33:1(OH))	746.5694	0.12
746.56949	[M+H] ⁺	C41H81NO8P	PE(O-36:2(OH))	746.5694	0.12
746.56949	[M+H] ⁺	C41H81NO8P	PE(P-36:1(OH))	746.5694	0.12
746.56949	[M+H-H ₂ O] ⁺	C41H81NO8P	PS(O-35:0)	746.5694	0.12
754.53518	[M+Na] ⁺	C40H78NO8PNa	PC(32:1)	754.5357	-0.69
754.53518	[M+Na] ⁺	C40H78NO8PNa	PE(35:1)	754.5357	-0.69
754.53518	[M+Na] ⁺	C40H78NO8PNa	PC(P-32:1(OH))	754.5357	-0.69
754.53518	[M+Na] ⁺	C40H78NO8PNa	PE(O-35:2(OH))	754.5357	-0.69
754.53518	[M+Na] ⁺	C40H78NO8PNa	PE(P-35:1(OH))	754.5357	-0.69
756.55385	[M+H] ⁺	C42H79NO8P	PC(34:3)	756.5538	0.07
756.55385	[M+H] ⁺	C42H79NO8P	PC(O-34:4(OH))	756.5538	0.07
756.55385	[M+H] ⁺	C42H79NO8P	PE(37:3)	756.5538	0.07
756.55385	[M+H] ⁺	C42H79NO8P	PC(P-34:3(OH))	756.5538	0.07
756.55385	[M+H-H ₂ O] ⁺	C42H79NO8P	PS(O-36:2)	756.5538	0.07
756.55385	[M+H-H ₂ O] ⁺	C42H79NO8P	PS(P-36:1)	756.5538	0.07
762.50379	[M+Na] ⁺	C41H74NO8PNa	PC(33:4)	762.5044	-0.80
762.50379	[M+Na] ⁺	C41H74NO8PNa	PE(36:4)	762.5044	-0.80
762.50379	[M+Na] ⁺	C41H74NO8PNa	PE(O-36:5(OH))	762.5044	-0.80
762.50379	[M+Na] ⁺	C41H74NO8PNa	PE(P-36:4(OH))	762.5044	-0.80
764.52256	[M+H] ⁺	C43H75NO8P	PC(35:6)	764.5225	0.08
764.52256	[M+H] ⁺	C43H75NO8P	PE(38:6)	764.5225	0.08
764.52256	[M+H] ⁺	C43H75NO8P	PE(P-38:6(OH))	764.5225	0.08
766.53838	[M+H] ⁺	C43H77NO8P	PC(35:5)	766.5381	0.37
766.53838	[M+H] ⁺	C43H77NO8P	PE(38:5)	766.5381	0.37
766.53838	[M+H] ⁺	C43H77NO8P	PE(O-38:6(OH))	766.5381	0.37
766.53838	[M+H] ⁺	C43H77NO8P	PE(P-38:5(OH))	766.5381	0.37
768.55387	[M+H] ⁺	C43H79NO8P	PC(35:4)	768.5538	0.09
768.55387	[M+H] ⁺	C43H79NO8P	PE(38:4)	768.5538	0.09
768.55387	[M+H] ⁺	C43H79NO8P	PE(O-38:5(OH))	768.5538	0.09
768.55387	[M+H] ⁺	C43H79NO8P	PE(P-38:4(OH))	768.5538	0.09
768.55387	[M+H-H ₂ O] ⁺	C43H79NO8P	PS(P-37:2)	768.5538	0.09
770.5098	[M+K] ⁺	C40H78NO8PK	PC(32:1)	770.5097	0.13
770.5098	[M+K] ⁺	C40H78NO8PK	PE(35:1)	770.5097	0.13

Continue Appendix 4. Summary of the mouse liver positive ionization LESA-FT-ICR MS1 exact mass assignments with multiple lipid identifications.

Precursor <i>m/z</i>	species	Chemical Composition	Short Name	Theo. <i>m/z</i>	ppm
770.5098	[M+K] ⁺	C40H78NO8PK	PC(P-32:1(OH))	770.5097	0.13
770.5098	[M+K] ⁺	C40H78NO8PK	PE(O-35:2(OH))	770.5097	0.13
770.5098	[M+K] ⁺	C40H78NO8PK	PE(P-35:1(OH))	770.5097	0.13
770.5098	[M+H] ⁺	C38H76NO12S	SHexCer(t32:0)	770.5083	1.95
770.5098	[M+Na] ⁺	C43H74NO7PNa	PE(P-38:6)	770.5095	0.39
772.54885	[M+H] ⁺	C42H79NO9P	PC(34:3(OH))	772.5487	0.19
772.54885	[M+H] ⁺	C42H79NO9P	PE(37:3(OH))	772.5487	0.19
772.54885	[M+H-H ₂ O] ⁺	C42H79NO9P	PS(36:1)	772.5487	0.19
772.54885	[M+H-H ₂ O] ⁺	C42H79NO9P	PS(O-36:2(OH))	772.5487	0.19
772.54885	[M+H-H ₂ O] ⁺	C42H79NO9P	PS(P-36:1(OH))	772.5487	0.19
772.54885	[M+H] ⁺	C42H79NO9P	PS(O-36:3)	772.5487	0.19
772.54885	[M+H] ⁺	C42H79NO9P	PS(P-36:2)	772.5487	0.19
772.58513	[M+H] ⁺	C43H83NO8P	PC(35:2)	772.5851	0.04
772.58513	[M+H] ⁺	C43H83NO8P	PE(38:2)	772.5851	0.04
772.58513	[M+H] ⁺	C43H83NO8P	PC(P-35:2(OH))	772.5851	0.04
772.58513	[M+H] ⁺	C43H83NO8P	PE(O-38:3(OH))	772.5851	0.04
772.58513	[M+H] ⁺	C43H83NO8P	PE(P-38:2(OH))	772.5851	0.04
772.58513	[M+H-H ₂ O] ⁺	C43H83NO8P	PS(O-37:1)	772.5851	0.04
772.58513	[M+H-H ₂ O] ⁺	C43H83NO8P	PS(P-37:0)	772.5851	0.04
773.49371	[M+Na] ⁺	C39H75O11PNa	PG(33:1(OH))	773.4939	-0.25
778.47853	[M+K] ⁺	C41H74NO8PK	PC(33:4)	778.4784	0.17
778.47853	[M+K] ⁺	C41H74NO8PK	PE(36:4)	778.4784	0.17
778.47853	[M+K] ⁺	C41H74NO8PK	PE(O-36:5(OH))	778.4784	0.17
778.47853	[M+K] ⁺	C41H74NO8PK	PE(P-36:4(OH))	778.4784	0.17
778.53575	[M+Na] ⁺	C42H78NO8PNa	PC(34:3)	778.5357	0.06
778.53575	[M+Na] ⁺	C42H78NO8PNa	PC(O-34:4(OH))	778.5357	0.06
778.53575	[M+Na] ⁺	C42H78NO8PNa	PE(37:3)	778.5357	0.06
778.53575	[M+Na] ⁺	C42H78NO8PNa	PC(P-34:3(OH))	778.5357	0.06
786.50463	[M+K] ⁺	C40H78NO9PK	PC(32:1(OH))	786.5046	0.04
786.50463	[M+Na] ⁺	C43H74NO8PNa	PC(35:6)	786.5044	0.29
786.50463	[M+K] ⁺	C40H78NO9PK	PE(35:1(OH))	786.5046	0.04
786.50463	[M+Na] ⁺	C43H74NO8PNa	PE(38:6)	786.5044	0.29
786.50463	[M+H] ⁺	C45H73NO8P	PE(40:9)	786.5068	-2.76
786.50463	[M+Na] ⁺	C43H74NO8PNa	PE(P-38:6(OH))	786.5044	0.29
786.50463	[M+K] ⁺	C40H78NO9PK	PS(O-34:1)	786.5046	0.04
786.50463	[M+K] ⁺	C40H78NO9PK	PS(P-34:0)	786.5046	0.04
787.66895	[M+H] ⁺	C45H92N2O6P	PE-Cer(d43:1)	787.6687	0.32
787.66895	[M+H] ⁺	C45H92N2O6P	SM(d40:1)	787.6687	0.32
788.61658	[M+H] ⁺	C44H87NO8P	PC(36:1)	788.6164	0.23
788.61658	[M+H] ⁺	C44H87NO8P	PC(O-36:2(OH))	788.6164	0.23
788.61658	[M+H] ⁺	C44H87NO8P	PE(39:1)	788.6164	0.23
788.61658	[M+H] ⁺	C44H87NO8P	PC(P-36:1(OH))	788.6164	0.23
788.61658	[M+H-H ₂ O] ⁺	C44H87NO8P	PS(O-38:0)	788.6164	0.23
789.4676	[M+K] ⁺	C39H75O11PK	PG(33:1(OH))	789.4679	-0.38

Continue Appendix 4. Summary of the mouse liver positive ionization LESA-FT-ICR MS1 exact mass assignments with multiple lipid identifications.

Precursor <i>m/z</i>	Precursor <i>m/z</i>	Precursor <i>m/z</i>	Precursor <i>m/z</i>	Precursor <i>m/z</i>	Precursor <i>m/z</i>
789.4676	[M+Na] ⁺	C42H71O10PNa	PG(36:6)	789.4677	-0.13
790.53906	[M+H] ⁺	C45H77NO8P	PC(37:7)	790.5381	1.21
790.53906	[M+H] ⁺	C45H77NO8P	PE(40:7)	790.5381	1.21
790.55947	[M+K] ⁺	C44H81NO8K	HexCer(d38:3)	790.5594	0.09
790.55947	[M+H] ⁺	C42H81NO10P	PS(36:1)	790.5593	0.22
790.55947	[M+H-H ₂ O] ⁺	C42H81NO10P	PI-Cer(d36:1)	790.5593	0.22
790.55947	[M+H-H ₂ O] ⁺	C42H81NO10P	PS(36:0(OH))	790.5593	0.22
790.55947	[M+H] ⁺	C42H81NO10P	PS(O-36:2(OH))	790.5593	0.22
790.55947	[M+H] ⁺	C42H81NO10P	PS(P-36:1(OH))	790.5593	0.22
792.55403	[M+H] ⁺	C45H79NO8P	PC(37:6)	792.5538	0.29
792.55403	[M+H] ⁺	C45H79NO8P	PE(40:6)	792.5538	0.29
792.55403	[M+H] ⁺	C45H79NO8P	PE(P-40:6(OH))	792.5538	0.29
794.5099	[M+K] ⁺	C42H78NO8PK	PC(34:3)	794.5097	0.25
794.5099	[M+K] ⁺	C42H78NO8PK	PC(O-34:4(OH))	794.5097	0.25
794.5099	[M+K] ⁺	C42H78NO8PK	PE(37:3)	794.5097	0.25
794.5099	[M+H] ⁺	C40H76NO12S	SHexCer(t34:2)	794.5083	2.01
794.5099	[M+K] ⁺	C42H78NO8PK	PC(P-34:3(OH))	794.5097	0.25
794.53093	[M+Na] ⁺	C42H78NO9PNa	PC(34:3(OH))	794.5306	0.42
794.53093	[M+H] ⁺	C44H77NO9P	PC(36:6(OH))	794.533	-2.61
794.53093	[M+Na] ⁺	C42H78NO9PNa	PE(37:3(OH))	794.5306	0.42
794.53093	[M+H] ⁺	C44H77NO9P	PE(39:6(OH))	794.533	-2.61
794.53093	[M+H-H ₂ O] ⁺	C44H77NO9P	PS(38:4)	794.533	-2.61
794.53093	[M+H-H ₂ O] ⁺	C44H77NO9P	PS(O-38:5(OH))	794.533	-2.61
794.53093	[M+H-H ₂ O] ⁺	C44H77NO9P	PS(P-38:4(OH))	794.533	-2.61
794.53093	[M+Na] ⁺	C42H78NO9PNa	PS(O-36:3)	794.5306	0.42
794.53093	[M+H] ⁺	C44H77NO9P	PS(O-38:6)	794.533	-2.61
794.53093	[M+Na] ⁺	C42H78NO9PNa	PS(P-36:2)	794.5306	0.42
794.53093	[M+H] ⁺	C44H77NO9P	PS(P-38:5)	794.533	-2.61
796.58511	[M+H] ⁺	C45H83NO8P	PC(37:4)	796.5851	0.01
796.58511	[M+H] ⁺	C45H83NO8P	PE(40:4)	796.5851	0.01
796.58511	[M+H] ⁺	C45H83NO8P	PE(O-40:5(OH))	796.5851	0.01
796.58511	[M+H] ⁺	C45H83NO8P	PE(P-40:4(OH))	796.5851	0.01
798.54122	[M+K] ⁺	C42H82NO8PK	PC(34:1)	798.541	0.28
798.54122	[M+K] ⁺	C42H82NO8PK	PC(O-34:2(OH))	798.541	0.28
798.54122	[M+K] ⁺	C42H82NO8PK	PE(37:1)	798.541	0.28
798.54122	[M+K] ⁺	C42H82NO8PK	PC(P-34:1(OH))	798.541	0.28
798.54122	[M+K] ⁺	C42H82NO8PK	PE(O-37:2(OH))	798.541	0.28
798.54122	[M+K] ⁺	C42H82NO8PK	PE(P-37:1(OH))	798.541	0.28
798.54122	[M+H] ⁺	C40H80NO12S	SHexCer(t34:0)	798.5396	2.03
798.54122	[M+Na] ⁺	C45H78NO7PNa	PE(P-40:6)	798.5408	0.53
802.47868	[M+K] ⁺	C43H74NO8PK	PC(35:6)	802.4784	0.35
802.47868	[M+K] ⁺	C43H74NO8PK	PE(38:6)	802.4784	0.35
802.47868	[M+K] ⁺	C43H74NO8PK	PE(P-38:6(OH))	802.4784	0.35
802.53599	[M+K] ⁺	C41H82NO9PK	PC(33:0(OH))	802.5359	0.11

Continue Appendix 4. Summary of the mouse liver positive ionization LESA-FT-ICR MS1 exact mass assignments with multiple lipid identifications.

Precursor <i>m/z</i>	Precursor <i>m/z</i>	Precursor <i>m/z</i>	Precursor <i>m/z</i>	Precursor <i>m/z</i>	Precursor <i>m/z</i>
802.53599	[M+Na] ⁺	C44H78NO8PNa	PC(36:5)	802.5357	0.36
802.53599	[M+H] ⁺	C46H77NO8P	PC(38:8)	802.5381	-2.63
802.53599	[M+K] ⁺	C41H82NO9PK	PE(36:0(OH))	802.5359	0.11
802.53599	[M+Na] ⁺	C44H78NO8PNa	PE(39:5)	802.5357	0.36
802.53599	[M+Na] ⁺	C44H78NO8PNa	PC(P-36:5(OH))	802.5357	0.36
802.53599	[M+H-H ₂ O] ⁺	C46H77NO8P	PS(P-40:6)	802.5381	-2.63
802.53599	[M+K] ⁺	C41H82NO9PK	PS(O-35:0)	802.5359	0.11
802.59588	[M+H] ⁺	C44H85NO9P	PC(36:2(OH))	802.5956	0.35
802.59588	[M+H] ⁺	C44H85NO9P	PE(39:2(OH))	802.5956	0.35
802.59588	[M+H-H ₂ O] ⁺	C44H85NO9P	PS(38:0)	802.5956	0.35
802.59588	[M+H-H ₂ O] ⁺	C44H85NO9P	PS(O-38:1(OH))	802.5956	0.35
802.59588	[M+H-H ₂ O] ⁺	C44H85NO9P	PS(P-38:0(OH))	802.5956	0.35
802.59588	[M+H] ⁺	C44H85NO9P	PS(O-38:2)	802.5956	0.35
802.59588	[M+H] ⁺	C44H85NO9P	PS(P-38:1)	802.5956	0.35
804.49465	[M+K] ⁺	C43H76NO8PK	PC(35:5)	804.494	0.81
804.49465	[M+K] ⁺	C43H76NO8PK	PE(38:5)	804.494	0.81
804.49465	[M+K] ⁺	C43H76NO8PK	PE(O-38:6(OH))	804.494	0.81
804.49465	[M+K] ⁺	C43H76NO8PK	PE(P-38:5(OH))	804.494	0.81
806.50992	[M+K] ⁺	C43H78NO8PK	PC(35:4)	806.5097	0.27
806.50992	[M+K] ⁺	C43H78NO8PK	PE(38:4)	806.5097	0.27
806.50992	[M+K] ⁺	C43H78NO8PK	PE(O-38:5(OH))	806.5097	0.27
806.50992	[M+K] ⁺	C43H78NO8PK	PE(P-38:4(OH))	806.5097	0.27
806.55393	[M+H] ⁺	C42H81NO11P	PI-Cer(d36:2)	806.5542	-0.33
806.55393	[M+H] ⁺	C42H81NO11P	PS(36:1(OH))	806.5542	-0.33
806.55393	[M+H-H ₂ O] ⁺	C42H81NO11P	PI-Cer(t36:1)	806.5542	-0.33
810.54154	[M+K] ⁺	C43H82NO8PK	PC(35:2)	810.541	0.67
810.54154	[M+K] ⁺	C43H82NO8PK	PE(38:2)	810.541	0.67
810.54154	[M+K] ⁺	C43H82NO8PK	PC(P-35:2(OH))	810.541	0.67
810.54154	[M+K] ⁺	C43H82NO8PK	PE(O-38:3(OH))	810.541	0.67
810.54154	[M+H] ⁺	C41H80NO12S	SHexCer(t35:1)	810.5396	2.39
810.54154	[M+K] ⁺	C43H82NO8PK	PE(P-38:2(OH))	810.541	0.67
813.68481	[M+H] ⁺	C47H94N2O6P	PE-Cer(d45:2)	813.6844	0.50
813.68481	[M+H-H ₂ O] ⁺	C47H94N2O6P	PE-Cer(t45:1)	813.6844	0.50
813.68481	[M+H] ⁺	C47H94N2O6P	SM(d42:2)	813.6844	0.50
814.55975	[M+H] ⁺	C44H81NO10P	PS(38:3)	814.5593	0.55
814.55975	[M+H-H ₂ O] ⁺	C44H81NO10P	PI-Cer(d38:3)	814.5593	0.55
814.55975	[M+H-H ₂ O] ⁺	C44H81NO10P	PS(38:2(OH))	814.5593	0.55
814.55975	[M+H] ⁺	C44H81NO10P	PS(O-38:4(OH))	814.5593	0.55
814.55975	[M+H] ⁺	C44H81NO10P	PS(P-38:3(OH))	814.5593	0.55
815.70046	[M+H] ⁺	C47H96N2O6P	PE-Cer(d45:1)	815.7	0.56
815.70046	[M+H-H ₂ O] ⁺	C47H96N2O6P	PE-Cer(t45:0)	815.7	0.56
815.70046	[M+H] ⁺	C47H96N2O6P	SM(d42:1)	815.7	0.56
816.57528	[M+H] ⁺	C44H83NO10P	PS(38:2)	816.5749	0.47
816.57528	[M+H-H ₂ O] ⁺	C44H83NO10P	PI-Cer(d38:2)	816.5749	0.47
816.57528	[M+H-H ₂ O] ⁺	C44H83NO10P	PS(38:1(OH))	816.5749	0.47

Continue Appendix 4. Summary of the mouse liver positive ionization LESA-FT-ICR MS1 exact mass assignments with multiple lipid identifications.

Precursor <i>m/z</i>	Precursor <i>m/z</i>	Precursor <i>m/z</i>	Precursor <i>m/z</i>	Precursor <i>m/z</i>	Precursor <i>m/z</i>
816.57528	[M+H] ⁺	C44H83NO10P	PS(O-38:3(OH))	816.5749	0.47
816.57528	[M+H] ⁺	C44H83NO10P	PS(P-38:2(OH))	816.5749	0.47
818.51007	[M+K] ⁺	C44H78NO8PK	PC(36:5)	818.5097	0.45
818.51007	[M+K] ⁺	C44H78NO8PK	PE(39:5)	818.5097	0.45
818.51007	[M+K] ⁺	C44H78NO8PK	PC(P-36:5(OH))	818.5097	0.45
818.591	[M+K] ⁺	C46H85NO8K	HexCer(d40:3)	818.5907	0.37
818.591	[M+H] ⁺	C44H85NO10P	PS(38:1)	818.5906	0.49
818.591	[M+H-H ₂ O] ⁺	C44H85NO10P	PI-Cer(d38:1)	818.5906	0.49
818.591	[M+H-H ₂ O] ⁺	C44H85NO10P	PS(38:0(OH))	818.5906	0.49
818.591	[M+H] ⁺	C44H85NO10P	PS(O-38:2(OH))	818.5906	0.49
818.591	[M+H] ⁺	C44H85NO10P	PS(P-38:1(OH))	818.5906	0.49
822.54138	[M+K] ⁺	C44H82NO8PK	PC(36:3)	822.541	0.46
822.54138	[M+K] ⁺	C44H82NO8PK	PC(O-36:4(OH))	822.541	0.46
822.54138	[M+K] ⁺	C44H82NO8PK	PE(39:3)	822.541	0.46
822.54138	[M+H] ⁺	C42H80NO12S	SHexCer(t36:2)	822.5396	2.16
822.54138	[M+K] ⁺	C44H82NO8PK	PC(P-36:3(OH))	822.541	0.46
828.5155	[M+Na] ⁺	C45H76NO9PNa	PC(37:7(OH))	828.515	0.60
828.5155	[M+Na] ⁺	C45H76NO9PNa	PE(40:7(OH))	828.515	0.60
828.5155	[M+H] ⁺	C47H75NO9P	PE(42:10(OH))	828.5174	-2.29
828.5155	[M+K] ⁺	C42H80NO10PK	PS(36:1)	828.5151	0.48
828.5155	[M+K] ⁺	C42H80NO10PK	PS(O-36:2(OH))	828.5151	0.48
828.5155	[M+K] ⁺	C42H80NO10PK	PS(P-36:1(OH))	828.5151	0.48
828.53605	[M+Na] ⁺	C42H80NO11PNa	PI-Cer(d36:2)	828.5361	-0.06
828.53605	[M+Na] ⁺	C42H80NO11PNa	PS(36:1(OH))	828.5361	-0.06
828.53605	[M+H] ⁺	C44H79NO11P	PS(38:4(OH))	828.5385	-2.96
830.56698	[M+K] ⁺	C43H86NO9PK	PC(35:0(OH))	830.5672	-0.26
830.56698	[M+Na] ⁺	C46H82NO8PNa	PC(38:5)	830.567	-0.02
830.56698	[M+H] ⁺	C48H81NO8P	PC(40:8)	830.5694	-2.91
830.56698	[M+Na] ⁺	C46H82NO8PNa	PC(O-38:6(OH))	830.567	-0.02
830.56698	[M+K] ⁺	C43H86NO9PK	PE(38:0(OH))	830.5672	-0.26
830.56698	[M+Na] ⁺	C46H82NO8PNa	PE(41:5)	830.567	-0.02
830.56698	[M+H] ⁺	C48H81NO8P	PE(43:8)	830.5694	-2.91
830.56698	[M+Na] ⁺	C46H82NO8PNa	PC(P-38:5(OH))	830.567	-0.02
830.56698	[M+K] ⁺	C43H86NO9PK	PS(O-37:0)	830.5672	-0.26
830.56698	[M+H-H ₂ O] ⁺	C48H81NO8P	PS(P-42:6)	830.5694	-2.91
834.58539	[M+H] ⁺	C44H85NO11P	PI-Cer(d38:2)	834.5855	-0.13
834.58539	[M+H] ⁺	C44H85NO11P	PS(38:1(OH))	834.5855	-0.13
834.58539	[M+H-H ₂ O] ⁺	C44H85NO11P	PI-Cer(t38:1)	834.5855	-0.13
836.61702	[M+H] ⁺	C48H87NO8P	PC(40:5)	836.6164	0.74
836.61702	[M+H] ⁺	C48H87NO8P	PC(O-40:6(OH))	836.6164	0.74
836.61702	[M+H] ⁺	C48H87NO8P	PE(43:5)	836.6164	0.74
836.61702	[M+H] ⁺	C48H87NO8P	PC(P-40:5(OH))	836.6164	0.74
836.61702	[M+H-H ₂ O] ⁺	C48H87NO8P	PS(O-42:4)	836.6164	0.74

Continue Appendix 4. Summary of the mouse liver positive ionization LESA-FT-ICR MS1 exact mass assignments with multiple lipid identifications.

Precursor <i>m/z</i>	Precursor <i>m/z</i>	Precursor <i>m/z</i>	Precursor <i>m/z</i>	Precursor <i>m/z</i>	Precursor <i>m/z</i>
836.61702	[M+H-H ₂ O] ⁺	C48H87NO8P	PS(P-42:3)	836.6164	0.74
838.57286	[M+K] ⁺	C45H86NO8PK	PC(37:2)	838.5723	0.67
838.57286	[M+K] ⁺	C45H86NO8PK	PE(40:2)	838.5723	0.67
838.57286	[M+K] ⁺	C45H86NO8PK	PC(P-37:2(OH))	838.5723	0.67
838.57286	[M+K] ⁺	C45H86NO8PK	PE(O-40:3(OH))	838.5723	0.67
838.57286	[M+H] ⁺	C43H84NO12S	SHexCer(t37:1)	838.5709	2.34
838.57286	[M+K] ⁺	C45H86NO8PK	PE(P-40:2(OH))	838.5723	0.67
838.63255	[M+H] ⁺	C48H89NO8P	PC(40:4)	838.632	0.66
838.63255	[M+H] ⁺	C48H89NO8P	PC(O-40:5(OH))	838.632	0.66
838.63255	[M+H] ⁺	C48H89NO8P	PE(43:4)	838.632	0.66
838.63255	[M+H] ⁺	C48H89NO8P	PC(P-40:4(OH))	838.632	0.66
838.63255	[M+H-H ₂ O] ⁺	C48H89NO8P	PS(O-42:3)	838.632	0.66
838.63255	[M+H-H ₂ O] ⁺	C48H89NO8P	PS(P-42:2)	838.632	0.66
840.58875	[M+K] ⁺	C45H88NO8PK	PC(37:1)	840.5879	1.01
840.58875	[M+K] ⁺	C45H88NO8PK	PC(O-37:2(OH))	840.5879	1.01
840.58875	[M+K] ⁺	C45H88NO8PK	PC(P-37:1(OH))	840.5879	1.01
840.58875	[M+K] ⁺	C45H88NO8PK	PE(40:1)	840.5879	1.01
840.58875	[M+Na] ⁺	C48H84NO7PNa	PC(P-40:6)	840.5878	1.13
840.58875	[M+K] ⁺	C45H88NO8PK	PE(O-40:2(OH))	840.5879	1.01
840.58875	[M+H] ⁺	C43H86NO12S	SHexCer(t37:0)	840.5865	2.68
840.58875	[M+K] ⁺	C45H88NO8PK	PE(P-40:1(OH))	840.5879	1.01
842.59095	[M+H] ⁺	C46H85NO10P	PS(40:3)	842.5906	0.42
842.59095	[M+H] ⁺	C46H85NO10P	PS(O-40:4(OH))	842.5906	0.42
842.59095	[M+H-H ₂ O] ⁺	C46H85NO10P	PI-Cer(d40:3)	842.5906	0.42
842.59095	[M+H-H ₂ O] ⁺	C46H85NO10P	PS(40:2(OH))	842.5906	0.42
842.59095	[M+H] ⁺	C46H85NO10P	PS(P-40:3(OH))	842.5906	0.42
844.51057	[M+K] ⁺	C42H80NO11PK	PI-Cer(d36:2)	844.5101	0.56
844.51057	[M+K] ⁺	C42H80NO11PK	PS(36:1(OH))	844.5101	0.56
844.51057	[M+Na] ⁺	C45H76NO10PNa	PS(39:6)	844.5099	0.79
852.53638	[M+Na] ⁺	C44H80NO11PNa	PS(38:3(OH))	852.5361	0.33
852.53638	[M+H] ⁺	C46H79NO11P	PS(40:6(OH))	852.5385	-2.49
856.5834	[M+K] ⁺	C45H88NO9PK	PC(37:1(OH))	856.5828	0.70
856.5834	[M+Na] ⁺	C48H84NO8PNa	PC(40:6)	856.5827	0.82
856.5834	[M+H] ⁺	C50H83NO8P	PC(42:9)	856.5851	-1.98
856.5834	[M+K] ⁺	C45H88NO9PK	PE(40:1(OH))	856.5828	0.70
856.5834	[M+Na] ⁺	C48H84NO8PNa	PE(43:6)	856.5827	0.82
856.5834	[M+Na] ⁺	C48H84NO8PNa	PC(P-40:6(OH))	856.5827	0.82
856.5834	[M+K] ⁺	C45H88NO9PK	PS(P-39:0)	856.5828	0.70
860.50572	[M+K] ⁺	C42H80NO12PK	PI-Cer(t36:2)	860.505	0.84
860.50572	[M+Na] ⁺	C45H76NO11PNa	PS(39:6(OH))	860.5048	1.07
862.57304	[M+K] ⁺	C47H86NO8PK	PC(39:4)	862.5723	0.86
862.57304	[M+K] ⁺	C47H86NO8PK	PE(42:4)	862.5723	0.86
862.57304	[M+K] ⁺	C47H86NO8PK	PE(O-42:5(OH))	862.5723	0.86
862.57304	[M+K] ⁺	C47H86NO8PK	PE(P-42:4(OH))	862.5723	0.86

866.60422	[M+K]+	C47H90NO8PK	PC(39:2)	866.6036	0.72
866.60422	[M+K]+	C47H90NO8PK	PE(42:2)	866.6036	0.72
866.60422	[M+K]+	C47H90NO8PK	PE(O-42:3(OH))	866.6036	0.72
866.60422	[M+K]+	C47H90NO8PK	PE(P-42:2(OH))	866.6036	0.72
866.60422	[M+H]+	C45H88NO12S	SHexCer(t39:1)	866.6022	2.33
870.54177	[M+K]+	C48H82NO8PK	PC(40:7)	870.541	0.88
870.54177	[M+K]+	C48H82NO8PK	PE(43:7)	870.541	0.88
872.55731	[M+K]+	C48H84NO8PK	PC(40:6)	872.5566	0.81
872.55731	[M+K]+	C48H84NO8PK	PC(P-40:6(OH))	872.5566	0.81
872.55731	[M+K]+	C48H84NO8PK	PE(43:6)	872.5566	0.81
876.53741	[M+K]+	C43H84NO12PK	PI-Cer(t37:1)	876.5363	1.27
876.53741	[M+Na]+	C46H80NO11PNa	PS(40:5(OH))	876.5361	1.49
876.53741	[M+H]+	C48H79NO11P	PS(42:8(OH))	876.5385	-1.24
941.61883	[M+Na]+	C49H90O15Na	DGDG(34:1)	941.6172	1.73
941.61883	[M+H]+	C51H89O15	DGDG(36:4)	941.6196	-0.82

Appendix 5. Summary of the mouse brain negative ionization mode LESA-FT-ICR-MS (MS1 and MS/MS). The molecular ion species, chemical composition, lipid class, theoretical mass, mass error, and identifiers are provided. HG denotes the head group and FA denotes fatty acids.

Mouse Brain MS-								
ID	Precursor <i>m/z</i>	species	Chemical Composition	Main Class	Short Name	Theo. <i>m/z</i>	ppm	Identified fragments from AutoMS/MS or MS1 identification
1	656.5009	[M-H] ⁻	C37H71NO6P	CerP	CerP(d37:2)	656.5025	- 2.42	MS1
2	607.4582	[M+HCOO] ⁻	C36H63O7	DG	DG(32:3)	607.4579	0.56	MS1
3	500.2783	[M-H] ⁻	C25H43NO7P	LPE	LPE(20:4)	500.2783	- 0.06	MS1
4	524.2782	[M-H] ⁻	C27H43NO7P	LPE	LPE(22:6)	524.2783	- 0.13	MS1
5	619.2889	[M-H] ⁻	C29H48O12P	LPI	LPI(20:4)	619.2889	- 0.05	MS1
6	568.2682	[M-H] ⁻	C28H43NO9P	LPS	LPS(22:6)	568.2681	0.21	MS1
7	804.5760	[M+HCOO] ⁻	C43H83NO10P	PC	PC(34:1)	804.5760	0	M-HCOOCH3 (744.55468)
8	832.6078	[M+HCOO] ⁻	C45H87NO10P	PC	PC(36:1)	832.6073	0.53	M-HCOOCH3 (772.58579)
9	854.5932	[M+HCOO] ⁻	C47H85NO10P	PC	PC(38:4)	854.5917	1.74	M-FA 26:2(+OH)-HCOOCH3 (402.2883), M-FA 20:3(-H)-HCOOCH3 (506.28768), M-FA 17:0(+OH)-HCOOCH3 (524.27873), M-FA 15:0(+OH)-HCOOCH3 (552.2744), M-FA 11:4(-H)-HCOOCH3 (634.4084), M-HCOOCH3 (794.57164)
10	868.5627	[M+Cl] ⁻	C48H84NO8PCl	PC	PC(40:6)	868.5629	- 0.20	FA 13:6(+COO) (201.03787), FA 14:6(+COO) (215.03269)
11	700.5287	[M-H] ⁻	C39H75NO7P	PE	PE(O-34:2) or PE(P-34:1)	700.5287	0.06	MS1
12	728.5598	[M-H] ⁻	C41H79NO7P	PE	PE(O-36:2) or PE(P-36:1)	728.5600	- 0.27	MS1
13	726.5443	[M-H] ⁻	C41H77NO7P	PE	PE(O-36:3) or PE(P-36:2)	726.5443	- 0.01	MS1

Continue Appendix 5. Summary of the mouse brain negative ionization mode LESA-FT-ICR-MS (MS1 and MS/MS). The molecular ion species, chemical composition, lipid class, theoretical mass, mass error, and identifiers are provided. HG denotes the head group and FA denotes fatty acids.

ID	Precursor m/z	species	Chemical Composition	Main Class	Short Name	Theo. m/z	ppm	Identified fragments from AutoMS/MS or MS1 identification
14	722.5129	[M-H] ⁻	C41H73NO7P	PE	PE(O-36:5) or PE(P-36:4)	722.5130	- 0.10	MS1
15	750.5444	[M-H] ⁻	C43H77NO7P	PE	PE(O-38:5) or PE(P-38:4)	750.5443	0.17	MS1
16	748.5290	[M-H] ⁻	C43H75NO7P	PE	PE(O-38:6) or PE(P-38:5)	748.5287	0.36	MS1
17	776.5617	[M-H] ⁻	C45H79NO7P	PE	PE(O-40:6) or PE(P-40:5)	776.5600	2.14	MS1
18	746.5131	[M-H] ⁻	C43H73NO7P	PE	PE(P-38:6)	746.5130	0.08	MS1
19	774.5443	[M-H] ⁻	C45H77NO7P	PE	PE(P-40:6)	774.5443	0.03	MS1
20	865.5034	[M-H] ⁻	C50H74O10P	PG	PG(44:12)	865.5025	1.05	MS1
21	822.5783	[M-H] ⁻	C43H84NO11S	SHexCer	SHexCer(d37:0)	822.5771	1.47	MS1
22	820.5625	[M-H] ⁻	C43H82NO11S	SHexCer	SHexCer(d37:1)	820.5614	1.39	MS1
23	888.6238	[M-H] ⁻	C48H90NO11S	SHexCer	SHexCer(d42:2)	888.6240	- 0.28	MS1
24	681.2965	[M-H] ⁻	C34H49O12S	SQDG	SQDG(25:7)	681.2950	2.26	MS1

Appendix 6. Summary of the mouse liver negative ionization mode LESA-FT-ICR-MS (MS1 and MS/MS). The molecular ion species, chemical composition, lipid class, theoretical mass, mass error, and identifiers are provided. HG denotes the head group and FA here denotes fatty acids.

ID	Precursor <i>m/z</i>	species	Chemical Composition	Main Class	Short Name	Theo. <i>m/z</i>	ppm	Identified fragments from AutoMS/MS or MS1 identification
1	420.2883	[M+Cl] ⁻	C22H43NO4Cl	CAR	CAR(15:0)	420.2886	-0.69	MS1
2	574.4984	[M+Cl] ⁻	C34H69NO3Cl	Cer	Cer(d34:0)	574.4972	2.11	MS1
3	572.4816	[M+Cl] ⁻	C34H67NO3Cl	Cer	Cer(d34:1)	572.4815	0.14	MS1
4	656.5758	[M+Cl] ⁻	C40H79NO3Cl	Cer	Cer(d40:1)	656.5754	0.53	MS1
4	666.6038	[M+HCOO] ⁻	C41H80NO5	Cer	Cer(d40:1)	666.6042	-0.56	MS1
5	670.5901	[M+Cl] ⁻	C41H81NO3Cl	Cer	Cer(d41:1)	670.5911	-1.54	MS1
6	684.6067	[M+Cl] ⁻	C42H83NO3Cl	Cer	Cer(d42:1)	684.6067	-0.04	MS1
6	694.6355	[M+HCOO] ⁻	C43H84NO5	Cer	Cer(d42:1)	694.6355	-0.01	MS1
7	682.5910	[M+Cl] ⁻	C42H81NO3Cl	Cer	Cer(d42:2)	682.5911	-0.16	MS1
7	692.6192	[M+HCOO] ⁻	C43H82NO5	Cer	Cer(d42:2)	692.6199	-0.95	MS1
8	710.6303	[M+HCOO] ⁻	C43H84NO6	Cer	Cer(t42:1)	710.6304	-0.15	MS1
9	738.6621	[M+HCOO] ⁻	C45H88NO6	Cer	Cer(t44:1)	738.6617	0.53	MS1
10	736.6464	[M+HCOO] ⁻	C45H86NO6	Cer	Cer(t44:2)	736.6461	0.37	MS1
11	566.3383	[M+Cl] ⁻	C28H54NO6PCl	CerP	CerP(d28:2)	566.3383	0.04	MS1
12	602.4538	[M-H] ⁻	C33H65NO6P	CerP	CerP(d33:1)	602.4555	-2.90	MS1
13	630.4851	[M-H] ⁻	C35H69NO6P	CerP	CerP(d35:1)	630.4868	-2.70	MS1
14	628.4695	[M-H] ⁻	C35H67NO6P	CerP	CerP(d35:2)	628.4712	-2.67	MS1
15	629.4919	[M+Cl] ⁻	C37H70O5Cl	DG	DG(34:1)	629.4917	0.27	MS1
15	639.5201	[M+HCOO] ⁻	C38H71O7	DG	DG(34:1)	639.5205	-0.64	MS1
16	627.4761	[M+Cl] ⁻	C37H68O5Cl	DG	DG(34:2)	627.4761	-0.06	MS1
16	637.5050	[M+HCOO] ⁻	C38H69O7	DG	DG(34:2)	637.5049	0.11	MS1
17	625.4619	[M+Cl] ⁻	C37H66O5Cl	DG	DG(34:3)	625.4604	2.32	MS1
18	655.5071	[M+Cl] ⁻	C39H72O5Cl	DG	DG(36:2)	655.5074	-0.47	MS1

Continue Appendix 6. Summary of the mouse liver negative ionization mode LESA-FT-ICR-MS (MS1 and MS/MS). The molecular ion species, chemical composition, lipid class, theoretical mass, mass error, and identifiers are provided. HG denotes the head group and FA here denotes fatty acids.

ID	Precursor <i>m/z</i>	species	Chemical Composition	Main Class	Short Name	Theo. <i>m/z</i>	ppm	Identified fragments from AutoMS/MS or MS1 identification
18	665.5361	[M+HCOO] ⁻	C40H73O7	DG	DG(36:2)	665.5362	-0.15	MS1
19	653.4920	[M+Cl] ⁻	C39H70O5Cl	DG	DG(36:3)	653.4917	0.44	MS1
19	663.5203	[M+HCOO] ⁻	C40H71O7	DG	DG(36:3)	663.5205	-0.30	MS1
20	651.4761	[M+Cl] ⁻	C39H68O5Cl	DG	DG(36:4)	651.4761	0.02	MS1
20	661.5049	[M+HCOO] ⁻	C40H69O7	DG	DG(36:4)	661.5049	-0.05	MS1
21	611.5259	[M+HCOO] ⁻	C37H71O6	DG	DG(O-33:1) or DG(P-33:0)	611.5256	0.46	MS1
22	639.5563	[M+HCOO] ⁻	C39H75O6	DG	DG(O-35:1) or DG(P-35:0)	639.5569	-0.91	MS1
23	439.1379	[M+Cl] ⁻	C18H28O10Cl	FA	FA(18:0(OH4,Ke2,Ep2)	439.1377	0.50	MS1
23	449.1667	[M+HCOO] ⁻	C19H29O12	FA	FA(18:0(OH4,Ke2,Ep2)	449.1665	0.42	MS1
24	467.1684	[M+Cl] ⁻	C20H32O10Cl	FA	FA(20:0(OH4,Ke2,Ep2)	467.1690	-1.22	MS1
24	477.1979	[M+HCOO] ⁻	C21H33O12	FA	FA(20:0(OH4,Ke2,Ep2)	477.1978	0.29	MS1
25	465.1034	[M+HCOO] ⁻	C21H21O12	FA	FA(20:5(OH4,Ke2,Ep2, cyclo))	465.1039	-1.03	MS1
26	435.2963	[M+HCOO] ⁻	C22H43O8	FA	FA(21:0(OH4))	435.2964	-0.14	MS1
27	491.2143	[M+HCOO] ⁻	C22H35O12	FA	FA(21:0(OH4,Ke2,Ep2)	491.2134	1.81	MS1
28	463.3278	[M+HCOO] ⁻	C24H47O8	FA	FA(23:0(OH4))	463.3277	0.13	MS1
29	489.1403	[M+HCOO] ⁻	C24H25O11	FA	FA(23:6(OH3,Ke2,Ep2, cyclo))	489.1402	0.20	MS1
30	519.1508	[M+HCOO] ⁻	C25H27O12	FA	FA(24:6(OH4,Ke2,Ep2, cyclo))	519.1508	0.00	MS1

Continue Appendix 6. Summary of the mouse liver negative ionization mode LESA-FT-ICR-MS (MS1 and MS/MS). The molecular ion species, chemical composition, lipid class, theoretical mass, mass error, and identifiers are provided. HG denotes the head group and FA here denotes fatty acids.

ID	Precursor m/z	species	Chemical Composition	Main Class	Short Name	Theo. m/z	ppm	Identified fragments from AutoMS/MS or MS1 identification
31	533.1671	[M+HCOO] ⁻	C26H29O12	FA	FA(25:6(OH4,Ke2,Ep2, cyclo))	533.1665	1.13	MS1
32	411.3844	[M-H] ⁻	C26H51O3	FA	FA(26:0(OH))	411.3844	-0.07	MS1
33	537.1517	[M+Cl] ⁻	C26H30O10Cl	FA	FA(26:6(OH4,Ke2,Ep2, cyclo))	537.1533	-2.96	MS1
33	547.1806	[M+HCOO] ⁻	C27H31O12	FA	FA(26:6(OH4,Ke2,Ep2, cyclo))	547.1821	-2.80	MS1
34	409.3111	[M-H] ⁻	C28H41O2	FA	FA(28:6(cyclo))	409.3112	-0.17	MS1
35	575.2137	[M+HCOO] ⁻	C29H35O12	FA	FA(28:6(OH4,Ke2,Ep2, cyclo))	575.2134	0.54	MS1
36	529.2366	[M+Cl] ⁻	C30H38O6Cl	FA	FA(30:6(Ke2,Ep2,cyclo))	529.2362	0.83	MS1
37	615.2808	[M+HCOO] ⁻	C33H43O11	FA	FA(32:6(OH3,Ke2,Ep2, cyclo))	615.2811	-0.57	MS1
38	450.2707	[M+HCOO] ⁻	C21H40NO9	HexSph	HexSph(d14:1)	450.2709	-0.38	MS1
39	892.5575	[M+Cl] ⁻	C46H83NO13Cl	LacCer	LacCer(d34:3)	892.5559	1.74	MS1
40	950.6809	[M+HCOO] ⁻	C50H96NO15	LacCer	LacCer(d37:0)	950.6786	2.43	MS1
41	766.4963	[M-H] ⁻	C38H72NO14	LacCer	LacCer(t26:0)	766.4958	0.65	MS1
42	822.5579	[M-H] ⁻	C42H80NO14	LacCer	LacCer(t30:0)	822.5584	-0.56	MS1
43	632.3419	[M+Cl] ⁻	C28H55NO12Cl	LacSph	LacSph(d16:0)	632.3418	0.11	MS1
44	670.3930	[M+Cl] ⁻	C32H61NO11Cl	LacSph	LacSph(m20:1)	670.3939	-1.34	MS1
45	582.3145	[M-H] ⁻	C26H48NO13	LacSph	LacSph(t14:1)	582.3131	2.47	MS1
46	445.2115	[M+Cl] ⁻	C19H39O7PCl	LPA	LPA(16:0)	445.2128	-2.99	MS1
47	473.2427	[M+Cl] ⁻	C21H43O7PCl	LPA	LPA(18:0)	473.2441	-2.87	MS1
48	499.2594	[M+Cl] ⁻	C23H45O7PCl	LPA	LPA(20:1)	499.2597	-0.68	MS1
49	429.2173	[M+Cl] ⁻	C19H39O6PCl	LPA	LPA(P-16:0)	429.2178	-1.19	MS1

Continue Appendix 6. Summary of the mouse liver negative ionization mode LESA-FT-ICR-MS (MS1 and MS/MS). The molecular ion species, chemical composition, lipid class, theoretical mass, mass error, and identifiers are provided. HG denotes the head group and FA here denotes fatty acids.

ID	Precursor <i>m/z</i>	species	Chemical Composition	Main Class	Short Name	Theo. <i>m/z</i>	ppm	Identified fragments from AutoMS/MS or MS1 identification
50	485.2790	[M+Cl] ⁻	C23H47O6PCl	LPA	LPA(P-20:0)	485.2804	-2.84	MS1
51	554.3018	[M+Cl] ⁻	C26H50NO7PCl	LPC	LPC(18:2)	554.3019	-0.13	MS1
51	564.3308	[M+HCOO] ⁻	C27H51NO9P	LPC	LPC(18:2)	564.3307	0.18	MS1
52	552.2868	[M+Cl] ⁻	C26H48NO7PCl	LPC	LPC(18:3)	552.2863	0.87	MS1
52	562.3153	[M+HCOO] ⁻	C27H49NO9P	LPC	LPC(18:3)	562.3151	0.28	MS1
53	580.3174	[M+Cl] ⁻	C28H52NO7PCl	LPC	LPC(20:3)	580.3176	-0.33	MS1
54	578.3020	[M+Cl] ⁻	C28H50NO7PCl	LPC	LPC(20:4)	578.3019	0.19	MS1
54	588.3306	[M+HCOO] ⁻	C29H51NO9P	LPC	LPC(20:4)	588.3307	-0.19	MS1
55	614.3461	[M+HCOO] ⁻	C31H53NO9P	LPC	LPC(22:5)	614.3464	-0.54	MS1
56	602.3018	[M+Cl] ⁻	C30H50NO7PCl	LPC	LPC(22:6)	602.3019	-0.10	MS1
56	612.3307	[M+HCOO] ⁻	C31H51NO9P	LPC	LPC(22:6)	612.3307	0.07	MS1
57	476.2785	[M-H] ⁻	C23H43NO7P	LPE	LPE(18:2)	476.2783	0.34	MS1
58	502.2942	[M-H] ⁻	C25H45NO7P	LPE	LPE(20:3)	502.2939	0.54	MS1
59	500.2784	[M-H] ⁻	C25H43NO7P	LPE	LPE(20:4)	500.2783	0.18	MS1
60	528.3098	[M-H] ⁻	C27H47NO7P	LPE	LPE(22:4)	528.3096	0.28	MS1
61	524.2783	[M-H] ⁻	C27H43NO7P	LPE	LPE(22:6)	524.2783	0.04	MS1
62	590.3028	[M+Cl] ⁻	C29H50NO7PCl	LPE	LPE(24:5)	590.3019	1.52	MS1
63	543.2947	[M+HCOO] ⁻	C24H48O11P	LPG	LPG(17:0)	543.2940	1.20	MS1
64	571.3255	[M+HCOO] ⁻	C26H52O11P	LPG	LPG(19:0)	571.3253	0.37	MS1
65	617.3578	[M+Cl] ⁻	C29H59O9PCl	LPG	LPG(23:0)	617.3591	-2.09	MS1
66	543.2576	[M-H] ⁻	C23H44O12P	LPI	LPI(14:0)	543.2576	0.04	MS1
67	587.2459	[M+HCOO] ⁻	C24H44O14P	LPI	LPI(14:1)	587.2474	-2.62	MS1
68	571.2887	[M-H] ⁻	C25H48O12P	LPI	LPI(16:0)	571.2889	-0.42	MS1

Continue Appendix 6. Summary of the mouse liver negative ionization mode LESA-FT-ICR-MS (MS1 and MS/MS). The molecular ion species, chemical composition, lipid class, theoretical mass, mass error, and identifiers are provided. HG denotes the head group and FA here denotes fatty acids.

ID	Precursor <i>m/z</i>	species	Chemical Composition	Main Class	Short Name	Theo. <i>m/z</i>	ppm	Identified fragments from AutoMS/MS or MS1 identification
68	607.2644	[M+Cl] ⁻	C25H49O12PCl	LPI	LPI(16:0)	607.2656	-2.03	MS1
69	619.2886	[M-H] ⁻	C29H48O12P	LPI	LPI(20:4)	619.2889	-0.44	MS1
70	697.3573	[M+HCOO] ⁻	C32H58O14P	LPI	LPI(22:2)	697.3570	0.43	MS1
71	723.3740	[M+HCOO] ⁻	C34H60O14P	LPI	LPI(24:3)	723.3726	1.96	MS1
72	823.4032	[M+HCOO] ⁻	C35H69O17P2	LPIP	LPIP(25:0)	823.4016	1.91	MS1
73	540.2588	[M+HCOO] ⁻	C23H43NO11P	LPS	LPS(16:1)	540.2579	1.67	MS1
74	594.3046	[M+HCOO] ⁻	C27H49NO11P	LPS	LPS(20:2)	594.3049	-0.59	MS1
75	568.2691	[M-H] ⁻	C28H43NO9P	LPS	LPS(22:6)	568.2681	1.69	MS1
76	648.3517	[M+HCOO] ⁻	C31H55NO11P	LPS	LPS(24:3)	648.3518	-0.12	MS1
77	744.4018	[M+Cl] ⁻	C38H64NO9PCl	LPS	LPS(32:6)	744.4013	0.63	MS1
78	584.3569	[M+HCOO] ⁻	C27H55NO10P	LPS	LPS(O-20:0)	584.3569	-0.03	MS1
79	582.3413	[M+HCOO] ⁻	C27H53NO10P	LPS	LPS(P-20:0)	582.3413	0.02	MS1
80	691.4644	[M+HCOO] ⁻	C36H67O12	MGDG	MGDG(26:0)	691.4638	0.81	MS1
81	719.4955	[M+HCOO] ⁻	C38H71O12	MGDG	MGDG(28:0)	719.4951	0.61	MS1
82	669.4585	[M-H] ⁻	C37H65O10	MGDG	MGDG(28:2)	669.4583	0.24	MS1
83	697.4891	[M-H] ⁻	C39H69O10	MGDG	MGDG(30:2)	697.4896	-0.72	MS1
84	982.6231	[M-H] ⁻	C49H93NO16P	MIPC	MIPC(d37:1)	982.6238	-0.73	MS1
85	436.2997	[M+Cl] ⁻	C26H43NO2Cl	NAE	NAE(24:5)	436.2988	2.09	MS1
86	464.3311	[M+Cl] ⁻	C28H47NO2Cl	NAE	NAE(26:5)	464.3301	2.20	MS1
87	462.3156	[M+Cl] ⁻	C28H45NO2Cl	NAE	NAE(26:6)	462.3144	2.53	MS1
88	660.5231	[M+HCOO] ⁻	C37H74NO6S	NAT	NAT(34:0)	660.5242	-1.74	MS1
89	701.3968	[M+Cl] ⁻	C37H63O8PCl	PA	PA(34:5)	701.3955	1.85	MS1
90	601.3639	[M+Cl] ⁻	C29H59O8PCl	PA	PA(O-26:0(OH))	601.3642	-0.47	MS1

Continue Appendix 6. Summary of the mouse liver negative ionization mode LESA-FT-ICR-MS (MS1 and MS/MS). The molecular ion species, chemical composition, lipid class, theoretical mass, mass error, and identifiers are provided. HG denotes the head group and FA here denotes fatty acids.

ID	Precursor <i>m/z</i>	species	Chemical Composition	Main Class	Short Name	Theo. <i>m/z</i>	ppm	Identified fragments from AutoMS/MS or MS1 identification
91	792.5315	[M+Cl] ⁻	C42H80NO8PCl	PC	PC(34:2)	792.5316	-0.1	FA 15:1(+COO) (253.2171), FA 17:1(+COO) (281.2484), M-CH3 (742.5391)
91	802.5604	[M+HCOO] ⁻	C43H81NO10P	PC	PC(34:2)	802.5604	0	FA 17:2(+COO) (279.2328), FA 17:1(+COO) (281.2484), M-FA 18:2 (480.3103), M-CH3 (742.5392), M-2*H2O (766.5394)
92	826.5605	[M+HCOO] ⁻	C45H81NO10P	PC	PC(36:4)	826.5604	0.15	FA 17:1(+COO) (281.2484), M-CH3 (766.5394), M-2*H2O (790.539)
93	624.3879	[M+HCOO] ⁻	C30H59NO10P	PE	PE(24:0)	624.3882	-0.42	MS1
94	668.4313	[M-H] ⁻	C36H63NO8P	PE	PE(31:4)	668.4297	2.42	MS1
95	738.5080	[M-H] ⁻	C41H73NO8P	PE	PE(36:4)	738.5079	0.08	FA 15:0(+COO) (255.2327), FA 19:4(+COO) (303.2329), M-FA 20:4 (452.2772), M-C2H6N (695.4647)
96	778.5033	[M-H] ⁻	C43H73NO9P	PE	PE(38:6(OH))	778.5029	0.49	MS1
97	762.5077	[M-H] ⁻	C43H73NO8P	PE	PE(38:6)	762.5079	-0.2	FA 21:6(+COO) (327.2328), M-FA 22:6 (452.2777)
98	760.4917	[M-H] ⁻	C43H71NO8P	PE	PE(38:7)	760.4923	-0.83	MS1
99	788.5229	[M-H] ⁻	C45H75NO8P	PE	PE(40:7)	788.5236	-0.84	MS1
100	722.5122	[M-H] ⁻	C41H73NO7P	PE	PE(O-36:5) or PE(P-36:4)	722.5130	-1.12	MS1
101	972.8337	[M-H] ⁻	C57H115NO8P	PE	PE(O-52:0(OH))	972.8366	-2.99	MS1
102	617.4296	[M-H] ⁻	C32H62N2O7P	PE	PE-Cer(t30:2)	617.4300	-0.63	MS1
103	645.3556	[M+Cl] ⁻	C30H59O10PCl	PG	PG(24:0)	645.3540	2.53	MS1

Continue Appendix 6. Summary of the mouse liver negative ionization mode LESA-FT-ICR-MS (MS1 and MS/MS). The molecular ion species, chemical composition, lipid class, theoretical mass, mass error, and identifiers are provided. HG denotes the head group and FA here denotes fatty acids.

ID	Precursor <i>m/z</i>	species	Chemical Composition	Main Class	Short Name	Theo. <i>m/z</i>	ppm	Identified fragments from AutoMS/MS or MS1 identification
104	643.3398	[M+Cl] ⁻	C30H57O10PCl	PG	PG(24:1)	643.3383	2.30	MS1
105	785.4734	[M+Cl] ⁻	C39H75O11PCl	PG	PG(33:1(OH))	785.4741	-0.95	MS1
106	869.5659	[M+Cl] ⁻	C45H87O11PCl	PG	PG(39:1(OH))	869.5680	-2.44	MS1
107	879.5549	[M+Cl] ⁻	C46H85O11PCl	PG	PG(40:3(OH))	879.5524	2.83	MS1
108	887.5235	[M+Cl] ⁻	C47H81O11PCl	PG	PG(41:6(OH))	887.5211	2.66	MS1
109	909.6008	[M+Cl] ⁻	C48H91O11PCl	PG	PG(42:2(OH))	909.5993	1.64	MS1
110	881.5127	[M+Cl] ⁻	C48H79O10PCl	PG	PG(42:8)	881.5105	2.47	MS1
111	913.5392	[M+Cl] ⁻	C49H83O11PCl	PG	PG(43:7(OH))	913.5367	2.75	MS1
112	933.6013	[M+Cl] ⁻	C50H91O11PCl	PG	PG(44:4(OH))	933.5993	2.13	MS1
113	743.3988	[M+HCOO] ⁻	C34H64O15P	PI	PI(24:0)	743.3988	-0.04	MS1
114	863.4905	[M+HCOO] ⁻	C43H76O15P	PI	PI(33:3)	863.4927	-2.61	MS1
115	901.5440	[M-H] ⁻	C47H82O14P	PI	PI(38:4(OH))	901.5448	-0.91	MS1
116	885.5495	[M-H] ⁻	C47H82O13P	PI	PI(38:4)	885.5499	-0.5	FA 17:2(+COO) (279.2328)
117	939.5262	[M+HCOO] ⁻	C49H80O15P	PI	PI(39:7)	939.5240	2.32	MS1
118	830.4947	[M+Cl] ⁻	C40H78NO12PCl	PI-Cert	PI-Cer(t34:1)	830.4956	-1.12	MS1
119	783.2955	[M+HCOO] ⁻	C30H57O19P2	PIP	PIP(20:0(OH))	783.2975	-2.57	MS1
120	881.3630	[M+Cl] ⁻	C37H68O17P2Cl	PIP	PIP(28:2(OH))	881.3626	0.41	MS1
121	566.3098	[M-H] ⁻	C26H49NO10P	PS	PS(20:0)	566.3100	-0.35	MS1
122	594.3412	[M-H] ⁻	C28H53NO10P	PS	PS(22:0)	594.3413	-0.24	MS1
123	608.3568	[M-H] ⁻	C29H55NO10P	PS	PS(23:0)	608.3569	-0.20	MS1
124	622.3725	[M-H] ⁻	C30H57NO10P	PS	PS(24:0)	622.3726	-0.13	MS1
124	668.3776	[M+HCOO] ⁻	C31H59NO12P	PS	PS(24:0)	668.3780	-0.57	MS1
125	636.3518	[M-H] ⁻	C30H55NO11P	PS	PS(24:1(OH))	636.3518	0.03	MS1

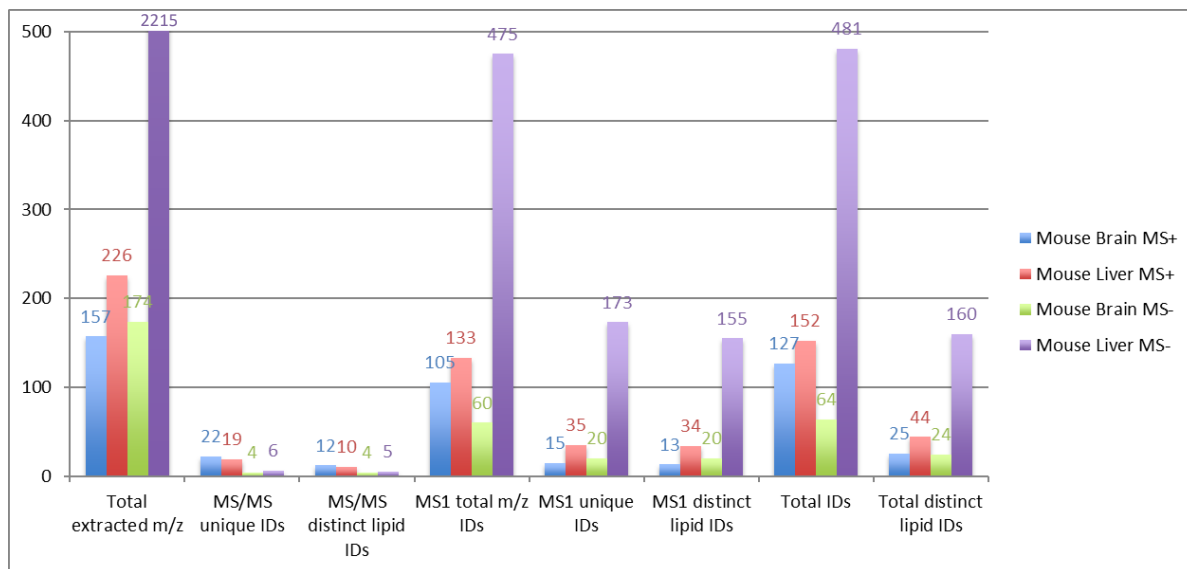
Continue Appendix 6. Summary of the mouse liver negative ionization mode LESA-FT-ICR-MS (MS1 and MS/MS). The molecular ion species, chemical composition, lipid class, theoretical mass, mass error, and identifiers are provided. HG denotes the head group and FA here denotes fatty acids.

ID	Precursor <i>m/z</i>	species	Chemical Composition	Main Class	Short Name	Theo. <i>m/z</i>	ppm	Identified fragments from AutoMS/MS or MS1 identification
126	666.3637	[M+HCOO] ⁻	C31H57NO12P	PS	PS(24:1)	666.3624	1.92	MS1
127	634.3724	[M-H] ⁻	C31H57NO10P	PS	PS(25:1)	634.3726	-0.36	MS1
128	700.3963	[M+Cl] ⁻	C33H64NO10PCl	PS	PS(27:0)	700.3962	0.17	MS1
129	674.4039	[M-H] ⁻	C34H61NO10P	PS	PS(28:2)	674.4039	-0.07	MS1
130	688.4197	[M-H] ⁻	C35H63NO10P	PS	PS(29:2)	688.4195	0.32	MS1
131	738.3970	[M-H] ⁻	C38H61NO11P	PS	PS(32:6(OH))	738.3988	-2.48	MS1
132	818.4824	[M+HCOO] ⁻	C41H73NO13P	PS	PS(34:3(OH))	818.4825	-0.12	MS1
133	842.4828	[M+HCOO] ⁻	C43H73NO13P	PS	PS(36:5(OH))	842.4825	0.34	MS1
134	874.5456	[M+HCOO] ⁻	C45H81NO13P	PS	PS(38:3(OH))	874.5451	0.54	MS1
135	850.4898	[M+HCOO] ⁻	C45H73NO12P	PS	PS(38:7)	850.4876	2.56	MS1
136	874.5802	[M+HCOO] ⁻	C46H85NO12P	PS	PS(39:2)	874.5815	-1.51	MS1
137	862.5355	[M+Cl] ⁻	C45H82NO10PCl	PS	PS(39:3)	862.5370	-1.70	MS1
138	878.5200	[M+HCOO] ⁻	C47H77NO12P	PS	PS(40:7)	878.5189	1.26	MS1
139	874.4894	[M+HCOO] ⁻	C47H73NO12P	PS	PS(40:9)	874.4876	2.08	MS1
140	904.5456	[M+Cl] ⁻	C47H84NO11PCl	PS	PS(41:4(OH))	904.5476	-2.24	MS1
140	914.5739	[M+HCOO] ⁻	C48H85NO13P	PS	PS(41:4(OH))	914.5764	-2.79	MS1
141	898.5800	[M+HCOO] ⁻	C48H85NO12P	PS	PS(41:4)	898.5815	-1.68	MS1
142	928.5456	[M+Cl] ⁻	C49H84NO11PCl	PS	PS(43:6(OH))	928.5476	-2.16	MS1
143	922.5788	[M+HCOO] ⁻	C50H85NO12P	PS	PS(43:6)	922.5815	-2.93	MS1
144	730.4430	[M+Cl] ⁻	C35H70NO10PCl	PS	PS(O-29:0(OH))	730.4431	-0.16	MS1
145	758.4734	[M+Cl] ⁻	C37H74NO10PCl	PS	PS(O-31:0(OH))	758.4744	-1.31	MS1
146	856.5382	[M+Cl] ⁻	C43H83NO11SCl	SHexCer	SHexCer(d37:1)	856.5381	0.12	MS1
147	510.2370	[M-H] ⁻	C22H40NO10S	SHexSph	SHexSph(d16:2)	510.2379	-1.74	MS1

Continue Appendix 6. Summary of the mouse liver negative ionization mode LESA-FT-ICR-MS (MS1 and MS/MS). The molecular ion species, chemical composition, lipid class, theoretical mass, mass error, and identifiers are provided. HG denotes the head group and FA here denotes fatty acids.

ID	Precursor <i>m/z</i>	species	Chemical Composition	Main Class	Short Name	Theo. <i>m/z</i>	ppm	Identified fragments from AutoMS/MS or MS1 identification
148	538.2687	[M-H] ⁻	C24H44NO10S	SHexSph	SHexSph(d18:2)	538.2692	-0.85	MS1
149	604.2991	[M+HCOO] ⁻	C25H50NO13S	SHexSph	SHexSph(t18:0)	604.3008	-2.76	MS1
150	669.2961	[M-H] ⁻	C33H49O12S	SQDG	SQDG(24:6)	669.2950	1.66	MS1
151	681.2963	[M-H] ⁻	C34H49O12S	SQDG	SQDG(25:7)	681.2950	1.89	MS1
152	965.5223	[M+Cl] ⁻	C52H82O12SCl	SQDG	SQDG(43:9)	965.5221	0.22	MS1
153	667.5158	[M+HCOO] ⁻	C39H71O8	TG	TG(35:1)	667.5155	0.43	MS1
154	695.5460	[M+HCOO] ⁻	C41H75O8	TG	TG(37:1)	695.5468	-1.11	MS1
155	709.5622	[M+HCOO] ⁻	C42H77O8	TG	TG(38:1)	709.5624	-0.24	MS1
156	737.5930	[M+HCOO] ⁻	C44H81O8	TG	TG(40:1)	737.5937	-0.92	MS1
157	683.5270	[M-H] ⁻	C43H71O6	TG	TG(40:5)	683.5256	2.09	MS1
158	709.5432	[M-H] ⁻	C45H73O6	TG	TG(42:6)	709.5413	2.68	MS1

Appendix 7. Dataset descriptions of the positive and negative MB and ML FT-ICR-MS(/MS) analyses.

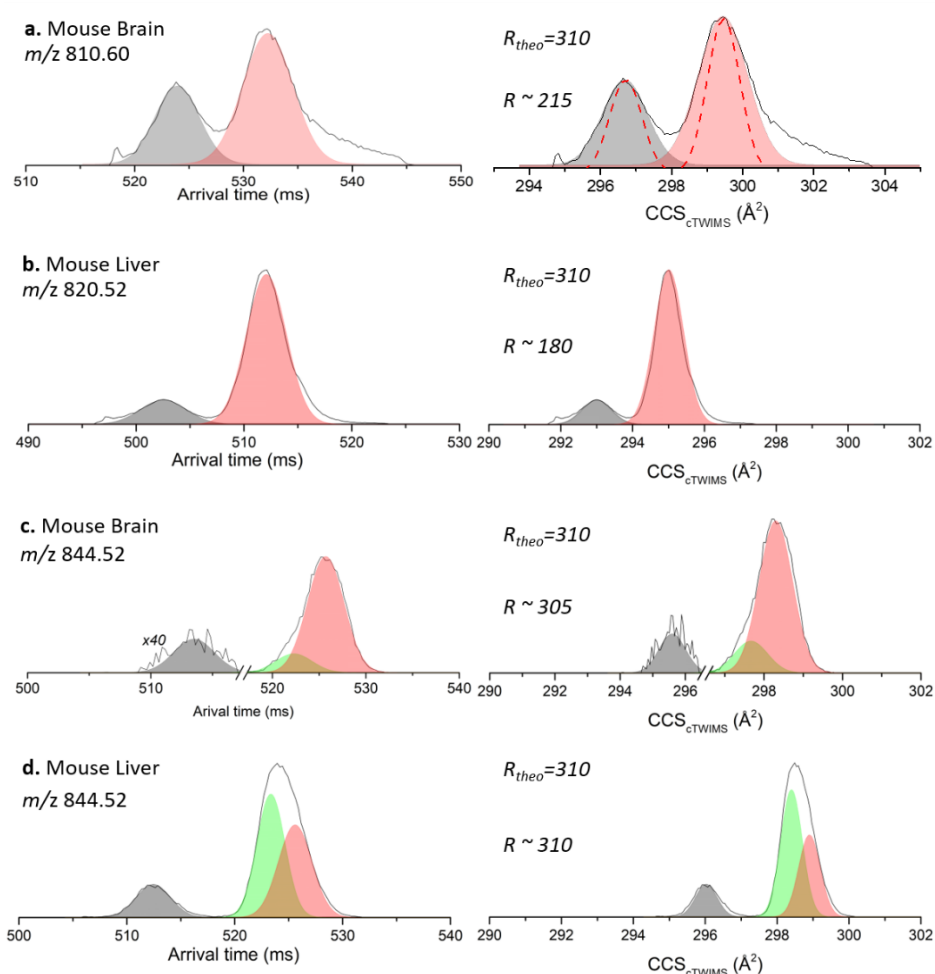


Appendix 8. Summary of the mouse brain and mouse liver lipid compositions, with the number of uniquely-identified lipids in each lipid class.

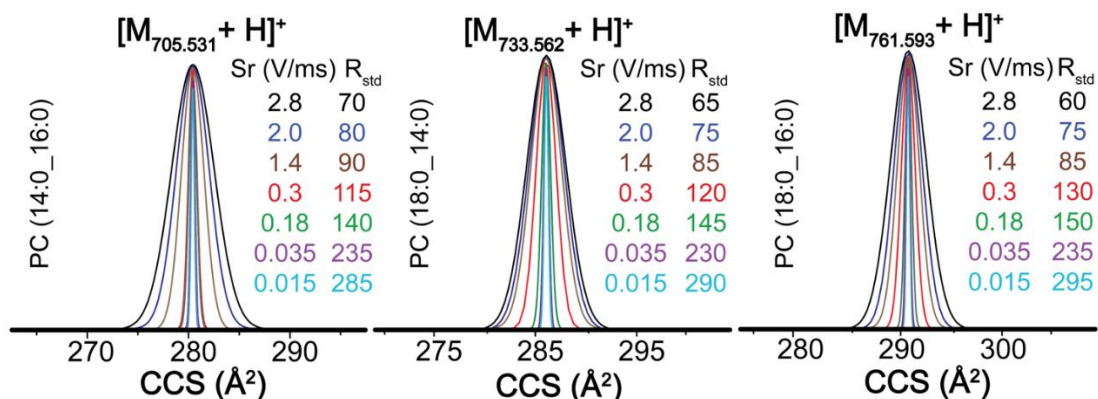
Lipid classes	MB	ML
CAR	2	2
Cer	1	9
CerP	1	4
DG	1	9
DGDG		1
FA		15
HexCer		3
HexSph		1
LacCer		4
LacSph		3
LPA		6
LPC	2	6
LPE	2	6
LPG		4
LPI	1	6
LPIP		3
LPS	3	8
MG		2
MGDG		8
MIPC		2
NAE		3
NAT		1
PA		2
PC	13	10
PE	10	9

Continue Appendix 8. Summary of the mouse brain and mouse liver lipid compositions, with the number of uniquely- identified lipids in each lipid class

Lipid classes	MB	ML
PE-Cer		1
PG	1	10
PI		5
PI-Cer		1
PIP		2
PS	1	27
SHexCer	3	1
SHexSph		3
SQDG	2	3
TG		6
WE		2



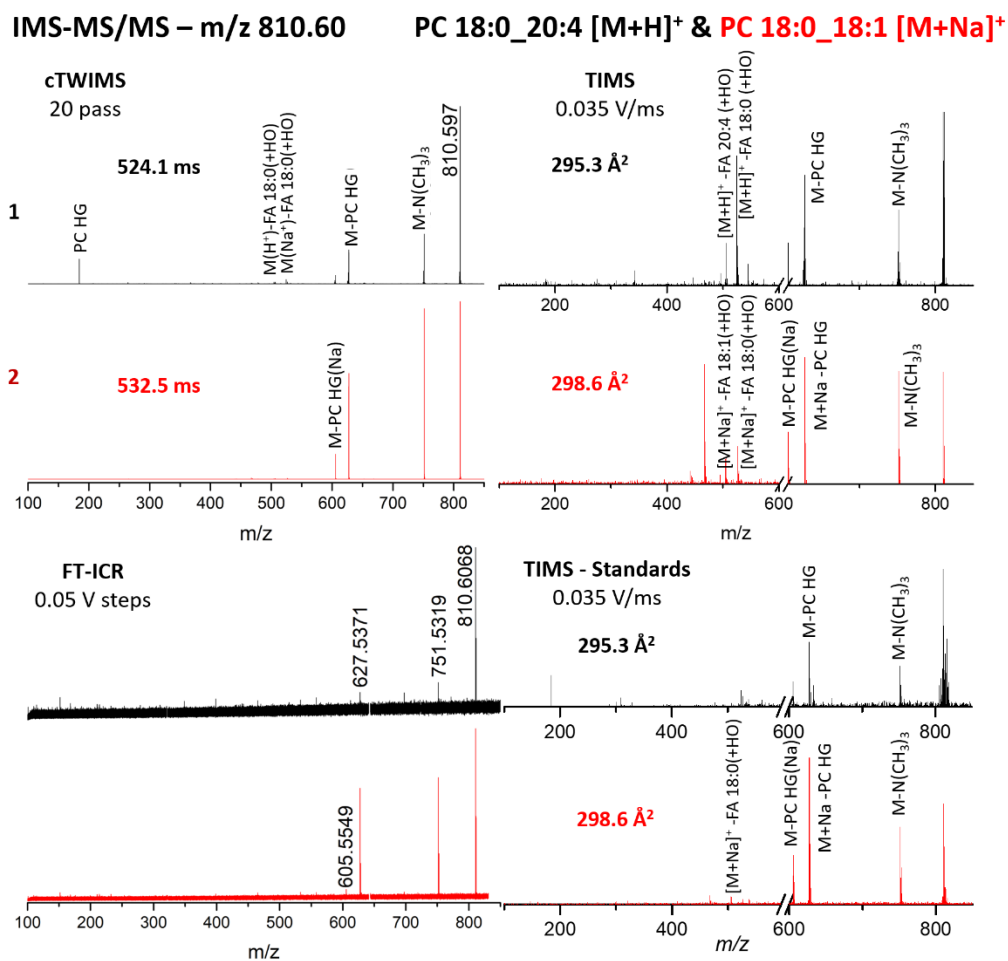
Appendix 9. Conversion of drift time cTWIMS to CCS cTWIMS from calibrated CCS values from TIMS of a. mouse brain m/z 810.60, b. mouse liver m/z 820.52, c. mouse brain m/z 844.60, and d. mouse liver m/z 844.60. R_{theo} refers to the theoretical resolving power ($cTWIMS, R=70\sqrt{n}$) and the R refers to the resolving power in terms of CCS.



Appendix 10. Typical CCS profiles of a lipid standard mix as a function of the scan rate: (a)PC (14:0_16:0), (b) PC (18:0_14:0) and (c) PC(18:0_16:0). The mobility resolving power can be increased nearly ~4-5x ($R = 60 - 295$), depending on the mobility range and scan time (data corresponds to up to 500 ms per scan).

Appendix 11. Comparison of the cTWIMS and TIMS instrument performances of different lipids in positive mode. “r” represents the peak resolution (see Eq. 2) between the two closest peaks and “R” represents the apparent resolving power (see Eq. 1). R expected is based on $R=70\sqrt{n}$ for cTWIMS and lipid standards from TIMS.

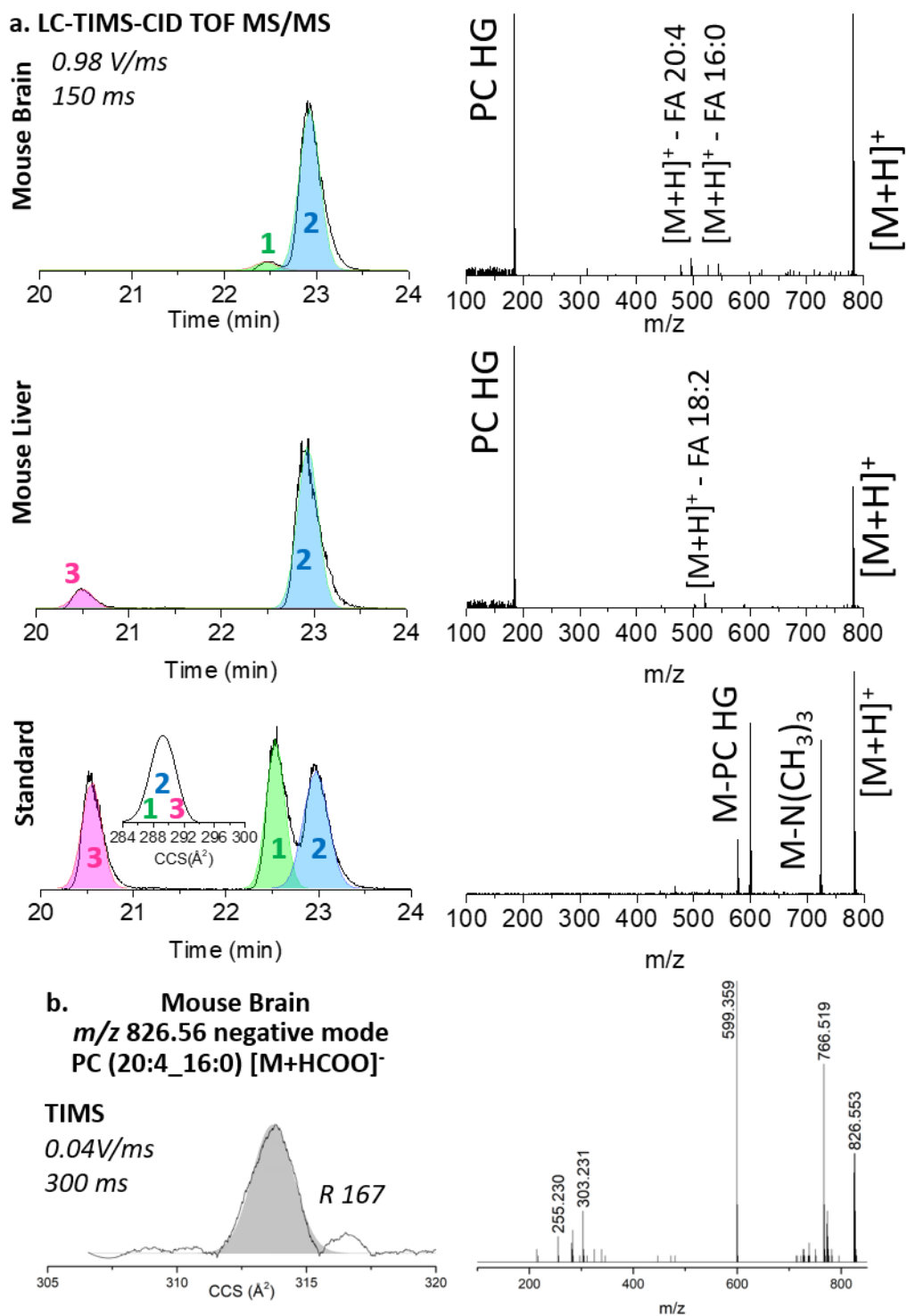
Mouse Tissue	m/z	Instrument	r ₁₋₂	r ₂₋₃	R measured (expected)
Brain	810.60	cTWIMS (20p)	1.6		215 (310)
		TIMS	1.6		240 (235)
	782.56	TIMS	1.4		150 (145)
Liver	782.56	TIMS		1.2	150 (145)



Appendix 12. Mobility- and quadrupole-selected cTWIMS-MS/MS, TIMS-MS/MS and FT-ICR CID spectra of m/z 810.60 from mouse brain.

Appendix 13. Fragment identification of positive mode m/z 810.60. “X” denotes the presence of the peaks in either the mouse brain or mouse liver tissue.

Fragment m/z	ID	cTWIMS	TIMS	FT-ICR
		1	2	1
751.52	$[M+Na]^+$ PC M-N(CH ₃) ₃	X	X	X
627.53	$[M+H]^-$ PC HG	X	X	X
605.55	$[M+H]^+$ M-PC HG(Na)	X	X	X
526.33	$[M+H]^+$ PC (38:4) M-FA 18:0(+HO)	X	X	X
	$[M+Na]^+$ PC (36:1) M-FA 18:0(+HO)			
506.36	$[M+H]^+$ PC (38:4) M-FA 20:4(+HO)	X	X	
184.07	PC HG	X		



Appendix 14. Targeted quadrupole-selected and mobility-selected TIMS-MS/MS of *m/z* 782.56 (PC (36:4)) from mouse brain and mouse liver.

Appendix 15. Fragment identification of positive mode m/z 782.56. “X” denotes the presence of the peaks in either the mouse brain or the mouse liver spectra.

Fragment m/z	ID	Mouse Brain	Mouse Liver
723.50	$[M+H]^+$ PC M-N(CH ₃) ₃	X	X
599.50	$[M+H]^+$ PC M-HG	X	
544.34	$[M+H]^+$ PC – FA 16:0	X	
496.34	$[M+H]^+$ PC – FA 20:4	X	
520.34	$[M+H]^+$ PC – FA 18:2		X
184.07	PC HG	X	X

Appendix 16. Negative mode TIMS-MS/MS fragment identification m/z 826.56.

Fragment m/z	ID
766.52	NL HCOOCH ₃
480.30	M-FA 20:4(-H)- HCOOCH ₃
303.23	FA 20:4
255.29	FA 16:0

Appendix 17. Mouse brain and mouse liver annotated lipids, extracted from a TIMS discovery run, for the lipid species previously identified using LESA-FT-ICR-MS(/MS)¹². The TIMS ramp was 90 V with a 500 ms ramp duration (Sr = 0.18 V/ms). The screened mass-to-charge range was m/z 150-1500. ^a Value is only present in Mouse Brain sample and ^b Value is only present in Mouse Liver sample.

Lipid ID	Species	Direct Infusion (nESI-TIMS-TOF)			Metaboscape (LESA-LC-TIMS-CID TOF MS/MS)			
		Experimental mass	Mass Error (ppm)	CCS (Å ²)	RT	CCS (Å ²)	MSMS Score	Mass Error (ppm)
LPC (14:0)	[M+H] ⁺	X	X	X	7.73	222.1	995.5	0.51
LPC(16:0)	[M+H-H ₂ O] ⁺	478.3293	0.21	223.6 226.5 ^a		225		
LPC(16:0)	[M+H] ⁺	496.3412	2.82	230.6	10	230.1	921.8	0.49
LPC(16:0)	[M+Na] ⁺	518.3234	3.28	234.2		233.65		
LPC(16:0)	[M+K] ⁺	534.298	4.49	235.0		X		
LPC (14:0)	[M+H] ⁺	X	X	X	7.73	222.1	995.5	0.51
LPC (16:1)	[M+H] ⁺	X	X	X	8.28	224.8	981.9	-0.039
LPC (17:0)	[M+H] ⁺ [M+Na] ⁺	X	X	X	10.92	233.6	952.9	-0.371
LPC (17:1)	[M+H] ⁺	X	X	X	9.36	228.5	991	0.184
PE 19:1	[M+H] ⁺	X	X	X	10.55	221	977.9	-0.702
LPC (18:3)	[M+H] ⁺	X	X	X	7.81	224.4	956.5	0.015
LPC(18:2)	[M+H] ⁺	520.3399	0.19	227.4 ^b 234.3 ^b	9.28	226.8	967.3	-0.85
LPC(18:2)	[M+Na] ⁺	542.3231	2.58	231.9 ^b		230.4		
LPC(18:1)	[M+H] ⁺	X	X	X	9.97	234.1	917.5	-0.887
LPC(18:0)	[M+H] ⁺	524.3721	-1.90	238.8	11.64	237.4	953.7	0.167
LPC (19:0)	[M+H] ⁺	X	X	X	12.35	241.2	978.1	0.387
LPC (20:0)	[M+H] ⁺ [M+Na] ⁺	X	X	X	13.17	244.7	974	-0.949
LPC (20:1)	[M+H] ⁺ [M+Na] ⁺	X	X	X	11.69	239.8	947.5	-0.535
LPC (20:3)	[M+H] ⁺	X	X	X	9.62	230.2	948.6	-0.907

Continue Appendix 17. Mouse brain and mouse liver annotated lipids, extracted from a TIMS discovery run, for the lipid species previously identified using LESA-FT-ICR-MS(/MS).

Lipid ID	Species	Direct Infusion (nESI-TIMS-TOF)			Metaboscape (LESA-LC-TIMS-CID TOF MS/MS)			
		Experimental mass	Mass Error (ppm)	CCS (Å ²)	RT	CCS (Å ²)	MSMS Score	Mass Error (ppm)
				230.3				
LPC(20:4)	[M+H] ⁺	544.3391	-1.29	235.7	8.81	229.5	969.1	-0.346
LPC(20:4)	[M+Na] ⁺	566.3231	2.47	236.2		234.3		
LPC(20:4)	[M+K] ⁺	582.3025	11.85	238.4		236.5		
LPC(20:3)	[M+H] ⁺	546.3557	-0.55	241.3	9.61	240.2	948.6	-0.751
PE 23:4	[M+H] ⁺	X	X	X	10.51	226.8	989.8	-0.894
LPC (20:5)	[M+H] ⁺	X	X	X	7.48	225.9	990.2	-0.407
LPC (22:5)	[M+H] ⁺	X	X	X	9.16	233.1	990.9	-1.012
LPC (22:6)	[M+H] ⁺	X	X	X	8.24	233.9	996.6	-0.878
LPE (18:0)	[M+H] ⁺	X	X	X	11.83	221.3	972.6	0.034
LPE (18:1)	[M+Na] ⁺	X	X	X	10.56	215.7	991.2	0.535
	[M+H-H ₂ O] ⁺							
LPE (19:0)	[M+H] ⁺	X	X	X	12.96	229.4	846.1	0.547
LPE (20:1)	[M+H] ⁺	X	X	X	11.87	223.6	963.3	0.106
LPE (22:4)	[M+H] ⁺	X	X	X	10.53	221.4	100	0.617
LPE (22:6)	[M+H] ⁺	X	X	X	8.51	218.8	958.8	-0.162
PC (17:0)	[M+H] ⁺	X	X	X	9.98	235.7	983	-0.941
PC (18:2)	[M+H] ⁺	X	X	X	9.37	231.1	900.3	0.074
				249.0				
DG(34:3)	[M+Na] ⁺	613.4802	2.12	253.9	X	X	X	X
				260.8				
DG(34:1)	[M+Na] ⁺	617.5115	3.40	249.0	X	X	X	X
DG(36:3)	[M+Na] ⁺	641.5115	11.54	253.3	X	X	X	X
				258.3				
DG(36:2)	[M+Na] ⁺	643.5272	4.35	257.8	X	X	X	X

Continue Appendix 17. Mouse brain and mouse liver annotated lipids, extracted from a TIMS discovery run, for the lipid species previously identified using LESA-FT-ICR-MS(/MS).

Lipid ID	Species	Direct Infusion (nESI-TIMS-TOF)			Metaboscape (LESA-LC-TIMS-CID TOF MS/MS)			
		Experimental mass	Mass Error (ppm)	CCS (Å ²)	RT	CCS (Å ²)	MSMS Score	Mass Error (ppm)
PE(30:2(OH))	[M+H] ⁺	676.4549	0.15	260.2 ^b	X	X	X	X
PE(30:1(OH))	[M+H] ⁺	678.4703	-0.15	264.2 266.9 ^a	X	X	X	X
PC(32:1)	[M+H] ⁺	732.5504	-4.64	274.2 ^a 283.7 ^a	21.51	282.3	994.7	0.153
PC(32:0)	[M+H] ⁺	734.5661	-4.49	286.8	26.04	286.3	997.7	0.911
PE(O-38:6) or PE(P-38:5)	[M+H] ⁺	750.5431	-0.13	277.8 285.2 276.6	X	X	X	X
PE(O-38:5) or PE(P-38:4)	[M+H] ⁺	752.5588	-0.13	283.6 287.5 ^a 283.5 ^b	X	X	X	X
PC(34:4) or PE(O-38:4))	[M+H] ⁺	754.5305	-10.07	286.9 290.5 ^a 294.8 ^a 284.2 ^b	29.65	283.9	741.2	1.626
PC(34:3)	[M+H] ⁺	756.5491	-6.21	286.7 ^b 292.0	19.55	282.6	995.3	0.9
PC(34:2)	[M+H] ⁺	758.5697	0.40	286.9 292.2 ^a	23.55	285.8	992.9	0.924
PC(34:1)	[M+H] ⁺	760.5836	-1.97	286.6 ^b 289.7	27.06	288.7	995.5	0.818
PE (38:4)	[M+H] ⁺	X	X	X	29.07	284.2	918.7	0.735
PE (38:5)	[M+H] ⁺ [M+Na] ⁺ [M+H] ⁺	X	X	X	24.31	280.3	915	0.626
PE (38:6)	[M+Na] ⁺	X	X	X	23.17	279.5	938.6	0.565

Continue Appendix 17. Mouse brain and mouse liver annotated lipids, extracted from a TIMS discovery run, for the lipid species previously identified using LESA-FT-ICR-MS(/MS).

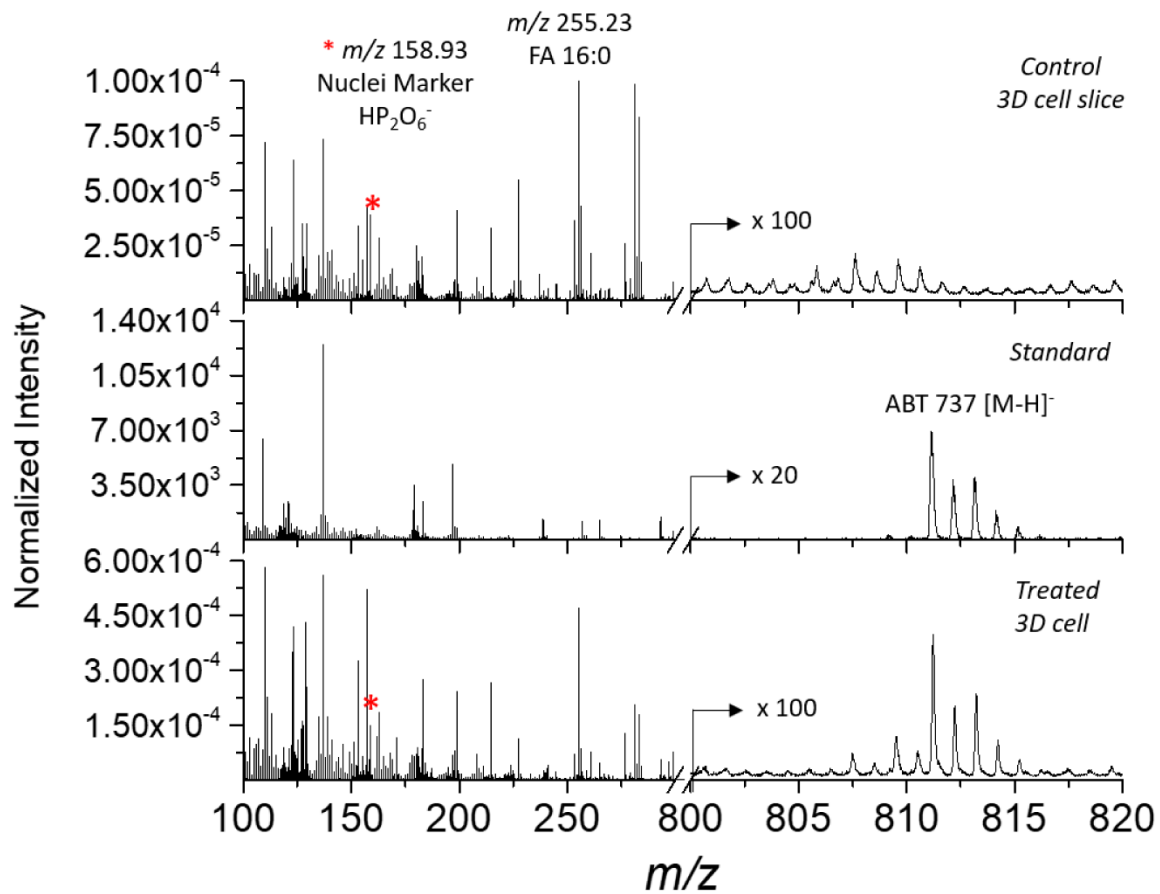
Lipid ID	Species	Direct Infusion (nESI-TIMS-TOF)			Metaboscape (LESA-LC-TIMS-CID TOF MS/MS)			
		Experimental mass	Mass Error (ppm)	CCS (Å ²)	RT	CCS (Å ²)	MSMS Score	Mass Error (ppm)
PC(O-37:9)	[M+H] ⁺	772.5261	-1.94	286.9 ^b 289.8	26.03	290.3	X	-0.764
PE(38:1)	[M+H] ⁺	774.5965	5.42	297.1 289.0	30.90	289.6	923.9	1.80
PC(36:5)	[M+H] ⁺	780.5519	-2.43	287.5 ^a 290.8	19.33	285.7	19.33	0.271
PC(36:4)	[M+H] ⁺	782.5672	-2.81	290.1 293.8	22.51	289.9	995.8	0.881
PC(36:3)	[M+H] ⁺	784.5826	-3.19	290.4 293.9	24.57	290.2	994.3	0.89
PC(36:2)	[M+H] ⁺	786.6004	-0.38	298.3 293.9	27.09	292.8	995.6	0.656
PC(36:1)	[M+H] ⁺	788.6099	-8.24	286.2 ^b 290.7 ^b 293.4 ^b 296.2 303.8 ^b	29.91	295	994.9	0.735
PE(40:7)	[M+H] ⁺	790.5443	7.84	286.6 290.8 296.2	23.49	283	936.8	-0.025
PC(37:6) and PE (40:6)	[M+H] ⁺	792.552	-2.27	287.4 ^b 291.5 ^b	28.31 (PE 40:6) 25.55 (PC 37:6)	286.6 (PE 40:6) 292.4 (PC 37:6)	0.312 (PE 40:6) -0.585 (PC 37:6)	936 (PE 40:6) 999.8 (PC 37:6)
PC(37:4) and PE(40:4)	[M+H] ⁺	796.5293	2.13	290.1 ^b 292.3 ^b 295.9 ^b	30.0 (PE 40:4) 25.4 (PC 37:4)	290.1 (PE 40:4) 292.0 (PC 37:4)	912.8 (PE 40:4) 994.4 (PC 37:4)	0.704 (PE 40:4) 0.451 (PC 37:4)
PC(O-36:4)	[M+H] ⁺	798.5422	-1.25	290.3 ^b	X	X	X	X

Continue Appendix 17. Mouse brain and mouse liver annotated lipids, extracted from a TIMS discovery run, for the lipid species previously identified using LESA-FT-ICR-MS(/MS).

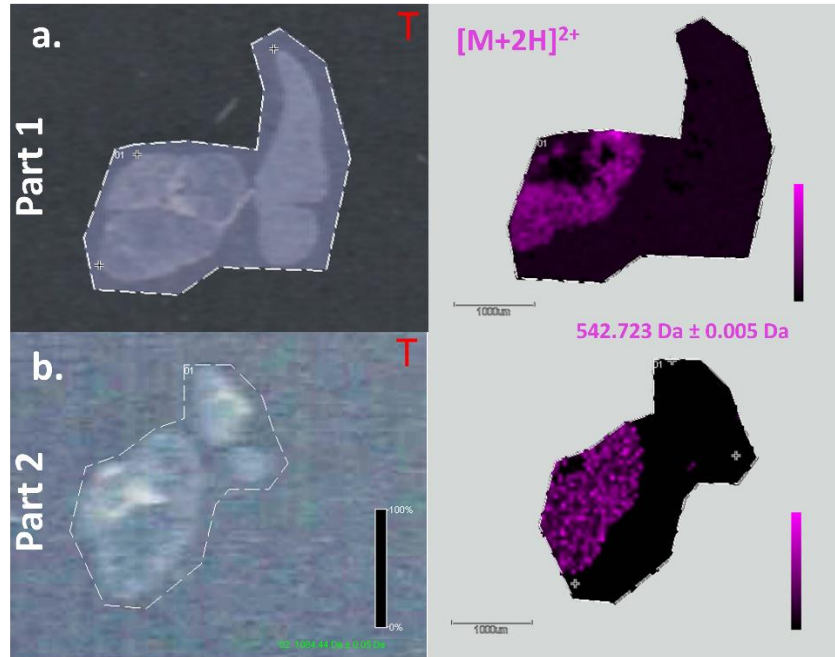
Lipid ID	Species	Direct Infusion (nESI-TIMS-TOF)			Metaboscape (LESA-LC-TIMS-CID TOF MS/MS)			
		Experimental mass	Mass Error (ppm)	CCS (Å ²)	RT	CCS (Å ²)	MSMS Score	Mass Error (ppm)
PC (37:2)	[M+H] ⁺	X	X	X	29.72	295.6	979.2	-0.104
PC(38:7)	[M+H] ⁺	804.5524	-1.74	291.0 294.0	1872	288.8	994.7	1.282
PC(38:6)	[M+H] ⁺	806.5656	-4.71	293.3	21.76	292.3	293.8	0.805
PC(38:5)	[M+H] ⁺	808.581	-5.07	294.4 297.6 295.3	24.46	294.9	994.7	0.455
PC(38:4)	[M+H] ⁺	810.596	-5.80	298.6 306.4 ^b 291.6 ^b	28.05	295.2	995.9	0.634
PC(38:3)	[M+H] ⁺	812.6165	-9.35	294.9 ^b 297.4 ^b 293.4	29.39	297.1	994.3	0.354
PC(38:2)	[M+H] ⁺	814.6343	2.82	298.8 306.8 ^b	30.24	298.1	995.3	0.283
PC (38:1)	[M+H] ⁺ [M+Na] ⁺	X	X	X	30.75	300.5	944	0.714
PC(39:7) or PE(42:7)	[M+H] ⁺	818.5723	3.54	290.4 ^b 296.1 ^b	X	X	X	X
PC(39:6)	[M+H] ⁺	820.5868	2.07	293.7	24.57	295.4	993.9	0.168
PC(O-41:11)	[M+H] ⁺	824.5585	-0.49	296.6 298.9 ^b 292.3 ^b	X	X	X	X
PC(O-41:10)	[M+H] ⁺	826.5733	-1.45	296.4 299.4 305.3 ^b	X	X	X	X
PC(40:9)	[M+H] ⁺	828.5552	1.69	293.8 ^b 296.6	21.78	294.8	X	-3.899

Continue Appendix 17. Mouse brain and mouse liver annotated lipids, extracted from a TIMS discovery run, for the lipid species previously identified using LESA-FT-ICR-MS(/MS).

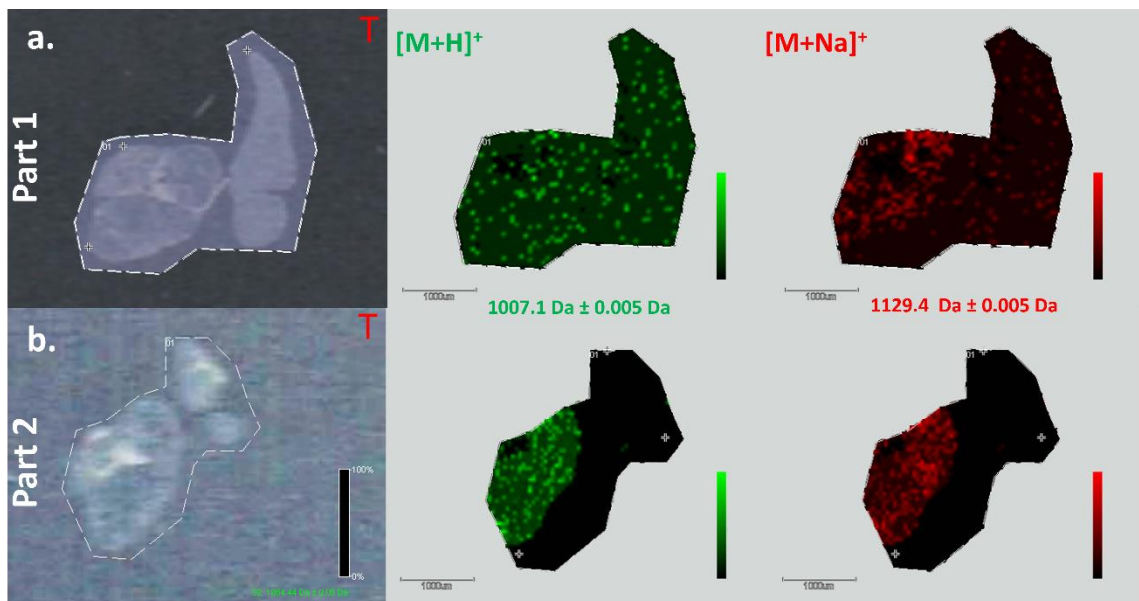
Lipid ID	Species	Direct Infusion (nESI-TIMS-TOF)			Metaboscape (LESA-LC-TIMS-CID TOF MS/MS)			
		Experimental mass	Mass Error (ppm)	CCS (Å ²)	RT	CCS (Å ²)	MSMS Score	Mass Error (ppm)
PC(40:8)	[M+H] ⁺	830.569	0.48	294.2 296.8	19.67	293	934.2	0.853
PC(40:7)	[M+H] ⁺	832.5792	-7.09	297.5 300.3	22.52	296	994.4	0.161
PC(40:6)	[M+H] ⁺	834.5953	-6.47	296.5 ^b 300.1	27.13	298.3	996	0.305
PC(40:5)	[M+H] ⁺	836.6075	-10.64	296.1 ^b 300.0 ^b	27.92	299.5	965.1	1.47
PC(40:4)	[M+H] ⁺	838.6321	0.12	295.9 ^b 299.4 ^b	29.82	301.5	966.1	0.862
PC(40:1)	[M+H] ⁺	844.6755	-4.14	293.6 ^b 296.8 ^b	31.88	306.8	993.7	0.774
PC(42:1)	[M+H] ⁺	854.5626	-5.85	298.2 ^a 300.5 ^a	19.08	296.2	994.8	0.195
PC (44:1)	[M+H] ⁺ [M+Na] ⁺	X	X	X	18.45	298.7	997.5	0.165
PS (38:1)	[M+H] ⁺	X	X	X	30.09	296.8	928.1	-0.967
PS (38:4)	[M+H] ⁺	X	X	X	24.94	288.1	914.5	0.312
PS (40:6)	[M+H] ⁺	X	X	X	24.14	291.2	933.7	0.125
PS (44:12)	[M+H] ⁺	X	X	X	16.81	291.6	914.5	0.766
SM (d34:1)	[M+H] ⁺	X	X	X	21.64	285.1	995.1	-0.135
SM (d41:1)	[M+H] ⁺	X	X	X	31.35	305.6	997.9	0.721
SM (d41:2)	[M+H] ⁺	X	X	X	30.25	303	981.1	-0.512
SM (d42:1)	[M+H] ⁺	X	X	X	31.87	308.4	999.1	0.621



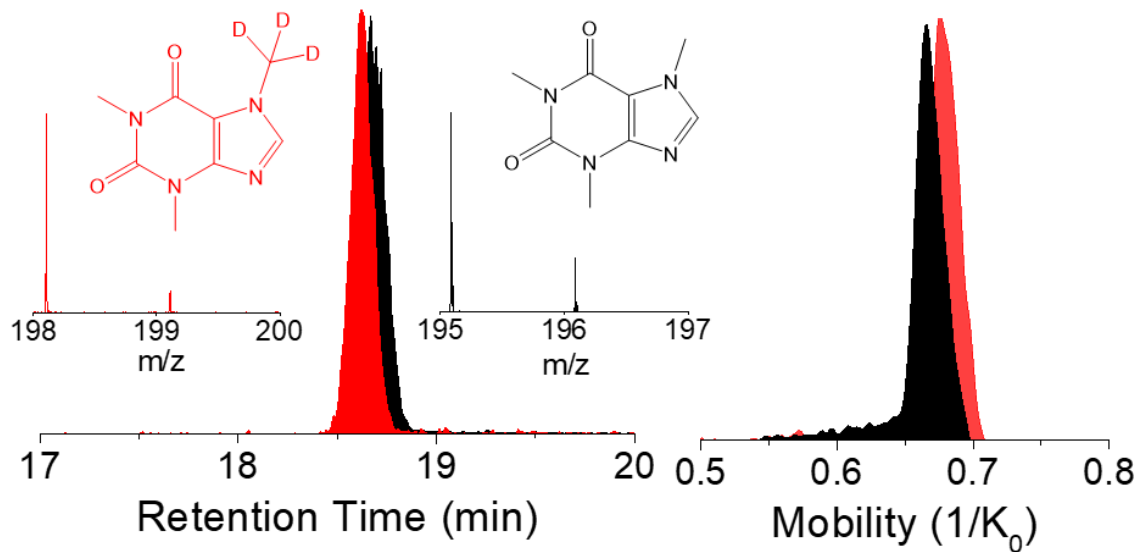
Appendix 18. Mass spectra comparing the control 3D cell spheroid slice (top), ABT-737 10 μM standard (center) and treated spheroid with 50 μM ABT 737 (bottom).



Appendix 19. MALDI-FT ICR images of doubly charged ions of Arg-Vasopressin species in sections through two different parts of human pituitary biopsy (a. part 1 and b. part 2).



Appendix 20. MALDI-FT ICR images of protonated and sodiated ions of Oxytocin species in sections through two different parts of human pituitary biopsy (a. part 1 and b. part 2)



Appendix 21. Caffeine D3 internal standard isotopic pattern, retention time and mobility, respectively.

Appendix 22. Complete list of identified compounds in saliva samples from HS and AS in positive and negative ionization mode.

Identification	RT (min)	Molecular Ion Form	Mobility (1/K ₀)	Neutral Mass	Formula	MS/MS score
Biological						
(2R)-2-[(2R)-1,1-Dimethoxy-3-nitro-2-propanyl]undecyl acetate	23.36	[M-H]-	0.904	361.25	C18H35NO6	Manual
(Z)-5,8,11-trihydroxyoctadec-9-enoic acid	30.04	[M-H]-	0.882	330.24	C18H34O5	948.6
1-beta-D-Arabinofuranosyluracil 5-monophosphate	15.86	[M-H]-	0.787	324.04	C9H13N2O9P	940.6
12-HETE	38.39	[M-H]-	0.878	320.24	C20H32O3	885.7
2'-Deoxycytidine 5-monophosphate	8.38	[M-H]-	0.778	307.06	C9H14N3O7P	735.3
2'-Deoxyinosine-5'-monophosphate	15.98	[M-H]-	0.822	332.05	C10H13N4O7P	756.4
2'-Deoxyuridine 5'-monophosphate	15.19	[M-H]-	0.762	308.04	C9H13N2O8P	907.1
2-O-Methylguanosine	14.71	[M-H]-	0.839	297.11	C11H15N5O5	929.1
3'-Azido-3'-deoxythymidide 5'-monophosphate	14.26	[M-H]-	0.812	347.06	C10H14N5O7P	931.3
3'-Cytidine monophosphate	8.52	[M-H]-	0.805	323.05	C9H14N3O8P	840.8
3'-O-Methylinosine	14.65	[M-H]-	0.771	282.10	C11H14N4O5	996.7
3-Hydroxyphenylalanine	12.56	[M-H]-	0.668	181.07	C9H11NO3	913.9
3-Methylxanthine	14.83	[M-H]-	0.581	166.05	C6H6N4O2	946
3-phenyllactic acid	24.85	[M-H]-	0.626	166.06	C9H10O3	808.3
4-Hydroxyphenyllactic acid	19.79	[M-H]-	0.655	182.06	C9H10O4	980.7
6-Phosphogluconate	7.95	[M-H]-	0.687	276.02	C6H13O10P	975
6:3+6O fatty acyl hexoside	9.93	[M-H]-	0.807	354.08	C12H18O12	993.9
9-(2,3-dihydroxypropoxy)-9-oxononanoic acid	22.96	[M-H]-	0.751	262.14	C12H22O6	983.4
alpha, alpha-Trehalose 6-phosphate	11.01	[M-H]-	0.878	422.08	C12H23O14P	454.4
Cytidine 5'-monophosphate	8	[M-H]-	0.789	323.05	C9H14N3O8P	922.9

Continue Appendix 22. Complete list of identified compounds in saliva samples from HS and AS in positive and negative ionization mode.

Identification	RT (min)	Molecular Ion Form	Mobility (1/K₀)	Neutral Mass	Formula	MS/MS score
D-Mannose 6-phosphate	10.93	[M-H]-	0.706	260.03	C6H13O9P	996
D-Ribose 5-phosphate	8.96	[M-H]-	0.663	230.02	C5H11O8P	924.4
D-Sorbitol	7.54	[M-H]-	0.609	182.08	C6H14O6	710.1
Decanedioic acid	28.52	[M-H]-	0.672	202.12	C10H18O4	979.5
Deoxinosine	13.99	[M-H]-	0.736	252.09	C10H12N4O4	994.1
Deoxyguanosine	13.98	[M-H]-	0.757	267.10	C10H13N5O4	984.6
Gluconate	7.84	[M-H]-	0.617	196.06	C6H12O7	952
Guanosine	13.66	[M-H]-	0.795	283.09	C10H13N5O5	976.8
Guanosine-5'-monophosphate	15.93	[M-H]-	0.826	363.06	C10H14N5O8P	837.6
Hypoxanthine	13.54	[M+H] ⁺	0.582	136.04	C5H4N4O	912.9
Indole-3-acetaldehyde	25.17	[M-H]-	0.598	159.068	C10H9NO	755.7
Indolelactic acid	25.61	[M-H]-	0.697	205.07	C11H11NO3	893.9
Indoline	17.45	[M+H] ⁺	0.574	119.07	C8H9N	990.8
Inosine	13.58	[M-H]-	0.751	268.08	C10H12N4O5	996.7
Isopropylmalic acid	20.63	[M-H]-	0.604	176.07	C7H12O5	864
Isoprostaglandin-f2 alpha	31.82	[M-H]-	0.893	354.24	C20H34O5	722.3
Laminaritetraose	7.68	[M-H]-	1.176	666.22	C22H30N14O11	579.6
L-carnitine	7.15	[M+H] ⁺	0.613	161.11	C7H15NO3	998.7
LPE 20:4	34.62	[M-H]-	1.06	501.29	C25H44NO7P	962.5
N-Acetylneuraminate	9.28	[M-H]-	0.76	309.11	C11H19NO9	960.8
N-Acetylneuraminic acid	9.30	[M+H] ⁺ [M-H]-	0.784 0.747	309.11	C11H19NO9	962.4
Niacinamide	8.64	[M+H] ⁺	0.565	122.05	C6H6N2O	376.6
Orthophosphate	10.52	[M-H]-	0.579	97.98	H3O4P	980.6

Continue Appendix 22. Complete list of identified compounds in saliva samples from HS and AS in positive and negative ionization mode.

Identification	RT (min)	Molecular Ion Form	Mobility (1/K ₀)	Neutral Mass	Formula	MS/MS score
Pantothenic Acid	15.45	[M+H] ⁺ [M-H] ⁻	0.701 0.690	219.11	C ₉ H ₁₇ NO ₅	871.9
Phosphocholine	7.33	[M+H] ⁺	0.636	183.07	C ₅ H ₁₄ NO ₄ P	961.5
Pseudo uridine	8.87	[M-H] ⁻	0.699	244.07	C ₉ H ₁₂ N ₂ O ₆	987.2
Riboflavin	18.89	[M+H] ⁺ [M-H] ⁻ [M+Cl] ⁻	0.908 0.928	376.14	C ₁₇ H ₂₀ N ₄ O ₆	969.5
Sorbitol-6-phosphate	11.04	[M-H] ⁻	0.697	262.05	C ₆ H ₁₅ O ₉ P	956.5
Taurine	7.45	[M-H] ⁻	0.528	125.01	C ₂ H ₇ NO ₃ S	998.6
Thymidine 5'-monophosphate	16.92	[M-H] ⁻	0.782	322.06	C ₁₀ H ₁₅ N ₂ O ₈ P	909.4
Tryptophan	16.46	[M-H] ⁻	0.708	204.09	C ₁₁ H ₁₂ N ₂ O ₂	992.7
Uric Acid	9.86	[M+H] ⁺ [M-H] ⁻	0.665 0.576	168.03	C ₅ H ₄ N ₄ O ₃	875.7
Uridine 5'-monophosphate	13.42	[M-H] ⁻	0.775	324.04	C ₉ H ₁₃ N ₂ O ₉ P	934.4
Xanthine	13.21	[M-H] ⁻	0.549	152.03	C ₅ H ₄ N ₄ O ₂	995
Xanthosine	14.29	[M-H] ⁻	0.754	284.08	C ₁₀ H ₁₂ N ₄ O ₆	999.6
Drugs						
Acetaminophen	19.02	[M+H] ⁺	0.608	151.06	C ₈ H ₉ NO ₂	951.1
Albuterol	13.01	[M+H] ⁺ [M-H] ⁻	0.754 0.772	239.15	C ₁₃ H ₂₁ NO ₃	988.0
Cetirizine	24.22	[M+H] ⁺ [M-H] ⁻	0.965 0.942	388.16	C ₂₁ H ₂₅ CIN ₂ O ₃	730.7
Hesperidin	22.07	[M-H] ⁻	1.135	610.19	C ₂₈ H ₃₄ O ₁₅	999.5
Hydroxycine	22.09	[M+H] ⁺	0.951	374.18	C ₂₁ H ₂₇ CIN ₂ O ₂	995.8

Continue Appendix 22. Complete list of identified compounds in saliva samples from HS and AS in positive and negative ionization mode.

Identification	RT (min)	Molecular Ion Form	Mobility (1/K ₀)	Neutral Mass	Formula	MS/MS score
Nadolol	15.43	[M+H] ⁺	0.825	309.19	C ₁₇ H ₂₇ N ₁ O ₄	970.9
Food						
Aspartame	13.65	[M+H] ⁺	0.815	294.12	C ₁₄ H ₁₈ N ₂ O ₅	849.0
Caffeine	18.67	[M+H] ⁺	0.629	194.08	C ₈ H ₁₀ N ₄ O ₂	996.9
D-(-)-Quinic acid	8.16	[M-H] ⁻	0.626	192.06	C ₇ H ₁₂ O ₆	757.4
Piperine	34.2	[M+H] ⁺	0.801	285.14	C ₁₇ H ₁₉ N ₁ O ₃	986.9
Theobromine	15.81	[M+H] ⁺	0.612	180.07	C ₇ H ₈ N ₄ O ₂	829.1
Theophylline	17.04	[M+H] ⁺ [M-H] ⁻	0.623 0.609	180.07	C ₇ H ₈ N ₄ O ₂	997.0
Trigonelline	7.55	[M+H] ⁺	0.562	137.05	C ₇ H ₇ N ₁ O ₂	909.5
Contaminants						
1-hexadecylpyridinium	30.97	[M+H] ⁺	0.934	303.29	C ₂₁ H ₃₇ N	948.1
2-Aminonaphthalene	7.27	[M+H] ⁺	0.59	109.06	C ₅ H ₇ N ₃	992.0
Bis(p-methylbenzylidene)sorbitol	32.8	[M+H] ⁺	0.88	386.17	C ₂₂ H ₂₆ O ₆	991.6
Bisphenol S	29.97	[M-H] ⁻	0.734	250.03	C ₁₂ H ₁₀ O ₄ S	918.1
CocamidopropylBetaine	29.6	[M+H] ⁺	0.954	342.29	C ₁₉ H ₃₈ N ₂ O ₃	997.0
Lauryl sulfate	25.04	[M-H] ⁻	0.793	266.16	C ₁₂ H ₂₆ O ₄ S	984.7
Undecanedioic acid	31.1	[M-H] ⁻	0.697	216.14	C ₁₁ H ₂₀ O ₄	991.3
Peptides						
(S)-3,5-Dihydroxyphenylglycine	16.04	[M+H] ⁺	0.68	194.11	C ₁₀ H ₁₄ N ₂ O ₂	998.2
4-Methylene-L-glutamine	7.27	[M+H] ⁺	0.619	158.07	C ₆ H ₁₀ N ₂ O ₃	276.8
7-Methylguanine	8.36	[M+H] ⁺	0.607	165.06	C ₆ H ₇ N ₅ O	995.0
Ala-Ile	13.34	[M-H] ⁻	0.7	202.13	C ₉ H ₁₈ N ₂ O ₃	892.5
Ala-Lys	5.39	[M-H] ⁻	0.725	217.14	C ₉ H ₁₉ N ₃ O ₃	934.6

Continue Appendix 22. Complete list of identified compounds in saliva samples from HS and AS in positive and negative ionization mode.

Identification	RT (min)	Molecular Ion Form	Mobility (1/K₀)	Neutral Mass	Formula	MS/MS score
Ala-Phe	14.7	[M-H]-	0.731	236.12	C12H16N2O3	890.4
Asp-Phe	13.39	[M-H]-	0.792	280.11	C13H16N2O5	733.7
Ala Pro Pro Gln Pro Phe	16.88	[M+H] ⁺	1.149	655.33	C32H45N7O8	-
Asn Thr Gly Pro Pro Pro	12.67	[M+H] ⁺	1.065	581.28	C25H39N7O9	-
Asp-His-Glu-Leu-Arg	7.5	[M+H+H] ²⁺	0.728	668.33	C27H44N10O10	-
Cyclo(leucylprolyl)	20.64	[M+H] ⁺	0.745	210.14	C11H18N2O2	945.2
Diprotin B	15.7	[M+H] ⁺	0.857	327.22	C16H29N3O4	988.4
gamma-Glutamylglutamine	7.18	[M-H]-	0.759	275.11	C10H17N3O6	751.9
gamma-Glutamylleucine	16.64	[M-H]-	0.755	260.14	C11H20N2O5	888.2
gamma-Glutamylmethionine	14.52	[M-H]- [M-H-H ₂ O]-	0.783 0.765	278.09	C10H18N2O5S	938.8
gamma-Glutamyltyrosine	15.67	[M-H]-	0.805	310.12	C14H18N2O6	953.1
Gln Gly Pro Pro Leu	15.52	[M+H] ⁺	1.056	510.28	C23H38N6O7	-
Gln-Ile	13.75	[M-H]-	0.777	259.15	C11H21N3O4	264.9
Gln-Leu	13.32	[M-H]-	0.766	259.15	C11H21N3O4	814.4
Gln-phe	14.59	[M-H]-	0.799	293.14	C14H19N3O4	941.3
Gly-Leu	13.41	[M-H]-	0.673	188.12	C8H16N2O3	976.2
Gly Pro Pro Gln Gln Asn His Gln Gln	7.17	[M+H+H] ²⁺	0.823	1032.48	C46H64N16O15	-
Gly Pro Pro Pro Pro Pro Gly Lys Pro Gln	9.73	[M+H+H] ²⁺	0.837	970.52	C45H70N12O12	-
Gly-Tyr	13.25	[M-H]-	0.733	238.10	C11H14N2O4	797.7
His-Ser	5.48	[M-H]-	0.718	242.10	C9H14N4O4	928.6
His Gly Tyr	8.01	[M+H] ⁺	0.883	375.15	C17H21N5O5	788.2
Ile-Ile	15.75	[M-H]-	0.821	244.18	C12H24N2O3	812.9

Continue Appendix 22. Complete list of identified compounds in saliva samples from HS and AS in positive and negative ionization mode.

Identification	RT (min)	Molecular Ion Form	Mobility (1/K ₀)	Neutral Mass	Formula	MS/MS score
Leu-Asp	8.88	[M-H]-	0.749	246.12	C10H18N2O5	981.5
Leu Asp Glu Glu Arg	8.49	[M+H+H]2+	0.71	660.31	C26H44N8O12	-
L-Histidine	7.27	[M+H]+	0.591	155.07	C6H9N3O2	860.3
Lys-ser	7.27	[M-H]-	0.707	233.10	C8H15N3O5	927.7
N-Acetyl-L-proline	17.8	[M+H]+	0.612	157.07	C7H11NO3	624.8
Phe Gly Tyr	17.03	[M+H]+	0.895	385.16	C20H23N3O5	782.4
Phe Leu Ser Leu	19.97	[M+H]+	1.055	478.28	C24H38N4O6	772.5
Pro Ala Pro	8.22	[M+H]+	0.785	283.15	C13H21N3O4	818.3
Pro Gly Gln Pro	7.76	[M+H]+ [M-H]-	0.914 0.942	397.20	C17H27N5O6	716.6
Pro Gly Pro Pro Gln	8.14	[M+H]+ [M+2H]2+	1.013 0.678	494.25	C22H34N6O7	-
Pro Gly Pro Pro Pro	13.5	[M+H]+ [M+2H]2+	1.095 0.709	560.30	C27H40N6O7	-
Pro Gly Pro Pro Pro Pro Gln	9.83	[M+H+H]2+	0.704	688.35	C32H48N8O9	-
Pro-Ile	13.94	[M-H]-	0.75	228.15	C11H20N2O3	835.5
Pro Pro Gln	9.83	[M+H]+	0.703	340.17	C15H24N4O5	943.3
Pro Pro Pro Pro	9.76	[M+H]+	0.923	406.22	C20H30N4O5	305.9
Pro Pro Pro Pro Pro Pro Gly Lys Pro Gln	9.76	[M+H+H]2+	0.807	1010.55	C48H74N12O12	-
Pro Ser Pro	8.06	[M+H]+ [M-H]-	0.800 0.800	299.15	C13H21N3O5	625.3
Pyroglu-ile	20.39	[M-H]-	0.759	242.13	C11H18N2O4	805.5
Pyroglu-phe	21.84	[M+H]+ [M-H]-	0.838 0.788	276.11	C14H16N2O4	939.7

Continue Appendix 22. Complete list of identified compounds in saliva samples from HS and AS in positive and negative ionization mode.

Identification	RT (min)	Molecular Ion Form	Mobility (1/K₀)	Neutral Mass	Formula	MS/MS score
Ser-Arg	5.45	[M-H]-	0.753	261.14	C ₉ H ₁₉ N ₅ O ₄	919.6
Ser-Gln	5.45	[M-H]-	0.731	233.14	C ₉ H ₁₉ N ₃ O ₄	947.1
Ser-Leu	13.05	[M-H]-	0.709	218.13	C ₉ H ₁₈ N ₂ O ₄	989
Ser-Phe	14.44	[M-H]-	0.747	252.11	C ₁₂ H ₁₆ N ₂ O ₄	817.7
Stachydrine	7.71	[M+H] ⁺	0.58	143.09	C ₇ H ₁₃ N ₂ O ₂	478.8
Thr-Leu	13.43	[M-H]-	0.734	232.14	C ₁₀ H ₂₀ N ₂ O ₄	973.2
Tyr Asp Gly Tyr	15.9	[M+H] ⁺ [M-H]-	1.044 1.000	516.19	C ₂₄ H ₂₈ N ₄ O ₉	-
Tyr Gly Tyr Gly Pro	16.73	[M+H] ⁺	1.092	555.23	C ₂₇ H ₃₃ N ₅ O ₈	478.8
Tyr Ile Asp Asn	14.3	[M+H] ⁺ [M+Na] ⁺ [M-H- H ₂ O]-	1.052 1.096 1.016	523.23	C ₂₃ H ₃₃ N ₅ O ₉	939.7
Tyr Leu Tyr Asp Asn	18.52	[M+H] ⁺	1.247	686.29	C ₃₂ H ₄₂ N ₆ O ₁₁	-

VITA

YARIXA L. CINTRON-DIAZ

Born, San Juan, Puerto Rico

- 2012 High School Diploma
University High School (UHS)
San Juan, Puerto Rico
- 2016 B.S., Chemistry
University of Puerto Rico, Rio Piedras Campus
San Juan, Puerto Rico
- 2020 Doctoral Candidate
Florida International University
Miami, Florida
- 2021 M.S., Chemistry
Florida International University
Miami, Florida
- 2021 Ph.D., Chemistry
Florida International University
Miami, Florida

PUBLICATIONS AND PRESENTATIONS

Haler, J.; Sisley, E.; Cintron-Diaz, Y.; Meitei, S.; Cooper, H.; Fernandez-Lima, F., Workflow for fast lipid screening using LESA-FT-ICR-MS. *Anal Methods*, 2019, 11, 2385. DOI: 10.1039/c8ay02739k

Cintron-Diaz, Y.; Acanda de la Rocha, A.; Castellanos, A.; Chambers, J.; and Fernandez-Lima, F., Mapping chemotherapeutic drug distribution in cancer cell spheroids using 2D-TOF-SIMS and LESA-TIMS-MS. *Analyst*, 2020, DOI: 10.1039/C9AN02245G

Cintron-Diaz, Y.; Haler, J.; Porter, J.; and Fernandez-Lima, F., Advantages of Time-Dispersive Cyclic Traveling Wave and Field-Dispersive Trapped Ion Mobility Spectrometries coupled to Mass Spectrometry for Fast Lipid Isomer Screening. *Talanta* (submitted)

Cintron-Diaz, Y.; Ramirez, C.; Hayeman, H.; and Fernandez-Lima, F., Discovery and targeted analysis of saliva using LC-TIMS-TOF MS/MS. *Rapid Communications in Mass Spectrometry* (submitted).

K. Jeanne Dit Fouque, M. Wellmann, D. Leyva Bombuse, M. Santos-Fernandez, Y. L. Cintron-Diaz, M. E. Gomez-Hernandez, D. Kaplan, V. G. Voinov and F. Fernandez-Lima, Effective

Discrimination of Gas-Phase Peptide Conformers using TIMS-ECD-ToF MS/MS. *Analytical Methods*, 2021, 13, 5216-5223.

Cintron-Diaz, Y.; Gomez-Hernandez, M.; Verhaert, M.; Verhaert, P.; and Fernandez-Lima, F. Spatially resolved neuropeptide characterization from neuropathological FFPE tissue sections by a combination of Imaging MALDI FT-ICR MSHC and LESA-TIMS-MS. *JASMS*. (submitted)

Cintron-Diaz, Y.; Gomez-Hernandez, M.; Jozic, I.; and Fernandez-Lima, F. Analysis of human skin chronic and acute wound healing process using 2D-TOF-SIMS. *In preparation*.

Yarixa L. Cintron-Diaz, Mario Gomez, and Francisco Fernandez-Lima, "Protein screening of native brain sections using LESA-TIMS-MS", Graduate School Appreciation Week (GSAW), Florida International University, April 1-5, 2019 (Poster presentation)

Yarixa L. Cintron-Diaz, Mario E. Gomez Hernandez, Jennifer Dziedzic, Tomas Guilarte, and Francisco Fernandez-Lima, "Protein screening of native brain sections using LESA-TIMS-MS", Florida Annual Meeting and Exposition (FAME), Tampa, Florida, May 9-11, 2019. (Poster presentation)

Yarixa L. Cintron-Diaz, Mario E. Gomez Hernandez, Jennifer Dziedzic, Tomas Guilarte, and Francisco Fernandez-Lima, "Protein screening of native brain sections using LESA-TIMS-MS", American Society of Mass Spectrometry (ASMS), Atlanta, Georgia, June 2-6, 2019. (Poster presentation)

Yarixa L. Cintron-Diaz, Arlet M. Acanda de la Rocha, Anthony Castellanos, Jeremy Chambers and Francisco Fernandez-Lima, "Mapping chemotherapeutic drug distribution in cancer cell spheroids using 2D-TOF-SIMS and LESA-TIMS-MS", American Society of Mass Spectrometry (ASMS), Online Meeting, June 1-12, 2020. (Poster presentation)

Yarixa L. Cintron-Diaz, Arlet M. Acanda de la Rocha, Anthony Castellanos, Jeremy Chambers and Francisco Fernandez-Lima. Mapping chemotherapeutic drug distribution in cancer cell spheroids using 2D-TOF-SIMS and LESA-TIMS-MS, Biomolecular Science Institute (BSI) Symposium, Online Meeting, July 30-31, 2020. (Poster presentation)

Yarixa L. Cintron-Diaz, Cesar Ramirez, Heino Hayeman, and Francisco Fernandez-Lima. Discovery and targeted analysis of saliva using LC-TIMS-TOF MS/MS. Biomolecular Science Institute (BSI) Symposium, Online Meeting, April 29-30, 2021. (Poster presentation)

Yarixa L. Cintron-Diaz, Mario Gomez-Hernandez, Marthe M. H. A. Verhaert, Peter D. E. M. Verhaert, and Francisco Fernandez-Lima. Spatially resolved neuropeptide characterization from neuropathological FFPE tissue sections by a combination of Imaging MALDI FT-ICR MSHC and LESA-TIMS-MS. American Society of Mass Spectrometry (ASMS), Philadelphia, Pennsylvania, October 31- November 4, 2021. (Poster presentation)